Coordination chemistry, kinetics and mechanistic studies of ring-opening polymerization of cyclic esters by formamidine and benzimidazolyl Mg(II), Cu(II) and Zn(II) complexes

by

EKEMINI DANIEL AKPAN

Submitted in fulfilment of the academic requirements for the degree of

Doctor of Philosophy

in Chemistry

School of Chemistry and Physics

College of Agriculture, Engineering and Science

University of KwaZulu-Natal

Westville

South Africa

(December, 2016)

As the candidate's supervisors, we have approved this thesis for examination.

Supervisors:

Signed:……..Name: Dr. Bernard O. Owaga Date:……

Signed:……..Name: Prof. Stephen O. Ojwach Date:…….

DECLARATION 1: PLAGIARISM

I, **Ekemini Daniel Akpan**, declare that:

(i) the research reported in this dissertation, except where otherwise indicated or acknowledged, is my original work;

(ii) this dissertation has not been submitted in full or in part for any degree or examination to any other university;

(iii) this dissertation does not contain other persons' data, pictures, graphs or other information, unless specifically acknowledged as being sourced from other persons;

(iv) this dissertation does not contain other persons' writing, unless specifically acknowledged as being sourced from other researchers. Where other written sources have been quoted, then:

(a) their words have been re-written but the general information attributed to them has been referenced;

(b) where their exact words have been used, their writing has been placed inside quotation marks, and referenced;

(v) where I have used material for which publications followed, I have indicated in detail my role in the work;

(vi) this dissertation is primarily a collection of material, prepared by myself, published as journal articles or presented as a poster and oral presentations at conferences. In some cases, additional material has been included;

(vii) this dissertation does not contain text, graphics or tables copied and pasted from the Internet, unless specifically acknowledged, and the source being detailed in the dissertation and in the References sections.

_____

Signed:

DECLARATION 2: PUBLICATIONS

DETAILS OF CONTRIBUTION TO PUBLICATIONS that form part and/or include research presented in this thesis (include papers published and in preparation). My role in each paper is indicated. The * indicates corresponding author.

Paper 1

Ekemini D. Akpan, Stephen O. Ojwach,* Bernard Omondi* and Vincent O. Nyamori. **Zn(II) and Cu(II) formamidine complexes: structural, kinetics and polymer tacticity studies in the ring-opening polymerization of ε-caprolactone and lactides**. *New Journal of Chemistry* **2016**, 40, 3499.

My contribution: The research reported on is based on the data I collected from the experimental study I did on structural, kinetics and polymer tacticity in the ring-opening polymerization of ε-caprolactone and lactides and drafted the article. These were achieved under the supervision of my supervisors.

Paper 2

Ekemini D. Akpan, Stephen O. Ojwach,* Bernard Omondi* and Vincent O. Nyamori. Structural and kinetic studies of the ring-opening polymerization of cyclic esters using *N,N'* diarylformamidines Zn(II) complexes. *Polyhedron* **2016**, 110, 63–72

My contribution: I synthesized the complexes, carried out the characterization and catalysis testing, and wrote the initial draft of the manuscript and carried out subsequent modifications towards publication of the paper. These were achieved under the guidance of my supervisors.

Paper 3

Ekemini D. Akpan, Stephen O. Ojwach,* and Bernard Omondi.* **Kinetics, mechanisms and polymer property studies of ring-opening polymerization of ε-caprolactone and lactides initiated by (benzimidazolylmethyl)amine Zn(II) alkoxides.** Manuscript submitted *Polymer Bulletin*, POBU-D-17-00157

My contribution: I synthesized the complexes, carried out the characterization and catalysis testing, and wrote the initial draft of the manuscript and carried out subsequent modifications towards publication of the paper under the supervision of my supervisors.

Paper 4

Ekemini D. Akpan, Stephen O. Ojwach,* and Bernard Omondi.* **Magnesium alkoxide complexes of (benzimidazolylmethyl) amine ligands: Synthesis and applications in ROP reactions of ε-caprolactone and lactides.** Manuscript in preparation

My contribution: I synthesized the complexes, carried out the characterization and catalysis testing, and wrote the initial draft of the manuscript and carried out subsequent modifications towards publication of the paper. These were achieved under the direction of my supervisors.

_____

Signed: Ekemini Daniel Akpan

Date:

CONFERENCE PARTICIPATION

1. Ekemini Akpan, Stephen Ojwach and Bernard Omondi **Zn(II) and Cu(II) Formamidine Complexes: Synthesis, Molecular Structures and Catalytic Activity in Ring-Opening Polymerization of ε-caprolactone and $_{D,L}$-lactide** (Poster presented at NAM 24 Catalysis at the Confluence of Science and Technology, 14–19th June 2015, Pittsburgh, PA, United States).

2. Ekemini D. Akpan, Stephen O. Ojwach and Bernard Omondi **Zn(II) Formamidine Complexes: Synthesis, Molecular Structures and Catalytic Activities in Ring-Opening Polymerization of cyclic esters** (Oral presentation at the Catalysis Society of South Africa, 27th Annual CATSA conference 2016 6–9th November 2016, Central Drakensberg, South Africa).

3. Ekemini D. Akpan, Stephen O. Ojwach and Bernard Omondi **Zn(II) Formamidine Complexes: Synthesis, Molecular Structures and Catalytic Activities in Ring-Opening Polymerization of cyclic esters** (Oral presentation at the College of Agriculture, Engineering and Science research day, 29th November 2016, Howard campus, UKZN).

PREFACE

The work in this thesis is presented in seven distinct chapters. The background of the study and general introduction of the ROP cyclic esters is given in **Chapter 1**, while a review of the use of metal complexes as catalysts in the ROP reactions of cyclic esters is covered in **Chapter 2**.

Chapter 3 describes the syntheses of Zn(II) and Cu(II) formamidine acetate complexes and their structural, kinetics and polymer tacticity studies in the ROP of ε-CL, $_{L}$-LA and $_{D,L}$-LA. The complexes were fully characterized by spectroscopic and crystallographic methods. These complexes formed active catalysts in the ROP of esters and afforded moderate molecular weight polymers exhibiting relatively moderate PDI and heterotactic PLAs. The findings have been published in *New J. Chem*., **2016**, 40, 3499–3510.

In **Chapter 4**, the role of the carboxylate anion is demonstrated by the syntheses and applications of Zn(II) complexes bearing *N,N′* diarylformamidines and benzoate anion in the ROP of esters. All the complexes were fully characterized by spectroscopic methods, and formed active initiators in the ROP of esters to afford moderate molecular weights polymers *via* coordination insertion mechanism. The nature of the *N,N′* diarylformamidines ligands, auxiliary benzoate anion and solvents were found to affect the catalytic activities as well as the properties of the polymers. The findings have been published in *Polyhedron*, **2016**, 110, 63–72.

Attempts to improve the control of the ROP reactions and polymer properties were made by the syntheses of Zn(II) and Mg(II) alkoxides supported on benzimidazolyl ligands and their investigations as initiators in the ROP of LAs and ε-CL. The complexes showed appreciable improvement in control of polymers properties. Stereoselectivity was achieved resulting in isotactic PLAs. The results of the Zn(II) and Mg(II) complexes as initiators in ROP are given in **Chapters 5** and **6**, respectively. Finally, **Chapter 7** contains the general conclusions and recommendations for future studies.

_____

Signed:

Date:

ABSTRACT

The synthesis and applications of new trinuclear Zn(II) and dinuclear Zn(II), Cu(II) and Mg(II) metal complexes derived from *N*,*N'*-diarylformamidines and (benzimidazolylmethyl) amine ligands as catalysts in ring-opening polymerization (ROP) of cyclic esters are described.

Compounds *N*,*N'*-bis(2,6-dimethylphenyl)formamidine (**L1**), *N*,*N'*-bis(2,6-diisopropylphenyl)formamidine (**L2**), and *N*,*N'*-dimesitylformamidine (**L3**) were synthesized by refluxing two mole equivalents of appropriate aniline and triethyl orthoformate in the presence of catalytic amount of acetic acid. Ligands **L1**–**L3** were reacted with either $Zn(OAc)_2.2H_2O$ or $Cu(OAc)_2.H_2O$ to produce the corresponding Zn(II) and Cu(II) *N*,*N'*-diarylformamidines complexes $[Zn_3(\mathbf{L1})_2(OAc)_6]$ (**1**), $[Zn_2(\mathbf{L2})_2(OAc)_4]$ (**2**), $[Zn_2(\mathbf{L3})_2(OAc)_4]$ (**3**) and $[Cu_2(\mathbf{L2})_2(OAc)_4]$ (**4**). All new compounds prepared were characterized by ^1H, ^{13}C, NOESY, COSY NMR spectroscopy, FT-IR, mass spectrometry, EPR and microanalyses. The coordination of **L1**–**L3** to the metal centers was through the imine nitrogen atom in a monodentate fashion. Complex **1** is trinuclear, while complexes **2**–**4** are dimeric as confirmed by single crystal X-ray crystallography. The X-band EPR spectra of complex **4** in solid and solution states confirmed retention of the dinuclear paddle-wheel core in the solution state.

Complexes **1**–**4** formed active catalysts in the ROP of ε-caprolactone (ε-CL) and lactides (LA). Complexes **1** and **3** exhibited higher rate constants of 0.1009 h^{-1} and 0.0963 h^{-1} compared to the rate constants of 0.0479 h^{-1} and 0.0477 h^{-1} observed for **2** and **4**, respectively in the ROP of ε-CL at 110 °C. Higher rate constants of 0.5963 h^{-1} and 1.2962 h^{-1} were obtained for complexes **1** and **3** in ROP of LAs compared to those reported in ROP of ε-CL at 110 °C. Activation parameters

were determined as $\Delta H^{\ddagger}$ = 25.08 kJ mol^{-1} and $\Delta S^{\ddagger}$ = −201.7 J K^{-1} mol^{-1} for ROP of ε-CL using **3**. Kinetic investigation of the polymerization of ε-CL and LAs revealed first order dependence of the ROP reactions on monomer concentration. Moderate molecular weight polymers of up to 21 286 g mol^{-1} exhibiting relatively moderate molecular weight distributions and moderately heterotactic PLAs with *Pr* up to 0.65 were obtained.

With the flexibility exhibited by ligands **L1** and **L2** in coordination with the metal centers, and its influences in the ROP reactions, auxiliary carboxylate ligands were introduced. The reactions of **L1**–**L2** with either $Zn(OAc)_2.2H_2O$ or $Cu(OAc)_2.2H_2O$ salts and auxiliary benzoate ligands produced the respective Zn(II) and Cu(II) formamidine benzoate complexes **4**–**9**. Single crystal X-ray diffraction analyses for complexes **5**, **6, 7** and **9** confirmed dinuclear solid state geometry of the complexes. Complexes **5**–**9** were active in the ROP of ε-CL, $_{D,L}$-lactide ($_{D,L}$-LA) and $_{L}$-lactide ($_{L}$-LA) monomers. The kinetic results indicated a *pseudo*-first order dependency on the monomers. The nature of the *N*,*N′* diarylformamidines ligands, auxiliary benzoate and solvent were found to affect the catalytic activity as well as the properties of the polymers. Activation parameters obtained from Eyring plots for the ROP of ε-CL using complex **8** pointed to coordination-insertion mechanism. While ROP of $_{L}$-LA resulted in moderate isotactic PLA with minimal epimerization, predominantly atactic PLA were obtained for ROP of $_{D,L}$-LA.

Attempts to improve the control of the ROP reactions and polymer properties metal alkoxide initiators were made using ligands *N*-((1H-benzo[*s*]imidazol-2-yl)methyl)-2,6-dimethylaniline (**L4**), *N*-((1H-benzo[*d*]imidazol-2-yl)methyl)-2,6-diisopropylaniline (**L5**) and *N*-((1H-benzo[*d*]imidazol-2-yl)methyl)-2,4,6-trimethylaniline (**L6**). Ligands **L4**–**L6** reacted with two

moles equivalent of either BnOH or *t*-BuOH and $ZnEt_2$ to form the Zn(II) alkoxide complexes **10**–**13**. The Mg(II) alkoxide analogous **14**–**17** were synthesized using a similar protocol with $Mg(^{n}Bu)_2$.

The Zn(II) alkoxide complexes formed effective catalysts in the ROP reactions of ε-CL, $_{D,L}$-LA. The ROP reactions initiated by the Zn(II) alkoxide complexes **10**–**13** in toluene demonstrated the effect of ligand architecture, and proceeded in *pseudo*-first order dependence on monomer concentration. The identity of the monomer and the stereochemistry of the LA monomer also had effect on the rates of ROP reaction. Complexes **10**–**13** produced predominantly crystalline isotactic poly($_{L}$-LA) and heterotactic poly($_{D,L}$-LA). Mg(II) alkoxide complexes **14**–**17** efficiently initiated the ROP of ε-CL, $_{D,L}$-LA and $_{L}$-LA to give polymers with moderate polydispersity indexes (PDI), but exhibited lower catalytic activities. Kinetic studies showed *pseudo* first-order dependency on monomer. ROP reactions using complexes **14**–**17** produced isotactic poly($_{L}$-LA) and atactic poly($_{D,L}$-LA).

ACKNOWLEDGMENTS

I give thanks, glory and honour to God Almighty who has given me all the love, strength, joy and courage to the completion of this research work.

I specially acknowledge my supervisors, Dr. Bernard Omondi Owaga and Prof. Stephen Otieno Ojwach for their sincere interest, invaluable love, patience, criticisms, spirit uplifting assistances, which all together made this work a success.

Very special appreciation goes to my parents, Elder Daniel U. Akpan and Deaconess (Mrs) Eno Daniel Akpan for totally bearing the burden of ensuring that I become a successful man in life, Dad and Mom, I say thank you so much. I am indebted to my siblings; Mrs Itohowo Benjamin, Itorobong and Mfonbong for their encouragement, support and patience, which played the greatest role in sustaining me through the challenge of being a postgraduate student.

My immeasurable thanks go to my fiancée, Elizabeth and daughter, Favour for waiting tirelessly and also being present for me at all times, I LOVE YOU ALL.

I appreciate my research colleagues especially Zamiza Sizwe, Michael Pillay, Vashan Moodley, Wisdom Munzeiwa and other colleagues in the synthetic lab. The technical and administrative staffs of the School of Chemistry and Physics, Westville campus, UKZN is highly appreciated for their help, especially Dilip Jagjivan and Mrs Malini Padayachee.

I owe the following a lot of gratitude for being there for me at one point or the other; Mr & Mrs Victor W. Akpan, Samson O. Akpotu, Elder Samuel Essien, Kempi Inyang, Drs. Ekemena Oseghe, Ovokeroye Abafe, and Isiaka Lawal, Osadolor Ebhuoma, Fru Fambo and Nwaokoro Henry. I also thank the College of Agriculture, Engineering and Science and University of KwaZulu-Natal for their financial support during this work.

The good Lord that gave me the enablement to carry out this study successfully will surely bless you all in Jesus Name, Amen.

This work is dedicated to **Mr Victor Wilson Akpan** for his invaluable contribution towards my academic pursuit.

Ekemini Akpan

LIST OF ABBREVIATIONS AND SYMBOLS

Å	Ångstrom
AM	Activated-monomer mechanism
br	Broad
CIM	Coordination-insertion mechanism
COSY	Correlation spectroscopy
calcd.	Calculated
EPR	Electron paramagnetic resonance
ε-CL	ε-caprolactone
°C	Degrees celsius
δ	Chemical shift
d	Doublet
$_{D}$-LA	$_{D}$-lactide
$_{D,L}$-LA	$_{D, L}$-Lactide
DMF	Dimethylformamide
DOSY	Diffusion-Ordered spectroscopy
DSC	Differential scanning calorimetry
ESI-MS	Electrospray ionization mass spectrometry
ε	Epsilon
FT-IR	Fourier transform infrared spectroscopy
g	Gram(s)

g mol^{-1}	Gram per mole
GPC	Gel permeation chromatography
h	Hour(s)
Hz	Hertz
^{i}Pr	Isopropyl
i	Isotactic
J	Coupling constant
k_{app}	Apparent rate of propagation
k_c	Equilibrium constant
LAs	Lactides
$_L$-LA	$_L$-lactide
m	Multiplet
Me	Methyl
min	Minute(s)
mL	Millilitres
mmol	Millimoles
mol	Moles
Mn	Number average molecular weight
M_w	Weight average molecular weight
NMR	Nuclear magnetic resonance
NOESY	Nuclear Overhauser effect spectroscopy

OAc	Acetate anion
PDI	Polydispersity index
PCL	Polycaprolactone
PLA(s)	Polylactide(s)
Pm	Probability of *meso* enchainment
ppm	Parts per million
Pr	Probability of racemic enchainment
ROP	Ring-opening polymerization
rac-LA	Racemic lactide
SEC	Size exclusion chromatography
s	Singlet
t	Triplet
TGA	Thermogravimetric analysis
T_r	Polymerization temperature
T_g	Glass transition temperature
THF	Tetrahydrofuran
T_m	Melting temperature

TABLE OF CONTENTS

LIST OF TABLES

LIST OF FIGURES

LIST OF SCHEMES

Chapter 1

Introduction to preparation, properties and applications of cyclic esters

1.1 Background

A polymeric material generally consists of many polymer chains of varying number of monomeric units and hence, different size and shape.[1] Polymers are large molecules that consist of a number of repeat units linked together in a repetitive fashion.

Large volumes of plastic materials in our daily lives are produced from oil-based sources.[2] With the disposable régime of the world population being on the increase, more and more waste plastic materials find their way into the environment.[2,3] Accumulations resulting from the persistent entrance of non-biodegradable polymer materials into the environment have become an environmental concern.[4] There is also an increased pressure on the world's oil reserves; as a result, polyesters from renewable biomass feedstock that possess excellent degradable and biocompatible properties are increasingly sort.[5,6] Polyesters obtained from renewable resources are thus fast replacing petrochemical-based plastics due to their biocompatible and biodegradable nature.[3,7]

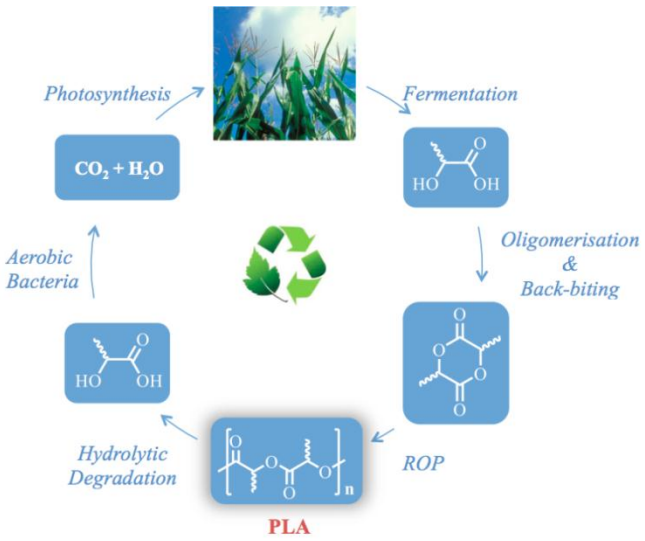

Figure 1. 1: Biodegradation cycle of a bio-based plastic.[8,9]

The raw materials for bio-based plastics are generally available from the fermentation of sugar (beet or cane) or starch (corn, wheat, potatoes, or manioc) (Figure 1.1).[8,9] Such bio-plastics are renewable and will eliminate concerns of long-term uses of these renewable materials. A typical polylactides (PLAs) cycle showing the formation of lactic acid, ring-opening polymerization (ROP) of lactide (LA) and degradation is as depicted in Figure 1.1. Polymers obtained from lactone and lactide are consider as a "green" alternative to oil based plastics largely due to their eco-friendly nature and for their physical properties such as stiffness and tensile strength of the resulting polymeric materials.[10,11,12]

In continuous search of aliphatic polyesters with useful biocompatible and biodegradable properties, ROP reactions of lactone and lactide have been employed.[13,14] Considering ring strains as imparting on the ROP reactions, monomers such as lactide (**1.1**), ε-caprolactone (**1.2**), δ-valerolactone (**1.3**) and β-butyrolactone (**1.4**) (Figure 1.2) are mainly used in the synthesis of polyesters.[15]

Lactide (**1.1**) | ε-caprolactone (**1.2**) | δ-valerolactone (**1.3**) | β-butyrolactone (**1.4**)

Figure 1. 2: Cyclic esters mostly employed in ROP reactions.

1.2 Synthesis of polyesters

Polyesters are hetero-chain macromolecules containing repeating ester groups.[16] The synthesis of polyesters such as polycaprolactone (PCL) and polylactides (PLAs) can occur mainly *via* two different approaches: the polycondensation of hydroxycarboxylic acids (Scheme 1.1), or by the ROP of cyclic esters (Scheme 1.2).

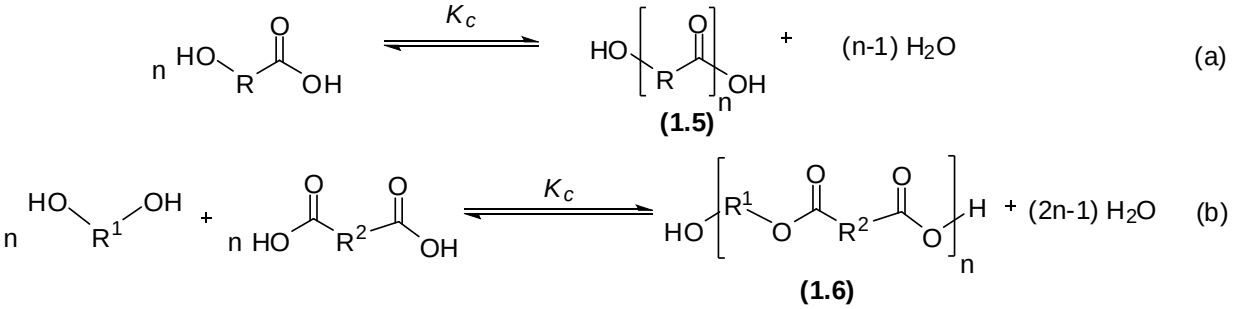

Scheme 1. 1: Polyesterification based on (a) homo polycondensation and (b) hetero condensation.[1]

Polycondensation can either be by the homo polycondensation of hydroxycarboxylic acid (Scheme 1.1a) or the hetero polycondensation of a diol with dicarboxylic acid (Scheme 1.1b).[1] The homo and hetero polycondensation route has an advantage of being less expensive compared

to the ROP method, but gives low molecular weight polymers because the process requires a sufficiently high equilibrium constant (K_c) and 1:1 stoichiometry must be obeyed in the case of hetero polycondensation.[1,17]

The ROP of PCL and PLAs has been used in the last forty five years as it is versatile in producing a variety of biodegradable, biocompatible and environmental friendly replacement of conventional oil-based materials polymers in a controlled manner.[18]

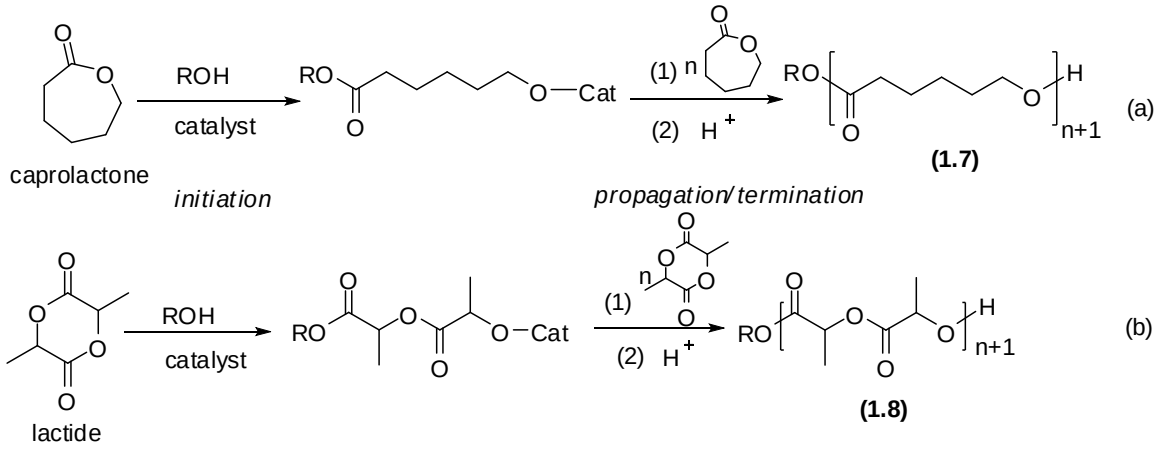

Scheme 1. 2: Ring opening of (a) lactones and (b) LA: alcohol initiation and polymer propagation, followed by termination by acid.[12,19]

A number of initiator and catalyst systems have been developed and applied to a diversity of monomers to produce all types of polymers since Carothers and co-workers[20,21] first extensively explored the ROP technique for lactones, anhydrides, and carbonates. Stridsberg and co-workers[17] enumerated several reasons for studying the polymerization of cyclic esters. In order

to find the best polymerization system for a desired technological or industrial process, factors such as optimized experimental conditions, economy, toxicology, and technical apparatus development are important. Over the years, well defined metal catalysts, organic catalysts and enzymatic catalysts have been developed, resulting in a certain of level control over polymer molecular weight, polydispersity index (PDI) and tacticity.[11,12]

1.2.1 Ring-opening polymerization of cyclic esters

ROP processes are generally defined by three separate stages; namely, initiation, propagation and termination (Scheme 1.2). Dubois and co-workers[22] reported three primary ROP mechanisms: cationic polymerization, anionic polymerization and "coordination-insertion" polymerization based on the initiation steps.

1.2.1.1 Anionic ring-opening polymerization

Anionic ROP involves the formation of an anionic species (**1.9**) that attacks the carbonyl carbon of the monomer as depicted in Scheme 1.3. Lithium complexes among other complexes involving potassium and magnesium are reported to have the highest stereocontrol in ROP of *rac*-lactide (*rac*-LA) *via* anionic ROP mechanism.[23]

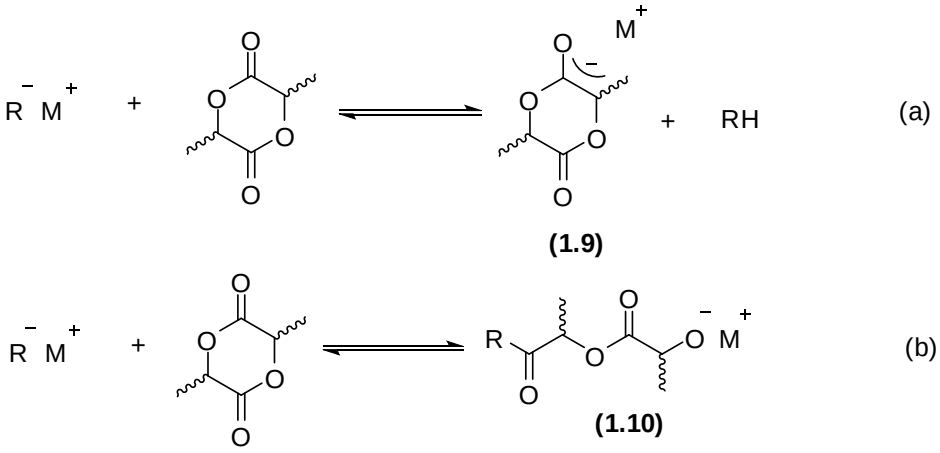

Scheme 1. 3: Anionic mechanism in the ROP of LA *via* (a) deprotonation of the methine proton of the monomer, and (b) direct nucleophilic attack.[12,24]

The anionic mechanism is initiated by either the deprotonation of the methine proton of the monomer (Scheme 1.3a) or nucleophilic attack on the carbonyl carbon of the monomer (Scheme 1.3b), breaking the acyl bond forming a metal alkoxide. Propagation occurs with the addition of another monomer forming a growing polymer chain (**1.10**).[24] The two initiation pathways are easily distinguished by end-group analysis. The deprotonation route is associated with the absence of initiator fragments whereas the nucleophilic attack route typically results in ester end groups derived from the alkoxide promoters.[12] Jedlinski and co-workers[25] reported polymers with molecular weights in agreement with the monomer-to-initiator ratios and relatively narrow molecular weight distribution in the anionic polymerization of $_{L}$-lactide ($_{L}$-LA) and $_{D,L}$-lactide ($_{D,L}$-LA) initiated with potassium methoxide. Anionic ROP tends to give uncontrolled molecular weights distributions (PDI) due to side reactions such as epimerization, chain termination and inter/intra molecular *trans*-esterification (**1.11 – 1.14**) (Scheme 1.4).[12,26]

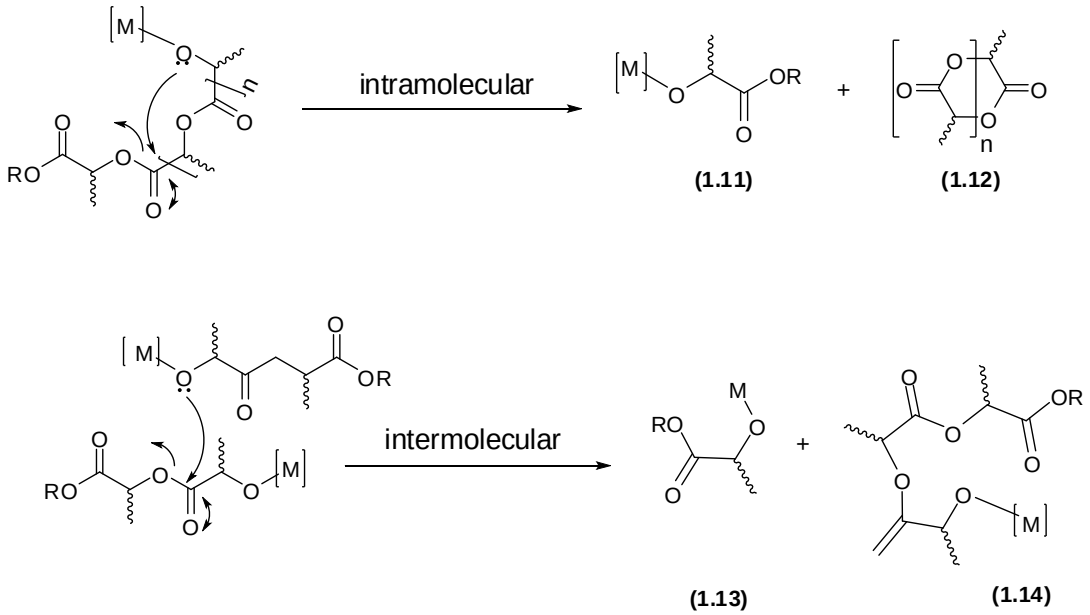

Scheme 1. 4: Intra- and inter-molecular *trans*-esterification side reactions in the ROP of LAs.[12,26]

1.2.1.2 Cationic ring-opening polymerization

Typically, cationic ROP reaction mechanism involves initiation by nucleophilic attack at the methine carbon in **1.15** and subsequent cleavage of the alkyl oxygen bond in **1.16** (Scheme 1.5).[12] The attack results in a ring opening of the positively charged species through an S_N2-type process.[17] The cationic polymerization is difficult to control and often only low molecular weight polymers are formed.[27] Few catalysts such as trifluoromethanesulfonate (MeOTf) and trifluoromethanesulfonic acid (HOTf) have been found to be active in the cationic polymerization of LA.[28,29]

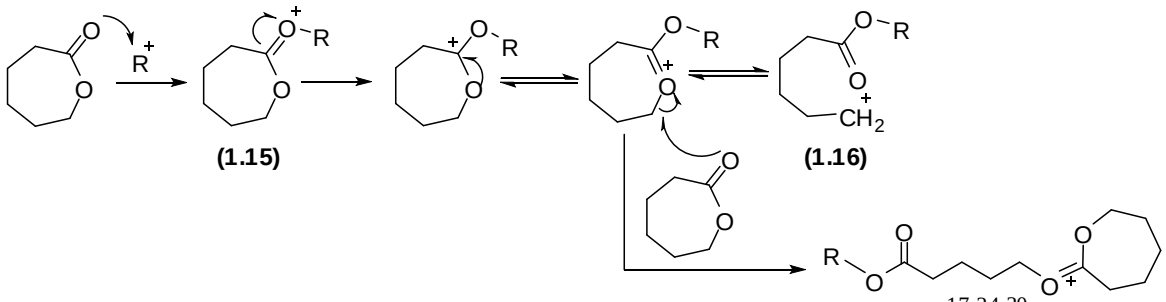

Scheme 1. 5: Schematic representation of the initiation steps for cationic ROP.[17,24,30]

1.2.1.3 Coordination-insertion ring-opening polymerization

The most common ROP mechanism observed with respect to inorganic and organometallic polymerization catalysts is the coordination-insertion mechanism as shown in Scheme 1.6.[28] Coordination-insertion mechanism is a special case of anionic polymerization in that the overall bonds formed and broken are identical; however, a portion of the initiating species remains bound to the propagating terminus of the growing polymer chain. The coordination of the monomer to the metal center of the catalyst through the carbonyl group is thought to control the characteristics of the polymer. Insertion proceeds *via* nucleophilic addition to the activated carbonyl carbon leading to the ring opening of the monomer and the breaking of the acyl-oxygen bond. Insertion of a new monomer propagates the growing polymer chain (**1.17**).[16] Quenching of the polymerization reaction by agents such as an alcohol may induce the termination of the reaction thereby liberating the polymer from the catalyst *via* protonation. This may also occur automatically if the propagating polymer chain undergoes deactivation thereby deactivating the propagating terminus. In principle, this process may be used to recover the catalytically active species, although success of this approach is largely dependent on the nature of the catalyst.[16]

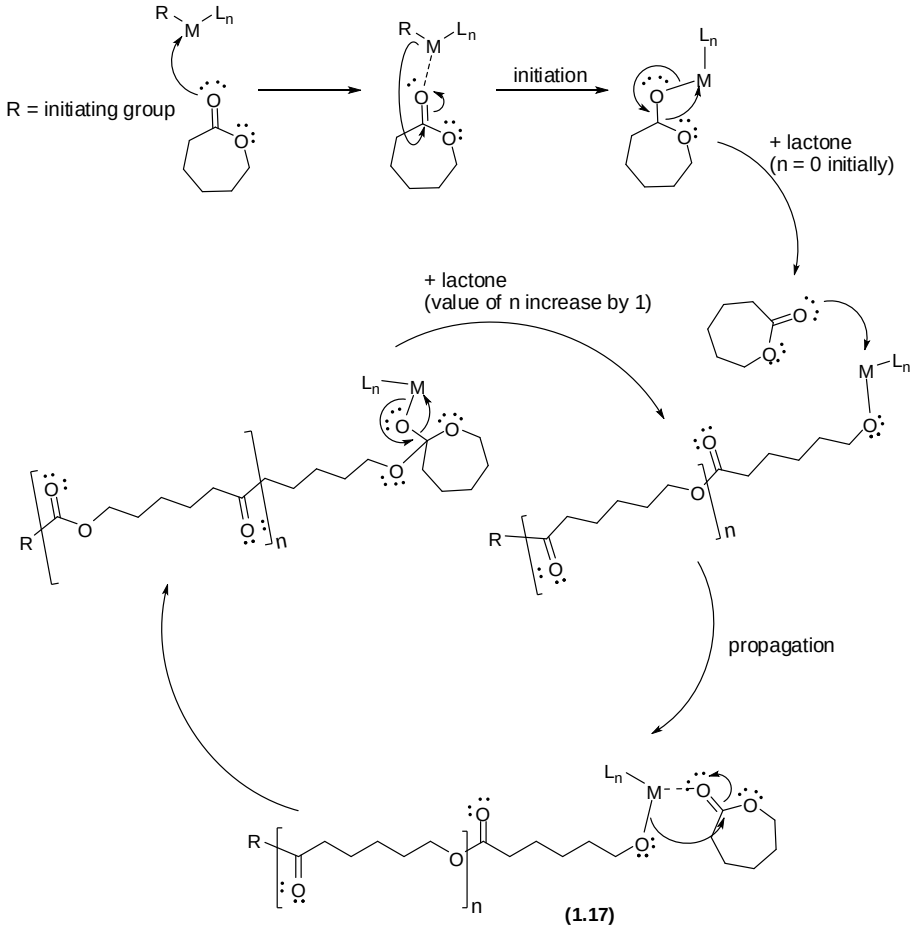

Scheme 1. 6: Polymerization of a lactone *via* the coordination-insertion mechanism. Note: M = metal center and L_n = Ligand (unspecified).[31]

ROP reactions occurring through coordination-insertion mechanism are also prone to side reactions such as intermolecular or intramolecular *trans*-esterification, leading to the termination of the polymerization process. The undesirable *trans*-esterification is associated with molecular weight broadening (manifested in a high PDI) and may produce low molecular weight polymers.[26] In the cases of LAs, developing growing PLA chain *via* chain end control and enantiomorphic site control gives stereocontrol in the polymer chain thereby reducing undesirable side reactions.

1.2.2 Stereochemistry of PLAs

There are three possible configurations of LAs because of the presence of two chiral centers in the molecule as shown in **1.18 – 1.20** (Figure 1.3). The relationship of the neighboring stereocenters in LAs could be described by considering the combination of the stereocenter pairs. When LAs undergo ROP reactions, four microstructures of PLA are possible; isotactic (**1.21**), atactic (**1.22**), heterotactic (**1.23**), and syndiotactic (**1.25**). Isotactic PLA (**1.24**) can be produced from either $_{L}$-LA (**1.18**) or $_{D}$-LA (**1.19**) or a mixture of both in combination with a stereoselective catalyst. Isotactic PLA (**1.24**) obtained has a pure enantiomeric enrichment in the polymer chain, i.e. -*SSSSSSSS*- or –*RRRRRRRR*- stereocenters. Heterotactic and atactic PLA can be synthesized from *rac*-LA, when each $_{L}$- and $_{D}$-LA are alternating resulting in a doubly alternating sequence in polymer chain. Stereocontrol ROP of *meso*-LA (**1.20**) can conceivably yield either syndiotactic PLA with alternating of *S* and *R* stereocenters in the polymer chain; -*SRSRSR*- or heterotactic PLA having the stereocenters doubly alternating -*SSRRSSRR*- throughout the polymer chain.

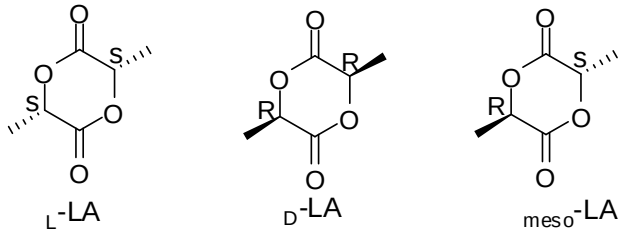

(1.18) **(1.19)** **(1.20)**

Figure 1. 3: Stereoisomer structures of LAs.

Stereocontrol in ROP of LAs is an important parameter because the polymer's tacticity influences its properties, for example, crystallinity is associated with isotactic PLA whereas atactic PLA is amorphous. The PLA tacticity depends on both the type of lactide and initiator selected (Figure 1.4). Metal alkoxide initiators' giving high stereoselectivity in the ROP of LAs

has been reported.[18,32,33] Aluminum tris(alkoxide) or tin bis(carboxylate) catalysts is known to produced isotactic PLA from the polymerization of optically active (*R*,*R*)-LA or (*S*,*S*)-LA. The polymerization of *rac*-LA or *meso*-LA with these catalysts also yields PLAs that were effectively atactic polymers [33,34]

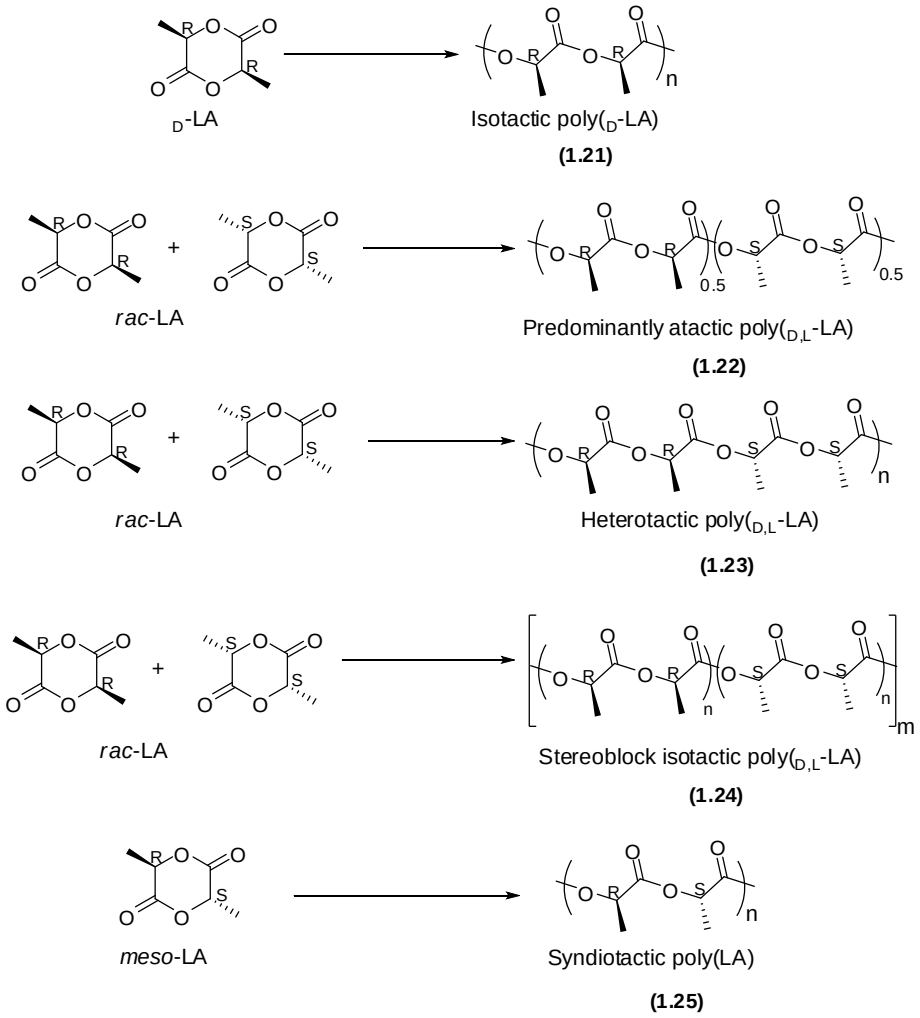

Figure 1. 4: Stereochemistry of PLAs microstructure for ROP of LAs.[10,34]

The stereochemistry of PLAs is normally studied and quantified by homonuclear decoupled ^{1}H NMR, together with ^{13}C NMR spectroscopy to obtained information about the microstructure of the polymer.

1.2.2.1 Homonuclear decoupled ^{1}H NMR spectroscopy

Homonuclear decoupled ^{1}H NMR spectroscopy study is a vital tool in the quantification of stereochemical microstructures of PLAs. Due to the different stereochemical environments experienced in the polymer, multiple resonances of the methine proton can be observed in the ^{1}H NMR spectrum of the polymer.[35] Conventionally, these resonances are assigned to different stereosequence combinations using notations '*i*' and '*s*'. The number of possible combinations for a stereosequence of *n* stereocenters is defined by $2^{(n-1)}$ and the probability of different stereosequence combinations occurring in the polymer chain can be calculated based on Bernoullian statistics (Table 1.1).[36]

Table 1. 1: Tetrad probabilities based on Bernoullian statistics.[36]

	Probability	
Tetrad	*rac*-lactide	*meso*-lactide
[iii]	$P_m^2 + P_rP_m/2$	0
[iis]	$P_rP_m/2$	0
[sii]	$P_rP_m/2$	0
[sis]	$P_r^2/2$	$(P_m^2 + P_rP_m)/2$
[sss]	0	$P_r^2 + P_rP_m/2$
[ssi]	0	$P_rP_m/2$
[iss]	0	$P_rP_m/2$
[isi]	$(P_r^2 + P_rP_m)/2$	$P_m^2/2$

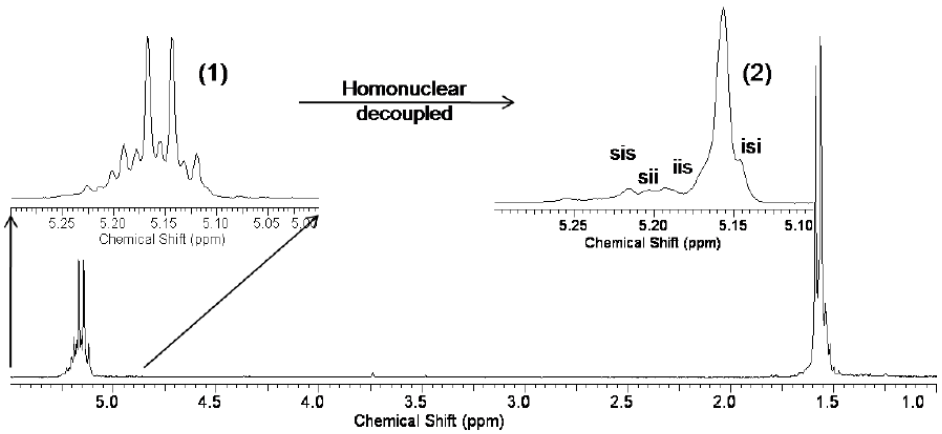

Figure 1. 5: ^{1}H NMR spectra illustrating expanded methine region before (1) and after (2) homonuclear decoupling.

Decoupling the methine proton from the methyl group in the ^{1}H NMR (Figure 1.5) removes the quartet splitting due to the adjacent methyl group and allows straightforward identification and quantification of the tetrads seen for PLA formed from $_{L}$-LA, $_{D}$-LA or mixtures thereof.[36] Assignment of tetrads of the PLA microstructure using spectra obtained from homonuclear decoupled ^{1}H NMR is well established and reported in literature.[35,37,38,39,40] For example, atactic PLA exhibit five resonances in the homonuclear decoupled ^{1}H NMR as depicted in Figure 1.6. ^{13}C NMR spectroscopy can also give information about the polymer microstructure and is generally used to support conclusions made from examination of the methine region of the homonuclear decoupled ^{1}H NMR spectrum of the polymer.

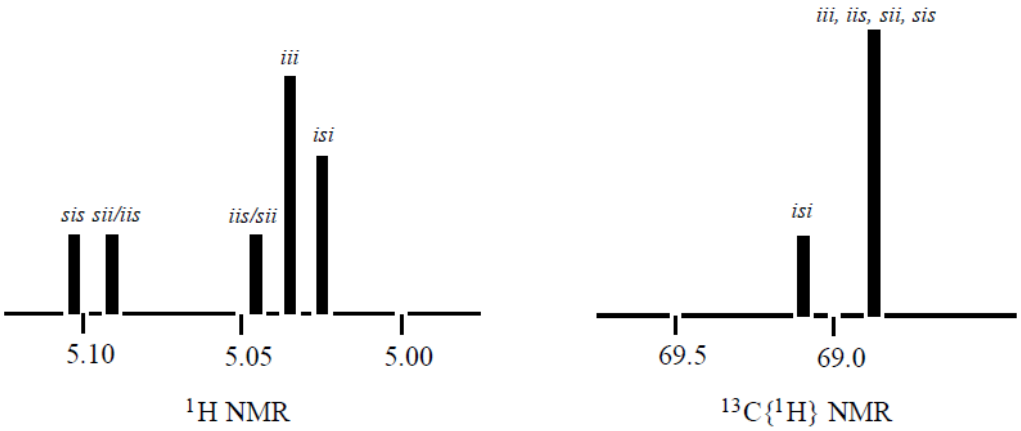

Figure 1. 6: Schematic representation of tetrad intensities for atactic PLAs.[41]

The probability of racemic enrichment P_r is calculated based on equation (1.1).[34]

$$P_r = \frac{2I_1}{(I_1 + I_2)} \qquad (1.1)$$

I_1 is the intensity of tetrad appearing between δ 5.20 – 5.25 ppm, and I_2 represent the intensity of tetrad between δ 5.13 – 5.20 ppm in the homonuclear decoupled ^{1}H NMR (Figure 1.6).

Kinetic data obtained from the kinetic studies of the ROP of *rac*-LA and $_L$-LA has been used in estimating the stereocontrol exhibited by the catalysts. The relationship in equation (1.2)[42] under the assumption that the concentration and order of initiator are kept constant and the *pseudo*-first order rate constant of ROP of *rac*-LA is directly proportional to the *pseudo*-first order rate constant of ROP of $_L$-LA is used in calculating P_r.

$$P_r = 1 - \frac{1}{2}\left[\frac{K_{app\,(L-lactide)}}{K_{app\,(rac-lactide)}}\right] \qquad (1.2)$$

1.3 Applications of PCL and PLAs

Biodegradable polymers are a special class of biomaterials that have received a lot of interest because they degrade through hydrolysis of the ester bonds, an example of applications of some of these polymers being that of degradable sutures.[43] Versatile bio-plastic obtained from ROP of ε-CL and LA have many applications like in food packaging[44] with readily composted waste materials, cutting down on problematic waste. The degradability of PLA to biocompatible molecules is utilized in medical applications such as in surgery.[45] In the medical field, degradable PLA have also been used in bone fixation as screws that will degrade *in vivo* and eliminate the need for follow-up surgery to remove the screws.[14] Polyesters from LA have also been used as a vehicle for controlled drug delivery enabling the controlled release of active ingredients at the required site in the body.[14,45] Biocompatible and biodegradable polymers obtained from the mentioned monomers have found applications in different fields as depicted in Figure 1.7.

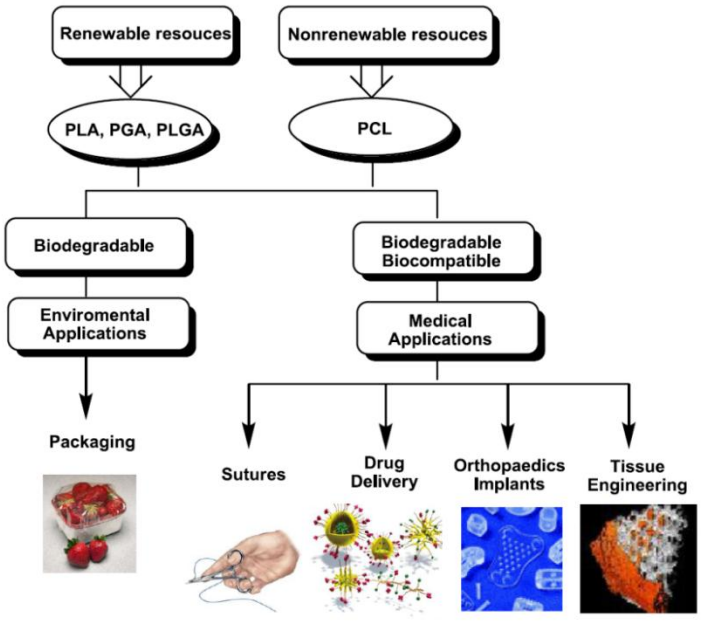

Figure 1. 7: Potential applications of polymers obtained from ε-CL and LAs.[7,12]

1.4 References

(1) Dubois, P.; Dubois, P.; Coulembier, O.; Raquez, J. M. *Handbook of Ring-Opening Polymerization*; Wiley, 2009.

(2) Thompson, R. C.; Moore, C. J.; vom Saal, F. S.; Swan, S. H. *Phil. Trans. R. Soc. B: Bio. Sci.* **2009**, *364*, 2153.

(3) Song, J. H.; Murphy, R. J.; Narayan, R.; Davies, G. B. H. *Phil. Trans. R. Soc. B: Bio. Sci.* **2009**, *364*, 2127.

(4) Barnes, D. K. A.; Galgani, F.; Thompson, R. C.; Barlaz, M. *Phil. Trans. R. Soc. B Bio. Sci.* **2009**, *364*, 1985.

(5) Divya, G.; Archana, T.; Manzano, R. A. *J. Pet. Environ. Biotechnol.* **2013**, *4*.

(6) Miller, S. A. *ACS Macro Lett*. **2013**, *2*, 550.

(7) Mooney, Brian P. *Biochem. J.* **2009**, *418*, 219.

(8) Platel, R. H.; Hodgson, L. M.; Williams, C. K. *Polym. Rev*. **2008**, *48*, 11.

(9) Manton, L. B., *Ring-opening polymerization of lactide and other related monomers. Doctor of Philosophy (PhD))*. University of Bath, **2014**.

(10) Stanford, M. J.; Dove, A. P. *Chem. Soc. Rev*. **2010**, *39*, 486.

(11) Dove, A. P. *Chem. Comm*. **2008**, 6446.

(12) Dechy-Cabaret, O.; Martin-Vaca, B.; Bourissou, D. *Chem. Rev*. **2004**, *104*, 6147.

(13) Nuyken, O.; Pask, S. *Polymers* **2013**, *5*, 361.

(14) Albertsson, A.-C.; Varma, I. K. *Biomacromolecules* **2003**, *4*, 1466.

(15) Williams, C. K. *Chem. Soc. Rev*. **2007**, *36*, 1573.

(16) Dubois, P.; Jacobs, C.; Jerome, R.; Teyssie, P. *Macromolecules* **1991**, *24*, 2266.

(17) Stridsberg, K.; Ryner, M.; Albertsson, A.-C. In *Degradable Aliphatic Polyesters*; Springer Berlin Heidelberg, 2002; Vol. 157.

(18) Yuan, Y.; Jing, X.; Xiao, H.; Chen, X.; Huang, Y. *J. Appl. Polym. Sci.* **2011**, *121*, 2378.

(19) Jérôme, C.; Lecomte, P. *Adv. Drug Delivery Rev.* **2008**, *60*, 1056.

(20) Natta, F. J. v.; Hill, J. W.; Carothers, W. H. *J. Am. Chem. Soc.* **1934**, *56*, 455.

(21) Carothers, W. H.; Dorough, G. L.; Natta, F. J. v. *J. Am. Chem. Soc.* **1932**, *54*, 761.

(22) Mecerreyes, D. J., R.; Dubios, P. *Macromol. Architect.* **1999**, 1.

(23) Kasperczyk, J. E. *Macromolecules* **1995**, *28*, 3937.

(24) Khanna, A.; Sudha, Y. S.; Pillai, S.; Rath, S. S. *J. Mol. Model.* **2008**, *14*, 367.

(25) Jedliński, Z.; Wałach, W.; Kurcok, P.; Adamus, G. Y. *Makromol. Chem.* **1991**, *192*, 2051.

(26) Dobrzynski, P.; Li, S.; Kasperczyk, J.; Bero, M.; Gasc, F.; Vert, M. *Biomacromolecules* **2004**, *6*, 483.

(27) Penczek, S. *J. Polym. Sci. A Polym. Chem.* **2000**, *38*, 1919.

(28) Kricheldorf, H. R.; Dunsing, R. *Die Makromol. Chemie* **1986**, *187*, 1611.

(29) Bourissou, D.; Martin-Vaca, B.; Dumitrescu, A.; Graullier, M.; Lacombe, F. *Macromolecules* **2005**, *38*, 9993.

(30) Labet, M.; Thielemans, W. *Chem. Soc. Rev.* **2009**, *38*, 3484.

(31) Ireland, B. J., *Cationic OrganoMagnesium complexes as homogeneous catalysts for the ring–opening polymerization of lactones (Doctoral dissertation)*University of Lethbridge, **2009**.

(32) Kowalski, A.; Duda, A.; Penczek, S. *Macromolecules* **2000**, *33*, 689.

(33) Ovitt, T. M.; Coates, G. W. *J. Polym. Sci. Part A: Polym. Chem.* **2000**, *38*, 4686.

(34) Ovitt, T. M.; Coates, G. W. *J. Am. Chem. Soc.* **2002**, *124*, 1316.

(35) Kricheldorf, H. R.; Boettcher, C.; Tönnes, K.-U. *Polymer* **1992**, *33*, 2817.

(36) Chamberlain, B. M.; Cheng, M.; Moore, D. R.; Ovitt, T. M.; Lobkovsky, E. B.; Coates, G. W. *J. Am. Chem. Soc.* **2001**, *123*, 3229.

(37) Thakur, K. A. M.; Kean, R. T.; Zell, M. T.; Padden, B. E.; Munson, E. J. *J. Chem. Commun.* **1998**, 1913.

(38) Thakur, K. A. M.; Kean, R. T.; Hall, E. S.; Kolstad, J. J.; Lindgren, T. A.; Doscotch, M. A.; Siepmann, J. I.; Munson, E. J. *Macromolecules* **1997**, *30*, 2422.

(39) Thakur, K. A. M.; Kean, R. T.; Hall, E. S.; Doscotch, M. A.; Munson, E. J. *Anal. Chem.* **1997**, *69*, 4303.

(40) Kasperczyk, J. *Polymer* **1996**, *37*, 201.

(41) H. Chisholm, M.; S. Iyer, S.; E. Matison, M. *Chem. Commun.* **1997**, 1999.

(42) Nomura, N.; Ishii, R.; Yamamoto, Y.; Kondo, T. *Chem. – Eur. J.* **2007**, *13*, 4433.

(43) Ikada, Y.; Tsuji, H. *Macromol. Rapid Commun.* **2000**, *21*, 117.

(44) Amass, W.; Amass, A.; Tighe, B. *Polym. Int.* **1998**, *47*, 89.

(45) Uhrich, K. E.; Cannizzaro, S. M.; Langer, R. S.; Shakesheff, K. M. *Chem. Rev.* **1999**, *99*, 3181.

Chapter 2

Literature review of metal complexes as catalysts/initiators in ROP of cyclic esters

2.1 Background

The driving force in the design of catalytic systems arises from the understanding of mechanisms of ROP of cyclic esters resulting in desirable polymers with properties such as biocompatibility, biodegradability, high molecular weight, narrow molecular weight distributions and certain degree of stereoselectivity in the case of PLAs. This has brought about research on the design of ligands and their complexes with transition metal centers both in the academic and the industrial sectors. Numerous publications[1,2,3] on catalyst design based on structure-activity relationship have appeared and the search for better and more efficient ROP catalyst systems is continuing. This chapter is a review of relevant works on design and synthesis of Al, Sn, Mg, Ca, Zn, and Cu complexes involving different ligand systems and their application as catalysts or initiators in ROP reactions of cyclic ester.

2.2 Review of Al, Sn, Mg, Ca, Zn, Cu complexes involving N,O and S-donor ligands as ROP catalysts/initiators

Several catalysts have been explored for the ROP of LAs and lactones,[4,5,6,7,8,9] with the majority being metal based. It is interesting to note that metal based compounds which take part in the ROP of cyclic esters are described as catalysts or initiators based on their behaviors, mostly determined *via* end group analysis Over the years, well defined metal catalysts, organic catalysts

and enzymatic catalysts have also been developed, resulting in a certain of level control over polymer molecular weight, PDI and tacticity.[1,10]

2.2.1 Tin and aluminum initiators

For the past three decades, research on homogeneous coordination insertion catalysts has focused on inorganic main group metals based on tin and aluminum.[11] Industrially, the initiator used to prepare commercial grade PCLs and PLAs is a tin compound **2.1** depicted in Figure 2.1.[12]

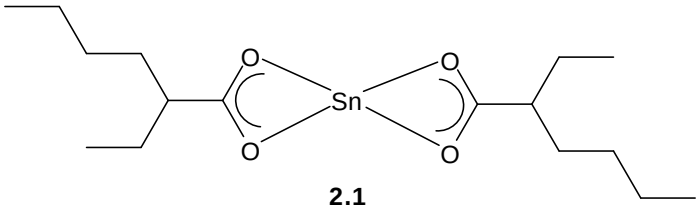

2.1

Figure 2. 1: Tin(II) 2-ethylhexanoate, an initiator used industrially to prepare polyesters.[12]

This commercially available initiator is soluble in both common organic solvents and in melt monomers. It may be used for the preparation of polymers with molecular weights of up to 10^6 g mol^{-1} with reaction times from a few hours to a few days when used with an alcohol co-initiator. However, there are toxicity issues related to organo-tin compounds and this has led to significant efforts to develop catalyst/initiator systems based on less controversial, more environmentally acceptable metals.

Salen-aluminum complexes have been intensively studied for the stereoselective polymerization of LAs (Figure 2.2). Moderate to high levels of isotactic enrichments in the ROP of LAs upon

using Schiff base ligands with non-substituted phenoxide groups were reported for compounds **2.2**[13] and **2.4**.[14]

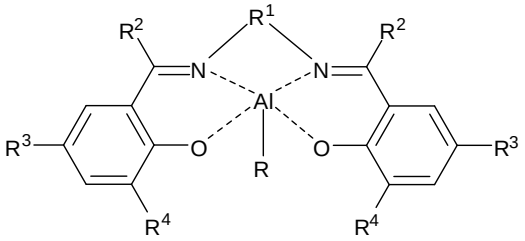

$R^1 = C_2H_4$, $R^2 = R^3 = R^4 = H$ (**2.2**)
$R^1 = C_2H_4$, $R^2 = CH_3$, $R^3 = R^4 = H$ (**2.3**)
$R^1 = C_2H_4$, C_3H_6 or $CH_2C(CH_3)_2CH_2$, $R^2 = R^3 = R^4 = H$ (**2.4**)

Figure 2. 2: Aluminum salen type complexes studied for the stereoselectivity polymerization of LAs.[13,14]

Nomura and co-workers also investigated a series of analogous aluminum/achiral Schiff base complexes [15,16], and reported much higher activities for ROP of *rac*-LA with complexes having propylene spacer ($R^1 = C_3H_6$) compared to the analogous ligands having an ethylene spacer ($R^1 = C_2H_4$), ascribing it to a higher flexibility imparted to the metal coordination sphere (Figure 2.3). Ma and co-workers[17] described the use of similar compound in the ROP of *rac*-LA and reported moderate activity when R^1 is an ethylene spacer (**2.6**) with resulting polymers showing no enrichment in stereoregular sequences (Figure 2.3). In contrast, when R^1 was an ortho-xylene spacer (**2.7**), polymers with moderate heterotactic enrichments (P_r = 0.65) were obtained. These differences in activity was attributed to the weak coordination between the aluminum and sulfur which causes rapid inter-conversion between conformations and no stereoselectivity is induced in this chain-end controlled polymerization when R^1 is an ethylene bridge.

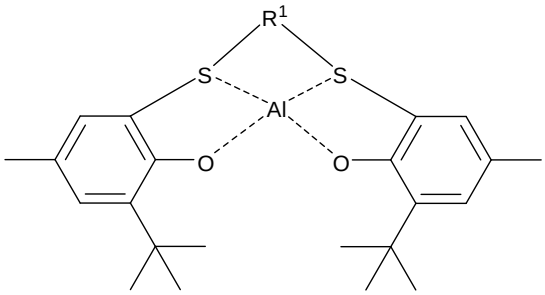

$R^1 = C_3H_6$ (**2.5**)
$R^1 = C_2H_4$ (**2.6**)
R^1 = ortho-xylene (**2.7**)

Figure 2. 3: Aluminum sulfanediyl bis(phenolate) complex in the ROP of *rac*-LA with resulting polymers showing no enrichment in stereoregular sequences.[15,16]

2.2.2 Magnesium and calcium based polymerization catalysts/initiators

Alkaline earth metals based catalysts have proven very attractive because of their high activity and low toxicity.[8] The most commonly used alkaline earth metals catalysts/initiators are Mg(II) and Ca(II) complexes because they combine high activity with relatively low toxicity. Indeed they are prevalent in many metalloenzymes both in vivo and in the environment. They are mostly grouped together because they show closely related properties and often their activities are studied via coordination with similar ligand systems. Magnesium is the most abundant alkali earth metal, and has become an interesting metal to use in the synthesis of polymers for biomedical applications.

Considerable attention on β-diketiminate (BDI) complexes emanated from the report of Coates and co-workers.[18] Mg(II) iso-propoxide β-diketiminate complexes were reported to show excellent activities and very high hetero-selectivity in *rac*-LA or *meso*-LA polymerization

(P_r:0.9 *rac*-LA, P_r:0.76 *meso*-LA).[19] The nature of the initiating groups was found to influence the polymerization reactions, resulting in predictable molecular weight and narrow PDI. The substituents on the BDI aryl rings affected both the rate and the stereochemistry: with apparent rate constant k_{app} decreasing in the order $^{i}Pr > Et > Pr$ and the heterotactic bias for *rac*-LA also decreased in the same order.[18]

Wu and co-workers[20] reported on the use of a mono-methylether Salen-type ligand in combination with magnesium (Figure 2.4). They reported the complexes as efficiently initiating the ROP of $_L$-LA and *rac*-LA in a controlled fashion, yielding polymers with very low PDI. Kinetic studies showed a second-order dependency on monomer concentration with magnesium complex as an initiator. Moderate isotactic enriched PLA was obtained in *rac*-LA polymerization in CH_2Cl_2 (P_m = 0.58, T_r = 0 °C), when the Mg(II) complex (**2.8**) was employed. The stereoselectivity was significantly increased upon lowering the polymerization temperature (P_m = 0.67, T_r = -30 °C).

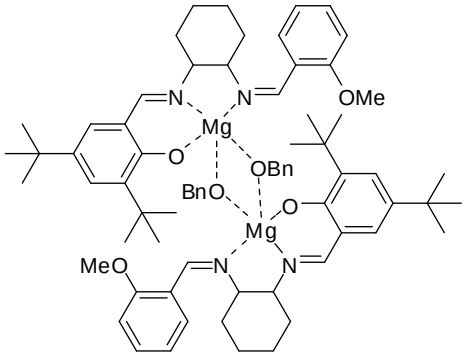

(2.8)

P_m = 0.58

Figure 2. 4: Mono-methylether Salen-complex reported by Wu and co-workers efficiently initiating the ROP of $_L$-LA and *rac*-LA in a controlled fashion.[20]

Sanchez-Barba and co-workers[21] reported alkyl-containing magnesium complexes with good polymerization properties, resulting in high molecular weight polymers with low to moderate PDI. The ROP reaction was initiated by alkyl transfer into the monomer chain. Shueh and co-workers[22] investigated a magnesium aryloxide as a catalyst and reported a ''living'' polymerization based on the linear relationship between the monomer : initiator ratio and the molecular weight of the polymer.

Magnesium *NNO*-tridentate ketiminate complexes used for the ROP of *rac*-LA were investigated by Huang and co-workers.[23] The magnesium complexes **2.9** and **2.10** shown in Figure 2.5 used as a catalyst afforded PLAs with high levels of heterotactic enrichment ($P_{r,50°C}$ = 0.79, $P_{r,0°C}$ = 0.85) in THF as the polymerization medium. When CH_2Cl_2 was used as a solvent, the P_r value became smaller ($P_{r,30°C}$ = 0.64).

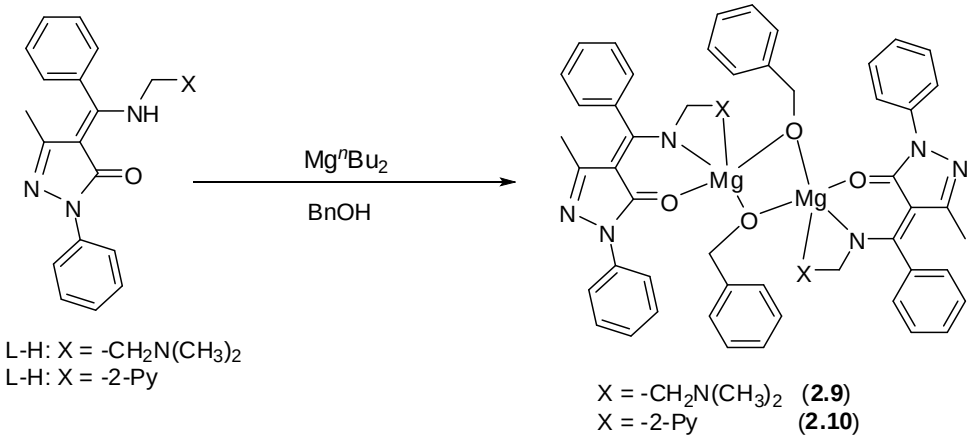

Figure 2. 5: *NNO*-tridentate ketiminate Mg complexes affording PLAs with high levels of heterotactic enrichment in THF as the polymerization medium .[23]

Organo-magnesium complexes,[20,23,24,25] are best known to exhibit this characteristics, and this has been attributed to the change in the stereogenic environment of the catalytic site in different solvent media.

The biocompatible nature of calcium and the difference in coordination chemistry from magnesium and zinc despite having +2 charges upon complex formation makes calcium attractive for polyesters production.[26] Calcium isopropyloxide (**2.11**) shown in Figure 2.6 generated in situ from the reaction of bis(tetrahydrofuran) calcium bis[bis(trimethylsilyl) amide] and isopropanol, is highly active for the controlled ROP of cyclic esters in THF using mild conditions (18 °C).[27] Complex **2.11** catalyzes the polymerization of cyclic esters, and the isolated polymers had high PDIs and much higher molecular weights as compared to the calculated values.

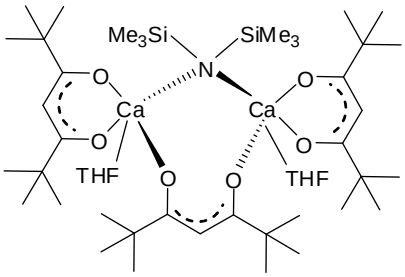

(2.11)

Figure 2. 6: Diketone supported calcium complex highly active for the controlled ROP of cyclic esters in THF.[27]

Chisholm and co-workers[28] also prepared monomeric Ca(II) complexes **2.12** and **2.13** for stereoselective ROP of $_{D,L}$-LA (Figure 2.7). In order to minimize aggregation, they employed a

strategy to encapsulate the metal center in a sterically bulky multidentate nitrogen donor framework specifically using tris(pyrazolyl) borate ligands. The Ca(II) complex was reported to be the most active for the ROP of $_{D,L}$–LA when compared with the corresponding Mg(II) and Zn(II) complexes. This was attributed to the increasing polarity of the M-OR bond on going from Zn(II) to Mg(II) to Ca(II) as the carbonyl carbon was presumed to be most effectively activated by the more electropositive metal.

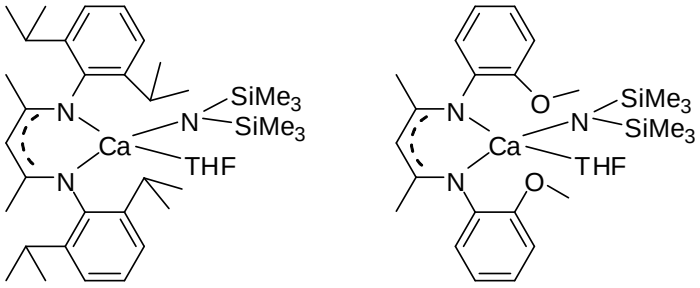

(2.12) **(2.13)**

Figure 2. 7: Calcium complexes supported by β-diketiminate ligands stereoselectivity in ROP of $_{D,L}$-LA.[28]

2.2.3 Zinc based polymerization catalysts/initiators

Dove[29], Chisholm[30] and co-workers investigated a potentially tridentate β-diiminate ligand in combination with zinc (**2.14**) (Figure 2.8), resulting in catalysts with higher activity, but less controlled and less stereoselective polymerizations than the β-diiminate complexes reported by Chamberlain and co-workers.[31] This was also explained by the fact that the extra O-donor with respect to the symmetric diisopropyl analogous was dissociated from the metal center.

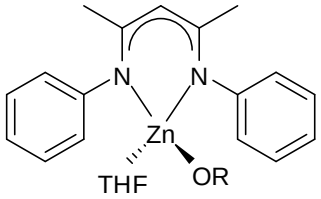

(2.14)

OR = O^{t}Bu

Figure 2. 8: BDI complexes reported by Chisholm and co-workers in the ROP reaction of cyclic esters.[32,33]

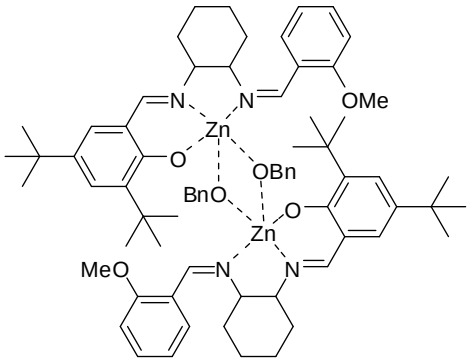

(2.15)

P_r = 0.75

Figure 2. 9: Mono-methylether Salen-complex reported by Wu and co-workers showing heterotactic enrichment in the ROP of $_{D,L}$-LA.[20]

Wu and co-workers[20] reported on the use of a mono-methylether Salen-type ligand in combination with Zn(II) alkoxides as depicted in Figure 2.9. Kinetic studies showed a first order dependency on both monomer concentrations. The Zn(II) complex **2.15** gave polymers with a significant heterotactic enrichment (P_r = 0.75, T_r = 25 °C) in CH_2Cl_2 as the polymerization medium.

Binuclear Zn(II) alkoxide complexes supported by a bis-salalen ligand have been reported and the complexes showed catalytic activities in the ROP of LA under a controllable mode.[34] Interestingly, the mechanisms of the ROP of LA were different at different temperatures, with coordination insertion mechanism being suitable under a melt condition (130 °C), while at a low temperature the ROP proceeded *via* an activated monomer mechanism. The complexes demonstrated stereoselectivity in the ROP of *rac*-LA affording a slightly isotactic preference (P_m = 0.59) in toluene and a heterotactic preference (P_m = 0.54) in THF, respectively.

Zn(II) *NNO*-tridentate ketiminate complexes used for the ROP of *rac*-LA have been investigated by Huang and co-workers (Figure 2.10).[23] The *NNO*-tridentate ketiminate Zn(II) complexes give higher stereoselectivity when the polymerization was performed in CH_2Cl_2 ($P_{r,0°C}$ = 0.71) (**2.16**) compared to THF ($P_{r,0°C}$ =0.61) (**2.17**). Huang and co-workers attributed the different stereoselective behavior upon using THF as the polymerization medium to the ability of THF to coordinate to the metal species

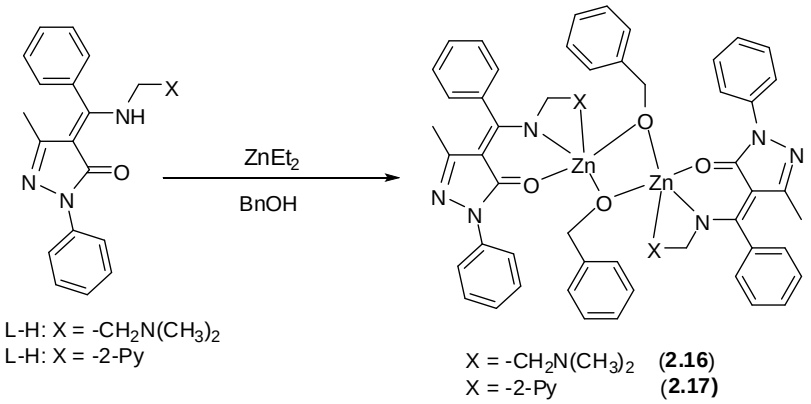

Figure 2. 10: *NNO*-tridentate ketiminate Zn(II) complexes used for the ROP of *rac*-LA investigated by Huang and co-workers giving higher stereoselectivity when the polymerization was performed in CH_2Cl_2.[23]

Wang and co-workers[35] reported Zn(II) complexes bearing the anilido-aldiminate ligand (**2.18** – **2.20**) shown in Figure 2.11 as efficient initiators in the ROP of ε-CL and β-BL in a "living" fashion, furnishing polymers with controlled molecular weights and very narrow PDI. The four-coordinate dinuclear Zn(II) alkoxide complex **2.20** dissociates to form a three coordinate monomeric zinc alkoxide complex at low temperatures, which was considered as an active species during the ROP process at relatively high temperatures. Chisholm and co-workers[32,33] reported the synthesis of related BDI complexes as THF adducts which were also efficient initiators in the ROP of LAs. The Zn(II) complex was reported to show good heteroselectivity in *rac*-LA polymerization in THF.

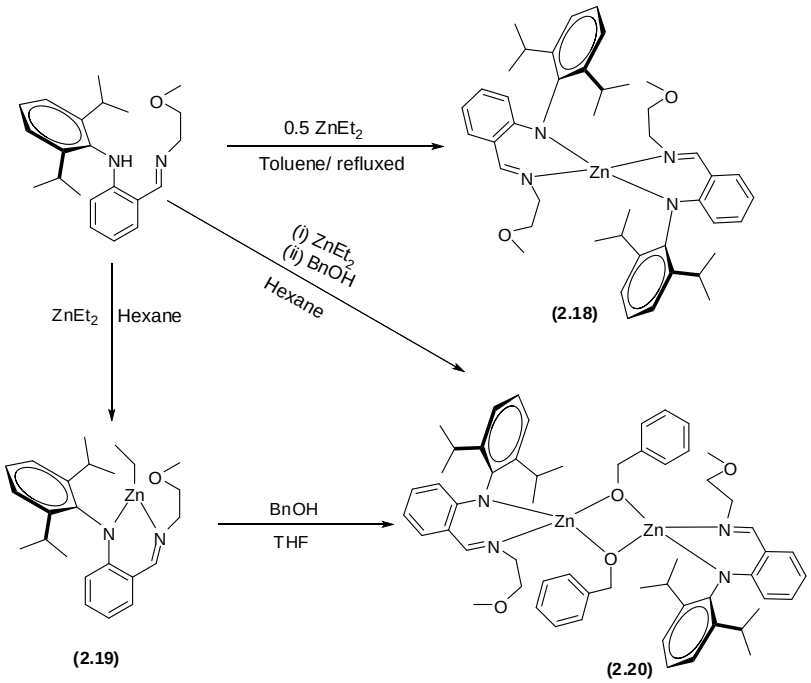

Figure 2. 11: Zinc alkoxide derivatives as initiators for ROP of cyclic esters.[35]

Zn(II) complexes prepared from the reactions of fluorous imino-alcohols with either $Zn[N(SiMe_3)_2]_2$ or $ZnEt_2$ when combined with benzyl alcohol (BnOH) showed activity for ROP of *rac*-LA and β-butyrolactone at 20–50 °C.[36] Atactic biased PLA with molecular weight up to

20,700 g mol^{-1} and PDI of 1.06–1.57 respectively, were reported. The use of excess benzyl alcohol as a transfer agent resulted in the immortal ROP of LA (or β-butyrolactone).

Jensen and co-workers[37,38] synthesized Zn(II) alkoxide catalyst **2.21** supported by an *N*-heterocyclic carbenes (Figure 2.12) and reported rapid polymerization of $_{D,L}$-LA to heterotactic enriched (P_r = 0.60) PLA while the free carbenes and analogs was also reported to polymerize LAs stereoselectively in the absence of a metal and yielded highly isotactic enriched PLA.

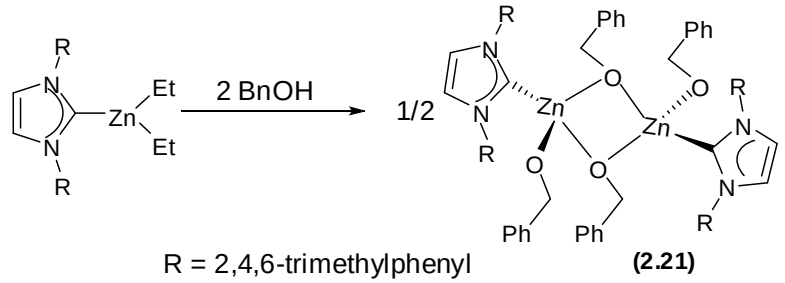

Figure 2. 12: *N*-heterocyclic carbene Zn(II) complex reported by Jensen and co-workers resulting in rapid polymerization of $_{D,L}$-LA to heterotactic enriched (P_r = 0.60) PLA .[37]

Jones and co-workers[39] reported a series of homogeneous/heterogeneous mononuclear and trinuclear Zn(II) metal complexes of salicylaldimine ligands. The presence of substituents in the phenyl ring of the ligands highly influenced the nature of complexes obtained. The heterogeneous salicylaldiminato Zn(II) system was shown to initiate the polymerization of LA but with less efficiency compared to the homogeneous systems evaluated. Higher M_n polymers were obtained over time as the percentage conversion increased. The PDI values of the polymers ranged from 1.34 to 1.85, with complexes with the least steric hindrance resulting in polymers with the highest PDI values.

Appavoo and co-workers[40] synthesized series of pyrazole Cu(II) and Zn(II) complexes **2.22** - **2.25** (Figure 2.13) and reported the activities of the complexes in the ROP of ε-CL and $_{D,L}$-LA to varied with respect to the metal center. No clear cut variation in the activities of initiators based on substituents on the benzoic acids that were used as ancillary ligands to introduce a metal–oxygen bond required for the polymerization was established. The reported stereoselectivity of the PLAs was heterotactic biased.

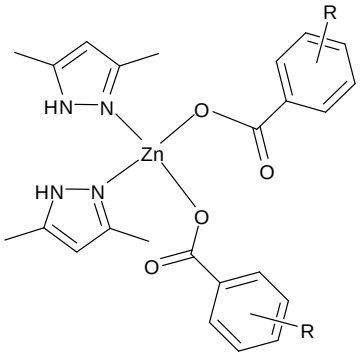

R = NO_2 (**2.22**)
R = Cl (**2.23**)
R = OH (**2.24**)
R = H (**2.25**)

Figure 2. 13: Pyrazole Zn(II) carboxylate complexes as catalysts in ROP of cyclic esters.[40]

Owjach and co-workers[41] studied the ROP of ε-CL using monometallic (pyrazol-1-ylmethyl)pyridine Zn(II) acetate complexes (Figure 2.14). The polymerization reactions followed *pseudo* first-order kinetic with respect to ε-CL monomer. Moderate molecular weights were obtained for the polymers and relatively broad molecular weight distributions associated with *trans*-esterification reactions was also obtained.

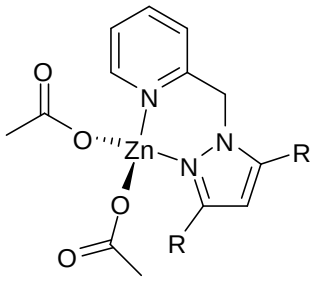

R = Me (**2.26**)
R = Ph (**2.27**)

Figure 2. 14: Monometallic (pyrazol-1-ylmethyl)pyridine Zn(II) acetate complexes as catalysts in ROP of ε-CL.[41]

Attandoh and co-workers[42] investigated (benzimidazolylmethyl)amine Zn(II) carboxylate complexes **2.28** – **2.30** as catalysts in polymerization reactions of ε-CL. The activities of these catalysts were dictated to a great extent by the nature of the metal center and the ligand architecture (Figure 2.15). The polymerization kinetics was first order with respect to both monomer and catalyst and proceeded through a coordination-insertion mechanism. Despite the inferior catalytic behavior of these complexes when compared with established zinc systems, they provided a convenient synthetic route to very stable catalysts.

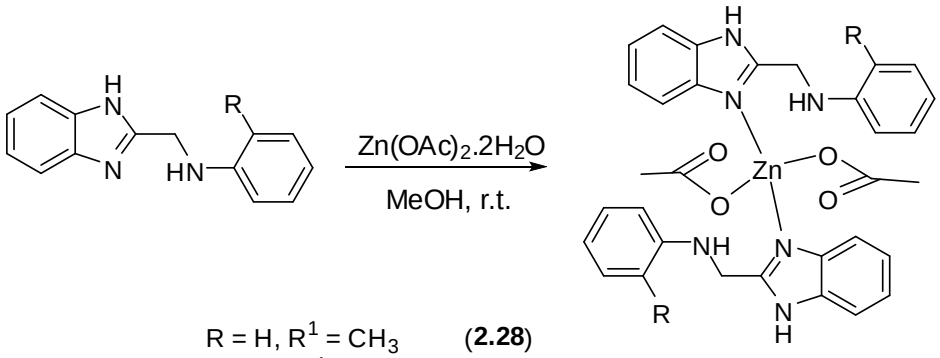

R = H, $R^1 = CH_3$ (**2.28**)
R = Br, $R^1 = CH_3$ (**2.29**)
R = SH, $R^1 = C_6H_5$ (**2.30**)

Figure 2. 15: ROP catalysts reported by Attandoh and co-workers.[42]

2.2.4 Copper based polymerization catalysts/initiators

Interest in copper complexes as catalysts for ROP reactions emanated following the first highly active Cu(II) based catalysts for the polymerization of *rac*-LA reported in literature.[43,44,45] John and co-workers synthesized Cu(II) complexes **2.31 - 2.33** of phenoxy-ketimine ligands (Figure 2.16) and reported that the Cu(II) complexes efficiently catalyzed the ROP of $_{L}$-LA at elevated temperatures under solvent- free melt conditions, producing PLA polymers of moderate molecular weights (M_n = 8000 –11 000, [M] : [I] = 50) and having narrow molecular weight distributions (PDI = 1.3 – 1.4 at 70–80% conversion).[46]

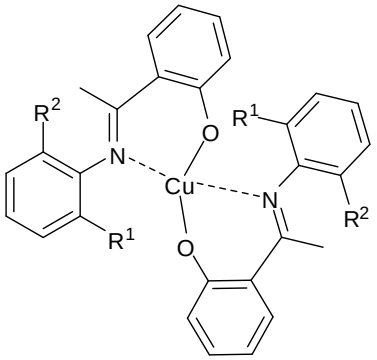

$R^1 = R^2 =$ Et (**2.31**)
$R^1 = R^2 =$ Me (**2.32**)
$R^1 =$ H, $R^2 =$ Me (**2.33**)

Figure 2. 16: Cu(II) phenoxy-ketimine based catalysts for the polymerization of $_{L}$-LA at elevated temperatures under solvent free melt conditions.[46]

Fortun and co-workers reported diiminopyrrolide Cu(II) alkoxide complexes **2.34** and **2.35**, LCuOR (OR^1 = *N*,*N*-dimethylamino ethoxide, OR^2=2-pyridyl methoxide) (Figure 2.17).[47] Compound **2.34** produces essentially atactic PLA (the typical slight heterotactic bias owing to chain-end control was observed), while compound **2.35** shows a strong isotactic preference with

P_m=0.68 – 0.70. The difference in stereocontrol was attributed to a dinuclear active species for LCuOR[2] in contrast to a mononuclear species for LCuOR[1].

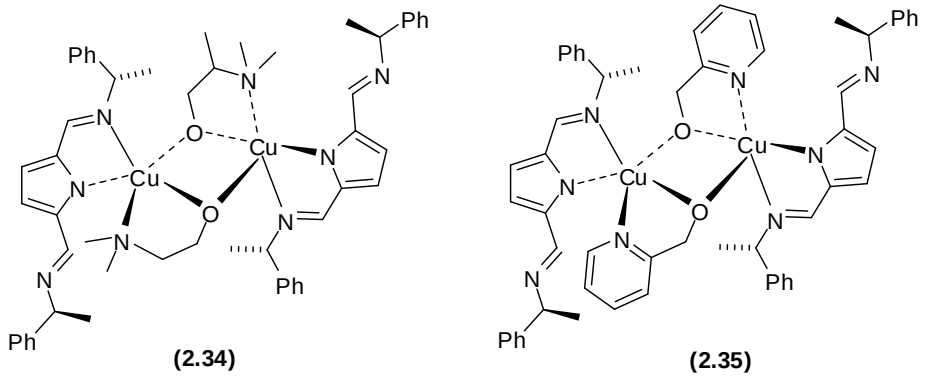

Figure 2. 17: Diiminopyrrolide Cu(II) alkoxide complexes employed in ROP of LAs.[47]

2.3 Statements of the problem

The toxicity and high cost of metal centers used in the synthesis of the most metal complexes employed as catalysts in the ROP of cyclic esters has become a concern. The inability to completely remove catalyst residues from synthesized polymer and potential toxicity of catalysts depending on the metal center is a major concern bearing the potential applications of the polymers. Most of the metal complex catalysts used in ROP produces polymers with low molecular weights, broad PDI, and lacks stereoselectivity in the case of PLAs. The challenge is to produce biodegradable polymers from LAs or ε-CL at low cost and with physical properties that would make them industrial competitors to non-biodegradable, well established commodity polymers such as poly(ethylene). Therefore, the development of non-toxic catalyst systems to synthesize polymer with high levels of control over polymer molecular weight, tacticity, PDI and end-group reliability has become highly desirable.

2.4 Justification of study

Polymers synthesized from lactones and LAs as biodegradable polymers have generated lot of interest as they are synthesized from bio-renewable resources and degrade into non-toxic product. These polymers have found applications in the fields of agriculture,[48] packaging,[49] biomedical,[50] and pharmaceutical industries.[51] In order to synthesize such polymers, developments in synthesis of catalysts and initiators (usually metal complexes) that form well-defined, stereospecific polymers with controlled molecular weights are required. Based on the overview of metal containing catalysts in this chapter, we decided to extend this research area further by developing and testing additional *N*-donor ligands containing formamidines and benzimidazole derivatives.

The flexibility of amidines, amidinates and benzimidazole derivative ligands to coordinate either as monodentate as well as chelating (η^2), rendering their respective complexes very promising for applications in catalysis.[52] The steric bulk of the ligand affects the coordination mode around the metal centers, and largely influences the control of polymer microstructure, and as such, careful design of the ligand motif could result in controlled ROP of cyclic esters.[41,53] The nature and chemical activities of the polymers obtained could be controlled *via* modification of the electronic and steric properties of these ligands. The metals Zn, Cu and Mg were chosen as metal centers because they are cheap and less toxic. Hence, any successful catalyst based on these metals will have lot of potentials from both the economic, health and environmental point of view. These observations have led to the motivation for this study.

2.5 Aim and objectives of this project

This study aimed to design and synthesize *N*-donor ligands and carry out complexation with less expensive, less toxic metals, and investigate their catalytic activities in the ROP of cyclic esters. The following specific objectives can thus be identified:

- Synthesis of formamidine ligands and their Zn(II) and Cu(II) complexes. The effect of metal and ligand stoichiometry in the synthesis of such complexes will be investigated and the coordination chemistry discussed.
- Synthesis of benzimidazole derivatives ligands and their Zn(II) and Mg(II) complexes. The effect of metal and ligand stoichiometry in the synthesis of such complexes will be investigated and the coordination chemistry discussed.
- Application of synthesized compounds as catalysts in the ROP of cyclic esters. It was envisaged that these catalysts will aid the synthesis of polymers with controlled architecture and controlled molecular weights.
- Kinetic and polymer tacticity studies of the ROP reactions.

2.6 References

(1) Dechy-Cabaret, O.; Martin-Vaca, B.; Bourissou, D. *Chem. Rev.* **2004**, *104*, 6147.

(2) Kamber, N. E.; Jeong, W.; Waymouth, R. M.; Pratt, R. C.; Lohmeijer, B. G. G.; Hedrick, J. L. *Chem. Rev.* **2007**, *107*, 5813.

(3) Labet, M.; Thielemans, W. *Chem. Soc. Rev.* **2009**, *38*, 3484.

(4) Albertsson, A.-C.; Varma, I. K. *Adv. Polym. Sci.* **2002**, *157*, 1.

(5) Gupta, A. P.; Kumar, V. *Eur. Polym. J.* **2007**, *43*, 4053.

(6) Jérôme, C.; Lecomte, P. *Adv. Drug Delivery Rev.* **2008**, *60*, 1056.

(7) Albertsson, A.-C.; Varma, I. K. *Biomacromolecules* **2003**, *4*, 1466.

(8) Platel, R. H.; Hodgson, L. M.; Williams, C. K. *Polym. Rev*. **2008**, *48*, 11.

(9) Stanford, M. J.; Dove, A. P. *Chem. Soc. Rev*. **2010**, *39*, 486.

(10) Dove, A. P. *Chem. Comm*. **2008**, 6446.

(11) Biela, T.; Duda, A.; Penczek, S. *Macromol. Symp*. **2002**, *183*, 1.

(12) Chisholm, M. H.; Zhou, M. *J. Mater. Chem*. **2004**, *14*, 3081.

(13) Le Borgne, A.; Wisniewski, M.; Spassky, N. *Abstr. Pap. Am. Chem. Soc*. **1995**, *210*, 217.

(14) Bhaw-Luximon, A.; Jhurry, D.; Spassky, N. *Polym. Bull.* **2000**, *44*, 31.

(15) Nomura, N.; Ishii, R.; Yamamoto, Y.; Kondo, T. *Chem. – Eur. J.* **2007**, *13*, 4433.

(16) Nomura, N.; Ishii, R.; Akakura, M.; Aoi, K. *J. Am. Chem. Soc.* **2002**, *124*, 5938.

(17) Ma, H.; Melillo, G.; Oliva, L.; Spaniol, T. P.; Englert, U.; Okuda, J. *Dalton Trans.* **2005**, 721.

(18) Chamberlain, B. M.; Cheng, M.; Moore, D. R.; Ovitt, T. M.; Lobkovsky, E. B.; Coates, G. W. *J. Am. Chem. Soc.* **2001**, *123*, 3229.

(19) Cheng, M.; Attygalle, A. B.; Lobkovsky, E. B.; Coates, G. W. *J. Am. Chem. Soc.* **1999**, *121*, 11583.

(20) Wu, J.-C.; Huang, B.-H.; Hsueh, M.-L.; Lai, S.-L.; Lin, C.-C. *Polymer* **2005**, *46*, 9784.

(21) Sanchez-Barba, L. F.; Garces, A.; Fajardo, M.; Alonso-Moreno, C.; Fernandez-Baeza, J.; Otero, A.; Antinolo, A.; Tejeda, J.; Lara-Sanchez, A.; Lopez-Solera, I. *Organometallics* **2007**, *26*, 6403.

(22) Shueh, M.-L.; Wang, Y.-S.; Huang, B.-H.; Kuo, C.-Y.; Lin, C.-C. *Macromolecules* **2004**, *37*, 5155.

(23) Huang, Y.; Hung, W.-C.; Liao, M.-Y.; Tsai, T.-E.; Peng, Y.-L.; Lin, C.-C. *J. Polym. Sci. Part A: Polym. Chem.* **2009**, *47*, 2318.

(24) Wu, J.; Pan, X.; Tang, N.; Lin, C.-C. *Eur. Polym. J.* **2007**, *43*, 5040.

(25) Chisholm, M. H.; Phomphrai, K. *Inorg. Chim. Acta* **2003**, *350*, 121.

(26) Voet, D.; Voet, J. G. *Biochemistry, 2nd ed.*,; John Wiley and Sons: New York, 1995.

(27) Zhong, Z.; Dijkstra, P. J.; Birg, C.; Westerhausen, M.; Feijen, J. *Macromolecules* **2001**, *34*, 3863.

(28) Chisholm, M. H.; Gallucci, J.; Phomphrai, K. *Chem. Commun.* **2003**, 48.

(29) chisholm, M. H.; Gallucci, J. C.; Phomphrai, K. *Inorg. Chem.* **2005**, *44*, 8004.

(30) Dove, A. P.; Gibson, V. C.; Marshall, E. L.; White, A. J. P.; Williams, D. J. *Dalton Trans.* **2004**, 570.

(31) Chamberlain, B. M.; Cheng, M.; Moore, D. R.; Ovitt, T. M.; Lobkovsky, E. B.; Coates, G. W. *J. Am. Chem. Soc.* **2001**, *123*, 3229.

(32) Chisholm, M. H.; Gallucci, J. C.; Phomphrai, K. *Inorg. Chem.* **2002**, *41*, 2785.

(33) Chisholm, M. H.; Huffman, J. C.; Phomphrai, K. *J. Chem. Soc. Dalton Trans.* **2001**, 222.

(34) Sun, Y.; Cui, Y.; Xiong, J.; Dai, Z.; Tang, N.; Wu, J. *Dalton Trans.* **2015**, *44*, 16383.

(35) Wang, C.-H.; Li, C.-Y.; Huang, B.-H.; Lin, C.-C.; Ko, B.-T. *Dalton Trans.* **2013**, *42*, 10875.

(36) Grunova, E.; Roisnel, T.; Carpentier, J.-F. *Dalton Trans.* **2009**, 9010.

(37) Jensen, T. R.; Breyfogle, L. E.; Hillmyer, M. A.; Tolman, W. B. *Chem. Commun.* **2004**, 2504.

(38) Jensen, T. R.; Schaller, C. P.; Hillmyer, M. A.; Tolman, W. B. *J. Organomet. Chem.* **2005**, *690*, 5881.

(39) Jones, M. D.; Davidson, M. G.; Keir, C. G.; Hughes, L. M.; Mahon, M. F.; Apperley, D. C. *Eur. J. Inorg. Chem*. **2009**, *2009*, 635.

(40) Appavoo, D.; Omondi, B.; Guzei, I. A.; van Wyk, J. L.; Zinyemba, O.; Darkwa, J. *Polyhedron* **2014**, *69*, 55.

(41) Ojwach, S. O.; Okemwa, T. T.; Attandoh, N. W.; Omondi, B. *Dalton Trans.* **2013**, *42*, 10735.

(42) Attandoh, N. W.; Ojwach, S. O.; Munro, O. Q. *Eur. J. Inorg. Chem*. **2014**, 3053.

(43) Whitehorne, T. J. J.; Schaper, F. *Chem. Commun.* **2012**, *48*, 10334.

(44) Whitehorne, T. J. J.; Schaper, F. *Inorg. Chem*. **2013**, *52*, 13612.

(45) Whitehorne, T. J. J.; Schaper, F. *Can. J. Chem*. **2013**, *92*, 206.

(46) John, A.; Katiyar, V.; Pang, K.; Shaikh, M. M.; Nanavati, H.; Ghosh, P. *Polyhedron* **2007**, *26*, 4033.

(47) Fortun, S.; Daneshmand, P.; Schaper, F. *Angew. Chem. Int. Ed.* **2015**, *54*, 13669.

(48) Kasirajan, S.; Ngouajio, M. *Agron. Sustain. Dev*. **2012**, *32*, 501.

(49) Amass, W.; Amass, A.; Tighe, B. *Polym. Int*. **1998**, *47*, 89.

(50) Uhrich, K. E.; Cannizzaro, S. M.; Langer, R. S.; Shakesheff, K. M. *Chem. Rev*. **1999**, *99*, 3181.

(51) Ikada, Y.; Tsuji, H. *Macromol. Rapid Commun.* **2000**, *21*, 117.

(52) Schmidt, S.; Schulz, S.; Bläser, D.; Boese, R.; Bolte, M. *Organometallics* **2010**, *29*, 6097.

(53) Thomas, C. M. *Chem. Soc. Rev*. **2010**, *39*, 165.

Chapter 3

Zn(II) and Cu(II) formamidine complexes: Structural, kinetics and polymer tacticity studies in ring-opening polymerization of ε-caprolactone and lactides

This chapter is adapted from the paper published in *New J. Chem*., **2016**, 40, 3499–3510 and is based on the experimental work of the first author, Ekemini D. Akpan. The contributions of the first author include synthesis and characterization of the ligands and complexes, ε-CL and LAs ROP catalysis and drafting the manuscript.

3.1 Introduction

The development of new catalysts or initiators for ROP of esters has generated great interest. Zn(II) and Cu(II) complexes have been shown to produce effective catalysts for the ROP reactions of cyclic esters largely because they are easily synthesized, they are stable, less toxic and more importantly biocompatible.[1]

The catalytic activities of β-diketiminate complexes employed in the ROP reactions of cyclic ester have been studied extensively.[2] Reports on amidines and amidinates complexes employed for ROP catalysis of cyclic esters are extremely rare.[3] Amidinate ligands have found many applications in coordination chemistry and also as ancillary ligands to form complexes as catalyst/initiators in organic transformation and polymerization reactions.[4] The flexibility of

amidines and amidinates ligands to coordinate either as monodentate as well as chelating (η^2) render their respective complexes very promising for applications in catalysis.[5] The steric bulk of the ligand affects the coordination mode around the metal centers, and largely influences the control of polymer microstructure, and as such, careful design of the ligand motif could result in controlled ROP of cyclic esters.[6] The nature and chemical activities of the polymers obtained could be controlled *via* modification of the electronic and steric properties of amidines/amidinates ligands. Neutral mono (amidinate) and bi-functional ligands with two amidinate moieties bridged by a linker with rare earth metal complexes show catalytic activity towards cyclic ester polymerization, giving high molecular weight and narrow molecular weight distribution polymers.[7] Phomphrai and coworkers[8] reported rapid polymerization of ε-CL and also found that bis(amidinate) tin(II) complexes with electron donating groups accelerated the polymerization reactions and enhance the catalytic activities of the complexes.

In this chapter, we report the synthesis of Zn(II) and Cu(II) formamidine complexes and their applications as catalysts in the ROP of ε-CL and LAs. The expected structural rigidity offered by these formamidine ligands as opposed to the more flexible (pyrazolylmethy)pyridine synthons previously used may result in better control of the ROP reactions. The rest of this chapter detailed the structural study of the complexes, kinetic and polymer tacticity of these ROP reactions.

3.2 Experimental Section

3.2.1 Materials and reagents

All experiments were carried out under argon using Schlenk techniques. All solvents (ACS reagent grades ≥ 99.5%) were obtained from Sigma-Aldrich. Reagent grade ethanol was distilled and dried from magnesium turnings; dichloromethane (DCM) and hexane were dried from a sodium-benzophenone mixture. Metal salts ($Cu(OAc)_2.H_2O$, $Zn(OAc)_2.2H_2O$), 2,6-dimethylaniline (99%), 2,6-diisopropylaniline (97%), 2,4,6-trimethylaniline (98%) and the monomers (ε-CL and LAs, 99%) were obtained from Sigma-Aldrich.

3.2.2 Instrumental characterization techniques

^1H and ^{13}C NMR spectra were measured at room temperature with Bruker 400 MHz spectrometer**.** ^1H NMR data were recorded in $CDCl_3$ listed as residual internal $CDCl_3$ (δ 7.26). Similarly, ^{13}C NMR data were recorded in $CDCl_3$ listed as residual internal $CDCl_3$ (δ 77.00). IR spectra were obtained on PerkinElmer Universal ATR spectrum 100 FTIR spectrometer. Mass spectra of compounds were obtained from Water synapt GR electrospray positive spectrometer.

3.2.3 Typical procedure for ligand syntheses L1–L3

Acetic acid (1.5 mole equivalents) was added to a round bottom flask charged with the aniline (2 mole equivalents) and triethyl orthoformate (1 mole equivalent). The reaction mixture was heated under reflux and temperature maintained at 130-140 °C. After 3 h, the temperature was increased to 150 °C and all volatiles removed *via* distillation. Upon cooling to room temperature, the reaction mixture solidified. The crude product was triturated with cold hexane and collected by vacuum filtration. The solids obtained was recrystallized in minimal hot acetone and stored at

4 °C. Crystals formed were collected *via* filtration and dried *in vacuo*, yielding the pure products (Figure 3.1).

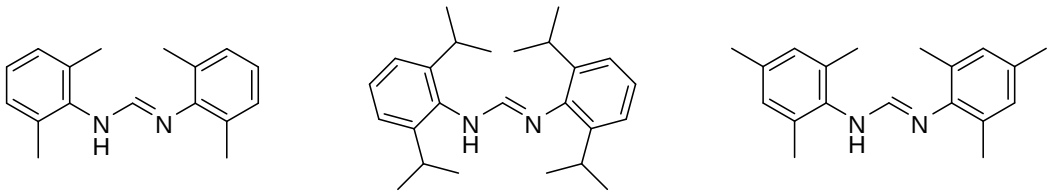

N,*N*′-bis(2,6-dimethylphenyl)formamidine (**L1**)
N,*N*′-bis(2,6-diisopropylphenyl)formamidine (**L2**)
N,*N*'-dimesitylformamidine (**L3**)

Figure 3. 1: Formamidine ligands used in this study

3.2.4 Synthesis of Zn(II) and Cu(II) formamidine complexes 1–4

3.2.4.1 $[Zn_3(L1)_2(OAc)_6]$ (1)

To a solution of $Zn(OAc)_2.H_2O$ (0.087 g, 0.396 mmol) in ethanol a solution of **L1** (0.200 g, 0.79 mmol) in ethanol was added drop wise. The resulting solution was stirred at room temperature for 24 h. The solvent was removed under vacuum, and the crude product washed with hexane and recrystallized from DCM/hexane solvent mixture to afford complex **1** as a white solid. (0.281 g, 67.2%) ^{1}H NMR ($CDCl_3$, 400 MHz): δ (ppm) 1.99 (s, 18H, Ac CH_3), 2.32 (s, 24H, CH_3), 6.07 (d, ^3J = 10.9 Hz, 1H, NH), 7.22 (m, 12H, Ar), 7.74 (d, ^3J = 9.8 Hz, 1H, N=CH). ^{13}C NMR ($CDCl_3$, 400 MHz) δ (ppm) 180.2, 133.7, 129.0, 129.0, 128.5, 127.6, 22.9, 18.4, 17.7. IR (Nujol): ν = 3333 (w), 1630 (s), 1588 (s), 1471 (m). ESI-TOF MS: *m/z* (%); 391.28 $[LZn_2 + Li]^+$ (90), 569.26 $[L_2Zn + H]^+$ (35). Anal. Calcd. For $C_{46}H_{58}N_4O_{12}Zn_3$: C, 52.16; H, 5.90; N, 5.29. Found: C, 52.20; H, 6.10; N, 5.24

3.2.4.2 $[Zn_2(L2)_2(OAc)_4]$ (2)

The reaction of compound **L2** (0.150 g, 0.410 mmol) and $Zn(OAc)_2.H_2O$ (0.045 g, 0.021 mmol) in ethanol afforded complex **2** as crystalline white solid. (0.150 g, 68%) ^{1}H NMR ($CDCl_3$, 400 MHz): δ (ppm) δ (ppm) 1.19 (d, ^3J = 6.80 Hz, 48H, CH_3), 1.89 (s, Ac CH_3, 6H), 3.33 (m, 8H, CH), 7.24 (m, 12H, Ar), 7.38 (d, ^3J = 11.7 Hz, 1H, N=CH), 5.72 (d, ^3J = 11.8 Hz, 1H, NH). IR (Nujol): ν = 2960 (m), 1661 (s), 1587 (m), 1382 (w). ESI-TOF MS: *m/z* (%); 731.58 $[LZn_2(OAc)_4 - H]^+$ (45); 792 $[L_2Zn]^+$ (100). Anal. Calcd. For $C_{58}H_{84}N_4O_8Zn_2$: C, 63.55; H, 7.72; N, 5.11. Found: C, 63.30; H, 7.66; N, 5.12

3.2.4.3 $[Zn_2(L3)_2(OAc)_4]$ (3)

The reaction of compound **L3** (0.130 g, 0.464 mmol) and $Zn(OAc)_2.H_2O$ (0.050 g, 0.023 mmol) in ethanol afforded the crude product. The crude product was washed with hexane and recrystallized from DCM/hexane solvent mixture to afford complex **3** as a white solid. (0.176 g, 82%) ^{1}H NMR ($CDCl_3$, 400 MHz): δ (ppm) 1.97 (s, 12H, Ac CH_3), 2.27 (m, 36H, CH_3), 5.99 (d, ^3J = 11.9 Hz, 1H, NH), 6.93 (m, 8H, Ar), 7.67 (d, ^3J = 9.5 Hz, 1H, N=CH). ^{13}C NMR ($CDCl_3$, 400 MHz) δ (ppm) 137.3, 133.7, 129.0, 129.0, 22.9, 20.8, 18.4, 18.3, 17.6. IR (Nujol): ν = 3147 (w), 2915 (m), 1641 (s), 1556 (m), 1478 (s), 1432 (s), 1369 (m). ESI-TOF MS: *m/z* (%); 561 $[LZn_2(OAc)_2 + K]^+$ (100), 812.28 $[L_2Zn_2(OAc)_2 + Na]^+$ (20). Anal. Calcd. For $C_{46}H_{60}N_4O_8Zn_2$: C, 59.42; H, 6.72; N, 6.03. Found: C, 59.07; H, 6.52; N, 6.19

3.2.4.4 $[Cu_2(L2)_2(OAc)_4]$ (4)

The reaction of compound **L2** (0.200 g, 0.55 mmol) and $Cu(OAc)_2.2H_2O$ (0.050 g, 0.250 mmol) in ethanol afforded the crude product. The crude product was washed with hexane and

recrystallized from DCM/hexane solvent mixture to afford complex **4** as a light green solid (0.200 g, 74%). IR (Nujol): ν = 3264 (w), 2963 (m), 2866 (w), 1652 (s), 1621 (s), 1436 (s), 1412 (s). ESI-TOF MS: *m/z* (%); 791.50 [M^+ - 4OAc] (100). Anal. Calcd. For $C_{58}H_{84}N_4O_8Cu_2$: C, 63.54; H, 8.09; N, 5.11. Found: C, 63.20; H, 7.79; N, 5.19.

3.2.5 Typical procedure for bulk polymerization of ε-CL

Bulk polymerization reactions were performed by introducing an appropriate amount of the complex and ε-CL monomer (1.14 g, 0.01 mol) to a Schlenk tube immersed in pre-heated oil bath at 110 °C and the reaction was initiated by stirring. Kinetics experiments were carried out by withdrawing samples at regular interval using a syringe into NMR tube containing $CDCl_3$ solvent. The tube and solution was then rapidly cooled down using ice water. The quenched samples were analyzed by ^1H NMR spectroscopy for determination of polymerization of ε-CL to PCL. The percentage conversion of $[PCL]/[CL]_o \times 100$, where $[CL]_o$ is the initial concentration of the monomer and [PCL] is the concentration of the polymer at time t, was evaluated by integration of the peaks for CL (4.2 ppm, OCH_2 signal) and PCL (4.0 ppm, OCH_2 signal) according to the equation $[PCL]/[CL]_o = I_{4.0}/(I_{4.2} + I_{4.0})$ where $I_{4.2}$ is the intensity of the CL monomer signal at 4.2 ppm and $I_{4.0}$ is the intensity of PCL signal at 4.0 ppm for OCH_2 protons. The observed rate constants were extracted from the slope of the line of best-fits of the plot of $\ln[CL]_o/[CL]_t$ *vs*. time.

3.2.6 Typical procedure for polymerization of $_{D,L}$-LA and $_L$-LA

A suitable LA (1.44 g, 0.01 mol) was dissolved in toluene in a Schlenk tube equipped with magnetic stirrer under argon and the required amount of complex was added. The reaction

mixture was stirred at 110 °C. Kinetics experiments were carried out by withdrawing samples at regular interval using a syringe and quenched quickly by rapid cooling into NMR tube containing $CDCl_3$ solvent using ice water. The quenched samples were analyzed by ^1H NMR spectroscopy for determination of polymerization of LAs to PLA. The integration values of the methine proton of the monomer and that of the polymer were used to calculate the percentage conversion using the equation $I_{CHpolymer}/(I_{CHmonomer} + I_{CHpolymer}) \times 100$.

3.2.7 Polymer characterization by size exclusion chromatography (SEC)

The samples were analyzed by SEC at Stellenbosch University. The samples were dissolved in Butylated hydroxytoluene (BHT) stabilized Tetrahydrofuran (THF) (2 mg/ml). Sample solutions were filtered *via* syringe through 0.45 µm nylon filters before subjected to analysis. The SEC instrument consists of a Waters 1515 isocratic HPLC pump, a Waters 717plus auto-sampler, Waters 600E system controller (run by Breeze Version 3.30 SPA) and a Waters in-line Degasser AF. A Waters 2414 differential refractometer was used at 30 °C in series with a Waters 2487 dual wavelength absorbance UV/Vis detector operating at variable wavelengths. THF (HPLC grade, stabilized with 0.125% BHT) was used as eluent at flow rates of 1 ml min^{-1}. The column oven was kept at 30 °C and the injection volume was 100 µl. Two PLgel (Polymer Laboratories) 5 µm Mixed-C (300 × 7.5 mm) columns and a pre-column (PLgel 5 µm Guard, 50 × 7.5 mm) were used. Calibration was done using narrow polystyrene standards ranging from 580 to 2 × 10^6 g mol^{-1}. All molecular weights were reported as polystyrene equivalents.

3.2.8 X-ray crystallography

The crystal evaluation and data collection of **1**, **2**, **3**, and **4** were done on a Bruker Smart APEXII diffractometer with Mo Kα radiation (λ = 0.71073 Å) equipped with an Oxford Cryostream low temperature apparatus operating at 100 K for all samples. Reflections were collected at different starting angles and the APEXII program suite was used to index the reflections.[9] Data reduction was performed using the SAINT[10] software and the scaling and absorption corrections were applied using SADABS[11] multi-scan technique. The structures were solved by the direct method using the SHELXS program and refined.[12] The visual crystal structure information was performed using OLEX2 system software.[13] Non-hydrogen atoms were first refined isotropically and then by anisotropic refinement with full-matrix least squares method based on F^2 using SHELXL.[12] All hydrogen atoms were positioned geometrically, allowed to ride on their parent atoms and refined isotropically. Disorder was found for one of the isopropyl methyl groups of complex **2**. The electron density was observed in the difference map and used to model the disorder using PART instructions resulting in 58% occupancy of the major component. The C–C bond distant in the disordered methyl group was improved using DFIX restraint. Disorder was also found for one of oxygen atoms of the acetate anions in complex **3** in which the electron density was observed in the difference map. The disorder was modelled using PART instructions resulting in a ~60% occupancy of the major component. Distant restraints (DFIX, DANG and SADI) was used to improve the C=O bond length in the disordered oxygen atoms of the acetate anions. The Cambridge Crystallographic Database contains supporting information with file numbers CCDC-1413137 for complex **1**, CCDC-1413165 for complex **2**, CCDC-1413216 for complex **3** and CCDC-1413168 for complex **4.** Crystal data collection and structural refinement parameters for complexes **1**–**4** are provided in Table 3.1.

Table 3. 1: Crystal data collection and structural refinement parameters for complexes **1**–**4**.

	1	**2**	**3**	**4**
Empirical formula	$C_{46}H_{58}N_4O_{12}Zn_3$	$C_{58}H_{84}N_4O_8Zn_2$	$C_{46}H_{60}N_4O_8Zn_2$	$C_{58}H_{84}Cu_2N_4O_8$
Formula weight	1055.07	1096.03	927.72	1092.37
Temperature (K)	173(2)	173(2)	293(2)	173(2)
Wavelength (Å)	0.71073	0.71073	0.71073	0.71073
Crystal system	Monoclinic	Triclinic	Triclinic	Monoclinic
Space group	$P2_1/c$	*P*-1	*P*-1	$P2_1/c$
a/Å	9.5958(6)	13.9570(3)	9.4219(7)	15.4331(10)
b/Å	15.6026(9)	21.3908(4)	12.1061(9)	12.4453(9)
c/Å	16.4916(10)	21.4967(5)	20.8673(18)	16.2537(11)
α	90°	94.542(10)°	85.831(5)°	90°
β	103.752(2)°	108.766(10)°	85.579(5)°	104.965(3)°
γ	90°	100.316(10)°	77.657(4)°	90°
Volume (Å^3)	2398.3(3)	5913.6(2)	2314.4(3)	3016.0(4)
Z	2	4	2	2
Density (calculated)	1.461 Mg/m^3	1.231 Mg/m^3	1.331 Mg/m^3	1.203 Mg/m^3
Absorption coefficient	1.552 mm^{-1}	0.864 mm^{-1}	1.091 mm^{-1}	0.757 mm^{-1}
F(000)	1096	2336	976	1164
Crystal size	0.41 x 0.36 x 0.32 mm^3	0.36 x 0.33 x 0.29 mm^3	0.18 x 0.15 x 0.12 mm^3	0.36 x 0.34 x 0.34 mm^3
Theta range for data collection	1.82 to 28.59°	0.978 to 28.433°	0.980 to 27.917°	1.366 to 25.493°
Index ranges	$-12 \le h \le 12$, $-20 \le k \le 20$, $-21 \le l \le 22$	$-17 \le h \le 18$, $-27 \le k \le 28$, $-27 \le l \le 28$	$-12 \le h \le 12$, $-15 \le k \le 14$, $-26 \le l \le 26$	$-18 \le h \le 18$, $-15 \le k \le 15$, $-19 \le l \le 19$
Reflections collected	53536	133169	36720	57141
Independent reflections	6033 [R(int) = 0.0176]	28279 [R(int) = 0.0230]	10307 [R(int) = 0.0342]	5593 [R(int) = 0.0338]
Completeness to theta = 28.59°	100%	100.0%	98.10%	100.0%
Absorption correction	Semi-empirical from equivalents	Semi-empirical from equivalents	Semi-empirical from equivalents	Semi-empirical from equivalents
Max. and min. transmission	0.609 and 0.524	0.791 and 0.683	0.877 and 0.822	0.773 and 0.769
Refinement method	Full-matrix least-squares on F^2	Full-matrix least-squares on F^2	Full-matrix least-squares on F^2	Full-matrix least-squares on F^2
Data / restraints / parameters	6032 / 0 / 302	28279 / 2 / 1348	10307 / 5 / 567	5593 / 0 / 325
Goodness-of-fit on F^2	1.059	1.041	1.135	1.095
Final R indices [I>2sigma(I)]	R1 = 0.0273, wR_2 = 0.0715	R1 = 0.0338, wR_2 = 0.0815	R1 = 0.0510, wR_2 = 0.1165	R1 = 0.0312, wR_2 = 0.0841
R indices (all data)	R1 = 0.0287, wR_2 = 0.0725	R1 = 0.0475, wR_2 = 0.0910	R1 = 0.0633, wR_2 = 0.1237	R1 = 0.0361, wR_2 = 0.0875
Largest diff. peak and hole	0.949 and -0.742 e.Å^{-3}	0.745 and -0.480 e.Å^{-3}	0.740 and -0.555 e.Å^{-3}	0.351 and -0.361 e.Å^{-3}

3.3 Results and discussion

3.3.1 Synthesis of *N,N′*-diarylformamidines Zn(II) and Cu(II) complexes

The *N,N′*-diarylformamidines ligands, *N,N′*-bis(2,6-dimethylphenyl)formamidine (**L1**), *N,N′*-bis(2,6-diisopropylphenyl)formamidine (**L2**), and *N,N′*-dimesitylformamidine (**L3**) were synthesized following literature procedure.[14] Reactions of **L1**–**L3** with two molar equivalents of $Zn(OAc)_2.2H_2O$ or $Cu(OAc)_2.H_2O$ salts afforded the corresponding trinuclear and dinuclear Zn(II) and Cu(II) complexes $[Zn_3(\mathbf{L1})_2(OAc)_6]$ (**1**), $[Zn_2(\mathbf{L2})_2(OAc)_4]$ (**2**), $[Zn_2(\mathbf{L3})_2(OAc)_4]$ (**3**) and $[Cu_2(\mathbf{L2})_2(OAc)_4]$ (**4**) in moderate to high yields (Scheme 3.1). Complexes **1**–**3** were isolated as white solids, while complex **4** was obtained as green solid.

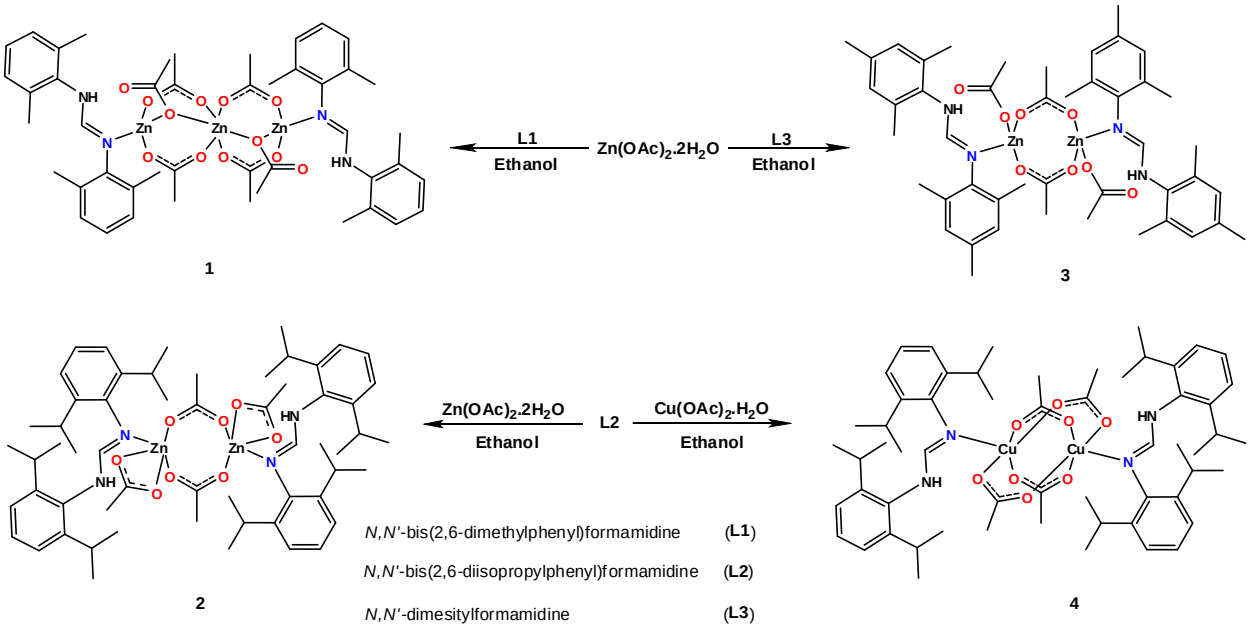

Scheme 3. 1: Synthesis of Zn(II) and Cu(II) formamidine complexes **1**–**4.**

Complexes **1**–**4** were characterized using ^{1}H and ^{13}C NMR spectroscopy, mass spectrometry, IR spectroscopy, elemental analyses and single crystal X-ray crystallography. For example, Figures 3.2 and 3.3 shows the ^{1}H and ^{13}C NMR spectra of complex **1.**

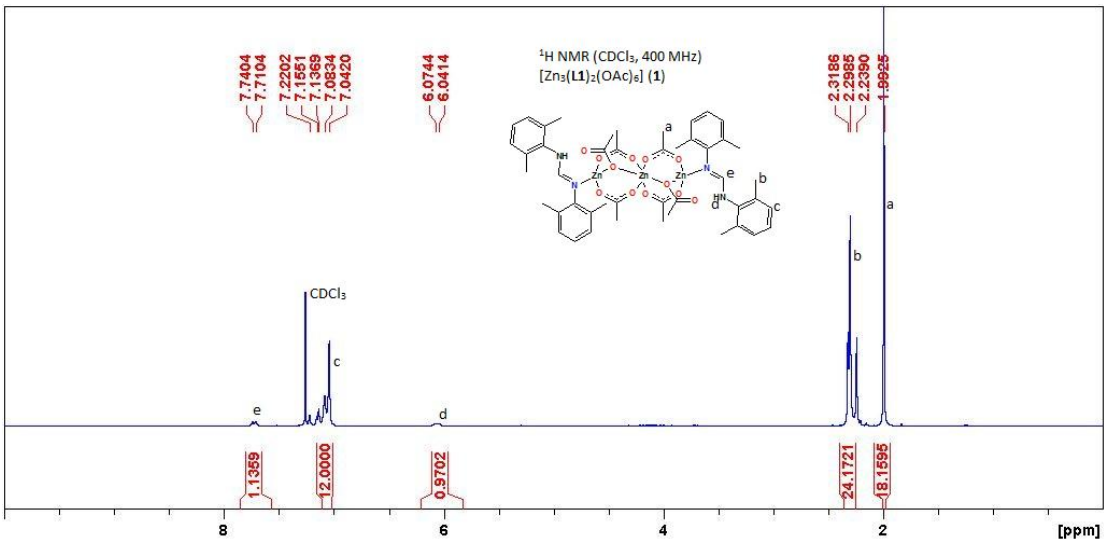

Figure 3. 2: ^{1}H NMR spectrum of complex **1** in $CDCl_3$ at room temperature.

COSY spectra of complex **1** (Figure 3.4) showed correlation between aromatic protons (7.16 – 7.04 ppm) and the CH_3 protons on the phenyl ring. A perfect correlation also existed between the NH proton (6.07 – 6.04 ppm) and the CH=N methine proton (7.74 – 7.71 ppm). The cross peaks in NOESY spectrum (Figure 3.5) could be due to cross relaxation between neighboring protons in the ligand motif.[15] A distant of 2.779 Å between the two types of protons was measured in the crystal structure of complex **1**, affirming the NOESY NMR spectra**.** Mass spectra of complexes **1**–**4** showed *m/z* peaks corresponding to various fragments of the parent compounds. For example, complex **3** showed a *m/z* = 645.13 corresponding to $[LZn_2(OAc)_4 + H]^{+}$.

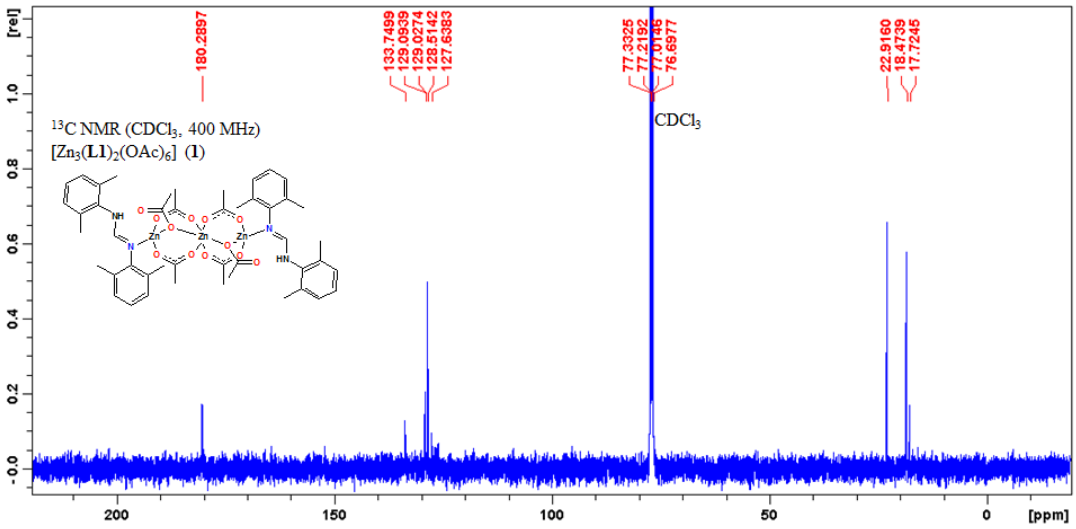

Figure 3. 3: ^{13}C NMR spectrum of complex **1** in $CDCl_3$ at room temperature.

FTIR spectra of complexes **1**–**4** displayed the characteristic carbonyl bands assignable to the ν_{asym} (OCO) and ν_{sym} (OCO) of the acetate ligands respectively.[16]

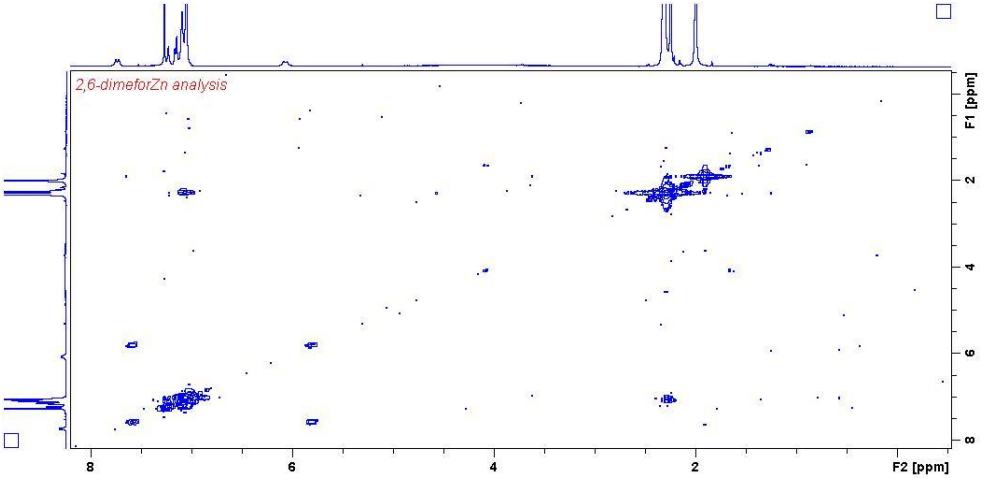

Figure 3. 4: COSY NMR spectrum of complex **1** in $CDCl_3$ at room temperature.

For example, the IR spectrum of complex **1** revealed two bands at 1639 cm^{-1} and 1588 cm^{-1} assignable to ν_{asym} (OCO) while the band at 1471 cm^{-1}, 1404 cm^{-1}, 1373 cm^{-1} bands could be

attributed to ν_{sym} (OCO). The IR spectra of complexes **1**–**4** showed shifts of the C=N bands at higher frequencies in comparison to the free ligands. The measured effective magnetic moment of the paramagnetic complex **4** at room temperature was 1.97 BM, signifying significant Cu···Cu interaction.[17]

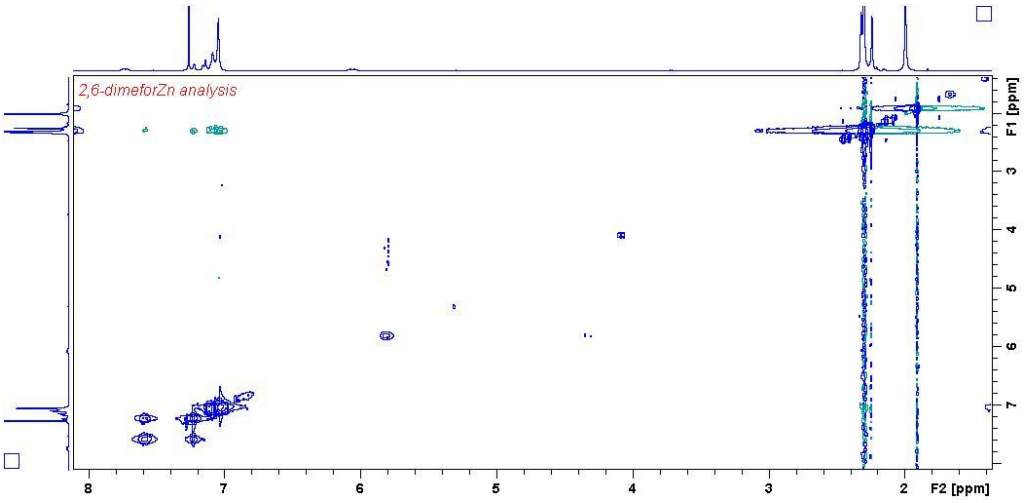

Figure 3. 5: Two dimensional (2D) ^{1}H-^{1}H nuclear overhauser effect spectroscopy (NOESY) NMR of complex **1** in $CDCl_3$ at room temperature.

3.3.2 Molecular structures of complexes 1, 2, 3 and 4

X-ray quality crystals of complexes **1**–**4** were obtained by slow diffusion of hexane into dichloromethane solutions of the respective complexes. Figures 3.6–3.9 show the molecular structures of complexes **1**–**4**, respectively while selected bond distances and angles are under the captions of each figure.

3.3.2.1 Crystal symmetry

The asymmetric unit of the trinuclear complex **1** has half a molecule of the complex with the other half generated by a center of inversion at the central Zn atom. Dinuclear complex **2** has one full molecule and two half molecules in the asymmetric unit and the molecules in **2** are related by a *d*-glide. Dinuclear complex **3** has two half molecules in its asymmetric unit with the other halves generated by a center of inversion located at <1 1 1> in one half and at <½ ½ ½> in the other half. The two full molecules are related by an *n*-glide but are however having different acetate environments as discussed later in this section. Complex **4** has half a molecule in the asymmetric unit.

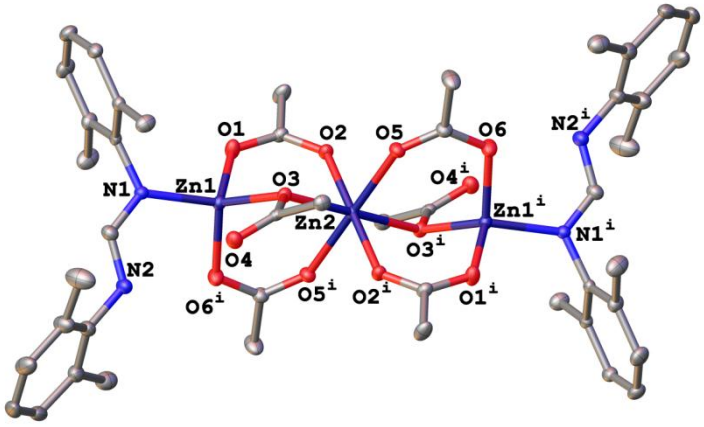

Figure 3. 6: X-ray crystal structure of complex **1** with thermal ellipsoids drawn at 40% probability level. Hydrogen atoms have been omitted for clarity. Selected bond lengths (Å) and angles (°): Zn(1)−Zn(2) 3.2099(3), N(1)−Zn(1) 1.9932(13), O(2)−Zn(2) 2.0312(11), O(1)−Zn(1) 1.9581(12), N(1)−C(9) 1.299(2), O(3)−Zn(2) 2.1441(10), Zn(1)−O(3)−Zn(2) 102.97(4), O(3)−Zn(1)−O(1) 104.24(5), O(2)−Zn(2)−O(3) 90.39(4), O(3)−Zn(1)−N(1) 123.34(5), O(1)−Zn(1)−N(1) 108.04(5), $O(6)^{i}$−Zn(1)−N(1) 101.75(5). Symmetry transformations used to generate equivalent atoms: (i) = −x+1, −y+1, −z+1.

3.3.2.2 Bonding modes of complexes 1, 2, 3 and 4

The coordination to the metal centers in all four complexes is through the imine N atom of the formamidine ligands (in a monodentate fashion) and O atoms of acetate anions in the remaining coordination sites in monodentate, bidentate or bridging fashions. The three Zn(II) centers in complex **1** are arranged in a linear fashion revealing the two bridging modes.

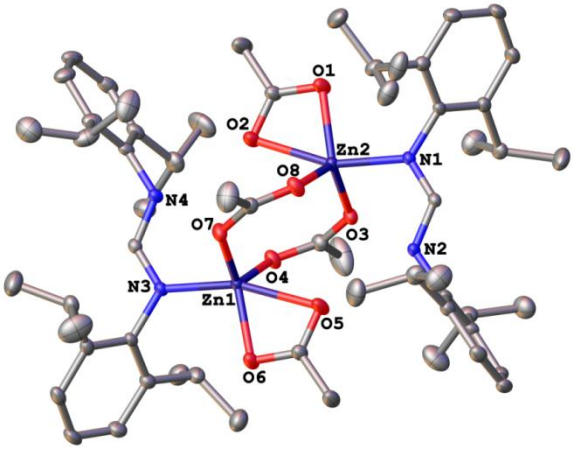

Figure 3. 7: X-ray crystal structure of complex **2** with thermal ellipsoids drawn at 40% probability level. Hydrogen atoms and the minor component of the disordered methyl groups have been omitted for clarity. Only one of the dimers in the asymmetry unit is shown for clarity. Selected bond lengths (Å) and angles (°): Zn(1)−Zn(2) 3.7648(6), N(1)−Zn(2) 2.0515(13), Zn(1)−O(6) 2.0256(12), Zn(2)−O(1) 2.0389(12), O(3)−Zn(2)−N(1) 97.05(5), O(1)−Zn(2)−O(3) 113.43(6), O(8)−Zn(2)−O(2) 91.50(5), N(1)−Zn(2)−O(1) 100.22(5).

In total six acetate anions are involved in the bridging environment where four are in the bidentate while two are in the monodentate bridging mode. The acetate anions in the dinuclear complex **2** coordinate to the Zn(II) centers in two modes. Two are bridging in a bidentate mode resulting in an eight member bi-metallacycle with two Zn atoms and two O—C—O moieties of

the acetate anion. Each of the remaining two are chelating to the Zn(II) centers in a bidentate manner based on bond distances and angles.[18] Complex **3** as mentioned earlier has two half molecules with the other halves generated by inversion. Both molecules form similar eight member bi-metallacycles through two of the four acetate anions as in complex **2**. However the remaining two anions coordinate differently to the Zn(II) centers, one in an anisodentate fashion (Figure 3.8a) **3** and the other a monodentate fashion (Figure 3.8b) **3**. The conformations of the bi-metallacycle moieties in **3** are different from that of complex **3** and so is the coordination of the acetate anions probably due to steric influences. Complex **4** exhibits a familiar dinuclear paddle wheel conformation in which all four acetate anions bridge the two Cu(II) centers in a bidentate bridging mode.

3.3.2.3 Coordination environment, geometry and hydrogen bond

The three Zn(II) centers in complex **1** adopt two coordination geometries in which the two axial Zn atoms are in a distorted tetrahedral environment with a N atom and three O atoms from the formamidine and the acetate anions, respectively while the middle Zn atom is in a distorted octahedral environment in which the equatorial and axial coordination site are occupied by O atoms. In complex **2** the geometries around the Zn atoms adopt a severely distorted trigonal bipyramidal geometry due to the coordination of one of the acetate anions being anisobidentate in manner, while the Zn(II) atoms in complex **3** adopt a distorted tetrahedral geometry in one of the molecules and a distorted trigonal pyramidal geometry in the second molecule. The distortions from a regular arrangement and the selective formation of either trinuclear and dinuclear complexes could be due to the flexibility in binding modes of the acetate ligands, in addition to steric restriction imposed by **L1**–**L3** respectively.[6b,19]

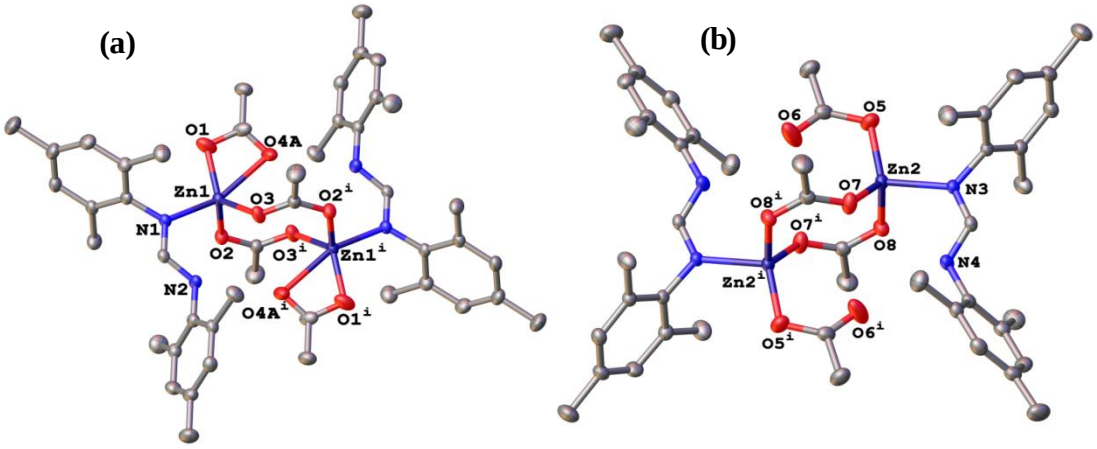

Figure 3. 8: X-ray crystal structure of complex **3** with thermal ellipsoids drawn at 30% probability level. Hydrogen atoms and the minor component of the disordered O atom have been omitted for clarity. Selected bond lengths (Å) and angles (°): (a) molecule with anisodentate coordination acetates, Zn(1)−N(1) 2.022(2), Zn(1)−O(2) 1.984(2), Zn(1)−O(1) 1.960(3), Zn(1)−O(4A) 2.34(2), O(1)−Zn(1)−O(2) 112.26(11), O(2)−Zn(1)−N(1) 98.58(9), O(3)−Zn(1)−O(2) 111.28(10), Symmetry transformations used to generate equivalent atoms: (i) = −x+2, −y+2, −z+2. (b) molecule with monodentate coordination acetate, Zn(2)−N(3) 2.018(2), Zn(2)−O(5) 1.923(2), Zn(2)−O(7) 1.964(2), O(7)−Zn(2)−O(5) 121.90(11), O(7)−Zn(2)−N(3) 98.20(9), O(8)−Zn(2)−O(5) 111.61(11), Symmetry transformations used to generate equivalent atoms: (i) = 1 −x+1, −y+1, −z+1.

The trigonal planar nature of the secondary amine group suggest conjugation of the amine lone pair with the π−electron system of the aryl ring, possibly accounting for its apparently rather poor σ−donor strength, and could justify its inability to facilitate chelation of the metal ion.[20] The Zn−O bond distances in complexes **1**–**3** falls within the ranges of similar complexes in literature.[21, 22, 23] Only one of these seems a little longer as seen in complex **2** and complex **3**a,

respectively resulting in anisobidentate chelating behavior.[20] The observed metal to metal distances in complexes **1**–**3** is greater than the sum of the van der Waal radii of Zn (1.39 Å) indicating the absence of any meaningful Zn···Zn interatomic metal bond vis-à-vis metal-metal interaction[20]. Complex **4** exhibit Cu···Cu distance of 2.6796(3) Å typical of binuclear copper (II) acetates that possess N-donating apical ligands.[24]

In the crystals of all four complexes fairly strong intramolecular hydrogen bonds and interactions exist in which acetate oxygen atoms are the acceptor atoms and the ligand N atom the donor atoms. These interactions seem to play a significant role in the packing of the molecules in crystals.[21c,21f]

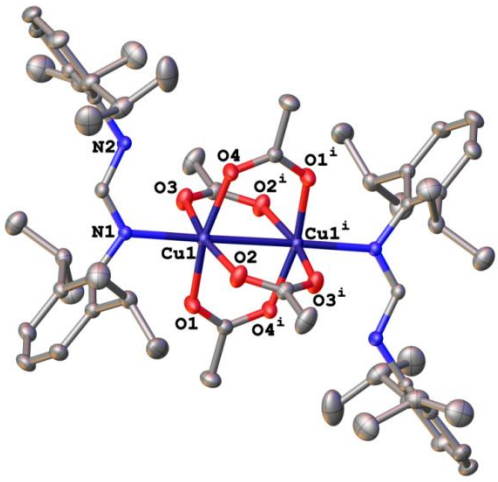

Figure 3. 9: X-ray crystal structure of complex **4** with thermal ellipsoids drawn at 30% probability level. Hydrogen atoms have been omitted for clarity. Selected bond lengths (Å) and angles (°): Cu(1)−Cu(1) 2.6797(5), N(1)−Cu(1) 2.1821(13), O(4)−Cu(1) 1.9891(13), O(3)−Cu(1) 1.9654(14), N(1)−Cu(1)−O(2) 100.55(5), O(1)−Cu(1)−O(4) 166.70(5), O(4)−Cu(1)−O(3) 87.21(6), Symmetry code: (i) = −x+1, −y+1, −z.

3.3.3 Electron Paramagnetic Resonance spectra of complex 4

In order to gain additional insight into the coordination environment of the paddle-wheel Cu(II) complex in both solid state and solution, X-band EPR spectra of complex **4** were acquired in methanol solution and solid at 295 K (Figure 3.10). In methanol solution, the EPR spectrum of complex **4** (Figure 3.10a) is almost perfectly isotropic and is characterized by a single line (g = 2.1062). This indicates that there is a total symmetric environment where the electrons in the different d-orbitals have equal interactions in all direction (all the principal g-factors are the same).

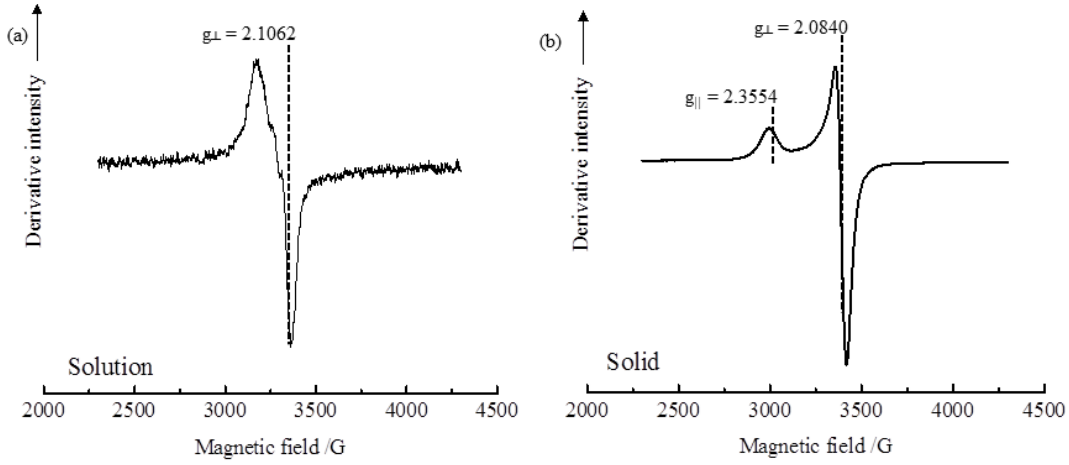

Figure 3. 10: **(**a) EPR spectrum of complex **4** in methanol solution (295 K, 9.786 GHz) and (b) Solid state EPR spectrum of complex **4** (295 K, 9.870 GHz).

The spin-allowed $\Delta m_s = \pm 1$ transitions are thus degenerate and occur at a resonant frequency governed by g^{iso}. The significant g-shift of g^{iso} = 2.1062 to g_e (2.0025) reflects spin-orbit coupling effect in the paddlewheel complex.[20] The solid state EPR spectrum (Figure 3.10b)

shows axial symmetry such that the total magnetic moment in the Z-direction is rather large ($g_x = g_y \neq g_z$). The magnetic parameters for the exchange-couple copper-copper pairs are $g_{//}$ = 2.3554 and $g_{\perp}$ = 2.0840. A consistent interpretation of these data is presented on the basis of a weak metal-metal interaction.[25] The similarity in the solution and solid state EPR spectra of complex **4** confirm the retention of the paddle-wheel structure in solution.

3.3.4 Ring-opening polymerization of ε-CL and LAs

The ring-opening polymerization (ROP) reactions of ε-CL using complexes **1**–**4** as catalysts were initially investigated at 110 °C using [M]/[catalyst] ratio of 200 (M = monomer). Under these conditions, complexes **1**–**4** exhibited significant catalytic activities giving maximum conversions between 48 h to 76 h. Complexes **1** and **3** were also investigated in the ROP of $_{D,L}$-LA and $_{L}$-LA at 110 °C using [M]/[catalyst] ratio of 200 in toluene and afforded conversions of 97% and 99% within 3.5 and 9 h, respectively. Tables 3.2 and 3.3 contain a summary of the ROP data of ε-CL and LAs for complexes **1**–**4**, respectively.

Table 3. 2: Summary of polymerization of ε-CL data by complexes **1**–**4**[a]

Catalyst	Time (h)	Conversion (%)	k_{app} (h^{-1})	M_w[b]	PDI[b]	IE[c]
1	48	98	0.1009 ±0.0111	12632	2.11	0.56
2	72	96	0.0479 ±0.039	5426	1.86	0.25
3	53	96	0.0963 ±0.0108	10342	2.14	0.47
4	76	98	0.0441 ±0.0059	3838	1.66	0.17

[a]Reaction conditions, bulk polymerization, 110 °C, $[CL]_o/[catalyst] = 200$. [b]Molecular-weight average and Polydispersity index (PDI) determined by GPC relative to polystyrene standard values, the values obtained from GPC × correction factor of 0.56.[19] [c]Initiator efficiency (IE) = M_{wexp}/M_{wcalc} where $M_{wcalc} = M_{w(monomer)} \times [CL]_o/[I] \times [PCL]/[CL]_o + M_{w(chain\text{-}end\ group)}$.

Having established that complexes **1**–**4** form effective catalysts in the ROP of ε-CL and LAs, we carried out detailed kinetic and polymer property studies to gain insight into the influence of catalyst structure and reaction conditions on the kinetics of the polymerization reactions and nature of polymers obtained.

Table 3. 3: ROP of $_{D,L}$-LA and $_{L}$-LA using complexes **1** and **3**[a]

Entry	Catalyst	Time (h)	Conversion[b] (%)	k_{app} (h^{-1})	M_w[c]	PDI[c]	IE[d]
1[e]	**1**	3.5	97	1.2765 ±0.0885	10376	2.25	0.37
2[f]	**1**	5	96	0.8737 ±0.0437	21286	1.79	0.77
3[e]	**3**	9	99	0.6412 ±0.0679	15867	1.99	0.55
4[f]	**3**	9	99	0.5963 ±0.0236	18054	1.85	0.63

[a]Reaction conditions: $[CL]_o/[I]$ = 200; solvent, toluene; temperature, 110 °C. [b]Maximum conversion achieved [c]Molecular-weight average and PDI determined by GPC relative to polystyrene standard values, the values obtained from GPC × correction factor of 0.58.[19] [d]Initiator efficiency (IE) = M_{wexp}/M_{wcalc} where $M_{wcalc} = M_{w(monomer)} \times [CL]_o/[I] \times [PCL]/[CL]_o + M_{w(chain\text{-}end\ group}$ [e]$_{D,L}$-LA and [f]$_{L}$-LA.

3.3.4.1 Kinetics of ROP reactions of ε-CL and LAs

Kinetic studies of the ROP of ε-CL were investigated for complexes **1**–**4** and monitored by ^{1}H NMR spectroscopy. The rates of the reaction were determined by plot of $\ln[CL]_o/[CL]_t$ *vs.* time (Figure 3.11a). Linear relationships consistent with *pseudo*-first-order dependency on the monomer were observed in all cases (Figure 3.11a). Thus, the rate of ε-CL polymerization can be written as shown in equation (3.1).

$$\frac{d[\mathrm{CL}]}{dt} = k[\mathrm{CL}] \qquad (3.1)$$

where $k = k_p[I]^x$; k_p is the rate of chain propagation, I is the initiator, and x is the order of reaction.

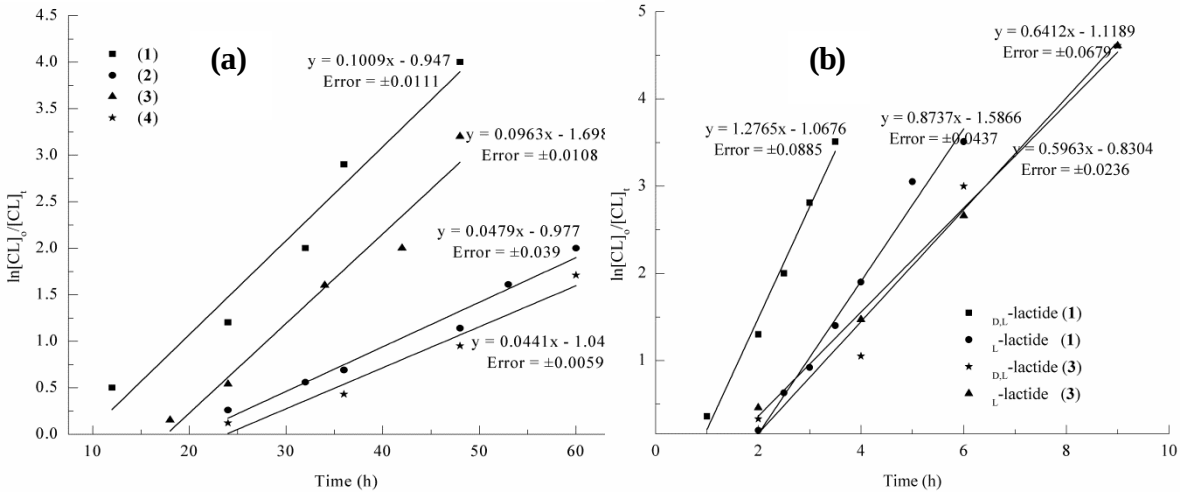

Figure 3. 11: **(a)** First order kinetic plots of $\ln[CL]_o/[CL]_t$ *vs.* time for complexes **1–4** in the bulk polymerization of ε-CL at 110 °C, $[CL]_o/[I] = 200$. (b) First order kinetic plots of $\ln[CL]_o/[CL]_t$ *vs.* time for complexes **1** and **3** in the polymerization of $_{D,L}$-LA and $_{L}$-LA to PLA in toluene at 110 °C, $[CL]_o/[I] = 200$.

The apparent rate constants for catalysts **1–4** in ROP of ε-CL were extracted from Figure 3.11a and are given in Table 3.2. More discerning was the drastic decrease in catalytic activity observed for catalyst **2** (0.0479 $\pm$0.039 h^{-1}**)** bearing isopropyl groups relative to catalyst **1** (0.1009 $\pm$0.0111 h^{-1}) containing the less bulky methyl groups. Reduction of catalytic activity with increase in steric bulk of the ligand framework may be rationalized by inhibition of monomer coordination to the metal center.[26] Similar trends have been observed for bis(thiophosphinic amine) yttrium catalyst systems.[27]

Kinetic studies of the ROP of LAs were also investigated using complexes **1** and **3**. A linear relationship of the plot of $\ln[CL]_o/[CL]_t$ *vs.* time was also obtained consistent with a *pseudo*-first-

order dependency on LA concentration (Figure 3.11b). The apparent rate constants for complexes **1** and **3** in ROP of LAs were extracted from Figure 3.11b and are given in Table 3.3. We observed that the reaction rates of ROP of ε-CL were much slower than that those of LA reactions. This is in good agreement with literature finding and has largely been attributed to the larger ring size of ε-CL.[28] The six-membered ring in LA increases the strain resulting in rapid ROP reactions.[29]

3.3.4.2 Order of ROP of ε-CL reaction with respect to catalysts 1 and 3

ROP reactions at different catalyst concentrations at constant ε-CL monomer concentration were carried out to determine the order of reaction with respect to catalysts **1** and **3** (Table 3.4). A Plot of $\ln k_{app}$ *vs.* ln[**1**/**3**] gave linear relationships which allowed us to determine the order of reaction with respect to **1** and **3** (Figure 3.12). The order of reaction with respect to **1** and **3** were extracted from the gradients of the lines of best fit (Figure 3.12) and were obtained as 2.1420 ≈ 2 and 0.6343 respectively.

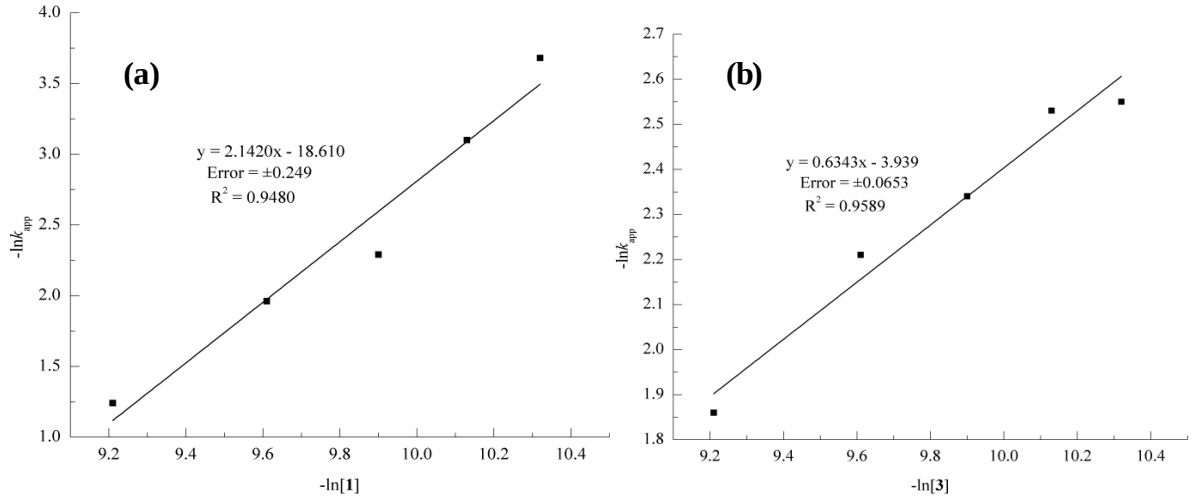

Figure 3. 12: (a) Plot of $\ln k_{app}$ *vs.* ln[**1**] and (b) $\ln k_{app}$ *vs.* ln[**3**] for the determination of order of reactions with respect to catalysts **1** and **3**.

Table 3. 4: Effect of catalyst concentrations on polymerization kinetics of ε-CL[a]

Catalyst	$[CL]_o/[Cat]$	Time (h)	Conversion[b] (%)	k_{app} (h^{-1})	M_w[c]	PDI[c]	IE[d]
1	100	18	97	0.2894	7666	2.01	0.69
1	150	30	97	0.1409	7879	2.36	0.47
1	250	48	96	0.0450	13252	2.47	0.48
1	300	68	82	0.0252	13646	2.15	0.49
3	100	30	97	0.1557	5141	1.91	0.46
3	150	48	98	0.1097	7864	2.41	0.47
3	250	48	95	0.0797	13506	1.92	0.50
3	300	48	95	0.0781	14124	2.14	0.43

[a]Reaction conditions, bulk polymerization, 110 °C. [b]Maximum conversion achieved [c]Molecular-weight average and Polydispersity index (PDI) determined by GPC relative to polystyrene standard values, the values obtained from GPC × 0.56.[19] [d]Initiator efficiency (IE) = M_{wexp}/M_{wcalc} where $M_{wcalc} = M_{w(monomer)} \times [CL]_o/[Cat] \times [PCL]/[CL]_o + M_{w(chain\text{-}end\ group)}$.

Fractional orders of reaction with respect to catalysts have been previously reported and largely attributed to catalyst aggregation especially in bulk polymerization reactions.[5, 30] DOSY NMR experiment was carried out in other to ascertain if complexes **1** and **3** indeed undergo aggregation.

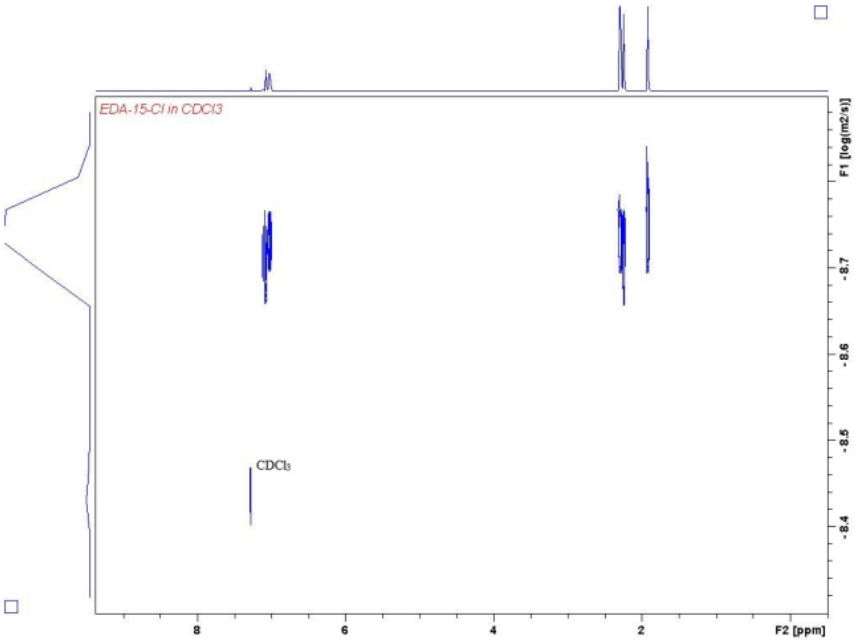

Figure 3. 13: DOSY NMR spectra of complex **1** showing single species in solution, and negating the possibility of complex aggregations.

The DOSY spectrum (Figures 3.13 and 3.14) is consistent with one species in solution thereby negating the possibility of complex aggregation. A slight difference in diffusion co-efficient of 1.666×10^{-9} m^2/s and 1.112×10^{-9} m^2/s was observed at 30 °C for **1** and **3**, respectively. More intriguing is the large difference in reaction orders with respect to catalysts **1** and **3**. This might be associated to the nuclearity and structures of the complexes; while complex **1** is trinuclear, complex **3** is dinuclear.

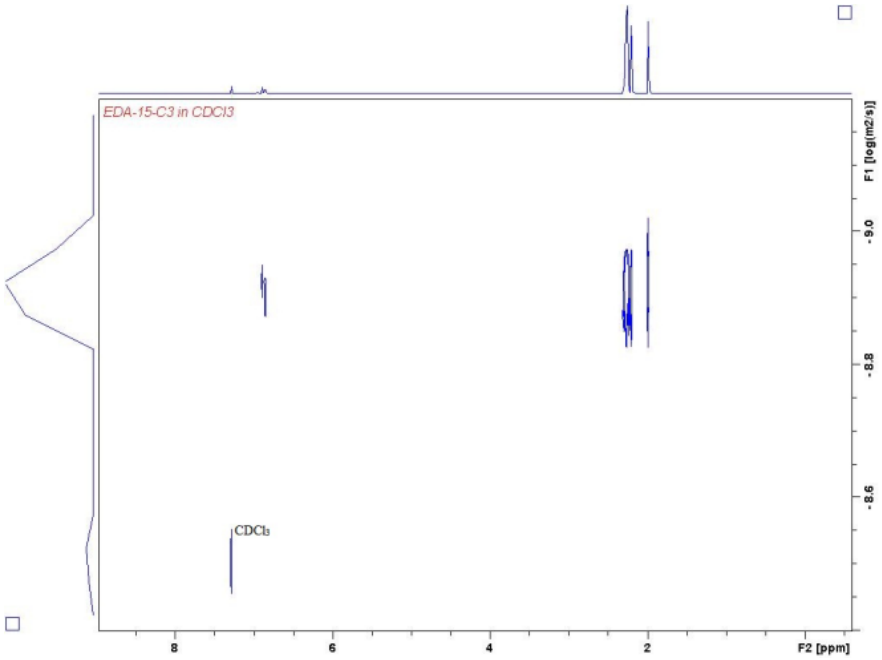

Figure 3. 14: DOSY NMR spectra of complex **3** showing single species in solution, and negating the possibility of complex aggregations.

It is therefore conceivable to conclude that the active catalytic species produced from complexes **1** and **3** are structurally different and that the solid state structures are likely to be retained in solution. The overall order of the polymerization reactions catalyzed by complexes **1** and **3** could thus be described according to equations (3.2) and (3.3), respectively.

$$\frac{d[\mathrm{CL}]}{dt} = k[\mathrm{CL}][\mathbf{1}]^2 \qquad (3.2)$$

$$\frac{d[\mathrm{CL}]}{dt} = k[\mathrm{CL}]\,[\mathbf{3}]^{0.6} \qquad (3.3)$$

3.3.4.3 Effect of solvent and temperature on the ROP kinetics of ε-CL

To understand the influence of solvent on the polymerization kinetics of ε-CL, we compared the activity of complex **3** in bulk and solution polymerization reactions. Table 3.5 shows a summary of the bulk and solution ROP of ε-CL data and at different reactions temperatures. The rate of polymerization reactions recorded in toluene solvent was comparable to that in the bulk experiment (Table 3.4). This contrasts previous reports where we observed higher catalytic activities in bulk reactions in comparison to solution experiments.[16]

Table 3.5: Effect of solvents and reaction temperature on polymerization kinetics of ε-CL using complex **3**

Entry	$[CL]_o/[I]$	Time (h)	Conversion[a] (%)	k_{app} (h^{-1})	M_w (GPC)[b]	PDI[b]	IE[c]
1	200[d]	52	98	0.0778	7073	2.02	0.32
2	200[e]	96	97	0.0640	4108	1.74	0.19
3	200[f]	156	97	0.0371	2186	1.46	0.10
4	200[g]	168	93	0.0283	4319	1.76	0.20
5	200[h]	240	95	0.0257	2153	1.43	0.10

[a]Maximum conversion achieved [b]Molecular-weight average and Polydispersity index (PDI) determined by GPC relative to polystyrene standard values, the values obtained from GPC × 0.56.[19] [c]Initiator efficiency (IE) = M_{wexp}/M_{wcalc} where $M_{wcalc} = M_{w(monomer)} \times [CL]_o/[I] \times [PCL]/[CL]_o + M_{w(chain\text{-}end\ group)}$. [d]Solvent, toluene. [e]Temp., 90 °C. [f]Temp., 80 °C. [g]Temp., 70 °C. [h]Temp., 60 °C.

The dependence of the kinetics of the ROP of ε-CL reaction on reaction temperature was studied by determination of the rate constants at various temperatures (60 °C to 110 °C) using complex

3. After induction periods observed at lower temperatures, linear relationships consistent with *pseudo* first-order dependency on the monomer were observed. A significant decrease in rate constant from 0.0963 h^{-1} to 0.064 h^{-1} was recorded with decrease in the reaction temperature from 110 °C to 90 °C. The observed rate constants extracted from the semi-logarithmic plots are shown in Table 3.5.

The overall activation energy of the ROP of ε-CL using complex **3** calculated from the slope of Arrhenius plot of ln*k vs.* T^{-1} was found to be 28.05 kJ mol^{-1} (Figure 3.15a). This value is lower than that reported for ROP reactions using the lanthanide tris(2,4,6-tri-tert-butylphenolate) catalyst of 39.3 kJ mol^{-1}[131] but higher than the value of 12.05 kJ mol^{-1} reported by Mei and co-workers.[30] The low energy barrier hints to greater number of actives sites in the system at lower temperatures. From the Eyring plot in Figure 3.15b, the enthalpy of activation $\Delta H^{\ddagger}$ and entropy $\Delta S^{\ddagger}$ of activation were obtained as 25.08 kJ mol^{-1} and −201.7 J K^{-1} mol^{-1}, respectively for complex **3** at $[CL]_o/[I]$ = 200. These results are consistent with highly ordered transition state systems and are in good agreement with those reported for coordination-insertion mechanisms in the ROP of ε-CL.[32]

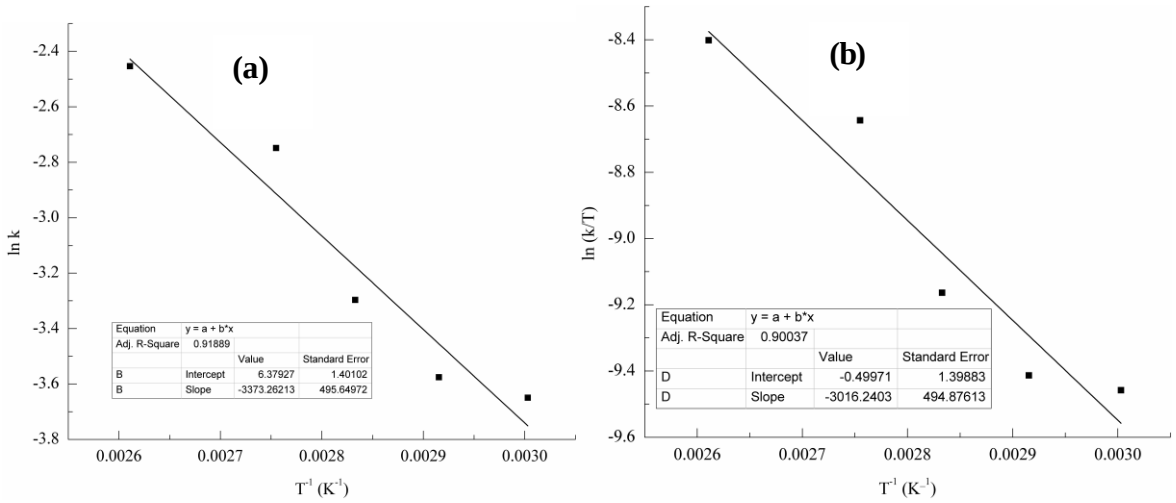

Figure 3. 15: (a) Arrhenius plot of Ink *vs.* T^{-1} for the bulk polymerization of ε-CL initiated by **3**, M/I = 200. (b) Eyring plot of temperature dependence of rate constant.

3.3.5 Molecular weight and molecular weight distribution of polymers

The molecular weight and molecular weight distribution of polymers obtained were determined by GPC and compared with the theoretical values calculated from ^{1}H NMR spectra (Tables 3.2–3.5). Generally higher molecular weights of up to 21 286 g mol^{-1} were obtained for PLA compared to maximum values of 14 124 g mol^{-1} reported for PCL. ESI-MS spectra of Poly($_{D,L}$-LA) showed some minor signals in addition to the main peaks while that of Poly($_L$-LA) showed mainly one signal corresponding to the mass of LA repeat unit (72 Da) (Figure 3.17) The minor signals in the mass spectrum of poly($_{D,L}$-LA) is believed to originate from *trans*-esterification process (back-biting) occurring in the system.[33]

The ROP reactions of cyclic esters by metal-based catalysts is likely to proceed either *via* coordination-insertion mechanism (CIM) or activated-monomer mechanism (AMM).[34] In the

CIM route, the polymer end chain bears the nucleophile on one end and the metal center on the other end. However, hydrolysis of one end of the polymer chain to form an –OH end group could be promoted by chain transfer agents such as water or alcohols.[35] To establish the nature of the initiating and chain-end groups in this study, ^{1}H NMR and ESI-MS spectra of Poly($_L$-LA) obtained were analyzed. ^{1}H NMR spectra of all the polymers revealed the absence of acetate methyl signals at about 2.00 ppm (Figure 3.16). Similarly, no signals associated with ligand moiety in the complexes were observed. However, analyses of the ESI-MS spectra of poly($_L$-LA) exhibited signals indicating the presence of Zn-OH end groups, associated with the hydrolysis and ligand dissociation of the zinc complex (Figure 3.17). These results are in agreement with those reported by Pilone and co-workers[36] in which water molecules hydrolyzed the polymer end chains. From these data, the polymerization reactions in our system can thus be said to proceed through coordination insertion mechanism followed by hydrolysis of the acetate end groups.

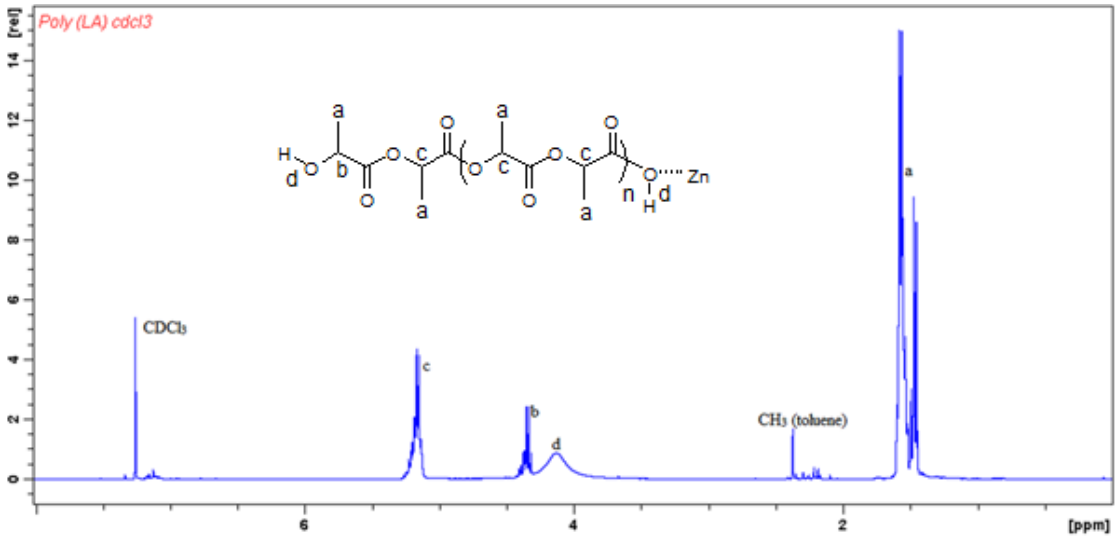

Figure 3. 16: ^{1}H NMR spectrum of poly($_L$-LA) produced by complex **1** obtained at room temperature.

A linear relationship of the plot of the molecular weight *vs.* monomer conversion (Figure 3.18) established the living polymerization behavior of these catalysts.[37,38] The observed increase in polymer weight with increase in [CL]/[Catalyst] ratio (low catalyst concentration) further supported this living polymerization nature (Table 3.4) and is consistent with small numbers of active sites at lower concentration of the catalyst. Generally, the polymers obtained exhibited narrow to moderate molecular weight distributions; 1.12–2.47 and 1.79–2.25 for PCLs and PLAs, respectively indicating some degree of control of the ROP and minima esterification and epimerization reactions.

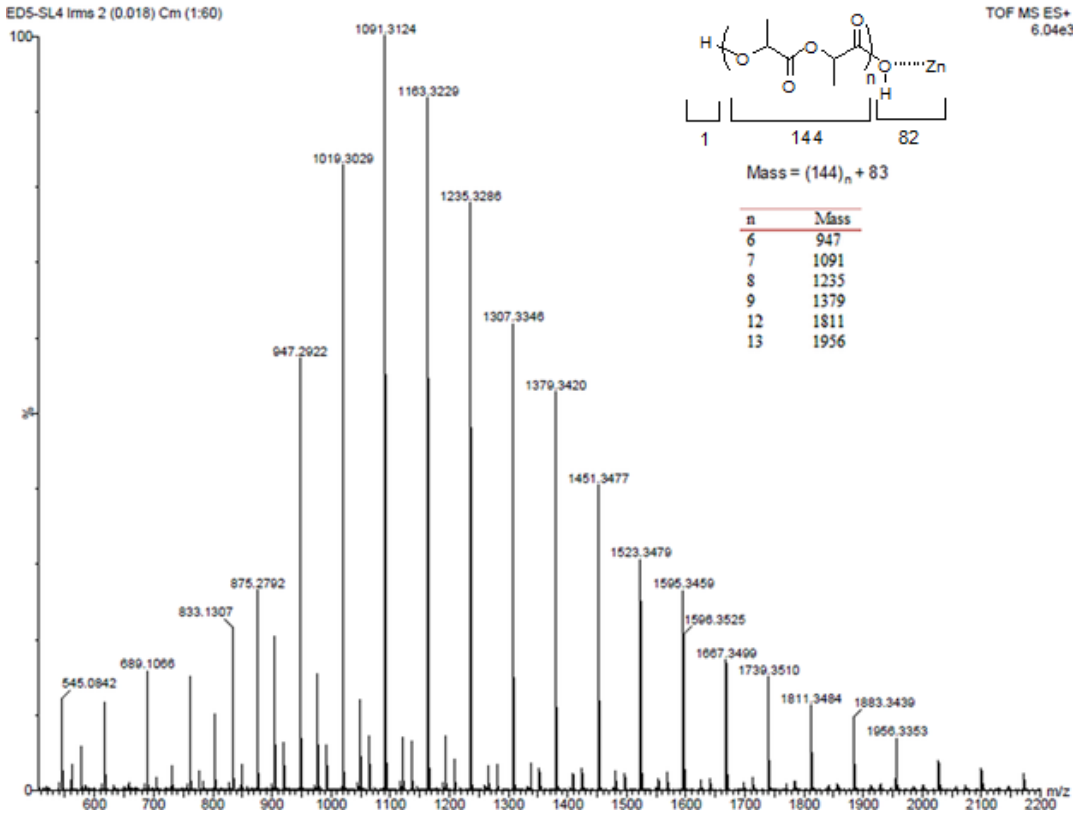

Figure 3. 17: ES-MS of the crude PLA (from $_L$-LA) from catalyst **3**, $[CL]_o/[\mathbf{3}]$ = 200, 9 h, showing distribution of one structural components.

The catalyst structure was also found to influence the molecular weights of the polymers obtained. Contrary to expectations,[36] increasing the steric bulk of the ligands resulted in decreased PCL molecular weights. For example, molecular weight of 22 550 g mol^{-1} were obtained using complex **1** bearing the less sterically demanding methyl substituents on the phenyl ring compared to molecular weight of 9 689 g mol^{-1} observed for complex **2**, containing the bulkier isopropyl groups (Table 3.2, entries 1 and 2).[39]

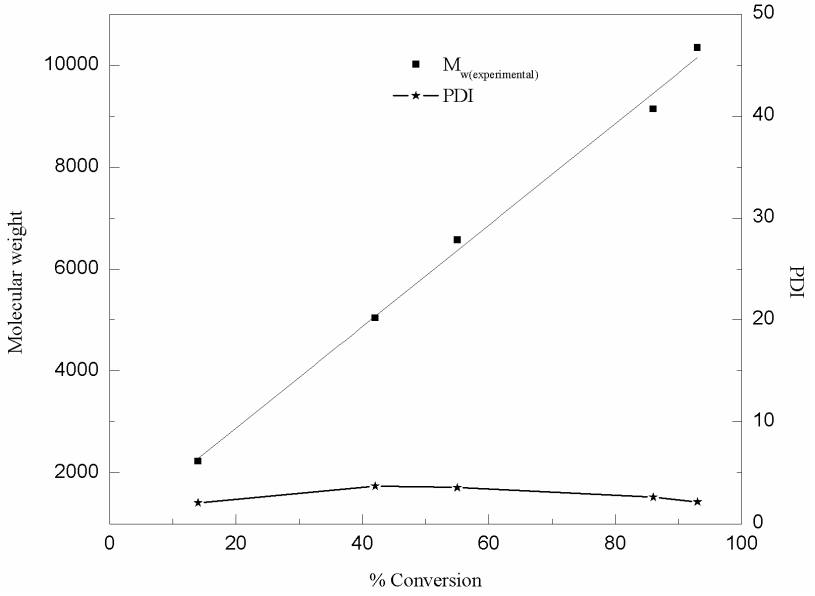

Figure 3. 18: Plot of experimental molecular weight against % conversion, showing the living polymerization nature complex **3** in bulk ROP of ε-CL at 110 °C, $[CL]_o/[I]$ = 200.

The dependence of PCL molecular weight and molecular weight distributions on the identity of the solvent used in the ROP of ε-CL was also noted. Interestingly, PCL obtained in methanol solvent exhibited narrow PDI of 1.12 compared to PDI of 2.02 recorded in toluene solvent. It is known that methanol as initiator increases the number of active sites, resulting in several polymer chains per unit catalyst.

3.3.6 Stereochemistry of PLAs

Poly(LA) tacticity was studied by inspecting the methine regions and tetrad sequences in the homonuclear decoupled ^{1}H NMR and ^{13}C NMR spectra of the polymers.[40] Figures 3.19 – 3.21 show the methine resonances of the homonuclear decoupled ^{1}H and ^{13}C NMR spectra of poly($_{L}$-LA) and poly($_{D,L}$-LA). The peaks were assigned to the appropriate tetrads in accordance with literature reports.[35] The *iii* tetrad is the predominant peak in the spectrum, thereby yielding moderate isotactic poly($_{L}$-LA).[41] However, minor signals in the decoupled ^{1}H NMR spectra could be attributed to the epimerization of the chiral centers, thus randomizing their absolute configuration therefore resulting to loss of control of polymer stereo-regularity.[35] Attempt was made to use homonuclear decoupled ^{1}H NMR to quantify the number of defects in poly($_{L}$-LA) chain. In the homonuclear decoupled ^{1}H NMR spectra of the methine region of poly($_{L}$-LA) (Figure 3.19), the poly($_{L}$-LA) or the defect content was estimated from the total *iii* cored tetrad intensities by assuming a certain defect fraction and then continually corrected for changes in defects fraction calculated from *iis* and *sis*/*sii* intensities.[42] Based on the composition analysis, we estimated the presence of 97.02% of poly($_{L}$-LA) and 2.98% of defects resulting from epimerization reactions. As reported in the literature,[42-43] polymer sequence showing a characteristic resonance at δ = 5.21 ppm in a decoupled ^{1}H NMR spectrum contains a single defect, whereas the stereoregular sequence shows a resonance at δ = 5.17 ppm. In addition, double stereodefects shows two characteristic resonances at δ = 5.22 and δ = 5.23 ppm, respectively. Considering the ^{1}H homonuclear decoupled NMR of the methine region of poly(L-LA) formed with complexes **1** and **3**, respectively, it is therefore conceivable to state that the poly($_{L}$-LA) chain has double stereodefects arising from epimerization reactions. The core tetrad stereosequences in poly($_{D,L}$-LA) are well resolved and peak assignments are consistent with

literature [41,43] and production of predominantly moderate heterotactic poly($_{D,L}$-LA) with *Pr* of up to 0.65.

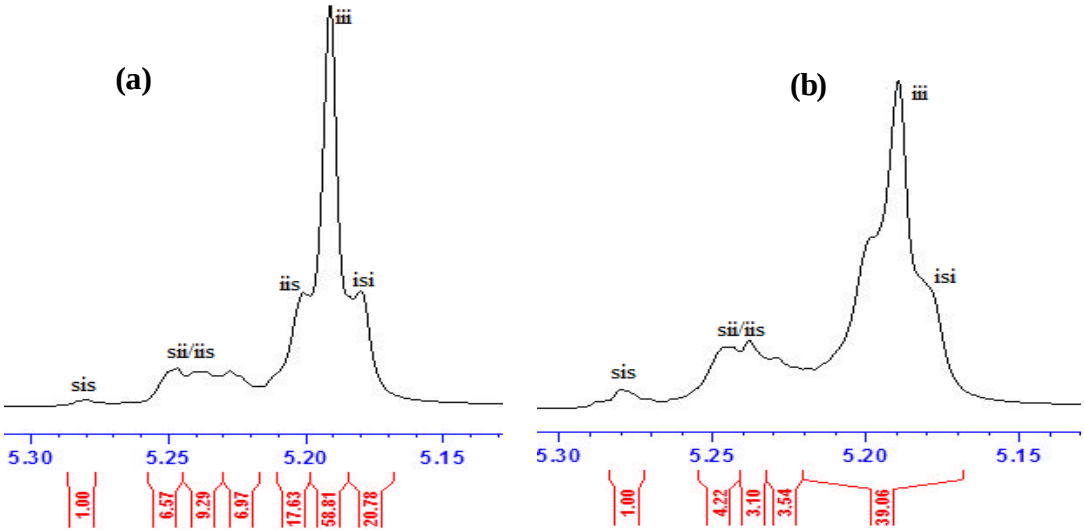

Figure 3. 19: ^{1}H homonuclear decoupled NMR of the methine region of poly($_{L}$-LA) formed with (a) complex **1** and (b) complex **3**, respectively.

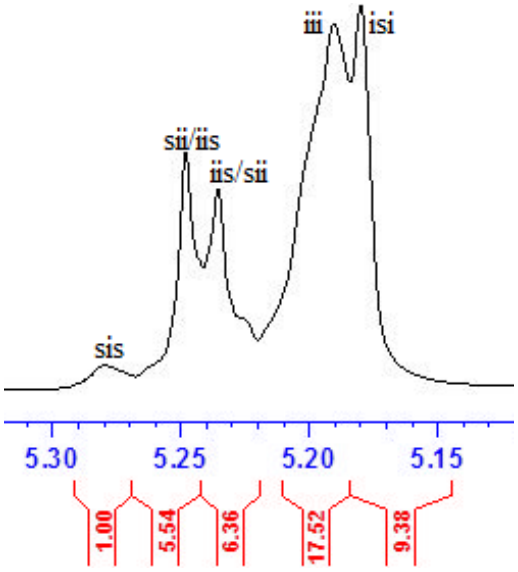

Figure 3. 20: ^{1}H homonuclear decoupled NMR of the methine region of poly($_{D,L}$-LA).

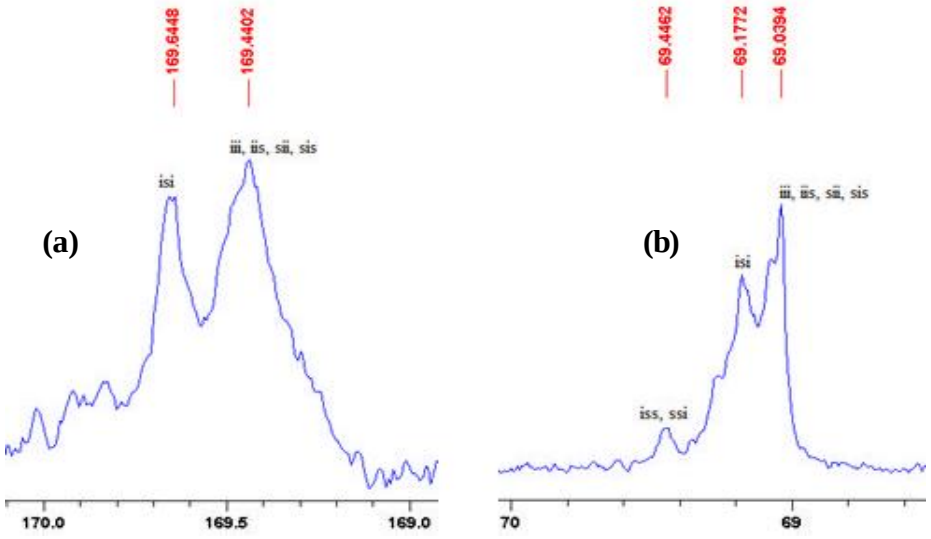

Figure 3. 21: (a) ^{13}C NMR spectra carbonyl region and (b) ^{13}C NMR methine region of poly($_{D,L}$-LA).

3.4 Conclusions

This work demonstrates the coordination chemistry and the applications of Zn(II) and Cu(II) formamidine complexes in the ring-opening polymerization of ε-caprolactone and lactides. It has shown that the substituents on the phenyl ring of the ligand backbone significantly affect the coordination chemistry of the complexes to afford dinuclear and trinuclear complexes. Complexes **1**–**4** formed active and stable catalysts in the ring-opening polymerization of ε-caprolactone and $_{D,L}$-Lactide and $_{L}$-Lactide to produce polymers with moderate weights and molecular weight distributions. The catalytic activities of the complexes were largely controlled by the ligand architecture and metal atom. The kinetics of the ROP reactions was *pseudo*-first order with respect to both ε-caprolactone and lactides monomers. Both the temperature and solvent significantly influenced the ring-opening polymerization of ε-caprolactone and overall

activation energy of 28.5 kJ mol^{-1} was obtained. The catalysts display reasonable degree of control of polymer stereo-regularity producing predominantly heterotactic poly($_{D,L}$-Lactide).

With the flexibility exhibited by compounds **L1** and **L2** in coordination with the metal centers, and its influences in the ROP reactions, A auxiliary carboxylate ligands has been introduced, and it is envisaged that the structural rigidity may result in controlled polymerization. This work is described in chapter **4**.

3.5 References

(1) Wheaton, C. A.; Hayes, P. G.; Ireland, B. J. *Dalton Trans.* **2009**, 4832.

(2) (a) Chen, H.-Y.; Huang, B.-H.; Lin, C.-C. *Macromolecules* **2005**, *38*, 5400 (b) Cheng, M.; Attygalle, A. B.; Lobkovsky, E. B.; Coates, G. W. *J. Am. Chem. Soc.* **1999**, *121*, 11583 (c) Drouin, F.; Oguadinma, P. O.; Whitehorne, T. J. J.; Prud'homme, R. E.; Schaper, F. *Organometallics* **2010**, *29*, 2139.

(3) Collins, S. *Coord. Chem. Rev*. **2011**, *255*, 118.

(4) (a) Sanchez-Barba, L. F.; Alonso-Moreno, C.; Garces, A.; Fajardo, M.; Fernandez-Baeza, J.; Otero, A.; Lara-Sanchez, A.; Rodriguez, A. M.; Lopez-Solera, I. *Dalton Trans.* **2009**, 8054 (b) Edelmann, F. T. In *Adv. Organomet. Chem.*; Anthony, F. H., Mark, J. F., Eds.; Academic Press, 2008; Vol. Volume 57.

(5) Schmidt, S.; Schulz, S.; Bläser, D.; Boese, R.; Bolte, M. *Organometallics* **2010**, *29*, 6097.

(6) (a) Thomas, C. M. *Chem. Soc. Rev*. **2010**, *39*, 165 (b) Ojwach, S. O.; Okemwa, T. T.; Attandoh, N. W.; Omondi, B. *Dalton Trans.* **2013**, *42*, 10735.

(7) (a) Wang, J.; Yao, Y.; Zhang, Y.; Shen, Q. *Inorg. Chem.* **2009**, *48*, 744 (b) Wang, J.; Cai, T.; Yao, Y.; Zhang, Y.; Shen, Q. *Dalton Trans.* **2007**, 5275 (c) Luo, Y.; Xu, P.; Lei, Y.; Zhang, Y.; Wang, Y. *Inorg. Chim. Acta* **2010**, *363*, 3597.

(8) Phomphrai, K.; Pongchan-o, C.; Thumrongpatanaraks, W.; Sangtrirutnugul, P.; Kongsaeree, P.; Pohmakotr, M. *Dalton Trans.* **2011**, *40*, 2157.

(9) Bruker *APEXII Bruker AXS Inc.* **2009**, *Madison, Wisconsin, USA*.

(10) Bruker *SAINT Bruker AXS Inc.* **2009**, *Madison, Wisconsin, USA*.

(11) Bruker *Bruker SADABS Bruker AXS Inc.* **2009**, *Madison, Wisconsin, USA*.

(12) Sheldrick, G. *Acta Crystallogr. Sect. A* **2008**, *64*, 112.

(13) Dolomanov, O. V.; Bourhis, L. J.; Gildea, R. J.; Howard, J. A. K.; Puschmann, H. *J. Appl. Crystallogr.* **2009**, *42*, 339.

(14) (a) Elkin, T.; Kulkarni, N. V.; Tumanskii, B.; Botoshansky, M.; Shimon, L. J. W.; Eisen, M. S. *Organometallics* **2013**, *32*, 6337 (b) Taylor, E. C.; Ehrhart, W. A. *J. Org. Chem.* **1963**, *28*, 1108.

(15) Zhang, J.; Higashi, K.; Ueda, K.; Kadota, K.; Tozuka, Y.; Limwikrant, W.; Yamamoto, K.; Moribe, K. *Int. J. Pharm.* **2014**, *465*, 255.

(16) Kumar, U.; Thomas, J.; Thirupathi, N. *Inorg. Chem.* **2009**, *49*, 62.

(17) Devereux, M.; O'Shea, D.; O'Connor, M.; Grehan, H.; Connor, G.; McCann, M.; Rosair, G.; Lyng, F.; Kellett, A.; Walsh, M.; Egan, D.; Thati, B. *Polyhedron* **2007**, *26*, 4073.

(18) Parkin, G. *Chem. Rev.* **2004**, *104*, 699.

(19) Wu, J.-C.; Huang, B.-H.; Hsueh, M.-L.; Lai, S.-L.; Lin, C.-C. *Polymer* **2005**, *46*, 9784.

(20) Attandoh, N. W.; Ojwach, S. O.; Munro, O. Q. *Eur. J. Inorg. Chem.* **2014**, 3053.

(21) (a) Börner, J.; Flörke, U.; Döring, A.; Kuckling, D.; Jones, M.; Herres-Pawlis, S. *Sustainability* **2009**, *1*, 1226 (b) Wang, L.; Qin, W.; Liu, W. *Inorg. Chem. Commun.* **2010**, *13*, 1122 (c) Huo, Y.-P.; Zhu, S.-Z.; Hu, S. *Tetrahedron* **2010**, *66*, 8635 (d) Zhang, G.; Wang, S.; Gan, Q.; Zhang, Y.; Yang, G.; Shi Ma, J.; Xu, H. *Eur. J. Inorg. Chem.* **2005**, *2005*, 4186 (e) Hui, R.-H.; Zhou, P.; You, Z.-L. *Indian J. Chem. -Sect. A:* **2009**, *48A*, 663 (f) Yuan, G.; Huo, Y.; Nie, X.; Jiang, H.; Liu, B.; Fang, X.; Zhao, F. *Dalton Trans.* **2013**, *42*, 2921.

(22) Knight, P. D.; White, A. J. P.; Williams, C. K. *Inorg. Chem.* **2008**, *47*, 11711.

(23) Maiti, P.; Khan, A.; Chattopadhyay, T.; Das, S.; Manna, K.; Bose, D.; Dey, S.; Zangrando, E.; Das, D. *J. Coord. Chem.* **2011**, *64*, 3817.

(24) Stephens, J. C.; Khan, M. A.; Houser, R. P. *Inorg. Chem.* **2001**, *40*, 5064.

(25) Kokoszka, G. F.; Linzer, M.; Gordon, G. *Inorg. Chem.* **1968**, *7*, 1730.

(26) O'Keefe, B. J.; Breyfogle, L. E.; Hillmyer, M. A.; Tolman, W. B. *J. Am. Chem. Soc.* **2002**, *124*, 4384.

(27) Hodgson, L. M.; Platel, R. H.; White, A. J. P.; Williams, C. K. *Macromolecules* **2008**, *41*, 8603.

(28) Appavoo, D.; Omondi, B.; Guzei, I. A.; van Wyk, J. L.; Zinyemba, O.; Darkwa, J. *Polyhedron* **2014**, *69*, 55.

(29) Duda, A.; Kowalski, A. In *Handbook of Ring-Opening Polymerization*; Wiley-VCH Verlag GmbH & Co. KGaA, 2009.

(30) Mei, Y.; Kumar, A.; Gross, R. *Macromolecules* **2003**, *36*, 5530.

(31) Zhang, L.; Niu, Y.; Wang, Y.; Wang, P.; Shen, L. *J. Mol. Catal. A: Chem.* **2008**, *287*, 1.

(32) (a) Darensbourg, D. J.; Ganguly, P.; Billodeaux, D. *Macromolecules* **2005**, *38*, 5406 (b) Sun, H.; Ritch, J. S.; Hayes, P. G. *Dalton Trans.* **2012**, *41*, 3701.

(33) (a) Dubois, P.; Jacobs, C.; Jerome, R.; Teyssie, P. *Macromolecules* **1991**, *24*, 2266 (b) Kim, K.; Lee, J.; Chang, T.; Kim, H. *J. Am. Soc. Mass Spectrom.* **2014**, *25*, 1771 (c) Aluthge, D. C.; Ahn, J. M.; Mehrkhodavandi, P. *Chem. Sci.* **2015**, *6*, 5284.

(34) Wu, J.; Yu, T.-L.; Chen, C.-T.; Lin, C.-C. *Coord. Chem. Rev.* **2006**, *250*, 602.

(35) Ovitt, T. M.; Coates, G. W. *J. Polym. Sci. Part A: Polym. Chem.* **2000**, *38*, 4686.

(36) Pilone, A.; Lamberti, M.; Mazzeo, M.; Milione, S.; Pellecchia, C. *Dalton Trans.* **2013**, *42*, 13036.

(37) Kong, W.-L.; Wang, Z.-X. *Dalton Trans.* **2014**, *43*, 9126.

(38) Babu, H. V.; Muralidharan, K. *RSC Advances* **2014**, *4*, 6094.

(39) (a) Svejda, S. A.; Johnson, L. K.; Brookhart, M. *J. Am. Chem. Soc.* **1999**, *121*, 10634 (b) Deng, L.; Woo, T. K.; Cavallo, L.; Margl, P. M.; Ziegler, T. *J. Am. Chem. Soc.* **1997**, *119*, 6177.

(40) Zell, M. T.; Padden, B. E.; Paterick, A. J.; Thakur, K. A. M.; Kean, R. T.; Hillmyer, M. A.; Munson, E. J. *Macromolecules* **2002**, *35*, 7700.

(41) Yang, Y.; Wang, H.; Ma, H. *Inorg. Chem.* **2015**, *54*, 5839.

(42) Thakur, K. A. M.; Kean, R. T.; Hall, E. S.; Doscotch, M. A.; Munson, E. J. *Anal. Chem.* **1997**, *69*, 4303.

(43) Thakur, K. A. M.; Kean, R. T.; Hall, E. S.; Kolstad, J. J.; Lindgren, T. A.; Doscotch, M. A.; Siepmann, J. I.; Munson, E. J. *Macromolecules* **1997**, *30*, 2422.

Chapter 4

Structural and kinetic studies of the ring-opening polymerization of cyclic esters using *N,N'* diarylformamidines Zn(II) and Cu(II) complexes

This chapter is adapted from the paper published in *Polyhedron*, **2016**, 110, 63–72 and is based on the experimental work of the first author, Ekemini D. Akpan. The contributions of the first author include synthesis and characterization of the ligands and complexes, ε-CL and LAs ROP catalysis and drafting the manuscript.

4.1 Introduction

The major method that has been employed in the preparation of the polyesters is the ROP with the aid of a well-defined metal complexes[1]. The rational in the design and synthesis of metal carboxylates for ROP by employing new synthetic tools, varying the nature of reactants, synthetic conditions is currently under active investigations.[2] Research on metal carboxylates has always been fascinating in that they play important roles in synthetic chemistry largely due to the labile coordination modes of the carboxylate group.[3] The carboxylate group can adopt a wide range of bonding modes, including monodentate, symmetric and asymmetric chelating, bidentate and monodentate bridging as depicted in Figure 4.1, and is mostly incorporated as an ancillary ligand.[2,4,5,6,7] Appavoo and co-workers[8] recently reported pyrazole Cu(II) and Zn(II) carboxylate complexes as active catalysts in the ROP of ε-CL and $_{D,L}$-LA. More recently, (benzimidazolymethyl)amine and (pyrazolylmethyl)pyridine Zn(II) and Cu(II) carboxylate complexes catalyst for ROP of ε-CL have been reported.[9,10]

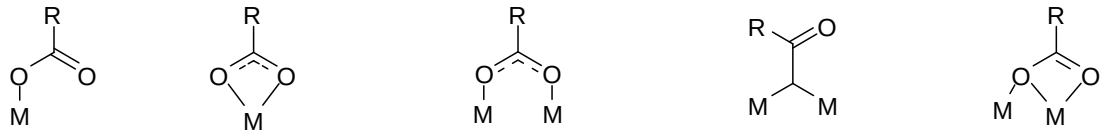

Figure 4. 1: Various coordination modes of carboxylate ligands to transition metals.[6]

Zn(II) and Cu(II) complexes in the presence of auxiliary carboxylate ligands and formamidine derivatives as catalyst for ROP of cyclic esters have not been reported and this has inspired us to design these complexes as potential catalysts in the ROP of cyclic esters. In this chapter, we envisaged that structural rigidity offered by the formamidine ligands together with the auxiliary carboxylate ligands as opposed to the more flexible (pyrazolylmethy)pyridine systems[7] previously reported may result in better control of the ROP reactions. Detailed structural and kinetics studies of the complexes in the ROP reactions of ε-CL and LAs have been performed and are herein discussed in this chapter.

4.2 Experimental Section

4.2.1 Materials and reagents

All experiments were carried out under argon using Schlenk techniques. All solvents were dried and purified by distillation over standard reagents under nitrogen prior to use. Compounds *N,N'*-bis(2,6-dimethylphenyl)formamidine (**L1**) and *N,N'*-bis(2,6-diisopropylphenyl)formamidine (**L2**) (Figure 4.2) were synthesized following literature procedure.[11,12] Benzoic acid, 2-nitrobenzoic acid, $Zn(OAc)_2.2H_2O$, $Cu(OAc)_2.2H_2O$, 2,6-dimethylaniline (99%), 2,6-diisopropylaniline (97%),

2,4,6-trimethylaniline (98%) and the monomers(ε-CL and LAs, 99%) were obtained from Sigma-Aldrich.

4.2.2 Instrumental characterization techniques

^{1}H and ^{13}C NMR spectra were measured at room temperature with Bruker 400 MHz spectrometer. The chemical shifts are reported in δ (ppm) and referenced to the residual proton and carbon signals 7.26 ppm and 77.00 ppm respectively of $CDCl_3$ NMR solvent. Elemental analyses were recorded on a Vario elementar III microcube CHN analyzer. IR spectra were obtained on PerkinElmer Universal ATR spectrum 100 FTIR spectrometer. Mass spectra of compounds were obtained from Water synapt GR electrospray positive spectrometer.

4.2.3 Synthesis of Zn(II) and Cu(II) complexes

4.2.3.1 $[Zn_2(L1)_2(C_6H_5COO)_4]$ (5)

A solution of $Zn(OAc)_2.2H_2O$ (0.130 g, 0.592 mmol) and benzoic acid (0.145 g, 1.187 mmol) in ethanol (10 mL) was heated at 80 °C for 5 h followed by drop wise addition of **L1** (0.149 g, 0.592 mmol) in ethanol (5 mL). The resulting solution was further refluxed for 24 h. After the specified period, the mixture was cooled to room temperature, filtered and the solvent removed under reduced pressure to afford a white solid. Recrystallization of the crude product from dichloromethane/hexane solvent mixture gave single crystals suitable for X-ray analysis (0.513 g, 77%). ^{1}H NMR (400 MHz, $CDCl_3$): δ (ppm) 1.94 [s, 2H, NH], 2.30 [s, 24H, CH_3], 6.92 [d, $^{3}J_{H,H}$ = 7.2 Hz, 1H, N=CH], 7.01 [s, 14H, Ar], 7.27 [m, 8H, Ar], 7.40 [t, $^{3}J_{H,H}$ = 6.8 Hz, 3H, Ar], 7.92 [d, $^{3}J_{H,H}$ = 7.2 Hz, 7H, Ar]. ^{13}C NMR (400MHz, $CDCl_3$) δ (ppm) 173.62, 134.03, 131.24 130.24, 128.52, 128.24, 127.63, 126.66, 121.80, 118.07, 18.60, 17.62. IR (Nujol): 3207 *ν*(N-H)

stretching, 1579 *v* (C=O) carbonyl. ESI-TOF MS: *m/z* (%); 567.25 $[LZn + 2C_6H_5COO]^+$ (100). Anal. Calcd. For $C_{62}H_{64}N_4O_8Zn_2$: C, 66.25; H, 5.74; N, 4.98. Found: C, 66.42; H, 5.85; N, 5.18.

Complexes **6**–**9** were prepared following the synthetic protocol described in **4.2.2.1**.

4.2.3.2 $[Zn_2(L2)_2(C_6H_5COO)_4]$ (6)

$Zn(OAc)_2.2H_2O$ (0.200 g, 0.911 mmol), benzoic acid (0.223 g, 1.822 mmol) and **L2** (0.332 g, 0.911 mmol). Recrystallization from dichloromethane/hexane solvent mixture gave white single crystals suitable for X-ray analysis (0.834 g, 68%). ^{1}H NMR (400 MHz, $CDCl_3$): δ (ppm) 1.27 [m, 48H, CH_3], 2.06 [s, 2H, NH], 3.43 [m, 8H, CH], 7.20 [d, $^3J_{H,H}$ = 7.6 Hz, 7H, Ar], 7.31 [m, 12H, Ar], 7.45 [t, $^3J_{H,H}$ = 7.2 Hz, 4H, Ar], 7.93 [d, $^3J_{H,H}$ = 6.24 Hz, 8H, Ar]. ^{13}C NMR (400MHz, $CDCl_3$) δ (ppm) 174.07, 146.00, 131.82, 130.46, 127.74, 123.77, 28.28, 23.83. IR (Nujol): 3264 *v*(N-H) stretching, 1647 *v* (C=O) carbonyl, 1574 *v*(N-H) amine bending vibration. ESI-TOF MS: *m/z* (%); 1223.54 $[M - C_6H_5COO]^+$ (100). Anal. Calcd. For $C_{78}H_{94}N_4O_8Zn_2$: C, 69.58; H, 7.04; N, 4.16. Found: C, 69.20; H, 7.31; N, 3.89.

4.2.3.3 $[Zn_2(L1)_2(C_6H_5COO)_4(NO_2)_4]$ (7)

$Zn(OAc)_2.2H_2O$ (0.130 g, 0.592 mmol), 2-NO_2-C_6H_4COOH (0.198 g, 1.184 mmol) and **L1** (0.149 g, 0.592 mmol). Recrystallization of the crude product from DMF/ethanol solvent mixture gave single crystals suitable for X-ray analysis (0.618 g, 80%). ^{1}H NMR (400 MHz, $CDCl_3$): δ (ppm) 2.26 [d, 24H, CH_3], 7.11 [m, , 12H, Ar], 7.68 [m, Hz, 12H, Ar], 7.79 [d, $^3J_{H,H}$ = 7.6 Hz, 10H, Ar], 7.45 [s, 2H, Ar], 8.43 [d, $^3J_{H,H}$ = 9.6 Hz, 4H, Ar]. ^{13}C NMR (400MHz, $CDCl_3$) δ (ppm) 168.52, 149.17, 131.93, 131.04, 130.54, 130.11, 127.63, 122.76, 18.33. IR (Nujol): 3207 *v*(N-H)

stretching, 1579 *v*(N-H) amine bending vibration. ESI-TOF MS: *m/z* (%); 1223.54 $[M - 2NO_2]^+$ (100). Anal. Calcd. For $C_{62}H_{61}N_8O_{16}Zn_2$: C, 57.11; H, 4.64; N, 8.59. Found: C, 57.17; H, 4.67; N, 8.51.

4.2.3.4 $[Zn_2(L2)_2(C_6H_5COO)_4(NO_2)_4]$ (8)

$Zn(OAc)_2.2H_2O$ (0.079 g, 0.362 mmol), 2-NO_2-C_6H_4COOH (0.121 g, 0.724 mmol) and compound **L2** (0.132 g, 0.362 mmol). White solid (0.415 g, 75%). ^1H NMR (400 MHz, $CDCl_3$): δ (ppm) 1.17 [d, $^3J_{H,H}$ = 5.6 Hz, 48H, CH_3], 3.2 [b, 8H, CH], 7.60 [d, $^3J_{H,H}$ = 7.5 Hz, 3H, Ar], 7.61 [d, $^3J_{H,H}$ = 6.8 Hz 12H, Ar], 7.68 [t, $^3J_{H,H}$ = 7.6 Hz, 6H, Ar], 7.75 [d, $^3J_{H,H}$ = 7.6 Hz, 4H, Ar], 7.76 [s, 2H, Ar], 7.81 [d, $^3J_{H,H}$ = 7.8 Hz, 4H, Ar], 7.82 [d, $^3J_{H,H}$ = 7.6 Hz, 2H, Ar]. ^{13}C NMR (400MHz, $CDCl_3$) δ (ppm) 169.05, 149.72, 132.31, 131.77, 130.87, 130.66, 123.17, 79.62, 79.40, 79.18, 27.95, 24.10.IR (Nujol): 3256 *v*(N-H) stretching, 1571 *v*(N-H) amine bending vibration. ESI-TOF MS: *m/z* (%); 1222.53 $[M - 4\text{-}NO_2\text{-}C_6H_5COO]^+$ (30). Anal. Calcd. For $C_{78}H_{92}N_8O_{16}Zn_2$: C, 61.29; H, 6.07; N, 7.33. Found: C, 61.28; H, 6.08; N, 7.38.

4.2.3.5 $[Cu_2(L2)_2(C_6H_5COO)_4]$ (9)

Compound **L2** (0.232 g, 0.636 mmol), benzoic acid (0.155 g, 1.273 mmol) and $Cu(OAc)_2.2H_2O$ (0.127 g, 0.636 mmol) in ethanol to afford complex **9** as green solid. (0.633 g, 74%). IR (Nujol): 3250 *v*(N-H) stretching, 1575 *v*(N-H) amine bending vibration. μeff = 1.87 BM. ESI-TOF MS: *m/z* (%); 1219.55 $[M - C_6H_5COO]^+$ (100). Anal. Calcd. For $C_{78}H_{96}N_4O_8Cu_2$: C, 69.67; H, 7.20; N, 4.17. Found: C, 69.91; H, 7.40; N, 4.13.

4.2.4 Typical procedure for bulk polymerization of ε-CL

Bulk polymerization reactions were performed by introducing an appropriate amount of the complex and ε-CL monomer (1.14 g, 0.01 mol) was added to Schlenk tube immersed in pre-heated oil bath at 110 °C and the reaction was initiated by stirring. Kinetics experiments were carried out by withdrawing samples at regular interval using a syringe and quenched quickly by rapid cooling into NMR tube containing $CDCl_3$ solvent using ice water. The quenched samples were analyzed by ^1H NMR spectroscopy for determination of polymerization of ε-CL to PCL. The percentage conversion of $[PCL]/[CL]_o \times 100$, where $[CL]_o$ is the initial concentration of the monomer and [PCL] is the concentration of the polymer at time t, was evaluated by integration of the peaks for CL (4.2 ppm, OCH_2 signal) and PCL (4.0 ppm, OCH_2 signal) according to the equation $[PCL]/[CL]_o = I_{4.0}/(I_{4.2} + I_{4.0})$ where $I_{4.2}$ is the intensity of the CL monomer signal at 4.2 ppm and $I_{4.0}$ is the intensity of PCL signal at 4.0 ppm for OCH_2 protons. The observed rate constants were extracted from the slope of the line of best-fits of the plot of $\ln[CL]_o/[CL]_t$ *vs.* time.

4.2.5 Typical procedure for polymerization of $_{D,L}$-LA and $_{L}$-LA

A suitable LA (1.44 g, 0.01 mol) was dissolved in toluene in a Schlenk tube equipped with magnetic stirrer under argon and the required amount of complex was added. The reaction mixture was stirred at 110 °C. Kinetics experiments were carried out by withdrawing samples at regular interval using a syringe and quenched quickly by rapid cooling into NMR tube containing $CDCl_3$ solvent using ice water. The quenched samples were analyzed by ^1H NMR spectroscopy for determination of polymerization of LAs to PLA. The integration values of the methine proton

of the monomer and that of the polymer were used to calculate the percentage conversion using the equation $I_{CHpolymer}/(I_{CHmonomer} + I_{CHpolymer}) \times 100$.

4.2.6 Polymer characterization by size exclusion chromatography (SEC)

The samples were analyzed by SEC at Stellenbosch University. The samples were dissolved in BHT stabilized THF (2 mg/ml). Sample solutions were filtered *via* syringe through 0.45 µm nylon filters before subjected to analysis. The SEC instrument consists of a Waters 1515 isocratic HPLC pump, a Waters 717plus auto-sampler, Waters 600E system controller (run by Breeze Version 3.30 SPA) and a Waters in-line Degasser AF. A Waters 2414 differential refractometer was used at 30 °C in series with a Waters 2487 dual wavelength absorbance UV/Vis detector operating at variable wavelengths. Tetrahydrofuran (THF, HPLC grade, stabilized with 0.125% BHT) was used as eluent at flow rates of 1 ml min^{-1}. The column oven was kept at 30 °C and the injection volume was 100 µl. Two PLgel (Polymer Laboratories) 5 µm Mixed-C (300 × 7.5 mm) columns and a pre-column (PLgel 5 µm Guard, 50 × 7.5 mm) were used. Calibration was done using narrow polystyrene standards ranging from 580 to 2×10^6 g mol^{-1}. All molecular weights were reported as polystyrene equivalents.

4.2.7 X-ray crystallography

The crystal evaluation and data collection of **5, 6, 7** and **9** were performed on a Bruker Smart APEXII diffractometer with Mo Kα radiation (λ = 0.71073 Å) equipped with an Oxford Cryostream low temperature apparatus operating at 100 K for all samples. Reflections were collected at different starting angles and the APEXII program suite was used to index the

reflections.[13] Data reduction was performed using the SAINT[14] software and the scaling and absorption corrections were applied using SADABS[15] multi-scan technique. The structures were solved by the direct method using the SHELXS program and refined.[16] The visual crystal structure information was performed using OLEX2 system software.[17] Non-hydrogen atoms were first refined isotropically and then by anisotropic refinement with full-matrix least squares method based on F^2 using SHELXL.[16] All hydrogen atoms were positioned geometrically, allowed to ride on their parent atoms and refined isotropically. Disorder was found for one of the phenyl rings of complex **5**. The electron density was observed in the difference map and used to model the disorder using PART instructions resulting in 52% occupancy of the major component. In the Crystallographic Information File for complexes **6** and **9**, hydrogen atoms are not assigned for the hexane molecule in the unit cell because of disorder as it renders refinement unstable. As such, the reported molecular formula for **6** and **9** in the crystallographic table is less by 14 hydrogen atoms, but the correct formula is reported in the experimental section. The Cambridge Crystallographic Database contains supporting information with file numbers CCDC- 1436109 for complex **5**, CCDC- 1436099 for complex **6** and CCDC- 1436101 for complex **7**.

4.3 Results and discussion

4.3.1 Synthesis and characterization of Zn(II) and Cu(II) carboxylate complexes supported by *N,N'* diarylformamidines ligands

Reactions of $Zn(OAc)_2.2H_2O$ salt with two molar equivalent of benzoic acid or substituted benzoic acid derivatives followed by *in situ* addition of *N,N'*-bis(2,6-dimethylphenyl)formamidine (**L1**) and *N,N'*-bis(2,6-diisopropylphenyl)formamidine (**L2**) afforded the corresponding dinuclear Zn(II) complexes $[Zn_2(\mathbf{L1})_2(C_6H_5COO)_4]$ **(5),** $[Zn_2(\mathbf{L2})_2(C_6H_5COO)_4]$ **(6),** $[Zn_2(\mathbf{L1})_2(2\text{–}NO_2\text{–}C_6H_4COO)_4]$ **(7)** and $[Zn_2(\mathbf{L2})_2(2\text{–}NO_2\text{–}$

$C_6H_4COO)_4$] **(8)** respectively (Scheme 4.1). Complexes **5–8** were isolated as white solids in moderate to high yields. Also, the reaction of $Cu(OAc)_2.2H_2O$ salt with two molar equivalent of benzoic acid followed by addition of *N,N'*-bis(2,6-diisopropylphenyl)formamidine (**L2**) *in situ* afforded the corresponding dinuclear Cu(II) complex $[Cu_2(\mathbf{L2})_2(C_6H_5COO)_4]$ **(9),** as green solid.

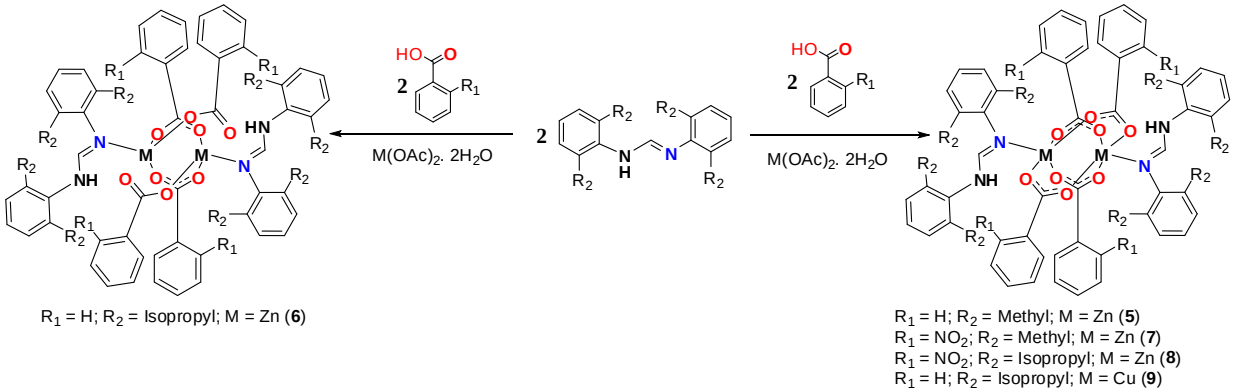

Scheme 4. 1: Synthesis of Zn(II) and Cu(II) carboxylate complexes **5–9.**

All the complexes were characterized by ^1H and ^{13}C NMR spectroscopy, CHN elemental analysis, mass spectroscopy, IR spectroscopy and single crystal X-ray crystallography for **5, 6, 7** and **9**. ^1H spectrum of the complexes showed appreciable shifts with respect to the ligand signals on complexation (Figures 4.2). For example, the HC=N proton signal was observed at 7.37 ppm in **L1** in comparison to 6.92 ppm in the corresponding complex **5**. In addition, signals in the ^1H NMR spectra of **5** observed in the region of 7.20 ppm to 7.92 ppm were typical for aromatic protons of the benzoate groups (Figure 4.2).

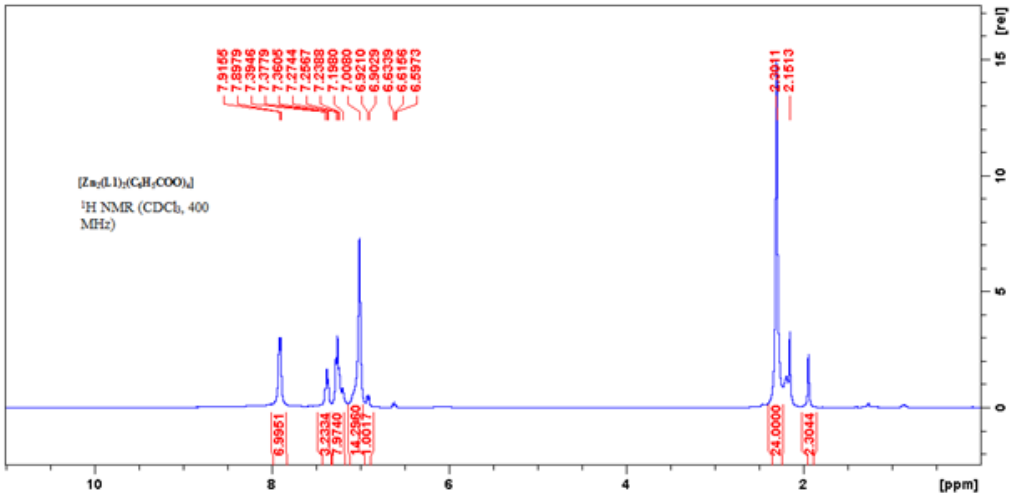

Figure 4. 2: ^{1}H NMR spectrum of complex **5** in $CDCl_3$ at room temperature.

Though detailed NMR spectroscopic analysis of the complexes was not carried out, NMR studies for amidine ligands *vis-à-vis* complexes in solutions is rather complex. This is majorly because amidine ligands exhibit various tautomeric structures in solutions.[11] Proton exchange at the formation stages of the complexes may result in symmetric and asymmetric isomer and the influence of deuterated NH group on the exchange rate of the different protons may result in the collapse of doublet into singlet peak, for example, as observed for 24H protons of the eight methyl groups on the formamidine ligands in complex **5** (Figure 4.2).[18,19] Mass spectra of complexes **5–9** showed *m/z* peaks of fragments that supported their formulation (Table 4.1).

FTIR spectra of complexes **5–9** showed shifts in the benzoate carbonyl signals by approximately v = 12 cm^{-1} in relation to the free benzoic acid, indicating possible metal benzoate formation. The frequency differences between v_{sym}(OCO) and v_{asym}(OCO) are in the range 184 cm^{-1} to 265

cm^{-1} indicative of syn-syn bidentate and monoatomic coordination modes (Figure 4.1) of the carboxylate ligands.[20]

Table 4. 1: ES-MS spectra of complexes **5-9** supporting the formation of the compounds

Complexes	Molecular formula	*m/z* (%)
5	$[LZn + 2C_6H_5COO]^+$	567.25 (100)
6	$[M - C_6H_5COO]^+$	1223.54 (100)
7	$[M - 2NO_2]^+$	1224.65 (100)
8	$[M - C_6H_5COO.4NO_2]^+$	1219.55 (30)
9	$[M - C_6H_5COO]^+$	1219.77 (100)

In addition, IR spectra of compounds **L1** and **L2** and their corresponding complexes showed the azomethine, *ν*C=N shift to higher frequencies in the corresponding complexes. For example, the strong band at 1630 cm^{-1} of the free ligand **L1** shifted to 1699 cm^{-1} in the corresponding complex **L3**. The measured effective magnetic moment of complex **9** at room temperature was 1.87 BM, signifying significant Cu···Cu interaction.[21] Elemental analyses data of complexes **5**–**9** were consistent with the proposed empirical formulae (Scheme 4.1) and confirmed their purity.

4.3.2 Molecular structures of complexes 5, 6, 7 and 9

Single crystals of complexes **5, 6** and **9** suitable for X-ray diffraction analyses were obtained by recrystallization in dichloromethane and hexane solutions at room temperature while crystals of

complex **7** were obtained from slow evaporation of a dimethylformamide/ethanol (1:1) solution at room temperature. Molecular structures and selected bond parameters of **5, 6, 7** and **9** are given in Figures 4.3–4.6, while structural refinement parameters and crystallographic data are given in Table 4.2.

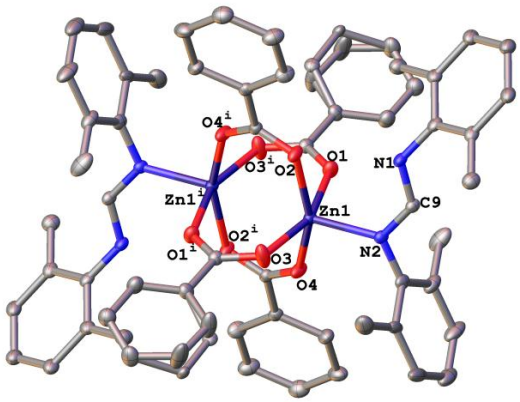

Figure 4. 3: Solid state structure of complex **5** drawn with 30% probability thermal ellipsoids. . Hydrogen atoms are omitted for clarity. Selected bond lengths (Å) and angles (°): N(2)−Zn(1) 1.946(2), O(1)−Zn(1) 1.962(2), O(3)−Zn(1) 1.928(2), O(2)−Zn(1) 1.984(2), N(2)−Zn(1)−O(1) 97.25(9), N(2)−Zn(1)−O(2) 102.51(8), O(3)−Zn(1)−O(4) 89.55(11), Symmetry transformations used to generate equivalent atoms: (i) = -x, -y, -z+1.

The solid state structures of complexes **5, 6,** and **7** are dinuclear and exhibit inversion symmetry between the two metal centers while complex **9** is dinuclear with no inversion symmetry. Complexes **5** and **7** contain half a molecule of the complex in their asymmetry units while **6** and **9** contain half a molecule of hexane in the asymmetric unit. The *N,N'* diarylformamidines ligand units in complexes **5, 6, 7** and **9** coordinate in a monodentate fashion through the imine N-atom. The coordination of the benzoate ligands in **5**, **7** and **9** is different from their coordination in **6**.

In **5**, **7** and **9**, the carboxylate ligands bridge two Zn(II) centers forming the familiar paddle wheel structure and a square pyramidal geometry around the Zn(II) and Cu(II) centers, respectively, in which four O atoms occupy the base while the formamidine N atom occupy the axial position of the pyramid.

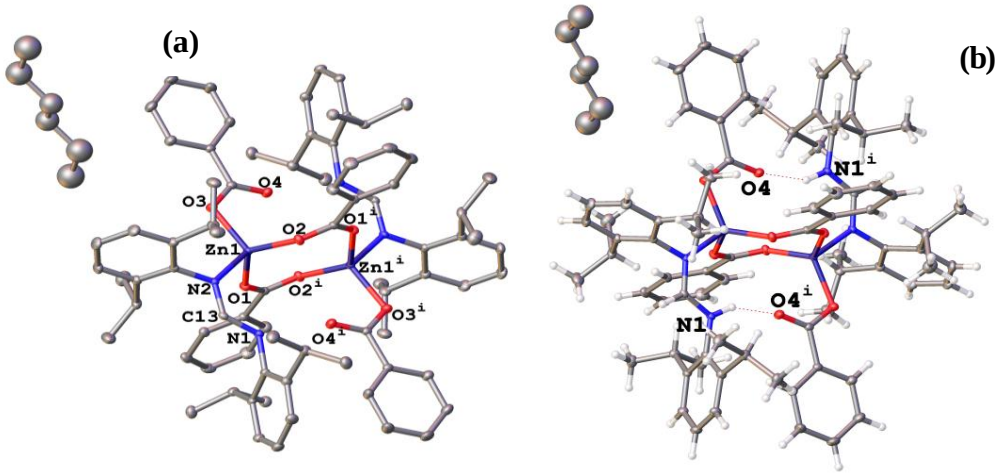

Figure 4. 4: (a) Solid state structure of complex **6** drawn with 30% probability thermal ellipsoids. Hydrogen atoms are omitted for clarity. (b) View of hydrogen bonded chain in the crystal structure of complex **6**. Selected bond lengths (Å) and angles (°): N(2)−Zn(1) 2.034(15), O(1)−Zn(1) 1.954(14), O(2)−Zn(1) 1.953(14), O(3)−Zn(1) 1.949(14), C(26)−O(4) 1.239(2), O(1)−Zn(1)−O(2) 124.57(6), O(2)−Zn(1)−O(3) 114.03(5), N(2)−Zn(1)−O(3) 102.62(6), O(3)−Zn(1)−O(1) 111.89(6). Symmetry transformations used to generate equivalent atoms: (i) = −x+2, −y, −z.

In complex **6** (Figure 4.4), one benzoate ligand bridges the two Zn(II) centers while the second unit coordinates in a monodentate fashion to give a distorted tetrahedral geometry around the Zn(II) atom. In the solid state structure of complex **6**, there is an intramolecular hydrogen bond interaction involving the non-zinc bonded carboxylate oxygen (O4) and the formamidine ligand

N−H atom. The mean interaction metric for the intramolecular N−H···O hydrogen bond is 2.849(2) Å; 149°, symmetry code: –x, –y, 2–z. This falls within the range of weak non-classical intramolecular hydrogen bond reported in literature[22] and is reported to play a significant role in the construction and stabilization of the dimeric Zn(II) units.

The average Zn–O bond distances of 1.955(8) Å in complexes **4** and **6** fall within the ranges reported for similar Zn(II) complexes in literature.[2,23] The longer Zn–O bond length of 2.0578 Å obtained in **7** (containing the nitrobenzoate) compared to 1.962(2) Å obtained for complex **5** (simple benzoate ligand) could be attributed to the more steric demands in the substituted benzoate ligand.

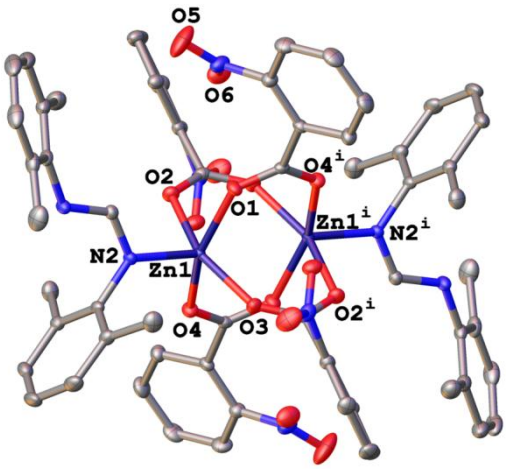

Figure 4. 5: Solid state structure of complex **7** drawn with 30% probability thermal ellipsoids. Hydrogen atoms are omitted for clarity. Selected bond lengths (Å) and angles (°): N(2)−Zn(1) 2.008(8), O(2)−Zn(1) 2.058(7), O(1)−Zn(1) 2.076(7), O(8)−N(4) 1.229(13), O(7)−N(4) 1.223(13), O(2)−Zn(1)−O(1) 86.45(3), N(2)−Zn(1)−O(2) 96.99(3). Symmetry transformations used to generate equivalent atoms: (i) = −x+1, −y+1, −z+1.

Table 4. 2: Crystal data collection and structural refinement parameters for complexes **5**, **6**, **7** and **9**.

	5	**6**	**7**	**9**
Empirical formula	$C_{62}H_{60}N_4O_8Zn_2$	$C_{84}H_{92}N_4O_8Zn_2$	$C_{62}H_{56}N_8O_{18}Zn_2$	$C_{78}H_{96}N_4O_8Cu_2$
Formula weight	1119.88	1416.35	1299.88	1412.70
Temperature (K)	173(2)	173(2)	173(2)	173(2)
λ (Å)	0.71073	0.71073	0.71073	0.71073
Crystal system	Monoclinic	Triclinic	Triclinic	Triclinic
Space group	$P2_1/n$	*P*-1	*P-1*	*P-1*
***a*/Å**	10.566(5)	11.3175(2)	11.3376(2)	11.5212(6)
***b*/Å**	15.140(7)	12.6100(3)	11.6384(2)	13.1171(7)
***c*/Å**	14.464(7)	14.1534(3)	12.0449(2)	15.3924(8)
α (°)	90	86.5030(10)	106.2300(10)	65.315(2)
β(°)	92.746(17)	75.2890(10)	97.4750(10)	70.273(2)
γ(°)	90	84.7960(10)	99.6980(10)	68.916(2)
Volume (Å^3)	2398.3(3)	1944.11(7)	1477.60(4)	1923.37(17)
Z	2	1	1	2
ρ_{calc} (mg/m^3)	1.609	1.210	1.461	1.220
μ (mm^{-1})	1.108	0.673	0.890	0.609
***F*(000)**	1168	748	672	746
Crystal size (mm^3)	0.24 x 0.21 x 0.15	0.27 x 0.23 x 0.17	0.41 x 0.34 x 0.32	0.23 x 0.32 x 0.19
Theta range for data collection	1.95 to 2.78°	1.489 to 28.501°	1.793 to 28.602°	1.49 to 28.43°.
Index ranges	$-12 \le h \le 13$, $-19 \le k \le 10$, $-12 \le l \le 18$	$-14 \le h \le 14$, $-15 \le k \le 16$, $-18 \le l \le 18$	$-15 \le h \le 15$, $-15 \le k \le 15$, $-16 \le l \le 16$	$-15 \le h \le 15$, $-17 \le k \le 17$, $-20 \le l \le 20$
Reflections collected	11880	32233	34388	40257
Independent reflections	5236 [R(int) = 0.0402]	9381 [R(int) = 0.0296]	7515 [R(int) = 0.0145]	16632 [R(int) = 0.0310]
Completeness to theta = 28.59°	98.9%	99.7%	99.9%	97.5%
Absorption correction	Semi-empirical from equivalents	Semi-empirical from equivalents	Semi-empirical from equivalents	Semi-empirical from equivalents
Max. and min. transmission	0.609 and 0.524	0.8802 and 0.8278	0.7828 and 0.7722	0.8604 and 0.8120
Refinement method	Full-matrix least-squares on F^2	Full-matrix least-squares on F^2	Full-matrix least-squares on F^2	Full-matrix least-squares on F^2
Data / restraints / parameters	5236 / 0 / 331	9381 / 0 / 435	7515 / 0 / 401	16632 / 3 / 883
Goodness-of-fit on F^2	1.047	1.016	1.045	1.032
Final R indices [I>2sigma(I)]	R1 = 0.0743, wR_2 = 0.1987	R1 = 0.0454, wR_2 = 0.1293	R1 = 0.0221, wR_2 = 0.0591	R1 = 0.0454, wR_2 = 0.1194
R indices (all data)	R1 = 0.0846, wR_2 = 0.2083	R1 = 0.0492, wR_2 = 0.1338	R1 = 0.0231, wR_2 = 0.0598	R1 = 0.0561, wR_2 = 0.1308
Largest diff. peak and hole	1.371 and -1.284 e.Å^{-3}	2.041 and -0.773 e.Å^{-3}	0.405 and -0.299 e.Å^{-3}	0.682 and -0.466 e.Å^{-3}

The Cu–O bond distances in **9** ranges from 1.957(6) Å to 1.992(7) Å averaging 1.970(7) Å. The Zn–N and Cu–N distances in all the complexes are compared well with Zn–N and Cu–N bond distances of similar complexes in reported in literature.[2,24,25] The observed Zn···Zn distances in the solid state structures of complexes **5, 6** and **7** are within the range reported for dinuclear Zn(II) complexes[26] and are also greater than the sum of the van der Waal radii of Zn (1.39 Å), signifying lack of meaningful Zn···Zn interatomic interactions.[24] The Zn···Zn bond separation (3.774 (4) Å) in **6** is longer than those in complexes **5** and **7**, but close to distance reported[7,27] for compounds with similar coordination environment around the two Zn(II) centers. The observed Cu···Cu distance of 2.685(5) Å in complex **9** is typical of binuclear Cu(II) complexes possessing N-donating apical ligands.[28]

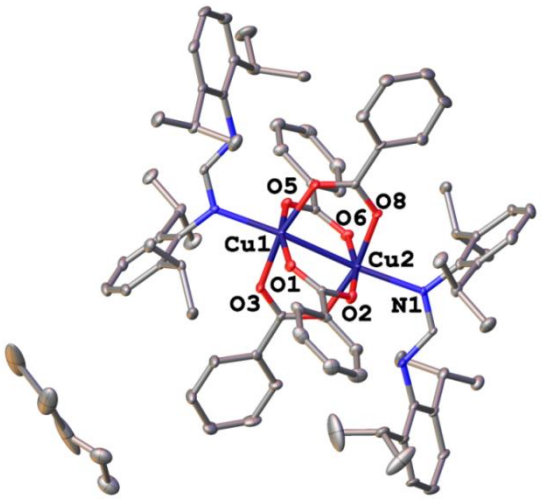

Figure 4. 6: Solid state structure of complex **9**. Hydrogen atoms are omitted for clarity. Selected bond lengths (Å) and angles (°): Cu(1)−Cu(2) 2.685(5), N(1)−Cu(2) 2.211(7), N(3)−Cu(2) 2.188(7), O(1)−Cu(1) 1.961(8), O(2)−Cu(2) 1.963(7), O(1)−Cu(1)−O(7) 88.4(3), O(6)−Cu(2)−O(2) 166.8(3), O(1)−Cu(1)−N(3) 102.6(3), O(8)−Cu(2)−N(1) 91.5(3).

4.3.3 ROP of ε-CL and LAs by Zn(II) and Cu(II) complexes 5–9 as catalysts

Initial investigations of complexes **5**–**9** as catalysts in the ROP reactions of ε-CL were performed at 110 °C using [M]/[I] ratio of 200 (Table 4.3). Under these conditions, complexes **5**–**9** were active in the ROP of ε-CL giving conversions above 90% between 24 h to 84 h. Complexes **5** and **8** were also investigated in the ROP of $_{D,L}$-LA and $_{L}$-LA at 110 °C using [M]/[I] ratio of 200 in toluene giving conversions of 97% and 98% within 36 and 48 h for $_{D,L}$-LA and $_{L}$-LA respectively.

4.3.3.1 Kinetics of ROP reactions of ε-CL and LAs

Detailed kinetic studies for the ROP of ε-CL with complexes **5**–**9** were performed by monitoring the reactions using ^{1}H NMR spectroscopy. Thus a plot of $\ln[CL]_o/[CL]_t$ *vs.* time (Figure 4.7a) was linear, consistent with *pseudo*-first order kinetics with respect to monomer. The apparent rate constants for catalysts **5**–**9** in ROP of ε-CL were extracted from Figure 4.7a and are given in Table 4.3. From the results obtained in Table 4.3, it is evident that no specific complex property showed a dominant influence on the resultant catalytic activities of the complexes. For example, while complex **8** (0.1553 $\pm$0.015 h^{-1}) bearing the nitro and isopropyl groups on the benzoate and phenyl rings respectively, exhibited the highest catalytic activity, the analogous complex **6** (0.0469 $\pm$0.0039 h^{-1}) showed the lowest rate constant. It is expected that bulky isopropyl groups would block access of monomer to the active site due to steric factor thus decreasing the catalytic activities of complexes **6** and **8** in comparison to catalysts **5**, **7** and **9** respectively (Table 4.3, entries 1-5).

Table 4. 3: ROP data of ε-CL and LAs by complexes **5**–**9**[a]

Entry	Catalyst	Time (h)	Conversion[b] (%)	k_{app} (h^{-1})	M_w (GPC)[c]	PDI[c]
1	**5**	30	96	0.1191 ±0.011	7112	1.97
2	**6**	84	96	0.0469 ±0.0039	8431	1.94
3	**7**	48	97	0.0778 ±0.0067	10831	2.25
4	**8**	24	96	0.1553 ±0.015	10063	2.31
5	**9**	60	95	0.0617±0.0057	5344	1.94
6[d]	**5**	36	97	0.102 ±0.0003	2200	1.74
7[e]	**5**	48	97	0.0746 ±0.0013	3936	2.52
8[d]	**8**	48	97	0.0772 ±0.0010	2067	1.69
9[e]	**8**	48	97	0.0480 ±0.0016	3450	1.84

[a]Reaction conditions: $[CL]_o/[I]$ = 200; bulk, temperature, 110 °C. [b]Maximum conversion achieved [c]Molecular-weight average and Polydispersity index (PDI) determined by GPC relative to polystyrene standard, values are the values obtained from GPC × correction factor of 0.56 for lactones and 0.58 for LAs[29]. [d]$_{D,L}$-LA, solvent, toluene; and [e]$_{L}$-LA, solvent, toluene.

Contrary to expectations, lower catalytic activity was obtained for complex **7** (0.0778 ±0.0067 h^{-1}), bearing the electron withdrawing NO_2 groups on the benzoate ring compared to complex **5** (0.1191 ±0.011 h^{-1}). Electron withdrawing groups on the ligand motif has been shown to enhance the electrophilicity of the metal center thus facilitate monomer coordination resulting in higher catalytic activity.[30,31] Thus it is conceivable that both the electronic and steric factors that control the catalytic activities of these complexes in the ROP reactions of ε-CL are more complex than was originally perceived.

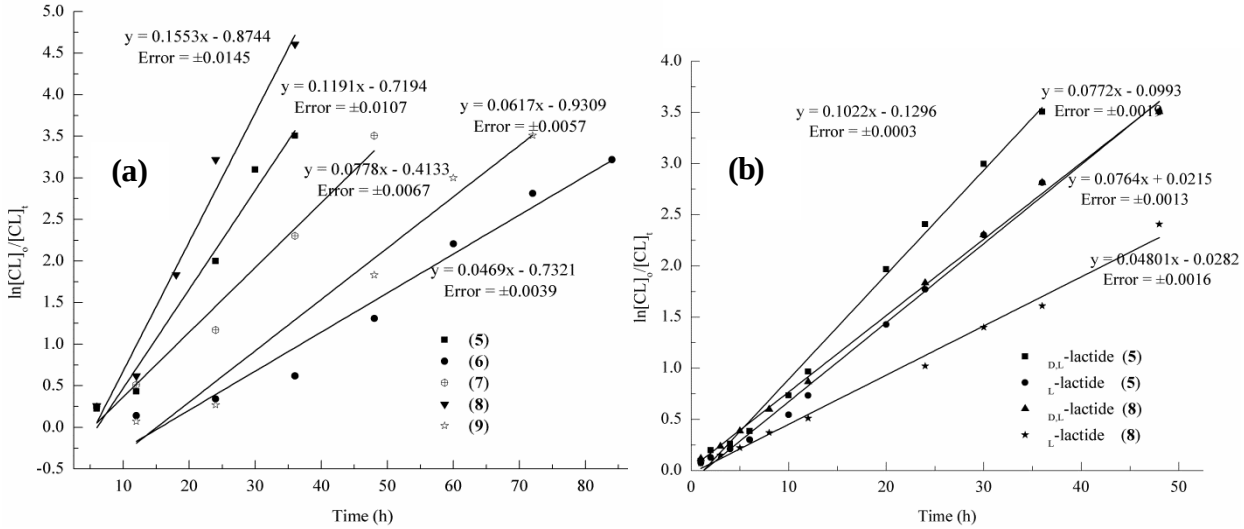

Figure 4. 7: (a) First order kinetic plots of $\ln[CL]_o/[CL]_t$ *vs.* time for complexes **5–9** in the bulk polymerization of ε-CL at 110 °C, $[CL]_o/[I] = 200$. (b) First order kinetic plots of $\ln[CL]_o/[CL]_t$ *vs.* time for complexes **5** and **8** in the polymerization of $_{D,L}$-LA and $_{L}$-LA to PLAs in toluene at 110 °C, $[CL]_o/[I] = 200$.

Kinetic investigation of the ROP of LAs using complexes **5** and **8** revealed that the ROP of LAs were also consistent with a *pseudo*-first-order with dependency on monomer (Figure 4.7b). Thus the ROP reactions of ε-CL and LAs follow simple *pseudo*-first-order kinetics with respect to monomer as shown in equations (4.1) and (4.2), respectively.

$$\frac{d[\mathrm{CL}]}{dt} = k[\mathrm{CL}] \qquad (4.1)$$

$$\frac{d[\mathrm{LA}]}{dt} = k[\mathrm{LA}] \qquad (4.2)$$

where $k = k_p[I]^x$; k_p is the rate of chain propagation, I is the initiator, and x is the order of reaction.

From the data obtained it was apparent that the reaction rates of ROP of ε-CL were slightly higher than that those of LA reactions. For example, rate constants of 0.1553 ± 0.015 h^{-1} and 0.0772 ± 0.0010 h^{-1} were obtained for ε-CL and $_{D,L}$-LA respectively using complex **8** (Table 4.3, entries 4 and 8). Similar observations have been reported in literature and have been largely associated with the larger ring size of ε-CL compared to LAs.[8] However, this contradicts other reports[32] where increased ring strain is expected to render LAs more reactive in ROP reactions. We also observed that the reaction rate of the ROP LAs was influenced by monomer stereochemistry. For instance, apparent rate constants of 0.102 ± 0.0003 h^{-1} and 0.0746 ± 0.0013 h^{-1} were obtained in the ROP of $_{D,L}$-LA and $_{L}$-LA respectively (Table 4.3, entries 6 and 7). This trend has been attributed to the differences in the stability of the $_{D,L}$-LA and $_{L}$-LA in the ground state as suggested by Buffet[33] and Chisholm[34] and co-workers. For example, the ROP reaction of *rac*-LA and $_{L}$-LA using the alkaline earth metal amide complexes appears to be slower than that of *meso*-LA, where full conversion was obtained in toluene in less than 30 min at room temperature.[33]

4.3.3.2 Determination of order of the ROP reactions of ε-CL with respect to complexes 5 and 8

To study the reaction order with respect to catalysts **5** and **8** the ROP reactions were carried at different catalyst concentrations at constant ε-CL monomer concentration (Figure 4.8, Table 4.4). A graph of $\ln k_{app}$ *vs.* ln[**5** or **8**] was plotted and the linear relationship obtained allowed us to extract the order of reaction from the gradient of the line of best fit (Figure 4.8). From Figure 4.8, the order of the reactions with respect to catalyst **5** and **8** were obtained as 0.31 ± 0.03 and 0.61 ± 0.08 respectively. Fractional orders of reactions with respect to catalysts or initiators

have been reported previously and are generally attributed to complicated aggregation of the active species arising during polymerization processes.[35] Variation in order of reaction with respect to complexes **5** and **8** thus hint to different nature of the active species and or level of aggregation for **5** and **8**.

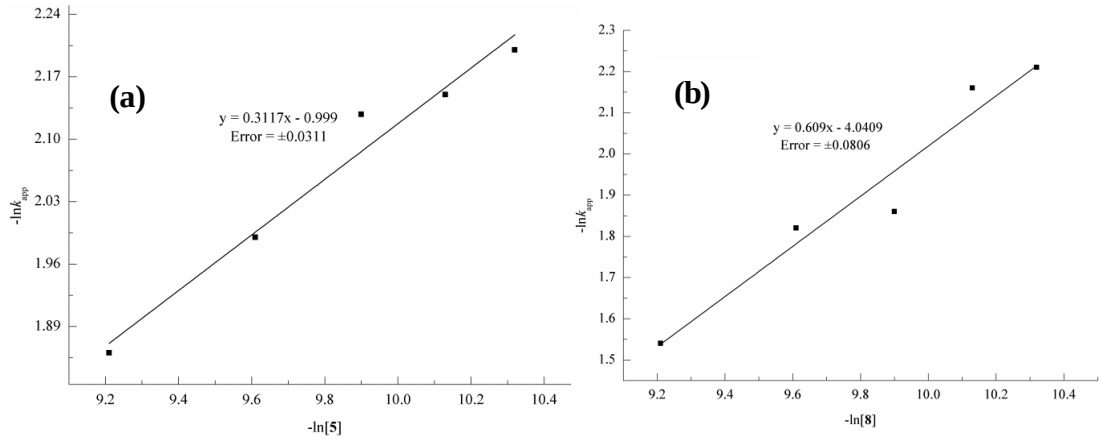

Figure 4. 8: (a) Plot of lnk_{app} *vs.* ln[**5**] and (b) lnk_{app} *vs.* ln[**8**] for the determination of order of reactions with respect to catalysts **5** and **8**.

4.3.3.3 Evaluation of the effect of alcohols initiators on the ROP kinetics of ε-CL using complex 5

In order to establish the influence of alcohols initiators in combination with complex **5**, methanol and benzyl alcohol was used in the catalyst:initiator:monomer ratio of 1:1:200 (Table 4.5). A substantial increase in catalytic activity was observed when benzyl alcohol (0.0254 ± 0.0016 min^{-1}) and methanol (0.0246 ± 0.0012 min^{-1}) were employed, respectively (Figure 4.9a and Table 4.5, entries 1 and 2), compared to the rate constant of 0.119 ± 0.011 h^{-1} obtained in bulk reactions. The higher catalytic activity recorded in benzyl alcohol and methanol could be as a

result of the *in situ* generation of Zn-alkoxides, known to form more active initiators in the ROP of cyclic esters.[36] Comparison of the bulk polymerization *vs.* solution polymerization was achieved by performing the experiments in toluene solvent and comparing the results to the bulk reactions. We noted that the use of toluene solvent resulted in a 2-fold drop in catalytic activity (0.0528 ± 0.0027 h^{-1}) compared to the bulk experiment (Figure 4.9b, Table 4.5, entry 3). Similar trend has been reported and attributed to reduced concentrations of the active species in the reaction mixture. For example, the use of toluene solvent resulted in a drop in k_{app} from 0.063 h^{-1} (bulk reaction) to 0.026 h^{-1}.[10]

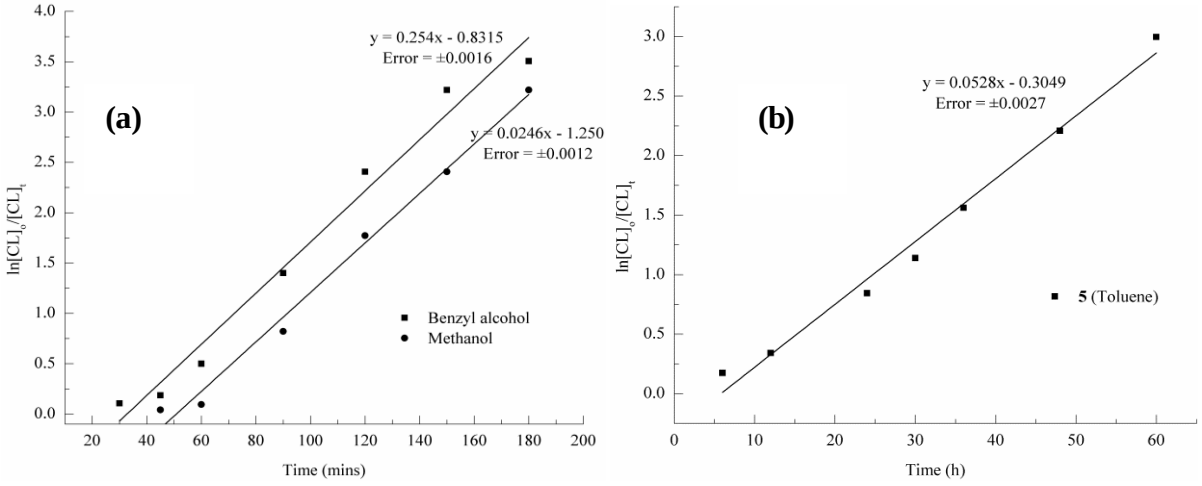

Figure 4. 9: First order kinetic plots of $\ln[CL]_o/[CL]_t$ *vs.* time for complex **5** in the polymerization of ε-CL in (a) benzyl alcohol and methanol as initiators, and (b) toluene at 110 °C, $[CL]_o/[I] = 200$.

Table 4. 4: ROP of ε-CL at different catalyst concentrations.

Catalyst	$[CL]_o/[I]$	Time (h)	Conversion[b] (%)	k_{app} (h^{-1})	M_w[c]	PDI[c]
5	100	30	97	0.156 ±0.013	6920	2.01
5	150	30	97	0.137 ±0.012	7012	2.15
5	250	48	99	0.117 ±0.010	7356	2.08
5	300	48	97	0.111 ±0.0088	7547	2.09
8	100	18	96	0.214 ±0.012	7122	1.98
8	150	24	97	0.162 ±0.0070	7292	1.86
8	250	36	98	0.115 ±0.011	8053	2.04
8	300	48	98	0.109 ±0.0090	9235	1.90

[a]Reaction conditions, bulk polymerization, 110 °C. [b]Maximum conversion achieved. [c]Molecular weight average and Polydispersity index (PDI) determined by GPC relative to polystyrene standard, values are the values obtained from GPC × correction factor of 0.58 [29].

4.3.3.4 Effect of temperature on the ROP kinetics of ε-CL and determination of activation parameters

ROP of ε-CL using complex **8** was carried out at various temperature (60 °C to 110 °C), to determine the activation parameters. A noticeable induction period was observed at lower temperatures, after which a linear relationship of the plot of $\ln[CL]_o/[CL]_t$ *vs.* time was obtained. The apparent rate constants extracted from the semi-logarithmic plot (Table 4.5) showed

significant decrease from 0.115 ±0.015 h^{-1} to 0.0627 ±0.0048 h^{-1} at temperature of 110 °C and 60 °C, respectively.

Table 4. 5: ROP of ε-CL data in different solvents and at varied temperature for complexes **5** and **8**.[a]

Entry	Catalyst	Time (h)	Conversion (%)[b]	k_{app} (h^{-1})	M_w (GPC)[c]	PDI[c]
1[d]	**5**	180	97	0.0254 ±0.0016	7 012	1.97
2[e]	**5**	180	96	0.0246 ±0.0012	8 431	1.94
3[f]	**5**	60	95	0.0528 ±0.0027	5 344	1.94
4[g]	**5**	48	99	0.131 ±0.011	7 711	1.94
5[h]	**8**	57	97	0.114 ±0.011	4996	2.55
6[i]	**8**	84	97	0.0631 ±0.0030	3689	1.60
7[j]	**8**	96	97	0.0627 ±0.0048	2295	1.44
8[k]	**5**	72	95	0.0389 ±0.0012	11 068	2.04

[a]Reaction conditions, 110 °C, $[CL]_o/[I]$ = 200. [b]Maximum conversion achieved. [c]Molecular weight average and Polydispersity index (PDI) determined by GPC relative to polystyrene standard. Values in parentheses are the values obtained from GPC × correction factor of 0.56.[29] [d]Initiator, benzyl alcohol, ratio, catalyst:initiator:monomer = 1;1:200; time (mins), k_{app}(min^{-1}). [e]Initiator, methanol, ratio catalyst:initiator:monomer = 1:1:200; time (mins), k_{app}(min^{-1}) . [f]Solvent, toluene. [g]Temp., 90 °C. [h]Temp., 80 °C. [i]Temp., 70 °C. [j]Temp., 60 °C. [k]Addition of second equivalent of ε-CL without adding the catalyst

The apparent rate constants at each reaction temperature was converted from h^{-1} to s^{-1}, and used to obtain the Eyring plot in Figure 4.10. From the Eyring plot, the enthalpies, $\Delta H^{\ddagger}$, and entropies, $\Delta S^{\ddagger}$, of activation were obtained as 18.77 $\pm$4.8 kJ mol^{-1} and -280.74 $\pm$13.6 J K^{-1} mol^{-1}, respectively for complex **8**. This data is consistent with an ordered transition state typical for coordination-insertion mechanisms in the ROP of cyclic esters by acyl oxygen bond cleavage (Scheme 4.2).[37,38] ^{1}H NMR spectra acquired of the PCL obtained was also consistent with a coordination mechanism due to the presence of signals associated with the complex/ligand motif (Figure 4.11). However, mass spectral data was inconclusive as we could not unambiguously assign all the signals or identify fragments associated with the complex or ligand molecules.

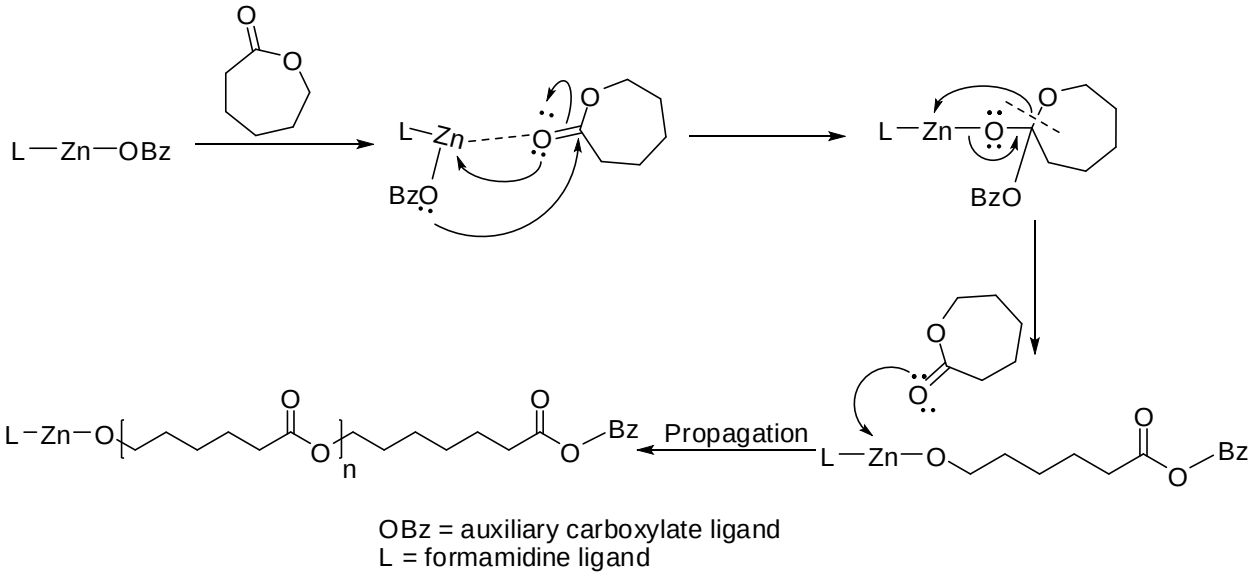

Scheme 4. 2 Proposed mechanism for bulk ROP of ε-CL *via* coordination-insertion.

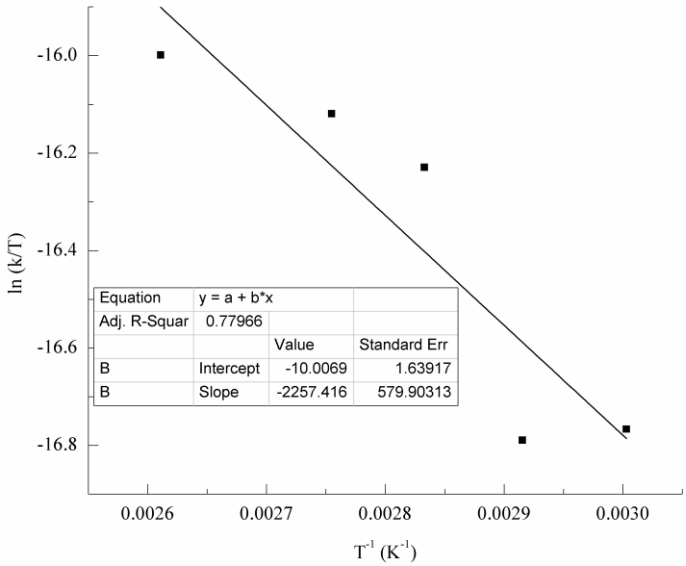

Figure 4. 10: Eyring plot of temperature dependence of rate constant of the ROP of ε-CL using complex **8**.

4.3.4 Molecular weight and molecular weight distribution of polymers

The molecular weight and molecular weight distribution of PCL and PLAs were determined by gel permeation chromatography (Tables 4.3–4.5). Generally, low to moderate molecular weights of up to 11 068 g mol^{-1} were obtained for PCL compared to a maximum molecular weight of 3 936 g mol^{-1} obtained for PLAs. The observed lower molecular weights in comparison to the theoretical values (Figure 4.12) points to substantial degree of intramolecular *trans*-esterification process (back-biting) during the polymerization reactions.[39,40] In addition, the broad molecular weight distributions reported were indicative of intermolecular *trans*-esterification reactions (Scheme 4.3). Indeed, analyses of the mass spectrum of a typical PCL gave *m/z* values corresponding to *n*(CL) + OH.[41] Despite the wide molecular weight distributions and side reactions observed, the increase in molecular weight of PCL with percentage conversion using complex **5** (Figure 4.12), established the "living" polymerization nature of the ROP reactions.

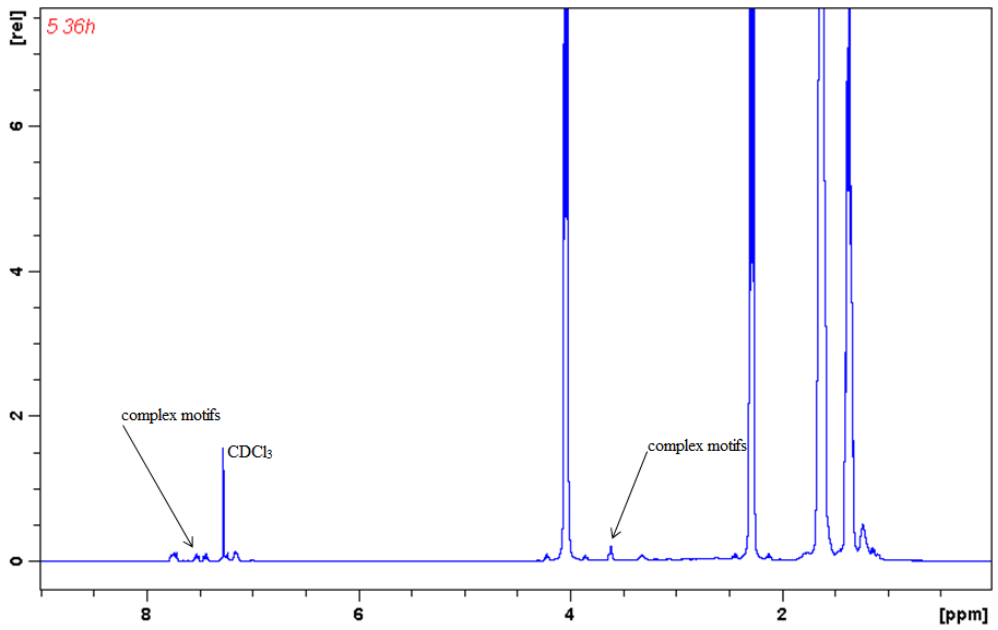

Figure 4. 11: ^{1}H NMR spectra of PCL obtained using complex **8** as catalyst.

To further support the "living" polymerization nature of **5**, increase in polymer molecular weight with increase in [CL]/[I] ratio was observed (Figure 4.12b and Table 4.4). Indeed, addition of a second ε-CL monomer after the first run without adding the initiator resulted in an increase in molecular weight from 7 012 g mol^{-1} to 11 068 g mol^{-1} respectively (Table 4.5, entries 1 and 8).

It was also evident that complex structure influenced the molecular weights of the PCL obtained. For example, molecular weights of 7 112 g mol^{-1} and 10 831 g mol^{-1} were obtained for complexes **5** and **7**, respectively. It is therefore conceivable to associate enhanced chain growth with increase in electrophilicity of the metal atom.

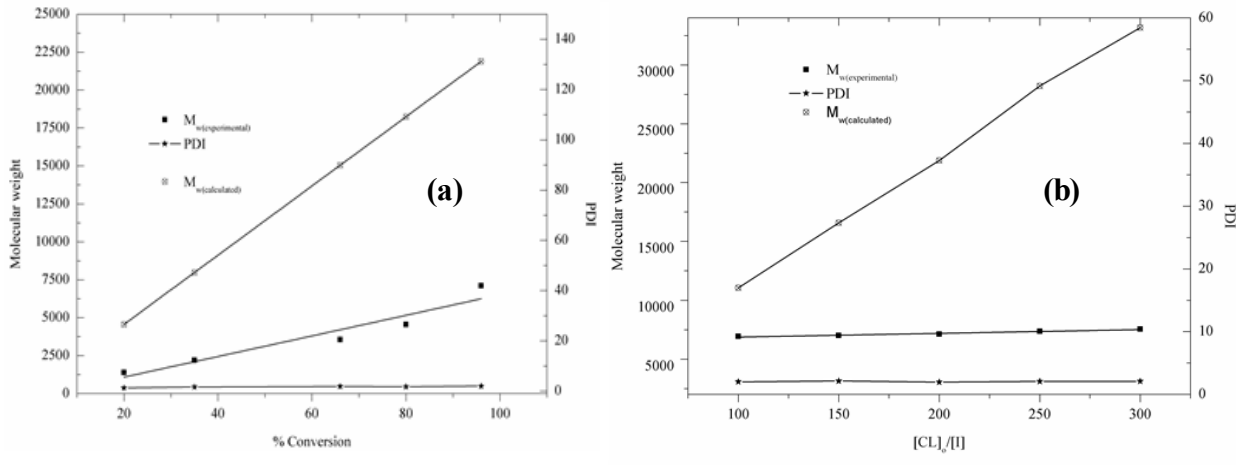

Figure 4. 12: Plot of experimental, theoretical molecular weight and PDI against (a) % conversion at fixed $[\varepsilon\text{-CL}]_o/[I]$ ratio of 200 and (b) different $[\varepsilon\text{-CL}]_o/[I]$ ratios, showing the living polymerization nature of complex **5** at 110 °C.

The dependency of molecular weight and molecular weight distributions on the identity of the initiator was assessed by comparing the values obtained in benzyl alcohol, methanol and in the absent of alcohol initiators. Interestingly, molecular weights obtained in benzyl alcohol (561 g mol^{-1}) and methanol (560 g mol^{-1}) were extremely low compared to molecular weights of 6 236 g mol^{-1} obtained in toluene (Table 4.5). Benzyl alcohol and methanol are known as chain transfer agents in ROP reactions thus promote chain termination to give low molecular weight polymers.[42] This observation correlates well with the lower rate constants of 0.0528 ± 0.0027 h^{-1} obtained in toluene compared to k_{app} of 0.0254 ± 0.0016 min^{-1} and 0.0246 ± 0.0012 min^{-1} recorded in benzyl alcohol and methanol solvents respectively. As expected, PCL obtained in benzyl alcohol (1.12) and methanol (1.10) exhibited narrow PDIs, respectively, compared to PDIs of 1.85 and 1.97 reported in toluene and bulk reactions respectively.

It was also observed an increase in PCL molecular weights with increase in reaction temperature for complex **8**. As an illustration, molecular weights of 10 063 g mol^{-1} and 7 711 g mol^{-1} were obtained at 110 °C and 90 °C respectively. These results agree with some literature reports[24,43] but contradict those by Dubois and co-workers[44,45] where higher molecular weights were reported at lower reaction temperatures. Generally, a decrease in PDI with decrease in reaction temperature was recorded, consistent with minimal side reactions at lower temperature (Table 4.5, entry 6).

4.3.5 Stereoselectivity of PLAs

Stereochemistry and tacticity of the PLAs were determined by inspecting the methine region of the homonuclear decoupled ^{1}H NMR and ^{13}C NMR spectroscopy (Figures 4.13 – 4.16). Peaks identities were based on assignments previously reported.[46,47] The occurrence of epimerization of $_{L}$-LA under our ROP reaction conditions was envisaged, thereby giving rise to traces of *isi*, *iis*, *sii* and *sis* tetrads (Figure 4.13). However, *iii* tetrad is predominant as seen in Figure 4.13 resulting in moderate isotactic PLA.[46,48] Figures 4.15 and 4.16 show homonuclear decoupled ^{1}H NMR and ^{13}C NMR spectra of PLA obtained from ROP of $_{D,L}$-LA , respectively. Predominantly atactic PLA were obtained consistent with interpretation of the NMR data. The probability of racemic enrichment, *Pr* of 0.64 and 0.69 was obtained for **5** and **8**, respectively based on calculations reported by Nomura and co-workers.[49]

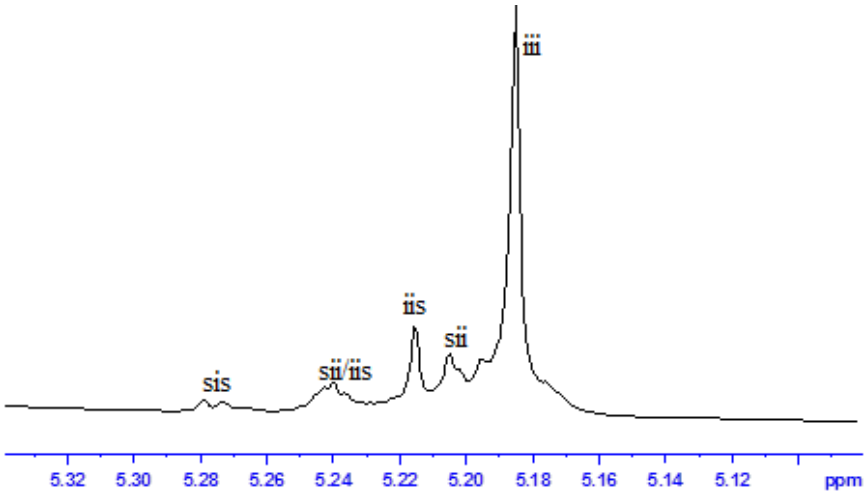

Figure 4. 13: ^{1}H homonuclear decoupled NMR of the methine region of poly(L-LA) showing moderate isotactic PLA.

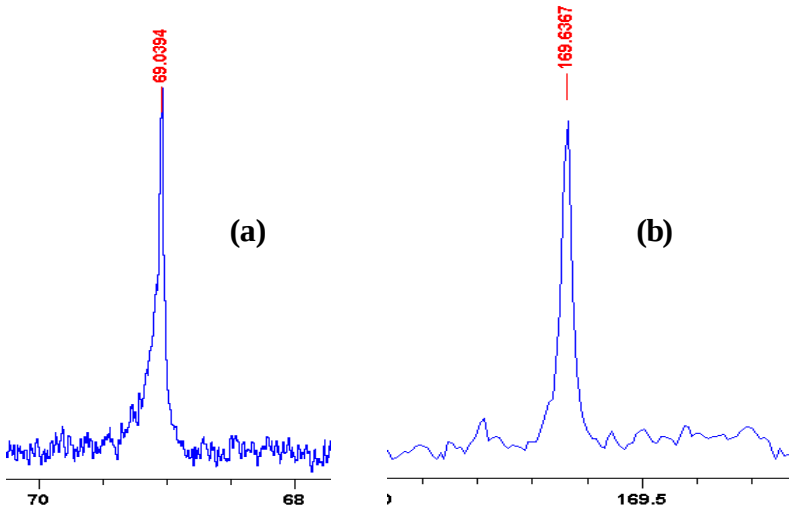

Figure 4. 14: (a) ^{13}C NMR methine region and (b) ^{13}C NMR spectra carbonyl region of poly(L-LA).

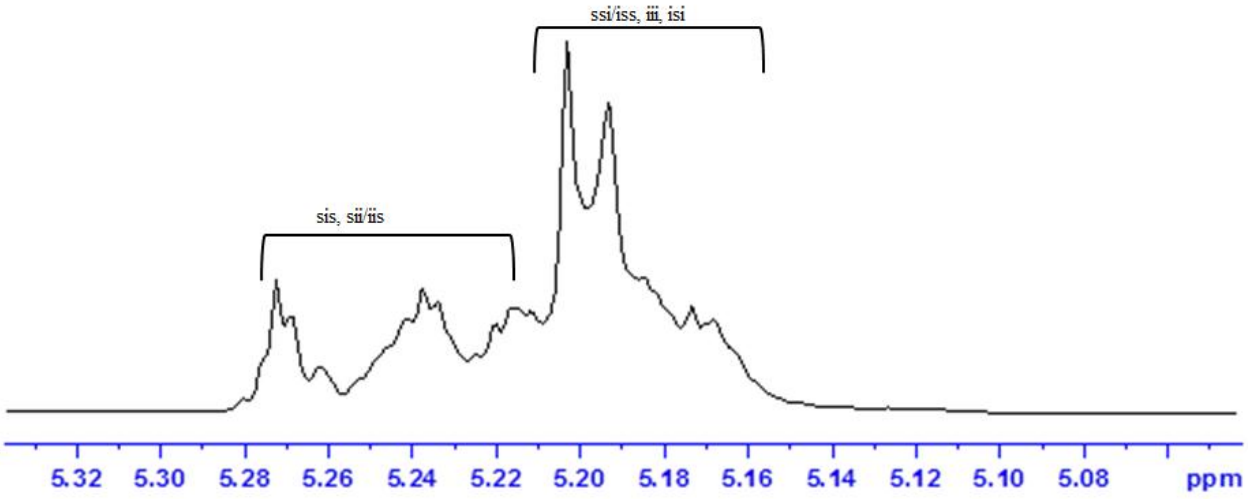

Figure 4. 15: ^{1}H homonuclear decoupled NMR of the methine region of poly($_{D,L}$-LA) showing atactic PLA.

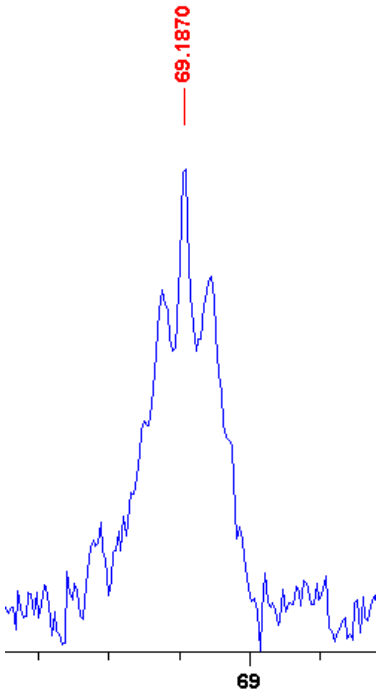

Figure 4. 16: ^{13}C NMR methine region of poly($_{D,L}$-LA).

4.4 Conclusions

In this chapter, Zn(II) and Cu(II) complexes bearing *N*,*N'* diarylformamidines and benzoate ligands was synthesized. The molecular structures of complexes **5, 6, 7** and **9** were confirmed by X-ray studies to adopt dinuclear species in which the ligands are monodentate. All the complexes formed active initiators in the ROP of ε-CL and LAs to afford moderate molecular weights polymers. Kinetic studies indicated a *pseudo*-first order dependency on monomer concentration. Activation parameters obtained from Eyring plot and ^{1}H NMR data point to a coordination-insertion mechanism of these ROP reactions.

Attempt was made to improve the control of the ROP reactions and polymer properties *via* the syntheses of alkoxides supported on benzimidazolyl ligands. The synthesis of Zn(II) alkoxides supported on benzimidazolyl ligands and their investigations as initiators in the ROP of ε-CL and LAs is described in chapter **5.**

4.5 References

(1) Hao, P.; Yang, Z.; Li, W.; Ma, X.; Roesky, H. W.; Yang, Y.; Li, J. *Organometallics* **2015**, *34*, 105.

(2) Dey, D.; Roy, S.; Purkayastha, R. N. D.; Pallepogu, R.; McArdle, P. *J. Mol. Struct*. **2013**, *1053*, 127.

(3) Jin, S.-W.; Ye, X.-H.; Jin, L.; Zheng, L.; Li, J.-W.; Jin, B.-P.; Wang, D.-Q. *Polyhedron* **2014**, *81*, 382.

(4) Policar, C.; Lambert, F.; Cesario, M.; Morgenstern-Badarau, I. *Eur. J. Inorg. Chem.* **1999**, 2201.

(5) Patra, A.; Sen, T. K.; Bhattacharyya, R.; Mandal, S. K.; Bera, M. *RSC Adv.* **2012**, *2*, 1774.

(6) Curtiss, A. B. S.; Bera, M.; Musie, G. T.; Powell, D. R. *Dalton Trans.* **2008**, 2717.

(7) Krajníková, A.; Gyepes, R.; Győryová, K.; Šubrt, J.; Imrich, J. *J. Chem. Cryst.* **2011**, *41*, 1036.

(8) Appavoo, D.; Omondi, B.; Guzei, I. A.; van Wyk, J. L.; Zinyemba, O.; Darkwa, J. *Polyhedron* **2014**, *69*, 55.

(9) Attandoh, N. W.; Ojwach, S. O.; Munro, O. Q. *Eur. J. Inorg. Chem.* **2014**, 3053.

(10) Ojwach, S. O.; Okemwa, T. T.; Attandoh, N. W.; Omondi, B. *Dalton Trans.* **2013**, *42*, 10735.

(11) Elkin, T.; Kulkarni, N. V.; Tumanskii, B.; Botoshansky, M.; Shimon, L. J. W.; Eisen, M. S. *Organometallics* **2013**, *32*, 6337.

(12) Taylor, E. C.; Ehrhart, W. A. *J. Org. Chem.* **1963**, *28*, 1108.

(13) Bruker *APEXII Bruker AXS Inc.* **2009**, *Madison, Wisconsin, USA*.

(14) Bruker *SAINT Bruker AXS Inc.* **2009**, *Madison, Wisconsin, USA*.

(15) Bruker *Bruker SADABS Bruker AXS Inc.* **2009**, *Madison, Wisconsin, USA*.

(16) Sheldrick, G. *Acta Crystallogr. Sect. A* **2008**, *64*, 112.

(17) Farrugia, L. *J. Appl. Crystallogra.* **2012**, *45*, 849.

(18) Komber, H.; Limbach, H.-H.; Böhme, F.; Kunert, C. *J. Am. Chem. Soc.* **2002**, *124*, 11955.

(19) Meschede, L.; Limbach, H. H. *J. Phys. Chem.* **1991**, *95*, 10267.

(20) Diop, M.; Aly-Gaye, P.; Bouyagui-Tamboura, F.; Gaye, M.; Pérez-Lourido, P.; Valencia, L.; Castro, G. *Z. Anorg. Allg. Chem*. **2014**, *640*, 1392.

(21) Devereux, M.; O'Shea, D.; O'Connor, M.; Grehan, H.; Connor, G.; McCann, M.; Rosair, G.; Lyng, F.; Kellett, A.; Walsh, M.; Egan, D.; Thati, B. *Polyhedron* **2007**, *26*, 4073.

(22) Yuan, G.; Huo, Y.; Nie, X.; Jiang, H.; Liu, B.; Fang, X.; Zhao, F. *Dalton Trans.* **2013**, *42*, 2921.

(23) Xiao, B.; Xiao, H.-Y.; Chen, M.-D. *J. Coord. Chem*. **2014**, *67*, 2455.

(24) Attandoh, N. W.; Ojwach, S. O.; Munro, O. Q. *Eur. J. Inorg. Chem*. **2014**, 3053.

(25) Obuah, C.; Lochee, Y.; Jordaan, J. H. L.; Otto, D. P.; Nyokong, T.; Darkwa, J. *Polyhedron* **2015**, *90*, 154.

(26) Sreehari, N.; Varghese, B.; Manoharan, P. T. *Inorg. Chem*. **1990**, *29*, 4011.

(27) Chen, F. J., Xu, H., Xu, H. and Huang, K. L. *Acta Cryst. E* **2009**, *65*, m540.

(28) Stephens, J. C.; Khan, M. A.; Houser, R. P. *Inorg. Chem*. **2001**, *40*, 5064.

(29) Wu, J.-C.; Huang, B.-H.; Hsueh, M.-L.; Lai, S.-L.; Lin, C.-C. *Polymer* **2005**, *46*, 9784.

(30) Hormnirun, P.; Marshall, E. L.; Gibson, V. C.; Pugh, R. I.; White, A. J. P. *Proc. Natl Acad. Sci. (USA)* **2006**, *103*, 15343.

(31) Bhunora, S.; Mugo, J.; Bhaw-Luximon, A.; Mapolie, S.; Van Wyk, J.; Darkwa, J.; Nordlander, E. *Appl. Organomet. Chem*. **2011**, *25*, 133.

(32) Duda, A.; Kowalski, A. In *Handbook of Ring-Opening Polymerization*; Wiley-VCH Verlag GmbH & Co. KGaA, 2009.

(33) Buffet, J.-C.; Davin, J. P.; Spaniol, T. P.; Okuda, J. *New J. Chem*. **2011**, *35*, 2253.

(34) Chisholm, M. H.; Eilerts, N. W.; Huffman, J. C.; Iyer, S. S.; Pacold, M.; Phomphrai, K. *J. Am. Chem. Soc.* **2000**, *122*, 11845.

(35) Schmidt, S.; Schulz, S.; Bläser, D.; Boese, R.; Bolte, M. *Organometallics* **2010**, *29*, 6097.

(36) Ikpo, N.; Hoffmann, C.; Dawe, L. N.; Kerton, F. M. *Dalton Trans.* **2012**, *41*, 6651.

(37) Chisholm, M. H.; Gallucci, J. C.; Krempner, C. *Polyhedron* **2007**, *26*, 4436.

(38) Sun, H.; Ritch, J. S.; Hayes, P. G. *Dalton Trans.* **2012**, *41*, 3701.

(39) Labet, M.; Thielemans, W. *Chem. Soc. Rev*. **2009**, *38*, 3484.

(40) Dubois, P.; Dubois, P.; Coulembier, O.; Raquez, J. M. *Handbook of Ring-Opening Polymerization*; Wiley, 2009.

(41) Chamberlain, B. M.; Cheng, M.; Moore, D. R.; Ovitt, T. M.; Lobkovsky, E. B.; Coates, G. W. *J. Am. Chem. Soc.* **2001**, *123*, 3229.

(42) Liu, Y.-C.; Ko, B.-T.; Lin, C.-C. *Macromolecules* **2001**, *34*, 6196.

(43) Zhang, L.; Niu, Y.; Wang, Y.; Wang, P.; Shen, L. *J. Mol. Catal. A: Chem*. **2008**, *287*, 1.

(44) Dubois, P.; Jacobs, C.; Jerome, R.; Teyssie, P. *Macromolecules* **1991**, *24*, 2266.

(45) Parvez, M. A.; Rahaman, M.; Suleiman, M. A.; Soares, J. B. P.; Hussein, I. A. *Int. J. Poly. Sci.* **2014**, *2014*, 10.

(46) Ovitt, T. M.; Coates, G. W. *J. Polym. Sci. Part A: Polym. Chem*. **2000**, *38*, 4686.

(47) Zell, M. T.; Padden, B. E.; Paterick, A. J.; Thakur, K. A. M.; Kean, R. T.; Hillmyer, M. A.; Munson, E. J. *Macromolecules* **2002**, *35*, 7700.

(48) Yang, Y.; Wang, H.; Ma, H. *Inorg. Chem*. **2015**, *54*, 5839.

(49) Nomura, N.; Ishii, R.; Yamamoto, Y.; Kondo, T. *Chem. – Eur. J.* **2007**, *13*, 4433.

Chapter 5

Kinetics, mechanisms and polymer property studies of ring-opening polymerization of ε-caprolactone and lactides initiated by (benzimidazolylmethyl)amine Zn(II) alkoxides

5.1 Introduction

Many metal alkoxide systems supported with various well-tailored ligands such as pyrazolone ketiminate,[1,2] bisphenolate, β-diketiminate, schiff base, amino-bis(phenolate),[3,4] have been reported to achieve impressive catalytic activities for ROP reactions in a well-controlled manner. The alkoxide based catalysts have been of great interest due to their unexpectedly diverse structures, together with the metal-oxygen bonds playing an important role in the ROP of ε-CL and LAs to the polymers.[5]

Most promising Zn(II) based initiators employed in the ROP reactions of cyclic esters are homogeneous Zn(II) alkoxides complexes due in part, to high rates of reaction, good selectivity and favorable properties of the metal ion such as lower toxicity.[6,7,8,9,10] Inoue and co-workers[6,11] were among the first to describe the use of diethylzinc with protic reagents to prepare *in situ* the alkoxide initiating system. However, in many of the zinc based complexes employed in the ROP of cyclic esters, undesired side reactions take place, impeding control over the ROP processes.[12,13,14] As a result, there is continued search for new initiators/catalysts that can yield well defined PCL and PLA.

Benzimidazole derivatives are known to be important class of ligands in coordination chemistry.[15] A series of Pd(II), Ni(II), Cu(II) and Zn(II) complexes ligated by benzimidazoles derivatives have been synthesized and has application in catalysis.[15,16,17] The ability to functionalize the aryl ring can turned the electronic and steric properties of the ligand backbone, which also impact on the coordination geometry around the metal centers it complexes and also envisaged to impact on the properties on the resulting polymers.

Attempts to improve the control of the ROP reactions and polymer properties reported in chapters **3** and **4** were made by the syntheses of Zn(II) alkoxides supported on benzimidazolyl ligands. This chapter reports the synthesis, characterization of Zn(II) alkoxide complexes of (benzimidazolylmethyl)amine ligands, as well as their catalytic activities towards ROP reactions ε-CL, $_{L}$–LA and $_{D, L}$–LA monomers.

5.2 Experimental section

5.2.1 Materials and reagents

All manipulations were carried out under a dry argon atmosphere except stated otherwise. Solvents (ACS reagent grades ≥ 99.5%) were dried by refluxing at least 24 h over sodium/benzophenone (hexane, DCM and tetrahydrofuran (THF), and reagent grade ethanol was distilled and dried from magnesium turnings. The monomers (ε-CL and LAs; 99%), $ZnEt_2$ (1.0 M in hexane), BnOH (anhydrous 99.8%), *t*-BuOH (anhydrous ≥ 99.5%), 2-(chloromethyl)benzimidazole (96%), 2,6-dimethylaniline (99%), 2,6-diisopropylaniline (97%), 2,4,6-trimethylaniline (98%), KI and KOH were purchased from Sigma Aldrich and used without further purification.

5.2.2 Instrumental characterization techniques

^{1}H and ^{13}C NMR spectra were measured at room temperature using a Bruker 400 MHz spectrometer. ^{1}H NMR data were recorded in $CDCl_3$ listed as residual internal $CDCl_3$ (δ 7.26). Similarly, ^{13}C NMR data were recorded in $CDCl_3$ listed as residual internal $CDCl_3$ (δ 77.00). Mass spectra of compounds were obtained from a Water synapt GR electrospray positive spectrometer. Synthesized polyester samples were analyzed by size exclusion chromatography at Stellenbosch University. Thermogravimetric analyses (TGA) were done on a TGA SDT Q600 V20.9 Build 20 modulus coupled with a thermal analyzer. The differential scanning calorimetric (DSC) measurements of dried samples were performed from 30 to 500 °C at a heating rate of 10 °C/min on a TA Instrument (TGA SDT Q600 V20.9 Build 20). An aluminum pan was loaded with ca. 5 mg of sample and heating ramped at 10 °C/min under a nitrogen atmosphere at a flow rate of (50 ml/min). A pinhole on the lid was made to prevent pressure build up due to gaseous products. The thermal analytical data was collected between 30 to 500 °C.

5.2.3 Typical procedure for the synthesis of (benzimidazolylmethyl) amine ligands

Equimolar amounts of 2-(chloromethyl)benzimidazole, KI and the respective amine were dissolved in ethanol (20 mL) and heated to reflux for 6 h at 80 °C. This was followed by addition of an equimolar amount of KOH and reflux was continued for a further 2 h. The reaction mixture was cooled to room temperature and poured into ice-cold water and stirred to give a precipitates. The precipitate was filtered and dried to yield the products.

5.2.3.1 *N*-((1H-benzo[s]imidazol-2-yl)methyl)-2,6-dimethylaniline (L4)

2-(chloromethyl)benzimidazole (0.50 g, 3.00 mmol), KI (0.50 g, 3.00 mmol), 2,6-dimethylaniline (0.36 g, 0.37 mL, 3.00 mmol) and KOH (0.17 g, 3.00 mmol) were reacted to give **L4** as a pale-yellow solid. (0.61 g, 81%). ^{1}H NMR ($CDCl_3$, 400 MHz): δ (ppm) 2.31 (s, 6H, CH_3), 4.45 (s, 2H, CH_2), 6.95 (t, ^{3}J = 7.5 Hz, 1H, Ar), 7.06 (d, ^{3}J = 7.5 Hz, 2H, Ar), 7.29 (m, 2H, Ar), 7.61 (m, 2H, Ar). ^{13}C NMR ($CDCl_3$, 400 MHz) δ (ppm) 153.3, 144.8, 130.2, 129.1, 123.3, 122.6, 46.7, 18.3. IR (Nujol): ν = 2927 (w), 1630 (m), 1533 (s), 1428 (s). ESI-TOF MS: *m/z* calculated for $C_{16}H_{17}N_3$ [M + H^+] 252.33; found 252.15. Anal. Calcd. For $C_{16}H_{17}N_3$: C, 76.46; H, 6.83; N, 16.72. Found: C, 76.40; H, 6.79; N, 16.69.

5.2.3.2 *N*-((1H-benzo[*d*]imidazol-2-yl)methyl)-2,6-diisopropylaniline (L5)

2-(chloromethyl)benzimidazole (0.50 g, 3.00 mmol), KI (0.50 g, 3.00 mmol), 2,6-diisopropylaniline (0.53 g, 0.56 mL, 3.00 mmol) and KOH (0.17 g, 3.00 mmol) were reacted to give **L5** as a pale-yellow solid. (0.82 g, 88%). ^{1}H NMR ($CDCl_3$, 400 MHz): δ (ppm) 1.26 (d, 12H, CH_3), 3.34 (m, 2H, CH), 4.39 (s, 2H, CH_2), 7.17 (s, 3H, Ar), 7.30 (m, 3H, Ar), 7.49 (t, 1H, Ar), 7.78 (t, 1H, Ar), 9.73 (1H, NH). ^{13}C NMR ($CDCl_3$, 400 MHz) δ (ppm) 152.9, 142.9, 141.6, 125.0, 123.9, 49.9, 27.8, 24.2. IR (Nujol): ν = 3354 (w), 2960 (s), 2869 (m), 1630 (m), 1544 (w), 1457 (s), 1432 (s). ESI-TOF MS: *m/z* calculated for $C_{20}H_{25}N_3$ [M + H^+] 308.43; found 308.58 Anal. Calcd. For $C_{20}H_{25}N_3$: C, 78.14; H, 8.20; N, 13.67. Found: C, 78.30; H, 8.29; N, 13.69.

5.2.3.3 *N*-((1H-benzo[*d*]imidazol-2-yl)methyl)-2,4,6-trimethylaniline (L6)

2-(chloromethyl)benzimidazole (0.50 g, 3.00 mmol), KI (0.50 g, 3.00 mmol), 2,4,6-trimethylaniline (0.41 g, 0.43 mL, 3.00 mmol) and KOH (0.17 g, 3.00 mmol) were reacted to

give **L6** as a pale-yellow solid. (0.72 g, 90%). ^{1}H NMR ($CDCl_3$, 400 MHz): δ (ppm) 2.27 (s, 6H, CH_3), 4.40 (s, 2H, CH_2), 6.88 (s, 2H, Ar), 7.29 (m, 3H, Ar), 7.44 (b, 1H, Ar), 7.76 (1H, Ar), 9.83 (s, 1H, NH). ^{13}C NMR ($CDCl_3$, 400 MHz) δ (ppm) 153.4, 143.4, 132.8, 130.5, 129.7, 122.9, 122.3, 119.4, 110.7, 46.9, 20.6, 18.1. IR (Nujol): ν = 2908 (m), 1630 (s), 1481 (s), 1420 (s). ESI-TOF MS: *m/z* calculated for $C_{17}H_{19}N_3$ [M + H^+] 266.35; found 266.25. Anal. Calcd. For $C_{17}H_{19}N_3$: C, 76.95; H, 7.22; N, 15.84. Found: C, 76.70; H, 7.29; N, 15.69.

5.2.4 Synthesis of (benzimidazolylmethyl) amine Zn(II) complexes

To a solution of benzyl alcohol (2 mmol) in dry THF (20 mL) at 0 °C under Ar was added drop wise $ZnEt_2$ (1 mmol equivalent) and the resulting solution was stirred at room temperature for 12 h. The mixture was further cooled to 0 °C and a solution of the respective ligand (1 mmol equivalent) in dry THF was added slowly and the mixture stirred at room temperature for further 24 h. Volatiles were removed under vacuum, and the product washed with DCM and hexane to afford the respective Zn(II) complexes **10**–**12**.

5.2.4.1 [(L4)Zn(OBn)]$_2$ (10)

Following the general procedure (**5.2.4**), **L4** (0.30 g, 1.19 mmol), benzyl alcohol (0.26 g, 0.25 mL) and $ZnEt_2$ (1.19 mL) were used as reagents. Pale yellow solid (0.85 g, 84%). ^{1}H NMR ($CDCl_3$, 400 MHz): δ (ppm) 2.14 (s, 12H, CH_3), 4.26 (s, 4H, NCH_2), 4.59 (s, 4H, CH_2Ph), 6.82 (t, 2H, Ar), 6.93 (d, ^{3}J = 7.44 Hz, 4H, Ar), 7.29 (m, 14H, Ar), 7.61 (b, 4H, Ar), 10.22 (s, 2H, NH). ^{13}C NMR ($CDCl_3$, 400 MHz) δ (ppm) 153.4, 144.8, 143.1, 141.0, 133.3, 130.3, 129.1, 128.5, 127.6, 127.6, 123.1, 122.6, 65.1, 46.6, 18.2. Anal. Calcd. For $C_{46}H_{46}N_6O_2Zn_2 \cdot 2CH_2Cl_2$: C, 56.77; H, 4.96; N, 8.28. Found: C, 57.02; H, 5.12; N, 8.58.

5.2.4.2 $[(L5)Zn(OBn)]_2$ (11)

Following the typical procedure (**5.2.4**), **L5** (0.50 g, 1.63 mmol), benzyl alcohol (0.34 g, 0.33 mL) and $ZnEt_2$ (1.63 mL) were used as reagents. Pale yellow solid (1.00 g, 64%). ^{1}H NMR ($CDCl_3$, 400 MHz): δ (ppm) 1.13 (d, ^3J = 6.92 Hz, 24H, CH_3), 3.19 (m, 4H, CH), 4.27 (d, 4H, NCH_2), 4.61 (s, 4H, CH_2Ph), 7.05 (s, 6H, Ar), 7.29 (m, 16H, Ar), 7.35 (t, 2H, Ar), 7.66 (t, 2H, Ar), 10.03 (s, 2H, NH). ^{13}C NMR ($CDCl_3$, 400 MHz) δ (ppm) 152.9, 143.3, 142.9, 141.6, 140.9, 133.2, 128.5, 127.6, 126.9, 124.9, 123.8, 122.9, 119.3, 110.7, 65.2, 49.8, 27.8, 24.2. Anal. Calcd. For $C_{54}H_{65}N_6O_2Zn_2 \cdot 2CH_2Cl_2$: C, 59.64; H, 5.90; N, 7.45. Found: C, 59.97; H, 5.96; N, 7.74.

5.2.4.3 $[(L6)Zn(OBn)]_2$ (12)

Following the general procedure (**5.2.4**), **L6** (0.45 g, 1.88 mmol), benzyl alcohol (0.37 g, 0.35 mL) and $ZnEt_2$ (1.69 mL) were used as reagents. Yellow solid (0.97 g, 66%). ^{1}H NMR ($CDCl_3$, 400 MHz): δ (ppm) 2.21 (s, 12H, CH_3), 2.26 (s, 6H, CH_3), 4.33 (s, 4H, NCH_2), 4.76 (s, 4H, CH_2Ph), 6.84 (s, 5H, Ar), 7.58 (m, 19H, Ar), 10.77 (b, 2H, Ar). ^{13}C NMR ($CDCl_3$, 400 MHz) δ (ppm) 153.5, 142.1, 141.1, 132.6, 130.4, 129.6, 128.5, 127.5, 126.6, 122.5, 64.9, 46.7, 20.6, 18.0. Anal. Calcd. For $C_{48}H_{50}N_6O_2Zn_2 \cdot CH_2Cl_2$: C, 61.39; H, 5.47; N, 8.77. Found: C, 60.98; H, 5.77; N, 8.52

5.2.4.4 $[(L5)Zn(t\text{-}BuO)]_2$ (13)

To a solution of *t*-BuOH (2 mmol, 0.14 g, 0.12 mL) in dry toluene (15 mL) at -78 °C was added drop wise $ZnEt_2$ (1 mmol,1.63 mL) and the resulting solution was warmed to room temperature and stirred for 3 h. **L5** (0.25 g, 0.81 mmol) in toluene (10 mL) was then added and the mixture

heated at 70 °C for 6 h. Volatiles were removed under vacuum, and the residue washed with hexane to afford complex **13**. Light yellow solid (0.97 g, 76%). ^{1}H NMR ($CDCl_3$, 400 MHz): δ (ppm) 1.30 (d, ^{3}J = 6.82 Hz, 24H, CH_3), 1.59 (s, 18H, CH_3), 2.98 (m, 4H, CH), 3.87 (s, 4H, CH_2), 6.83 (t, 1H, Ar), 7.06 (d, 2H, ^{3}J = 7.82 Hz Ar), 7.17 (s, 2H, Ar), 7.31 (, 2H, ^{3}J = 7.44 Hz Ar), 9.53 (b, 2H, NH). ^{13}C NMR ($CDCl_3$, 400 MHz) δ (ppm) 153.0, 142.5, 141.6, 132.4, 126.6, 120.9, 119.5, 110.7, 48.9, 27.9, 24.3,22.4. Anal. Calcd. For $C_{48}H_{66}N_6O_2Zn_2$: C, 64.78; H, 7.48; N, 9.44. Found: C, 64.95; H, 7.91; N, 9.55

5.2.5 Typical procedure for ROP of ε-CL

An appropriate amount of the complex was dissolved in toluene in a Schlenk tube immersed in pre-heated oil bath at 110 °C, and ε-CL monomer (1.14 g, 0.01 mol) was added and the reaction was initiated by stirring. Kinetics experiments were carried out by withdrawing samples at regular interval using a syringe and quenched quickly by rapid cooling into NMR tube containing $CDCl_3$ solvent using ice water. The quenched samples were analyzed by ^{1}H NMR spectroscopy for determination of polymerization of ε-CL to PCL. The percentage conversion of $[PCL]/[CL]_o \times 100$, where $[CL]_o$ is the initial concentration of the monomer and [PCL] is the concentration of the polymer at time t, was evaluated by integration of the peaks for CL (4.2 ppm, OCH_2 signal) and PCL (4.0 ppm, OCH_2 signal) according to the equation $[PCL]/[CL]_o = I_{4.0}/(I_{4.2} + I_{4.0})$ where $I_{4.2}$ is the intensity of the CL monomer signal at 4.2 ppm and $I_{4.0}$ is the intensity of PCL signal at 4.0 ppm for OCH_2 protons. The observed rate constants were extracted from the slope of the line of best-fits of the plot of $\ln[CL]_o/[CL]_t$ *vs*. time.

5.2.6 Typical procedure for polymerization of $_{D,L}$-LA and $_{L}$-LA

A suitable LA (1.44 g, 0.01 mol) was dissolved in toluene in a Schlenk tube equipped with magnetic stirrer under argon and the required amount of complex was added. The reaction mixture was stirred at 110 °C. Kinetics experiments were carried out by withdrawing samples at regular interval using a syringe and quenched quickly by rapid cooling into NMR tube containing $CDCl_3$ solvent using ice water. The quenched samples were analyzed by ^1H NMR spectroscopy for determination of polymerization of LAs to PLA. The integration values of the methine proton of the monomer and that of the polymer were used to calculate the percentage conversion using the equation 5.1.

$$\% \text{ Conversion} = \frac{I_{CH_{polymer}}}{I_{CH_{monomer}} + I_{CH_{polymer}}} \times 100 \qquad (5.1)$$

$I_{CH_{polymer}}$ = Intensity of the methine of the polymer obtained from proton NMR

$I_{CH_{monomer}}$ = Intensity of the methine of the monomer obtained from proton NMR

5.2.7 Polymer characterization by size exclusion chromatography (SEC)

The samples were analyzed by SEC at Stellenbosch University. The samples were dissolved in BHT stabilized THF (2 mg/ml). Sample solutions were filtered *via* syringe through 0.45 µm nylon filters before subjected to analysis. The SEC instrument consists of a Waters 1515 isocratic HPLC pump, a Waters 717 plus auto-sampler, Waters 600E system controller (run by Breeze Version 3.30 SPA) and a Waters in-line Degasser AF. A Waters 2414 differential refractometer was used at 30 °C in series with a Waters 2487 dual wavelength absorbance

UV/Vis detector operating at variable wavelengths. Tetrahydrofuran (THF, HPLC grade, stabilized with 0.125% BHT) was used as eluent at flow rates of 1 ml min^{-1}. The column oven was kept at 30 °C and the injection volume was 100 µl. Two PLgel (Polymer Laboratories) 5 µm Mixed-C (300 × 7.5 mm) columns and a pre-column (PLgel 5 µm Guard, 50 × 7.5 mm) were used. Calibration was done using narrow polystyrene standards ranging from 580 to 2 × 10^6 g mol^{-1}. All molecular weights were reported as polystyrene equivalents and corrected by a factor of 0.58 and 0.56 for PCL and PLAs, respectively

5.3 Results and discussion

5.3.1 Synthesis of (benzimidazolylmethyl) amine ligands

The (benzimidazolylmethyl) amine ligands, *N*-((1H-benzo[*d*]imidazol-2-yl)methyl)-2,6-dimethylaniline (**L4**), *N*-((1H-benzo[*d*]imidazol-2-yl)methyl)-2,6-diisopropylaniline (**L5**) and *N*-((1H-benzo[*d*]imidazol-2-yl)methyl)-2,4,6-trimethylaniline (**L6**) were synthesized by using a modified literature procedure[18] as presented in Scheme 5.1.

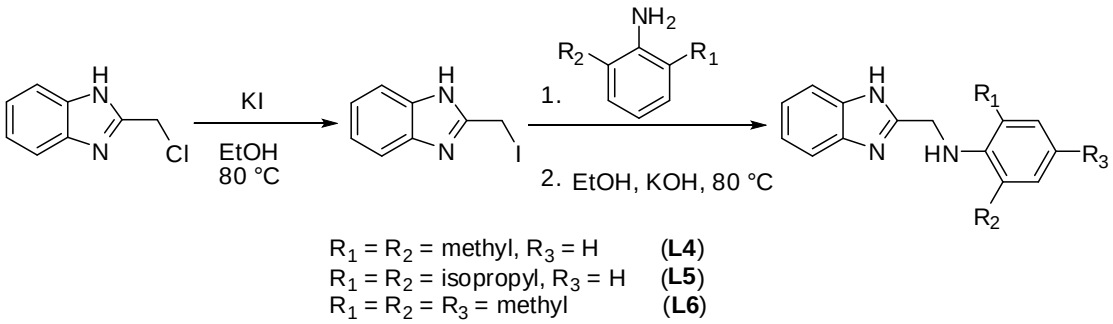

Scheme 5. 1: Synthesis of (benzimidazolylmethyl) amine ligands.

The compounds were isolated in good yields (83-85%) as pale-yellow solids and the identities of the compounds were established by ^1H and ^{13}C NMR, FTIR spectroscopy and mass

spectrometry. The NMR spectral signals were consistent with the respective proposed structures. For example, the ^{1}H NMR spectrum of the ligand **L4** exhibited signals at 4.45 ppm for the proton of CH_2 in the $–CH_2–NH–Ar$ backbone and the corresponding ^{13}C NMR spectral signal was around 46.70 ppm, which differ from those of the 2-(chloromethyl)benzimidazole starting material, indicating the formation of the desired ligand.

5.3.2 Synthesis and characterization of Zn(II) alkoxide complexes of (benzimidazolylmethyl) amine ligands L4–L6

Synthesis of Zn(II) alkoxide complexes **10**–**13** bearing (benzimidazolylmethyl) amine ligands **L4**–**L6** is shown in Scheme 5.2. Treatment of **L4**–**L6**, respectively, with BnOH and $ZnEt_2$, in THF at 0 °C for 24 h afforded complexes **10**–**12,** respectively. Also, treatment of **L5** with *t*-BuOH and $ZnEt_2$, in toluene at –78 °C and later heated to 70 °C for 6 h afforded complex **13.** Each of the complexes **10**–**13** was purified by recrystallizing from hexane and isolated as yellow (**10**–**12**) and light yellow (**13**) solids, respectively, in good yields. Compounds **10**–**13** were characterized ^{1}H and ^{13}C NMR spectroscopy, FT-IR, mass spectroscopy and elemental analyses. The elemental analysis of each of **10**–**13** was slightly different from the calculated values.

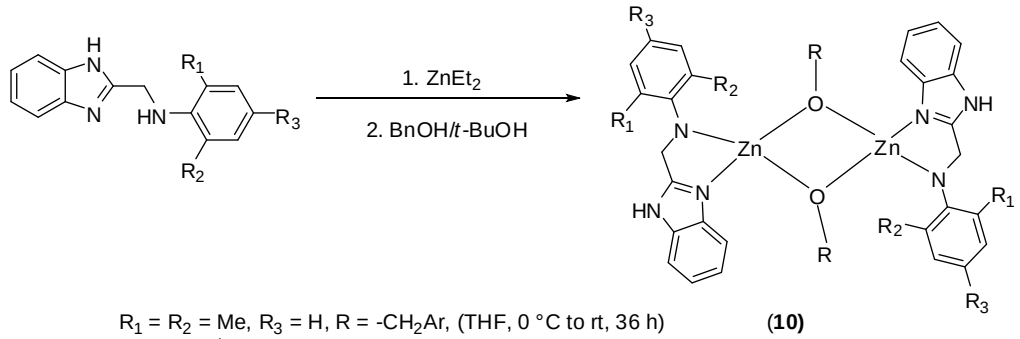

$R_1 = R_2 = Me$, $R_3 = H$, $R = -CH_2Ar$, (THF, 0 °C to rt, 36 h) (**10**)
$R_1 = R_2 = {}^{i}Pr$, $R_3 = H$, $R = -CH_2Ar$, (THF, 0 °C to rt, 36 h) (**11**)
$R_1 = R_2 = R_3 = Me$, $R = -CH_2Ar$, (THF, 0 °C to rt, 36 h) (**12**)
$R_1 = R_2 = {}^{i}Pr$, $R_3 = H$, $R = (CH_3)_3C$, (toluene, -78 °C to 70 °C, 9 h) (**13**)

Scheme 5. 2: Synthesis of complexes **10–13.**

In a typical ^{1}H NMR spectra, significant shifts of the ligand proton signals in the respective complexes relative to the respective free ligand signals was indicative of the formation of the Zn(II) complexes. For example, an upfield shift of the CH_2 proton in CH_2NH linkage from 4.40 ppm in **L6** to a resonance at 4.34 ppm was observed. In addition, the appearance of resonance of methylene hydrogen of the bridging benzyl alkoxides at 4.76 ppm in complex **12** indicated the formation of the alkoxide complexes (Figure 5.1). The ^{13}C NMR spectra of **12** (Figure 5.2) was significantly different from that of **L6**, and contain resonance peaks representative of the complex.

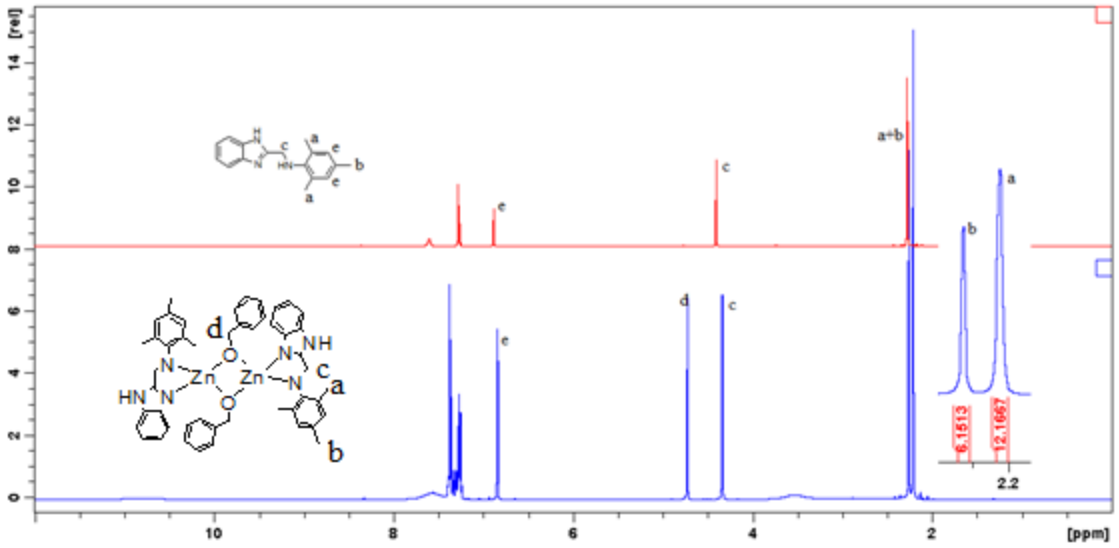

Figure 5. 1: ^{1}H NMR spectrum of ligand **L6** (top) and complex **12** (bottom) showing the appearance of resonance of methylene hydrogen of the bridging benzyl alkoxides at 4.76 ppm indicative of complex formation.

Typical IR spectra of complexes **10**–**13** showed shifts of the C=N bands to higher frequencies with respect to the ligands. For example, the C=N band of **L6** was recorded at 1576 cm^{-1} compared to 1601 cm^{-1} observed for the corresponding complex **12**. Strong bands associated with the *ν*(C-O) stretch around 1320, 1340, 1336 and 1343 cm^{-1} in complexes **10**, **11**, **12** and **13,** respectively, were also obtained. This suggested that the oxygen from the benzyl alcohol derivative coordinated to the Zn atom centers.[19]

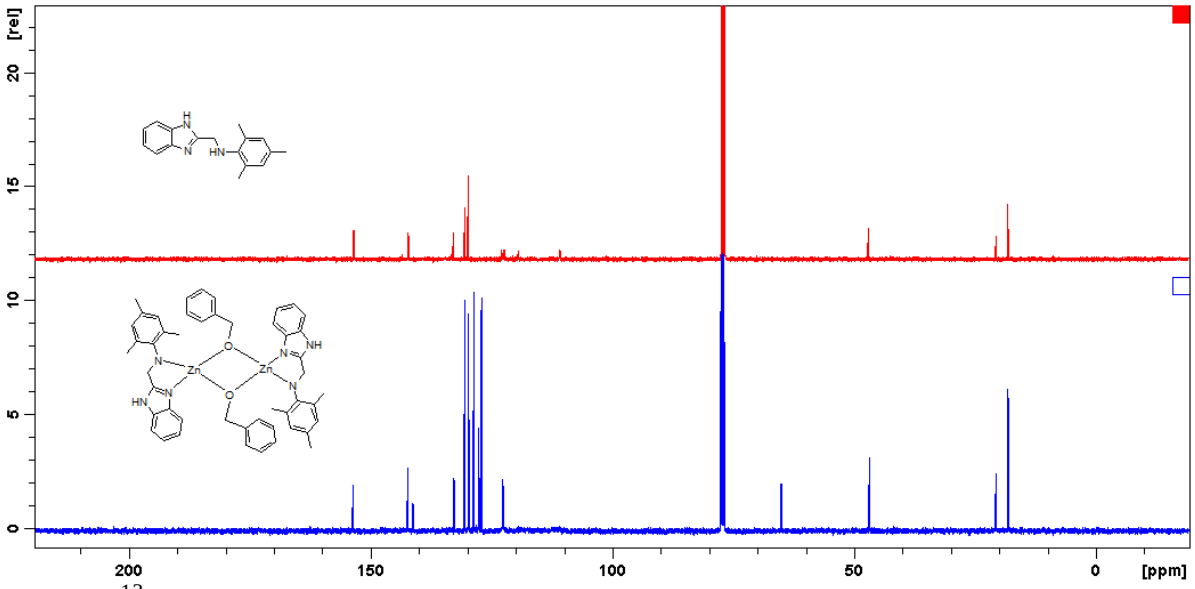

Figure 5. 2: ^{13}C NMR spectrum of ligand **L6** (top) and complex **12** (bottom) showing significant differences.

All the complexes were also characterized by mass spectroscopy and *m/z* values corresponding to various fragments of the complexes were observed. For example, the mass spectrum of complex **12** showed *m/z* peaks at 531 amu, 468 amu and a base peak at 266 amu (Figure 5.3) corresponding to $[C_{25}H_{29}N_3O_2Zn_2]^+$, $C_{20}H_{26}N_3O_2Zn_2$ and ligand **L6** fragments, respectively. Micro-analyses data of compounds **10**–**13** with solvent molecules (CH_2Cl_2) were in good agreement with the proposed structures and confirmed the purity of the isolated compounds. So far, attempts to isolate crystals suitable for single X-ray analyses have been unsuccessful.

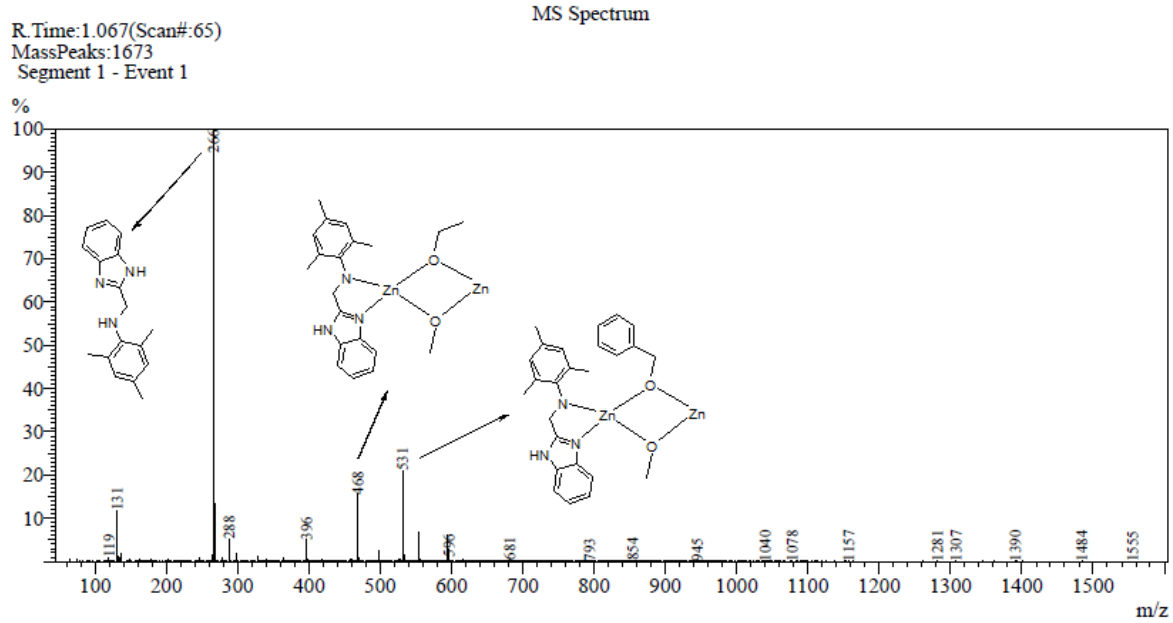

Figure 5. 3: Mass spectra showing complex **12** showing its fragmentation pattern to give a base peak at 266 amu corresponding to **L6** unit.

5.3.3 ROP of ε-CL and LAs using complexes 10–13 as catalysts

ROP reactions of ε–CL, $_{L}$–LA and $_{D,\ L}$–LA using complexes **10**–**13** generally progressed in toluene under a dry argon atmosphere and were systematically studied as listed in Table 5.1. The conversion of the monomers to the respective polymers at 110 °C using [M]/[I] ratio of 200 proceeded to near completion between 16 h to 36 h for complexes **10**–**13** (Table 5.1, entries 1–10). For example, complex **12** gave a conversion of 98% within 18 h for ε-CL, 95% within 16 h and 18 h for $_{D,L}$-LA and $_{L}$-LA, respectively (Table 5.1, entries 3, 7 and 10).

Table 5. 1: ROP data of ε-CL and LAs catalyzed by Zn(II) alkoxide complexes **10–13**[a]

Entry	Catalyst	Time (h)	Conversion[b] (%)	k_{app} (h^{-1})	M_w (GPC)[c]	PDI[c]	IE[d]
1	**10**	20	98	0.1839 ±0.0092	4456	1.34	0.20
2	**11**	26	96	0.1152 ±0.00582	3841	1.46	0.18
3	**12**	18	98	0.1988 ±0.0119	4744	1.38	0.21
4	**13**	32	97	0.1034 ±0.0065	nd	nd	–
5[e]	**10**	18	95	0.1556 ±0.00602	8326	1.24	0.30
6[e]	**11**	18	98	0.1974 ± 0.01	8675	1.34	0.31
7[e]	**12**	16	99	0.2715 ±0.0184	10650	1.33	0.37
8[f]	**10**	24	95	0.1258 ±0.00286	3946	1.53	0.14
9[f]	**11**	36	95	0.0818 ±0.00245	5428	1.29	0.20
10[f]	**12**	18	98	0.1390 ±0.00627	5678	1.16	0.20

[a]Reaction conditions: $[CL]_o/[I]$ = 200; solvent, toluene, temperature, 110 °C. [b]Maximum conversion achieved [c]Molecular-weight average and Polydispersity index (PDI) determined by GPC relative to polystyrene standard, values are the values obtained from GPC × correction factor of 0.56 for lactones and 0.58 for LAs., nd = not determine. [d]Initiator efficiency (IE) = M_{wexp}/M_{wcalc} where $M_{wcalc} = M_{w(monomer)} \times [CL]_o/[I] \times [PCL]/[CL]_o + M_{w(chain\text{-}end\ group.}$ [e]D,L-LA and [f]L-LA.[20]

5.3.3.1 Kinetic studies of ROP reactions of ε-CL and LAs

Kinetic studies for the polymerization of ε-CL, $_{D,L}$-LA and $_{L}$-LA using complexes **10–13** at $[CL]_o/[I]$ = 200 at 110 °C were performed The apparent rates constants of polymerization (k_{app}) using these complexes were extracted from Figures 5.4 and the results are shown in Table 5.1. The linearity of the semi logarithmic plots showed that the ROP reaction followed *pseudo*-first order kinetics dependence on monomer concentration for all the complexes.

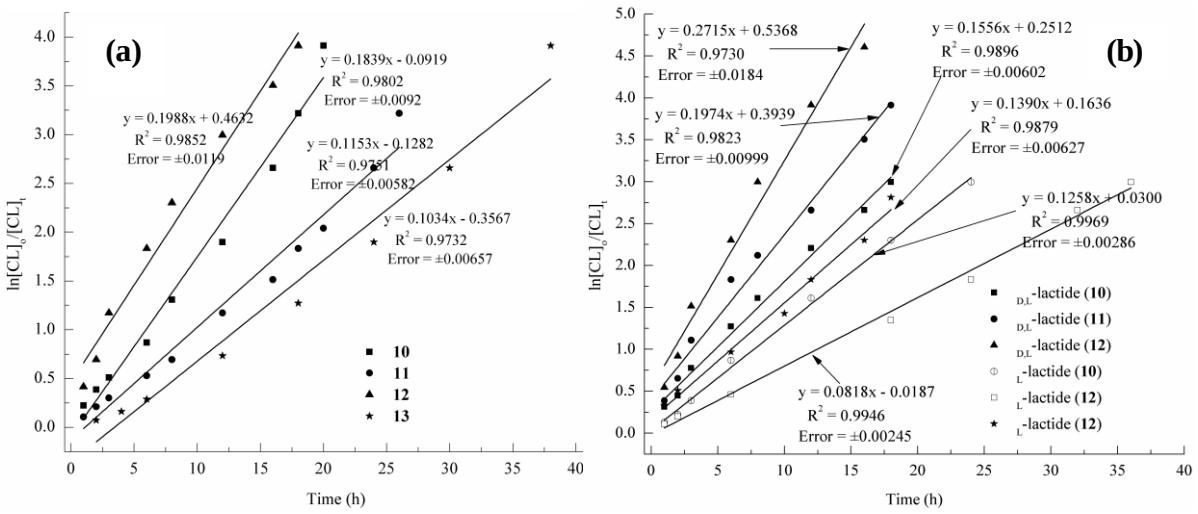

Figure 5. 4: (a) First order kinetic plots of $\ln[CL]_o/[CL]_t$ *vs.* time for complexes **10–13** in the polymerization of ε-CL at 110 °C, $[CL]_o/[I]$ = 200 in toluene. (b) First order kinetic plots of $\ln[CL]_o/[CL]_t$ *vs.* time for complexes **10–12** in the ROP of $_{D,L}$-LA and $_{L}$-LA to PLAs in toluene at 110 °C, $[CL]_o/[I]$ = 200.

The rate constants (k_{app}) for each of the ROP reaction of ε-CL were established to be 0.1839 ±0.0092, 0.1152 ±0.00582, 0.1988 ±0.0119 h^{-1} and 0.1034 ±0.00657 for complexes **10**, **11 12** and **13**, respectively (Table 5.1, entries 1, 2 3 and 4). From the ^{1}H and ^{13}C NMR spectrum, and elemental analyses data, complexes **10–13**, have similar structures with the only difference being

the methyl and isopropyl substituents on the phenyl ring of the ligand backbone (Scheme 5.1), and also *t*-BuOH initiating group in complex **13**. The lower apparent rate constant of 0.1152 $\pm$0.00582 h^{-1} and 0.1034 $\pm$0.00657 obtained using **11** and **13** (isopropyl group substituent) in comparison to complexes **10** and **12** with methyl group substituent on the ligand backbone point to the effect of ligand architecture on the polymerization activity. The increase in catalytic activity associated with sterically less bulky ligand complexes **10** and **12** is in agreement with literature reports.[21,22,23,24] It is believed that the sterically demanding isopropyl group blocks the Zn(II) center thus inhibiting access of the monomer to the active site resulting in lower activities.

The kinetics of ROP reactions of $_{D,L}$-LA and $_{L}$-L were monitored by ^{1}H NMR spectroscopy and the monomer consumption *vs.* reaction time plots are shown in Figure 5.4b. The apparent rate constants (k_{app}) extracted from the plots of $\ln[CL]_o/[CL]_t$ *vs.* time gave a higher rate of polymerization of 0.2715 $\pm$0.0184 h^{-1} ($_{D,L}$-LA) compared to a k_{app} of 0.1988 $\pm$0.0119 h^{-1} for ε-CL when complex **12** was employed as the catalyst. The six-membered ring in LA increases the strain resulting in rapid ROP reactions.[25] The stereochemistry of the LA monomer also had effect on the rates of ROP reaction rate. For instance, the k_{app} obtained for $_{D,L}$-LA (Table 5.1, entries 5, 6 and 7) were higher compared to $_{L}$-LA (Table 5.1, entries 8, 9 and 10) for complexes **10**–**12**. We also observed similar trend in the case of ROP of LA using *N,N'*diarylformamidines Zn(II) complexes reported in chapter **4**, and attributed this to the differences in the stability of the $_{D,L}$-LA and $_{L}$-LA in the ground state.[26,27] Although the recorded catalytic activities for complexes **10**–**13** were lower compared to some of the most active Zn(II) alkoxide complexes found in literature,[21,28,29,30] their catalytic activities were higher than those reported using

(benzimidazolylmethyl)amine Zn(II) and Cu(II) carboxylate complexes.[16] The recorded catalytic activities using complexes **10**–**13** were comparable to other reported Zn(II) alkoxide initiators.[31]

Table 5.2: Effect of catalyst concentrations on polymerization kinetics of ε-CL using complex **12**[a]

Entry	$[CL]_o/[12]$	Time (h)	Conversion[b] (%)	k_{app} (h^{-1})	M_w (GPC)[c]	PDI[c]	IE[d]
1	100	8	98	0.3803	4176	1.45	0.37
2	150	14	97	0.2672	4322	1.32	0.26
3	250	24	96	0.1328	6428	1.26	0.19
4	300	36	95	0.0728	6804	1.46	0.17

[a]Reaction conditions, Toluene, 110 °C. [b]Maximum conversion achieved [c]Molecular-weight average and Polydispersity index (PDI) determined by GPC relative to polystyrene standard values, the values obtained from GPC × 0.56.[20] [d]Initiator efficiency (IE) = M_{wexp}/M_{wcalc} where $M_{wcalc} = M_{w(monomer)} \times [CL]_o/[Cat] \times [PCL]/[CL]_o + M_{w(chain\text{-}end\ group)}$.

5.3.4 Order of ROP reactions of ε-CL using complex 12 at different concentrations

The kinetics of ROP reactions using complex **12** was evaluated at various $[CL]_o/[Cat]$ ratios of 100, 150, 250 and 300 using ε-CL as monomer in order to determine the order of ROP reactions with respect to complex **12**. The ROP reactions were carried out in toluene at 110 °C and data collected are presented in Table 5.2 (entries 1-4) and Figure 5.5a. The k_{app} values increased with increase in the concentration of the catalyst, confirming that the order with respect to the catalyst was first order.[24] A Plot of $\ln k_{app}$ *vs.* ln[**12**] (Figure 5.5b) gave linear relationship which allowed

us to determine the order of reaction with respect to **12**. From the plot, the order of the reaction extracted from the gradient of the line of best fit (Figure 5.5b) was obtained as 1.2132 ≈ 1. Thus, the overall kinetic equation for the ROP of ε-CL with **12** could be denoted as shown Equation 5.2.

$$-\frac{d[CL]}{dt} = k[CL][\mathbf{12}] \qquad (5.2)$$

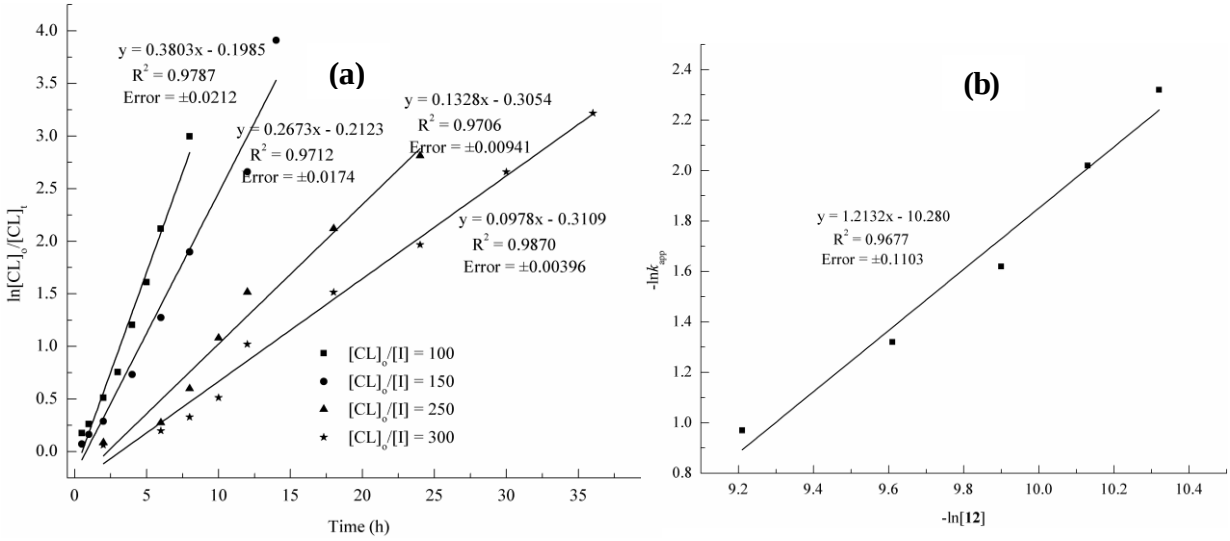

Figure 5. 5: (a) First order kinetic plots of $\ln[CL]_o/[CL]_t$ *vs.* time for complex **12** in the ROP of ε-CL in toluene at 110 °C, $[CL]_o/[I]$ = 100, 150, 250 and 300. (b) Plot of $\ln k_{app}$ *vs.* ln[**12**] for the determination of order of reactions with respect to complex **12** in the ROP of ε-CL.

5.3.5 Effect of BnOH as initiator in ROP reaction of ε-CL

The effect of BnOH initiator in the ROP reactions of ε-CL was evaluated by varying [BnOH] between 5, 10, 20 and 50, respectively. (Entries 1–4, Table 5.3). The apparent rate constant (K_{app}) obtained from the linear plots in Figure 5.6 indicated that catalytic activity using complex **12** increased with increase in concentrations of BnOH. For example, in the presence of 50

equivalent of BnOH, complex **12** displayed conversion of 98% in 14 h at 110 °C (entry 4; K_{app} = 0.2681 $\pm$0.01224 h^{-1}, Table 5.3), whereas in bulk reactions, conversion of 98% was obtained in 18 h (entry 3; K_{app} = 0.1998 $\pm$0.0119 h^{-1}, Table 5.1). Addition of BnOH is known to result in the formation of new benzyloxy-metal initiating groups,[32] thus providing additional catalytic sites for the of ROP reactions.[33,32] The increase of catalytically active sites upon addition of BnOH may be responsible for the higher catalytic activities observed. For example, in the presence of two equivalent of BnOH, Zn(II) bis(iminopyrrolide) alkoxide complex led to 95% conversion of 400 equivalent of ε-CL to PCL in 50 min at 50 °C, whereas the bulk reaction required 60 min and gave a lower conversion of monomer.[32]

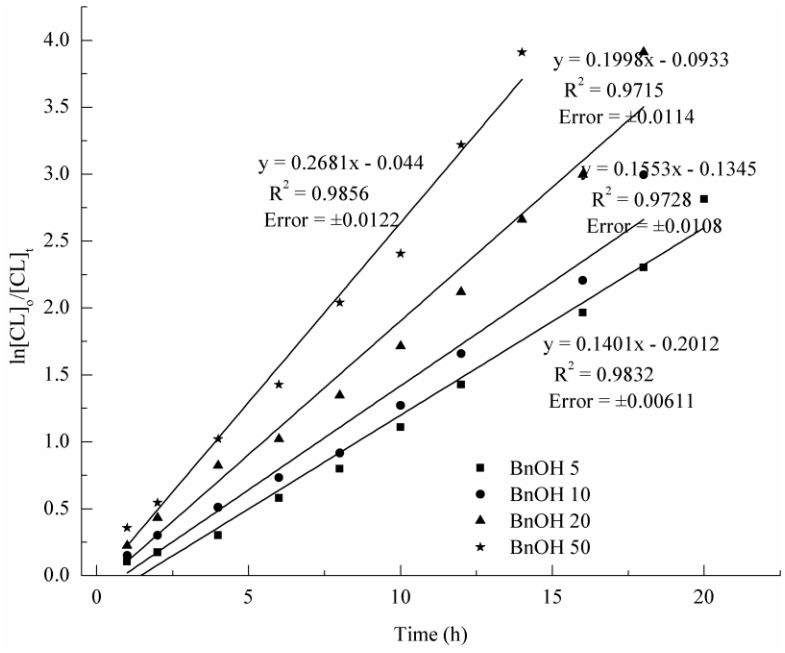

Figure 5. 6: First order kinetic plots of $\ln[CL]_o/[CL]_t$ *vs.* time for complex **12** in the ROP of ε-CL in toluene at 110 °C, $[CL]_o:[I]_o:[BnOH]_o$ = 200:1:5, 10, 20, 50.

Table 5. 3: The ROP of ε-CL using complex **12** in the presence of BnOH as initiator

Entry	$[CL]_o:[I]_o:[BnOH]_o$	Time (h)	Conversion[b] (%)	k_{app} (h^{-1})	M_w (GPC)[c]	PDI[c]	IE[d]
1	200:1:5	20	95	0.1401 ±0.006	2510	1.33	0.57
2	200:1:10	18	95	0.1553 ±0.011	2640	1.41	1.16
3	200:1:20	18	98	0.1998 ±0.011	1822	1.37	1.49
4	200:1:50	14	98	0.2681 ±0.012	1523	1.22	2.75

[a]Solvent: toluene, temperature, 110 °C. [b]Maximum conversion achieved [c]Molecular-weight average and Polydispersity index (PDI) determined by GPC relative to polystyrene standard, values are the values obtained from GPC × correction factor of 0.56 for lactones.[20] [d]Initiator efficiency (IE) = M_{wexp}/M_{wcalc} where $M_{wcalc} = 114 \times ([CL]_o/([BnOH]_o) \times$ conv. (%) + 108.

5.3.6 Molecular weight and molecular weight distributions of polymers

The molecular weights and molecular weight distributions (PDI) of the PCL and PLAs obtained from the ROP reactions using complexes **10**-**12** were determined by GPC (Table 5.1-5.3). For the ROP of ε-CL using **10**-**12**, weight average molecular weights (M_w) ranging from 1523 to 6804 g mol^{-1} was obtained. The experimental M_{ws} were obtained as 4456, 3841, 4744 g mol^{-1} for **10**, **11** and **12**, respectively. We observed a decrease in the average molecular weight of the PCL as the steric bulk of the ligand increased (Table 5.1, entries 1-3). This observation contradicts literature reports were an increased steric bulk increases the molecular weight by retarded chain transfer.[34,35] Thus at this stage, we are unable to definitely account for the observed trend. Generally higher M_w of PLAs was obtained compared to PCL. Significantly,

greater dependence of M_w on the stereochemistry of the LA monomer was observed. For example, M_w of PLA obtained from $_{D,L}$-LA (10 650 g mol^{-1}) was twofold greater than the M_w of 5678 g mol^{-1} from $_{L}$-LA monomer (Table 5.1, entries 7 and 10), respectively. Increasing the $[CL]_o$:$[BnOH]_o$ ratio resulted in low polymer molecular weights and narrower PDI (Table 5.3). The BnOH initiating groups increases the number of active site, resulting in many short polymer chains with low molecular weight.[33] Generally, the molecular weight distributions (PDI) of the polymers were relatively narrow ranging from 1.16 to 1.53. The molecular weight values of the resulting polymers catalyzed by complexes **10**-**12** were not in agreement with the calculated molecular weight values pointing that the growth of one polymer chain per zinc-benzyloxyl initiator was not obtained in our systems. This can be attributed to a slow initiation step compared to propagation. Similar results were also found for bridged bis(amidinate) Ytterbium alkoxide catalytic systems employed in ROP of ε-CL and LAs.[36]

5.3.7 Mechanism of ROP of ε-CL and LAs

To determine the nature of the active species and the chain end groups, a low molecular weight polymer sample was prepared and analyzed by ^{1}H NMR spectroscopy. For example, the proton NMR spectra of PCL obtained from complex **12** facilitated ROP reaction showed a benzyloxy end group on each polymer chain (Figure 5.7) indicating that the ROP was initiated from the BnO- initiating group. For instance, the ^{1}H NMR spectrum of PCL in Figure.5.7 shows the presence of phenyl ring protons (a, 7.37 ppm) and CH_2 (b, 5.12 ppm) suggesting that the ROP reaction was initiated by the insertion of BnO- group into CL *via* coordination-insertion mechanism.

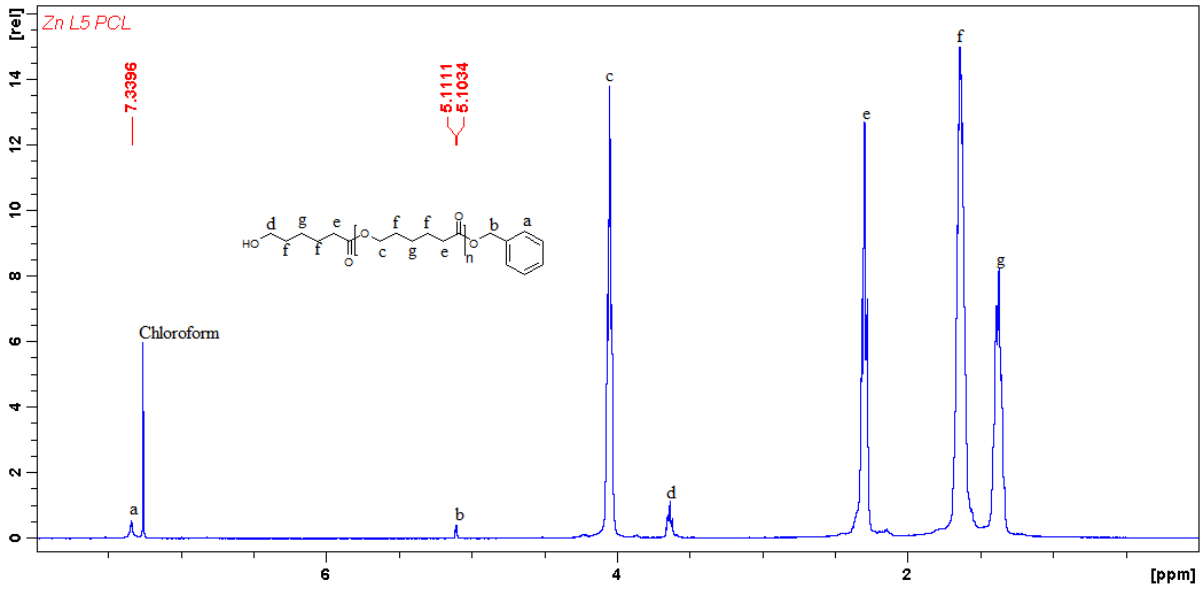

Figure 5. 7: ^{1}H NMR spectrum of PCL at 95% conversion revealing the presence of phenyl ring protons (a, 7.37 ppm) and CH_2 (b, 5.12 ppm) suggesting coordination-insertion mechanism. Reaction condition:$[CL]_o$:$[I]_o$ = 200:1 in toluene at 110 °C, 18 h.

The ESI-MS mass spectra of PLA obtained from catalyst **12** showed fragmentation pattern corresponding to the presence of benzyloxy end group in the polymer backbone. ESI-MS mass spectra show fragments with increments of 144 Da between consecutive peaks corresponding to the repeat units LA. For example, a potassium-cationized polymer chain with n = 12 has a mass of 1913.7 Da and confirmed the proposed polymer chain structure (Figure 5.8). The results from ^{1}H NMR spectroscopy and ESI-MS analyses showed presence of one benzyl ester group per polymer chain. Thus, it is plausible to conclude that there was incorporation of benzyl ester end-groups in the polymer back-bone, establishing a coordination-insertion mechanism.[37,38]

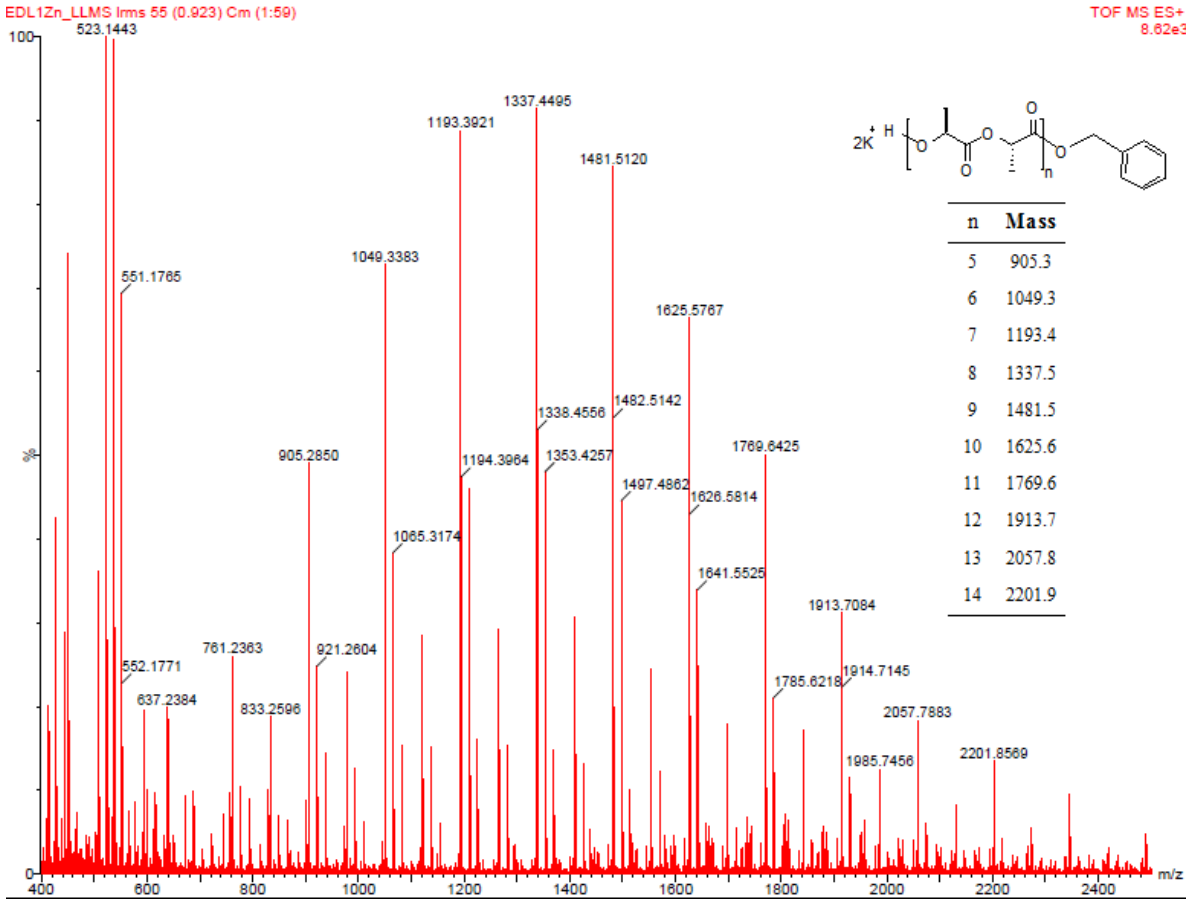

Figure 5. 8: ESI-MS spectrum of PCL obtained by using catalyst **12**, Reaction condition:$[CL]_o$:$[I]_o$ = 200:1 in toluene at 110 °C, 18 h, 98% conversion.

5.3.8 Polymer Tacticity

The microstructural architecture of the PLAs were investigated using homonuclear decoupled ^{1}H NMR. Figure 5.9 shows the methine region in the homonuclear decoupled ^{1}H NMR spectrum of poly($_{D,L}$-LA) produced by complex **10**. The peaks were assigned to the appropriate tetrads in accordance with their chemical shifts.[39] The methine region in the homonuclear decoupled ^{1}H NMR spectrum displays *isi* and *sis* tetrads which are more intense than for a totally random poly($_{D,L}$-LA) (Figure 5.9). The tacticity bias (*Pr* = 0.63) is similar to that reported for titanium

alkoxides[40] and for a single-site tin catalyst,[41] but the preference for heterotacticity is not as strong as reported, for example, for β-diketiiminate zinc alkoxide complexes.[42,43]

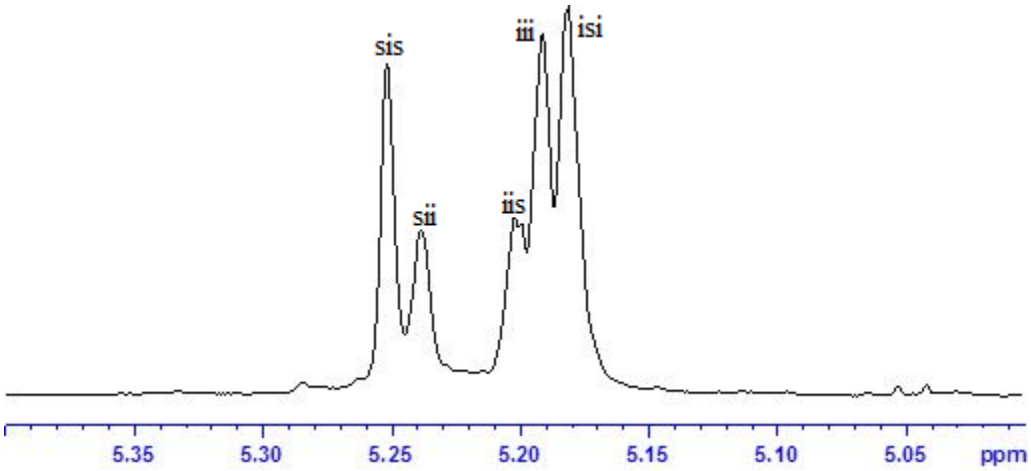

Figure 5. 9: ^{1}H homonuclear decoupled ^{1}H NMR (400 MHz, $CDCl_3$) spectrum of the methine region of partial heterotactic PLA prepared from $_{D,L}$-LA using complex **10.**

The results of ^{1}H homonuclear decoupled ^{1}H NMR spectra showed that complexes **10**-**13** hardly led to selective polymerization in toluene giving partially heterotactic selectivity.[44] The probability of racemic enrichment, *Pr* of 0.63 ,0.78 and 0.69 was obtained for **10, 11** and **12**, respectively based on calculations reported in literature[45,46]. The tacticity of the polymer was influenced by the ligand used. For instance, changing the ligand from **L4** to a sterically bulkier ligand **L5** resulted in an increase in *Pr* from 0.63 to 0.78. Similar observation were ligand architecture impacts on the stereoselectivity of PLAs has been reported.[30] Complex **11** (Pr = 0.78) gave a better stereocontrol PLA. It was envisaged that chain-end control by the growing polymer chain typically leads to a preference for alternating *RR*,*SS*-insertion, which can lead to modest stereoregular heterotactic PLA given sufficient bulk of the spectator ligands.[43] The

homonuclear decoupled ^{1}H NMR spectrum at the methine region of the PLA obtained from $_{L}$-LA *via* ROP with **11** and **15** is isotactic predominance without observable epimerization (Figure 5.10).

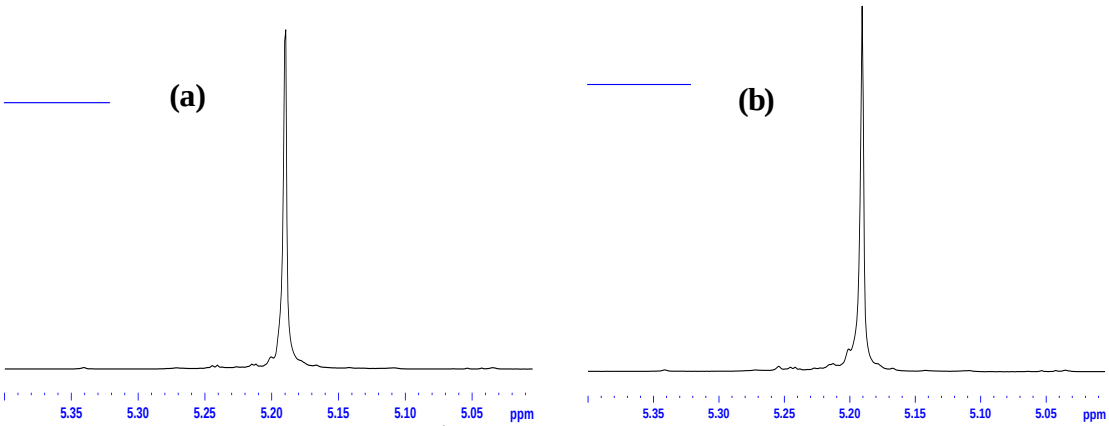

Figure 5. 10: Homonuclear decoupled ^{1}H NMR (400 MHz, $CDCl_3$) spectra of the methine region of isotactic PLA prepared from $_{L}$-LA using complexes (a) **11** and (b) **12.**

5.3.9 TGA and DSC analysis of PLAs

Thermal analyses of PLA using thermogravimetric analysis (TGA) and differential scanning calorimetry (DSC) were carried out (Figures 5.11). From the DSC thermogram, the glass transition temperature (T_g) and melting temperature (T_m) of PLA obtained from $_{L}$-LA occurred at 60 °C and 149 °C, respectively, which is consistent with the results reported in the literature for highly isotactic polymers.[47,48,49] The TGA trace gives the decomposition curve of the synthesized PLA, and shows that the PLA decomposed at 298 °C. The T_g, T_m and decomposition temperatures recorded points to synthesis of crystalline PLAs with long isotactic sequences in toluene.

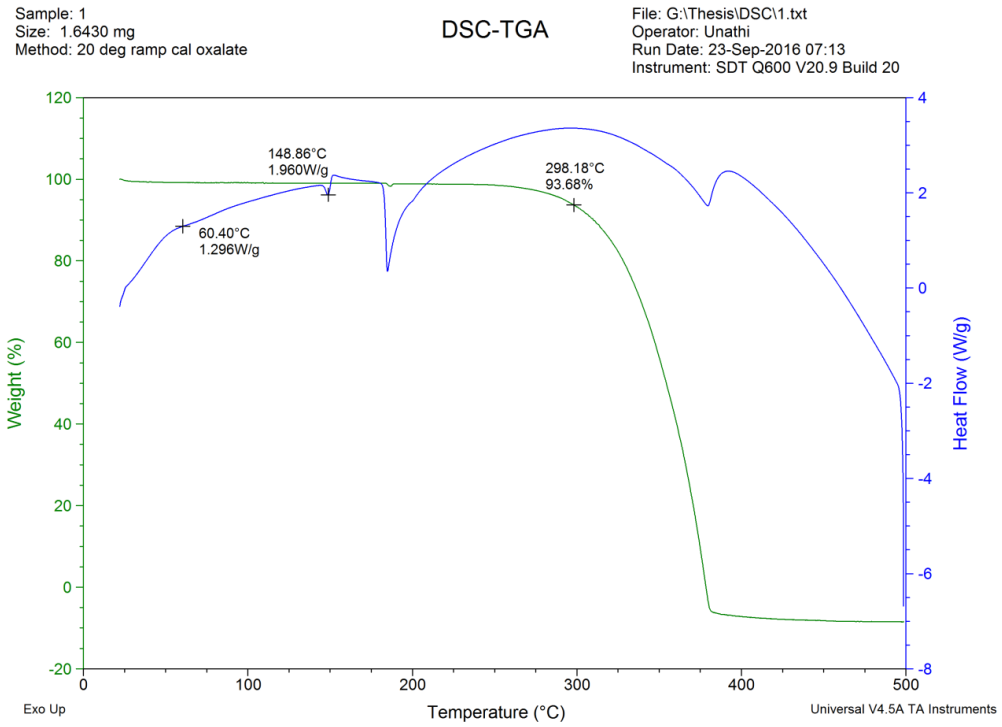

Figure 5. 11: DSC-TGA curves of PLA prepared from $_{L}$-LA in toluene at 110 °C, $[CL]_o/[I]$ = 200 using complex **12**.

5.4 Conclusions

A series of (benzoimidazolylmethyl)amine Zn(II) alkoxide complexes have been successfully synthesized and the identities of the compounds were established by ^{1}H and ^{13}C NMR, FTIR spectroscopy and mass spectrometry. The Zn(II) alkoxide complexes effectively catalyzed the ring opening polymerization of ε-caprolactone, $_{L}$–lactide and $_{D,\ L}$–lactides in controlled manner. All polymerization reactions follow *pseudo*-first order kinetics with respect to monomer. Both the complex architecture and monomer stereochemistry influence the reaction kinetics and gives better polymer properties. The Zn(II) complexes initiates ring opening polymerization of $_{L}$-lactide giving highly isotactic PLA, while ring opening polymerization of $_{D,L}$-lactide yields

heterotactic PLA. Benzyl alcohol initiator enhances the catalytic activities of the complexes compared to polymerization without benzyl alcohol, and the polymerization reactions proceeded *via* coordination-insertion mechanism.

5.5 References

(1) Tsai, C.-Y.; Du, H.-C.; Chang, J.-C.; Huang, B.-H.; Ko, B.-T.; Lin, C.-C. *RSC Advances* **2014**, *4*, 14527.

(2) Huang, Y.; Hung, W.-C.; Liao, M.-Y.; Tsai, T.-E.; Peng, Y.-L.; Lin, C.-C. *J. Polym. Sci. Part A: Polym. Chem.* **2009**, *47*, 2318.

(3) Wu, J.; Yu, T.-L.; Chen, C.-T.; Lin, C.-C. *Coord. Chem. Rev.* **2006**, *250*, 602.

(4) Sutar, A. K.; Maharana, T.; Dutta, S.; Chen, C.-T.; Lin, C.-C. *Chem. Soc. Rev.* **2010**, *39*, 1724.

(5) Albertsson, A.-C.; Varma, I. K. *Biomacromolecules* **2003**, *4*, 1466.

(6) Inoue, S. *J. Polym. Sci. Part A: Polym. Chem.* **2000**, *38*, 2861.

(7) Song, S.; Zhang, X.; Ma, H.; Yang, Y. *Dalton Trans.* **2012**, *41*, 3266.

(8) Gowda, R. R.; Chakraborty, D. *J. Mol. Catal. A: Chem.* **2010**, *333*, 167.

(9) Liu, Z.; Gao, W.; Zhang, J.; Cui, D.; Wu, Q.; Mu, Y. *Organometallics* **2010**, *29*, 5783.

(10) Ikpo, N.; Saunders, L. N.; Walsh, J. L.; Smith, J. M. B.; Dawe, L. N.; Kerton, F. M. *Eur. J. Inorg. Chem.* **2011**, *2011*, 5347.

(11) Inoue, S.; Koinuma, H.; Tsuruta, T. *J. Polym. Sci. Part B: Polym. Lett.* **1969**, *7*, 287.

(12) Platel, R. H.; Hodgson, L. M.; Williams, C. K. *Polym. Rev.* **2008**, *48*, 11.

(13) Stanford, M. J.; Dove, A. P. *Chem. Soc. Rev.* **2010**, *39*, 486.

(14) Thomas, C. M. *Chem. Soc. Rev.* **2010**, *39*, 165.

(15) Pal, S.; Hwang, W.-S.; Lin, I.; Lee, C.-S. *J. Mol. Catal. A* **2007**, *269*, 197.

(16) Attandoh, N. W.; Ojwach, S. O.; Munro, O. Q. *Eur. J. Inorg. Chem*. **2014**, 3053.

(17) Hao, P.; Zhang, S.; Sun, W.-H.; Shi, Q.; Adewuyi, S.; Lu, X.; Li, P. *Organometallics* **2007**, *26*, 2439.

(18) Achar, K. C. S.; Hosamani, K. M.; Seetharamareddy, H. R. *Eur. J. Med. Chem*. **2010**, *45*, 2048.

(19) Campos-Vallette, M. M.; Figueroa, K. A.; Latorre, R.; Manriquez, V.; Diaz, G.; Costamagna, J.; Otero, M. *Vib. Spectrosc*. **1992**, *4*.

(20) Wu, J.-C.; Huang, B.-H.; Hsueh, M.-L.; Lai, S.-L.; Lin, C.-C. *Polymer* **2005**, *46*, 9784.

(21) Wang, C.-H.; Li, C.-Y.; Huang, B.-H.; Lin, C.-C.; Ko, B.-T. *Dalton Trans.* **2013**, *42*, 10875.

(22) O'Keefe, B. J.; Breyfogle, L. E.; Hillmyer, M. A.; Tolman, W. B. *J. Am. Chem. Soc.* **2002**, *124*, 4384.

(23) Hodgson, L. M.; Platel, R. H.; White, A. J. P.; Williams, C. K. *Macromolecules* **2008**, *41*, 8603.

(24) Bhunora, S.; Mugo, J.; Bhaw-Luximon, A.; Mapolie, S.; Van Wyk, J.; Darkwa, J.; Nordlander, E. *Appl. Organomet. Chem*. **2011**, *25*, 133.

(25) Duda, A.; Kowalski, A. In *Handbook of Ring-Opening Polymerization*; Wiley-VCH Verlag GmbH & Co. KGaA, 2009.

(26) Buffet, J.-C.; Davin, J. P.; Spaniol, T. P.; Okuda, J. *New J. Chem*. **2011**, *35*, 2253.

(27) Chisholm, M. H.; Gallucci, J. C.; Krempner, C. *Polyhedron* **2007**, *26*, 4436.

(28) Sung, C.-Y.; Li, C.-Y.; Su, J.-K.; Chen, T.-Y.; Lin, C.-H.; Ko, B.-T. *Dalton Trans.* **2012**, *41*, 953.

(29) Wang, L.; Ma, H. *Dalton Trans.* **2010**, *39*, 7897.

(30) Chen, H.-Y.; Huang, B.-H.; Lin, C.-C. *Macromolecules* **2005**, *38*, 5400.

(31) Chisholm, M. H.; Eilerts, N. W.; Huffman, J. C.; Iyer, S. S.; Pacold, M.; Phomphrai, K. *J. Am. Chem. Soc.* **2000**, *122*, 11845.

(32) Kong, W.-L.; Wang, Z.-X. *Dalton Trans.* **2014**, *43*, 9126.

(33) Kong, W.-L.; Chai, Z.-Y.; Wang, Z.-X. *Dalton Trans.* **2014**, *43*, 14470.

(34) Collins, S. *Coord. Chem. Rev.* **2011**, *255*, 118.

(35) Kamber, N. E.; Jeong, W.; Waymouth, R. M.; Pratt, R. C.; Lohmeijer, B. G. G.; Hedrick, J. L. *Chem. Rev.* **2007**, *107*, 5813.

(36) Wang, J.; Yao, Y.; Zhang, Y.; Shen, Q. *Inorg. Chem.* **2009**, *48*, 744.

(37) Dubois, P.; Dubois, P.; Coulembier, O.; Raquez, J. M. *Handbook of Ring-Opening Polymerization*; Wiley, 2009.

(38) Dubois, P.; Jacobs, C.; Jerome, R.; Teyssie, P. *Macromolecules* **1991**, *24*, 2266.

(39) Thakur, K. A. M.; Kean, R. T.; Hall, E. S.; Kolstad, J. J.; Lindgren, T. A.; Doscotch, M. A.; Siepmann, J. I.; Munson, E. J. *Macromolecules* **1997**, *30*, 2422.

(40) Kim, Y.; Jnaneshwara, G. K.; Verkade, J. G. *Inorg. Chem.* **2003**, *42*, 1437.

(41) Dove, A. P.; Gibson, V. C.; Marshall, E. L.; White, A. J. P.; Williams, D. J. *Chem. Commun.* **2001**, 283.

(42) Chamberlain, B. M.; Cheng, M.; Moore, D. R.; Ovitt, T. M.; Lobkovsky, E. B.; Coates, G. W. *J. Am. Chem. Soc.* **2001**, *123*, 3229.

(43) Cheng, M.; Attygalle, A. B.; Lobkovsky, E. B.; Coates, G. W. *J. Am. Chem. Soc.* **1999**, *121*, 11583.

(44) Zhang, Y.; Gao, A.; Zhang, Y.; Xu, Z.; Yao, W. *Polyhedron* **2016**, *112*, 27.

(45) Kremer, A. B.; Osten, K. M.; Yu, I.; Ebrahimi, T.; Aluthge, D. C.; Mehrkhodavandi, P. *Inorg. Chem*. **2016**, *55*, 5365.

(46) Kasperczyk, J. E. *Macromolecules* **1995**, *28*, 3937.

(47) Petrus, R.; Sobota, P. *Organometallics* **2012**, *31*, 4755.

(48) Jamshidi, K.; Hyon, S.-H.; Ikada, Y. *Polymer* **1988**, *29*, 2229.

(49) Labet, M.; Thielemans, W. *Chem. Soc. Rev*. **2009**, *38*, 3484.

Chapter 6

Magnesium alkoxide complexes of (benzimidazolylmethyl) amine ligands: Synthesis and applications in ROP reactions of ε-caprolactone and lactides

6.1 Introduction

Magnesium alkoxides as catalyst in the ROP of cyclic esters have attracted considerable attention, because of their nontoxicity and high activity.[1,2,3,4,5] Magnesium alkoxides tend to polymerized *via* intermolecular O−Mg donor−acceptor bonds, and has the advantages of single-site catalyst system.[6] The alkoxide systems has been adjust as good catalysts/initiators because most alkoxide metal are redox-inactive and inert to hydrogen atom abstraction from the growing alkoxide polymer chain, thereby reducing side reactions(such as *trans*-esterification, epimerization) that could lead to chain termination with loss of catalytic activity.[7]

Tolman and co-workers investigated the effect of steric environment around the metal center and related the electrophilicity of the metal complex and the rate of coordination and insertion of monomers.[8,9] The electronegativity of the metal center has been reported to affects the coordination of monomers, as well as the bond energies in the transition states during insertion of the monomers into the metal−alkoxide bond. Recently, catalytic activities of (benzimidazolylmethyl)amine Zn(II) and Cu(II) carboxylate complexes in ROP reactions of ε-CL have been reported.[10] The activities of these catalysts were dictated to a great extent by the nature of the metal center and the ligand architecture.

Zn(II) alkoxides based on (benzimidazolylmethyl)amine ligands reported in chapter **5** exhibited improved control on ROP reactions and polymer properties, thus indicating that the alkoxide initiating species were a better initiators compared to the acetates and the benzoates. In this chapter, we aimed to build on the improved control of ROP process exhibited by the (benzimidazolylmethyl)amine based Zn(II) alkoxides complexes and developed analogous Mg(II) alkoxide complexes and investigate their potentials as catalysts in the ROP reactions of ε-CL, $_{L}$-LA and $_{D,L}$-LA.

6.2 Experimental section

6.2.1 Materials and reagents

All manipulations were carried out under a dry argon atmosphere unless stated otherwise. Solvents (ACS reagent grades ≥ 99.5%) were dried by refluxing at least 24 h over sodium/benzophenone (hexane, DCM and tetrahydrofuran (THF), and reagent grade ethanol was distilled and dried from magnesium turnings. The monomers (ε-CL and LAs; 99%), $Mg(^{n}Bu)_2$ (1.0 M in hexane), BnOH (anhydrous 99.8%), *t*-BuOH (anhydrous ≥ 99.5%), 2-(chloromethyl)benzimidazole (96%), 2,6-dimethylaniline (99%), 2,6-diisopropylaniline (97%), 2,4,6-trimethylaniline (98%) were purchased from Sigma Aldrich and used without further purification.

6.2.2 Instrumental characterization techniques

^{1}H and ^{13}C NMR spectra were measured at room temperature using a Bruker 400 MHz spectrometer. ^{1}H NMR spectral data were recorded in $CDCl_3$ listed as residual internal $CDCl_3$ (δ 7.26). Similarly, ^{13}C NMR data were recorded in $CDCl_3$ listed as residual internal $CDCl_3$ (δ

77.00). Mass spectra of compounds were obtained from a Water synapt GR electrospray positive spectrometer. Thermogravimetric analyses (TGA) were done on a TGA SDT Q600 V20.9 Build 20 modulus coupled with a thermal analyzer. The differential scanning calorimetric (DSC) measurements of dried samples were performed from 30 to 500 °C at a heating rate of 10 °C/min on a TA Instrument (TGA SDT Q600 V20.9 Build 20). An aluminum pan was loaded with ca. 5 mg of sample and heating ramped at 10 °C/min under a nitrogen atmosphere at a flow rate of (50 ml/min). A pinhole on the lid was made to prevent pressure build up due to gaseous products. The thermal analytical data was collected between 30 to 500 °C.

6.2.3 Synthesis of (benzimidazolylmethyl) amine Mg(II) complexes

To a solution of benzyl alcohol (2 mmol) in dry THF (20 mL) at 0 °C under Ar was added drop wise $Mg(^{n}Bu)_2$ (1 mmol) and the resulting solution was stirred at room temperature for 12 h. The mixture was again cooled to 0 °C and a solution of the ligand (1 mmol equivalent) in dry THF was added slowly and the mixture stirred at room temperature for further 24 h. Volatiles were removed under vacuum, and the product washed with hexane to afford the respective complexes.

6.2.3.1 $[(L4)Mg(OBn)]_2$ (14)

Following the general procedure (**6.2.3**), **L4** (0.50 g, 1.99 mmol), benzyl alcohol (0.43 g, 0.41 mL) and $Mg^{n}Bu_2$ (1.99 mL) were used as reagents. Pale yellow solid (0.93 g, 61%). ^{1}H NMR ($CDCl_3$, 400 MHz): δ (ppm) 2.21 (s, 12H, CH_3), 4.34 (s, 4H, NCH_2), 4.73 (s, 4H, CH_2Ph), 6.92 (t, 2H, Ar), 7.01 (d, ^{3}J = 7.44 Hz, 4H, Ar), 7.39 (m, 14H, Ar), 7.56 (b, 4H, Ar). ^{13}C NMR ($CDCl_3$, 400 MHz) δ (ppm) 153.6, 144.9, 141.2, 130.3, 129.1, 128.5, 127.5, 127.0, 123.1, 122.6,

64.9, 46.5, 18.2. IR (Nujol): ν = 1622 (s), 1330 (m), 1272 (m).). Anal. Calcd. For $C_{46}H_{46}N_6O_2Mg_2$: C, 72.36; H, 6.07; N, 11.01. Found: C, 72.68; H, 6.08; N, 11.38.

6.2.3.2 [(L5)Mg(OBn)]$_2$ (15)

Following the general procedure (**6.2.3**), **L5** (0.50 g, 1.63 mmol), benzyl alcohol (0.34 g, 0.33 mL) and Mg^{n}Bu$_2$ (1.63 mL) were used as reagents. Pale yellow solid (0.84 g, 59%). ^{1}H NMR ($CDCl_3$, 400 MHz): δ (ppm) 1.14 (d, ^3J = 6.92 Hz, 24H, CH_3), 3.20 (m, 4H, CH), 4.27 (s, 4H, NCH_2), 4.62 (s, 4H, CH_2Ph), 7.06 (s, 9H, Ar), 7.22 (m, 9H, Ar), 7.29 (m, 4H, Ar), 7.36 (b, 2H, Ar), 7.66 (b, 2H, Ar), 9.87 (s, 2H, NH). ^{13}C NMR ($CDCl_3$, 400 MHz) δ (ppm) 152.9, 143.3, 142.9, 141.6, 140.9, 133.2, 128.5, 127.6, 126.9, 124.9, 123.8, 122.9, 119.3, 110.7, 65.2, 49.8, 27.8, 24.2. IR (Nujol): ν = 1616 (s), 1324 (s). Anal. Calcd. For $C_{54}H_{62}N_6O_2Mg_2$: C, 74.06; H, 7.14; N, 9.60. Found: C, 74.68; H, 7.08; N, 9.38.

6.2.3.3 [(L6)Mg(OBn)]$_2$ (16)

Following the general procedure (**6.2.3**), **L6** (0.50 g, 1.88 mmol), benzyl alcohol (0.41 g, 0.39 mL) and Mg^{n}Bu$_2$ (1.88 mL) were used as reagents. Yellow solid (0.97 g, 65%). ^{1}H NMR ($CDCl_3$, 400 MHz): δ (ppm) 2.21 (s, 12H, CH_3), 2.26 (s, 6H, CH_3), 4.33 (s, 4H, NCH_2), 4.76 (s, 4H, CH_2Ph), 6.84 (s, 5H, Ar), 7.58 (m, 19H, Ar), 10.77 (b, 2H, Ar). ^{13}C NMR ($CDCl_3$, 400 MHz) δ (ppm) 153.5, 142.1, 141.1, 132.6, 130.4, 129.6, 128.5, 127.5, 126.6, 122.5, 64.9, 46.7, 20.6, 18.0. IR (Nujol): ν = 1611 (s), 1333 (s). Anal. Calcd. For $C_{48}H_{50}N_6O_2Mg_2$: C, 72.83; H, 6.37; N, 10.62. Found: C, 72.68; H, 6.78; N, 10.98.

6.2.3.4 [(L5)Mg(*t*-BuO)]$_2$ (17)

To a solution of *t*-BuOH (2 mmol, 0.14 g, 0.12 mL) in dry toluene (15 mL) at -78 °C was added drop wise Mg(^{n}Bu)$_2$ (1 mmol,1.63 mL) and the resulting solution was warmed to room temperature and stirred for 3 h. **L5** (0.25 g, 0.81 mmol) in toluene (10 mL) was then added and the mixture heated at 70 °C for 6 h. Volatiles were removed under vacuum, and the residue washed with hexane to afford complex **17**. Light yellow solid (0.97 g, ^{1}H NMR ($CDCl_3$, 400 MHz): δ (ppm) 1.16 (d, ^3J = 5.82 Hz, 24H, CH_3), 1.62 (s, 18H, CH_3), 3.21 (m, 4H, CH), 4.29 (s, 4H, CH_2), 7.07 (s, 1H, Ar), 7.20 (m, 2H, Ar), 7.39 (q, 2H, Ar), 7.69 (t, 2H, Ar), 9.62 (s, 2H, NH). ^{13}C NMR ($CDCl_3$, 400 MHz) δ (ppm) 152.6, 143.4, 142.9, 141.6, 133.2, 125.0, 123.9, 122.5, 122.7, 48.9, 27.9, 24.3,22.4. Anal. Calcd. For $C_{48}H_{66}N_6O_2Zn_2$: C, 64.78; H, 7.48; N, 9.44. Found: C, 64.85; H, 7.21; N, 8.99.

6.2.4 Typical procedure for ROP of ε-CL

An appropriate amount of the complex was dissolved in toluene in a Schlenk tube immersed in pre-heated oil bath at 110 °C, and ε-CL monomer (1.14 g, 0.01 mol) was added and the reaction was initiated by stirring. Kinetic experiments were carried out by withdrawing samples at regular interval using a syringe and quenched quickly by rapid cooling into NMR tube containing $CDCl_3$ solvent using ice water. The quenched samples were analyzed by ^{1}H NMR spectroscopy for determination of polymerization of ε-CL to PCL. The percentage conversion of $[PCL]/[CL]_o \times 100$, where $[CL]_o$ is the initial concentration of the monomer and [PCL] is the concentration of the polymer at time t, was evaluated by integration of the peaks for CL (4.2 ppm, OCH_2 signal) and PCL (4.0 ppm, OCH_2 signal) according to the equation $[PCL]/[CL]_o = I_{4.0}/(I_{4.2} + I_{4.0})$ where $I_{4.2}$ is the intensity of the CL monomer signal at 4.2 ppm and $I_{4.0}$ is the

intensity of PCL signal at 4.0 ppm for OCH_2 protons. The observed rate constants were extracted from the slope of the line of best-fits of the plot of $\ln[CL]_o/[CL]_t$ *vs*. time.

6.2.5 Typical procedure for polymerization of $_{D,L}$-LA and $_{L}$-LA

A suitable LA (1.44 g, 0.01 mol) was dissolved in toluene in a Schlenk tube equipped with magnetic stirrer under argon and the required amount of complex was added. The reaction mixture was stirred at 110 °C. Kinetics experiments were carried out by withdrawing samples at regular interval using a syringe and quenched quickly by rapid cooling into NMR tube containing $CDCl_3$ solvent using ice water. The quenched samples were analyzed by ^1H NMR spectroscopy for determination of polymerization of LAs to PLA. The integration values of the methine proton of the monomer and that of the polymer were used to calculate the percentage conversion using the equation 6.1.

$$\% \text{ Conversion} = \frac{I_{CH_{polymer}}}{I_{CH_{monomer}} + I_{CH_{polymer}}} \times 100 \qquad (6.1)$$

$I_{CH_{polymer}}$ = Intensity of the methine of the polymer obtained from proton NMR

$I_{CH_{monomer}}$ = Intensity of the methine of the monomer obtained from proton NMR

6.2.6 Polymer characterization by size exclusion chromatography (SEC)

The samples were analyzed by SEC at Stellenbosch University. The samples were dissolved in BHT stabilized THF (2 mg/ml). Sample solutions were filtered *via* syringe through 0.45 µm nylon filters before subjected to analysis. The SEC instrument consists of a Waters 1515

isocratic HPLC pump, a Waters 717plus auto-sampler, Waters 600E system controller (run by Breeze Version 3.30 SPA) and a Waters in-line Degasser AF. A Waters 2414 differential refractometer was used at 30 °C in series with a Waters 2487 dual wavelength absorbance UV/Vis detector operating at variable wavelengths. Tetrahydrofuran (THF, HPLC grade, stabilized with 0.125% BHT) was used as eluent at flow rates of 1 ml min^{-1}. The column oven was kept at 30 °C and the injection volume was 100 µl. Two PLgel (Polymer Laboratories) 5 µm Mixed-C (300 × 7.5 mm) columns and a pre-column (PLgel 5 µm Guard, 50 × 7.5 mm) were used. Calibration was done using narrow polystyrene standards ranging from 580 to 2 × 10^6 g mol^{-1}. All molecular weights were reported as polystyrene equivalents and corrected by a factor of 0.58 and 0.56 for PCL and PLAs, respectively

6.3 Results and discussion

6.3.1 Synthesis of (benzimidazolylmethyl) amine ligands and Mg(II) complexes

The (benzimidazolylmethyl) amine ligands, *N*-((1H-benzo[*d*]imidazol-2-yl)methyl)-2,6-dimethylaniline (**L4**), *N*-((1H-benzo[*d*]imidazol-2-yl)methyl)-2,6-diisopropylaniline (**L5**) and *N*-((1H-benzo[*d*]imidazol-2-yl)methyl)-2,4,6-trimethylaniline (**L6**) were synthesized using a modified literature procedure[11] as presented in Scheme 6.1.

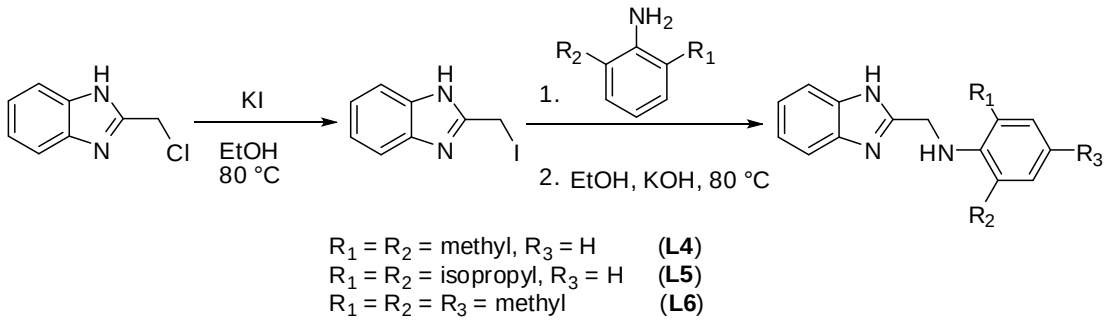

Scheme 6. 1: Synthesis of (benzimidazolylmethyl) amine ligands **L4–L6**.

The compounds were isolated in good yields (83-85%) as pale-yellow solids and the identities of the compounds were established by ^{1}H and ^{13}C NMR, FT-IR spectroscopy, mass spectrometry and elemental analysis. The ^{1}H and ^{13}C NMR spectral signals were consistent with the respective proposed structures. For example, the ^{1}H NMR spectrum of ligand **L4** exhibited signals at 4.45 ppm for the proton of CH_2 in the $–CH_2–NH–Ar$ backbone and the corresponding ^{13}C NMR signal was around 46.70 ppm, which differ from those of the 2-(chloromethyl)benzimidazole starting material, indicating the formation of the desired ligand. Further reaction of ligands **L4**–**L6** with $Mg(^{n}Bu)_2$ and BnOH or *t*-BuOH afforded the corresponding Mg(II) alkoxide complexes $[(\mathbf{L4})Mg(OBn)]_2$ (**14**), $[(\mathbf{L5})Mg(OBn)_2$ (**15**), $[(\mathbf{L6})Mg(OBn)_2$ (**16**) and $[(\mathbf{L5})Mg(t\text{-}BuO)]_2$ (**17**) (Scheme 6.2) in moderate yields (59–66%)

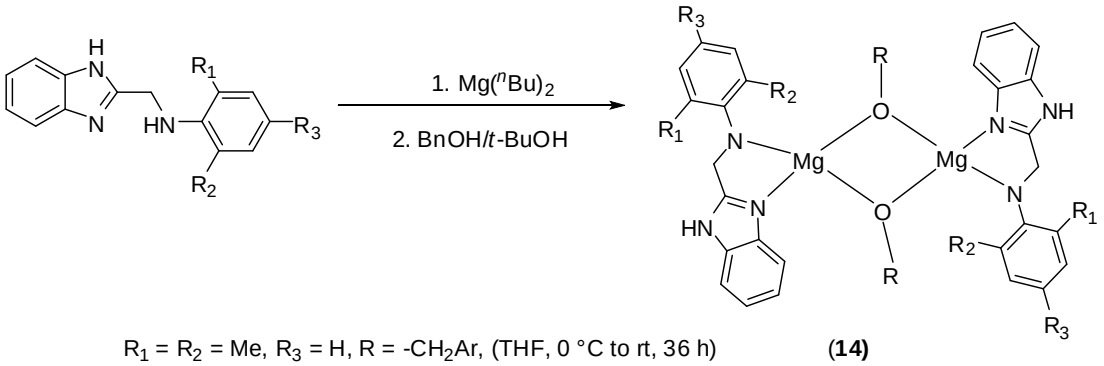

$R_1 = R_2 = Me$, $R_3 = H$, $R = -CH_2Ar$, (THF, 0 °C to rt, 36 h) (**14**)
$R_1 = R_2 = {}^{i}Pr$, $R_3 = H$, $R = -CH_2Ar$, (THF, 0 °C to rt, 36 h) (**15**)
$R_1 = R_2 = R_3 = Me$, $R = -CH_2Ar$, (THF, 0 °C to rt, 36 h) (**16**)
$R_1 = R_2 = {}^{i}Pr$, $R_3 = H$, $R = (CH_3)_3C$, (toluene, -78 °C to 70 °C, 9 h) (**17**)

Scheme 6. 2: Synthesis of Mg(II) alkoxide complexes **14–17**.

Complexes **14**–**17** were characterized using ^{1}H and ^{13}C NMR spectroscopy, mass spectrometry, IR spectroscopy and elemental analyses. The ^{1}H and ^{13}C NMR spectra of the Mg(II) complexes exhibited shifts relative to those of the respective ligands, which was useful in deducing complex formation (Figures 6.1 and 6.2). For instance, the resonance frequency for peaks corresponding to CH_3, CH_2NH and NH-Ar at 2.31, 4.45 and 7.06-6.93 ppm, respectively, for the free ligand **L4**

shifted upfield to 2.21, 4.34, and 6.99-6.88 ppm for complex **14** (Figure 6.1). Furthermore, the methylene hydrogen of the bridging benzyl alkoxides was revealed at 4.73 ppm (Figure 6.2). Also, ^{13}C NMR spectrum of ligand **L4** (top) and complex **14** (bottom) in Figure 6.2 showed the appearance of resonance peak at 64.88 ppm for the methylene linkage carbon of $–OCH_2C_6H_5$ derivative indicating the formation of desired complex

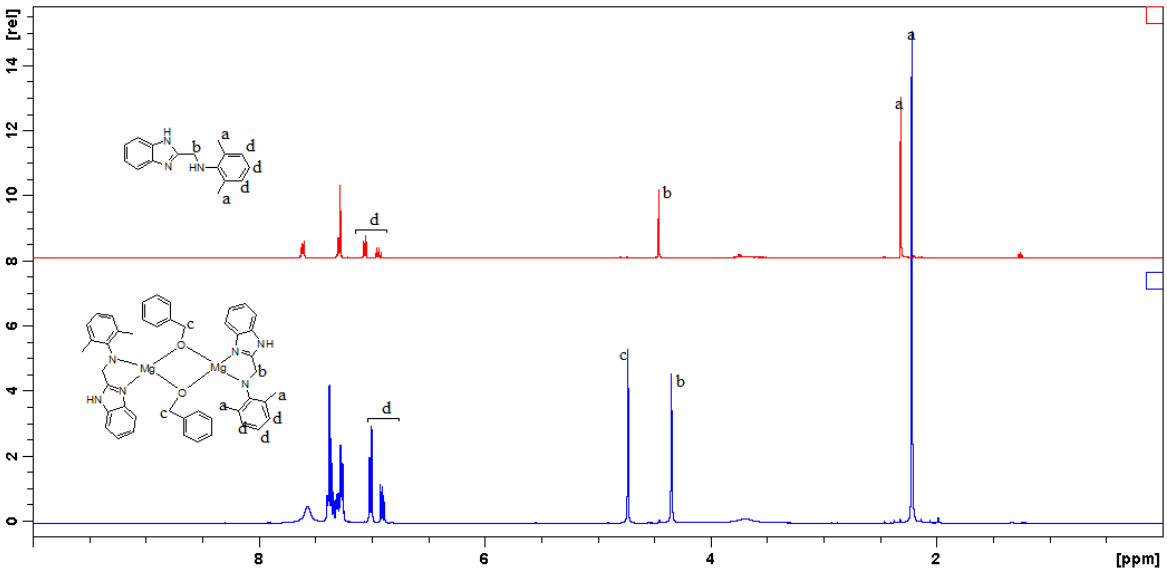

Figure 6. 1: ^{1}H NMR spectra of ligand **L4** (top) and complex **14** (bottom) showing the appearance of resonance of methylene hydrogen of the bridging benzyl alkoxides at 4.73 ppm indicative of complex formation.

All the complexes were characterized by mass spectroscopy and *m/z* values corresponding to various fragments of the complexes were observed. For instance, the mass spectrum of complex **14** showed *m/z* peaks at 512 amu, 382 amu and a base peak at 252 amu (Figure 6.3) corresponding to $[C_{30}H_{30}Mg_2N_3O_2]^+$, $[C_{23}H_{23}MgN_3O]^+$ and ligand **L4** fragments, respectively.

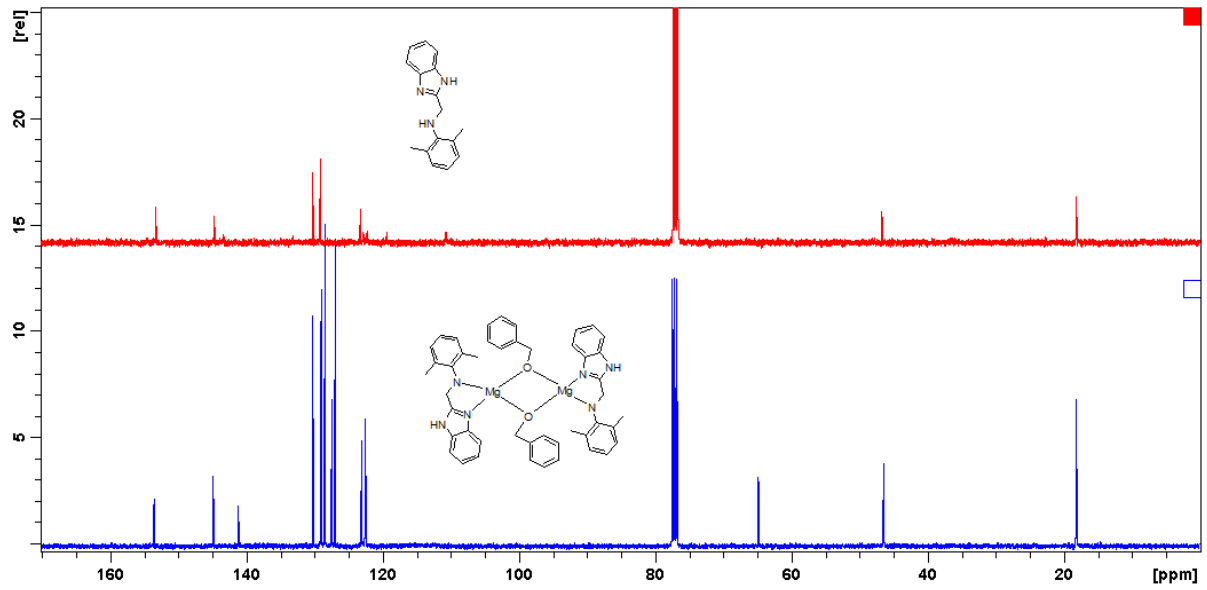

Figure 6. 2: ^{13}C NMR spectrum of ligand **L4** (top) and complex **14** (bottom) showing the appearance of resonance peak at 64.88 ppm for the methylene linkage carbon of $-OCH_2C_6H_5$ derivative indicating formation of complex.

The main stretching frequency bands observed in the FT-IR spectra of the complexes **14**–**17** were those of the ν(C=N) and ν(C-O) bands. From the FT-IR data, it was observed that these complexes showed a shift of the ν(C=N) peak from around 1630 cm^{-1} in the free ligands **L4**–**L6** to 1622, 1616, 1620 and 1611 cm^{-1} for complexes **14**, **15**, **16** and **17**, respectively. The shift of the imine ν(C=N) stretching frequency to lower wave numbers suggests the involvement of the nitrogen atom in the coordination to the magnesium center. Moreover, the strong bands associated with the ν(C-O) stretch around 1330, 1324, 1333 and 1328 cm^{-1} in **14**, **15**, **16** and **17**, respectively were also obtained. This suggested that the oxygen was also involved in complex formation.[12]

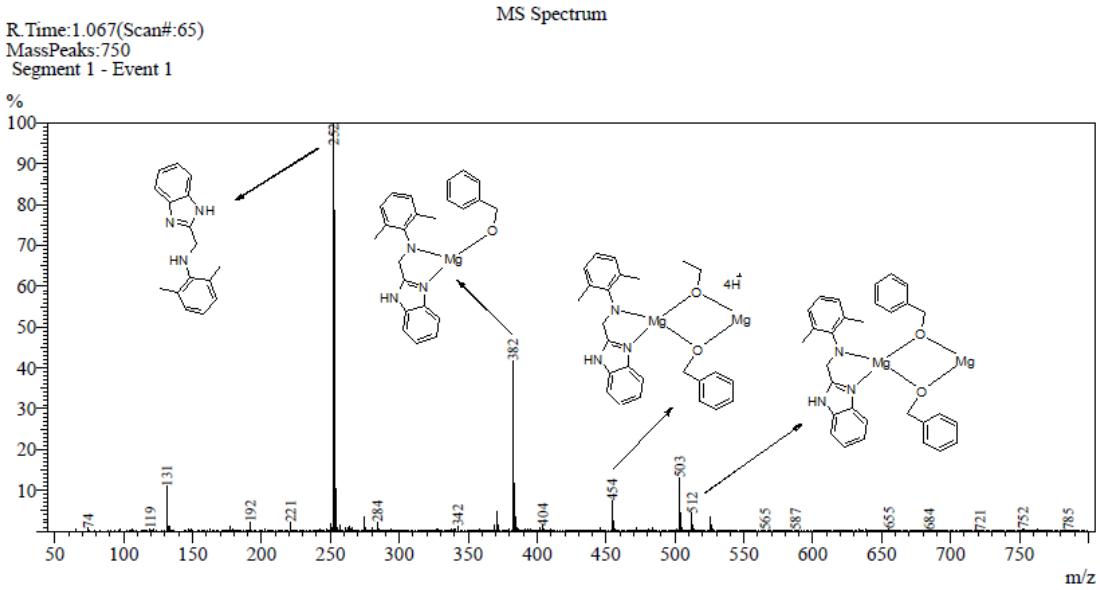

Figure 6. 3: Mass spectra showing complex **14** showing its fragmentation pattern to give a base peak at 252 amu corresponding to **L4** unit.

The NMR and mass spectrometry results, together with the result of elemental analysis were in good agreement with the proposed structures in Scheme 6.2. Attempts to isolate single crystals suitable for X-ray analysis to confirm the proposed structures of complexes **14-17** have so far been unsuccessful.

6.3.2 ROP of ε-CL and LAs using complexes 14–17 as catalysts

ROP of ε-CL and LAs catalyzed by Mg(II) alkoxide complexes **14–17** were investigated in toluene at 110 °C using [M]/[I] ratio of 200 and the results are listed in Table 6.1. Experimental results disclosed that all the (benzimidazolylmethyl) amine Mg(II) complexes **14–17** display good catalytic activities for the polymerization of ε-CL, $_{L}$-LA and $_{D,L}$-LA giving conversions

above 95% within 36 h for ε-CL , and 52 h for $_{L}$-LA and $_{D,L}$-LA, respectively (Table 6.1, Entries 1-10).

6.3.2.1 Kinetics of ROP reactions of ε-CL and LAs

In order to understand the influence of Mg(II) alkoxide complexes **10**–**12** in the mechanism of ROP reactions, the ROP of ε-CL and LAs catalyzed by the Mg(II) compounds were systematically investigated. Conversion of ε-CL with time was monitored by ^{1}H NMR spectroscopy and the rates of the reaction were determined from the semi logarithmic plots of $\ln[CL]_o/[CL]_t$ *vs.* time (Figure 6.4a). The plots were linear, indicating that the kinetics of ROP reactions obey *pseudo*-first order dependency on the monomer concentrations. The apparent rate constants (k_{app}) were extracted from Figure 6.4a and are presented in Table 6.1. Although no clear dominant influence of ligand/complex property on the catalytic activities of the Mg(II) alkoxide complexes was obtained, the experimental results revealed that the catalytic activities were enhanced by the sterically bulky isopropyl group as in complex **15** (Table 6.1, entry 2, $k_{app} = 0.1765 \pm 0.00165$). Bulky substituents are generally known to inhibit the coordination of monomer to metal center thereby impeding the reaction rate.[13,14] The increase in activity associated with complex **15** can be rationalized by the effective separation of the electrophilic active metal center and the counterion induced by the steric environment from the ligand.[15] Similar observation where a higher reaction rate was obtained in ROP reaction involving Mg(II) and Al complexes containing sterically bulky ligand have been reported.[5,16] The apparent rate constants obtained for complexes **14**–**17** were higher in comparison to those recently reported using (benzimidazolylmethyl)amine Zn(II) and Cu(II) carboxylate complexes on the ROP ε-CL monomer[17],.

Table 6. 1: ROP data of ε-CL and LAs by Mg(II) alkoxide complexes **14–17**[a]

Entry	Catalyst	Time (h)	Conversion[b] (%)	k_{app} (h^{-1})	M_w (GPC)[c]	PDI[c]	IE[d]
1	**14**	30	97	0.1330 ±0.00619	6185	1.58	0.28
2	**15**	30	98	0.1765 ±0.00165	8416	1.43	0.38
3	**16**	36	95	0.1075 ±0.00790	3584	1.39	0.17
4	**17**	38	98	0.1034 ±0.00658	nd	nd	–
5[e]	**14**	48	94	0.0574 ±0.00310	2560	1.30	0.10
6[e]	**15**	36	97	0.1006 ±0.00171	2340	1.48	0.08
7[e]	**16**	48	97	0.0714 ±0.00207	2500	1.31	0.09
8[f]	**14**	52	95	0.0520 ±0.00420	1249	1.35	0.05
9[f]	**15**	36	95	0.0815 ±0.00288	2528	1.44	0.10
10[f]	**16**	48	96	0.0641±0.00583	1916	1.28	0.07

[a]Reaction conditions: $[CL]_o/[I]$ = 200; solvent, toluene, temperature, 110 °C. [b]Maximum conversion achieved [c]Molecular-weight average and Polydispersity index (PDI) determined by GPC relative to polystyrene standard, values are the values obtained from GPC × correction factor of 0.56 for lactones and 0.58 for LAs. [d]Initiator efficiency (IE) = M_{wexp}/M_{wcalc} where $M_{wcalc} = M_{w(monomer)} \times [CL]_o/[I] \times [PCL]/[CL]_o + M_{w(chain\text{-}end\ group.}$ [e]D,L-LA and [f]L-LA.[18] nd = not determine.

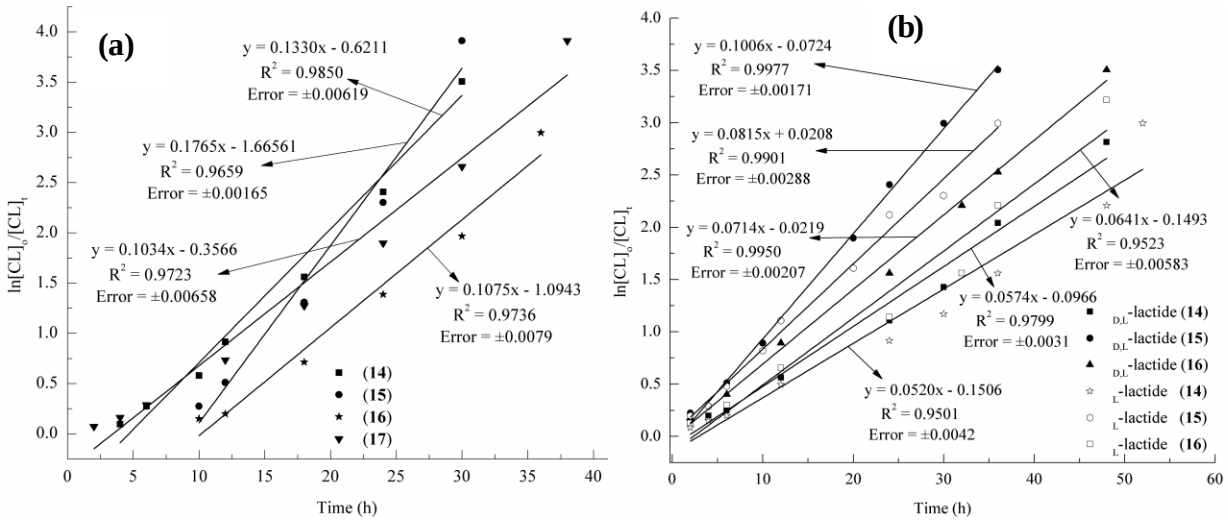

Figure 6. 4: (a) First order kinetic plots of $\ln[CL]_o/[CL]_t$ *vs.* time for complexes **14**–**17** in the ROP of ε-CL in toluene at 110 °C, $[CL]_o/[I] = 200$. (b) First order kinetic plots of $\ln[CL]_o/[CL]_t$ *vs.* time for complexes **14**–**16** in the ROP of $_{D,L}$-LA and $_{L}$-LA to PLAs in toluene at 110 °C, $[CL]_o/[I] = 200$.

Kinetic studies for the ROP of $_{D,L}$-LA and $_{L}$-LA using complexes **14**–**16** in ratio $[CL]_o/[I] = 200$ at 110 °C were also performed. The $\ln[CL]_o/[CL]_t$ *vs.* time plots (Figure 6.4b) exhibited linear variation. From the slope of the plots, the values of the apparent rate constant (k_{app}) for ROP reactions were obtained and presented in Table 6.1, entries 5–10. The semi-logarithmic plots exhibited a good linear relationship manifesting that the ROP reaction proceeded with first-order dependence on monomer concentration. High reaction rates were also recorded for complexes with sterically bulky isopropyl group in the ROP of $_{D,L}$-LA and $_{L}$-LA (Table 6.1, entries 6 and 9). Similar trend have been reported in the case of dialkylaluminium alkoxides[19,20] and monomeric Ti(IV) homopiperazine complexes.[21] The bulky isopropyl group could also improve the solubility of the complex and in return the activity. Coates and co-workers[22,23] also reported

increased catalyst activities upon increasing bulkiness of the ligand substituents and the observation was explained by the fact that the more bulky substituents could possibly force the catalyst in its monomeric and more active state. Generally, the reaction rates of ROP of ε-CL were slightly higher than that those of LA reactions. For example, rate constants of 0.1765 ± 0.00165 h^{-1}, 0.1006 ± 0.00171 h^{-1} and 0.0815 ± 0.00288 h^{-1} were obtained for ε-CL, $_{D,L}$-LA and $_{L}$-LA respectively using complex **15** (Table 6.1, entries 2, 6 and 9). Similar trend was reported in chapter **4**, and attributed it to the larger ring size of ε-CL compared to LAs.[24]

Table 6. 2: Effect of catalyst concentrations on polymerization kinetics of ε-CL and $_{L}$-LA [a]

Catalyst	$[CL]_o/[11]$	Time (h)	Conversion[b] (%)	k_{app} (h^{-1})	M_w (GPC)[c]	PDI[c]	IE[d]
15	100	15	98	0.2630	6185	1.58	0.55
15	150	20	97	0.1808	6469	1.44	0.39
15	250	36	96	0.1109	8280	1.40	0.30
15	300	48	95	0.0728	8560	1.30	0.26
15[e]	100	20	98	0.1754	2026	1.56	0.14
15[e]	150	30	97	0.1181	2430	1.41	0.12
15[e]	250	40	96	0.0778	2717	1.29	0.08
15[e]	300	48	96	0.0659	3016	1.39	0.07

[a]Reaction conditions, Toluene, 110 °C. [b]Maximum conversion achieved [c]Molecular-weight average and Polydispersity index (PDI) determined by GPC × correction factor of 0.56 for lactones and 0.58 for LAs. [e]$_{L}$-LA.[18] [d]Initiator efficiency (IE) = M_{wexp}/M_{wcalc} where $M_{wcalc} = M_{w(monomer)} \times [CL]_o/[Cat] \times [PCL]/[CL]_o + M_{w(chain\text{-}end\ group)}$. [e]$_{L}$-LA.

6.3.3 Order of ROP of ε-CL and $_L$-LA reaction with respect to catalyst 15

Conversion of ε-CL and $_L$-LA in toluene with time was monitored by ^{1}H NMR for various concentrations of **15**, $[CL]_o/[I]$ = 100, 150, 250, 300 respectively, at 110 °C to determine the reaction orders with respect to catalyst (Table 6.2). A graph of $\ln k_{app}$ *vs.* ln[**15**] was plotted and the linear relationship obtained allowed us to extract the order of reaction from the gradient of the line of best fit (Figure 6.5). From this plot, the order of the reactions in the ROP of ε-CL and $_L$-LA with respect to catalyst **15** were obtained as 1.08 $\pm$ 0.13 (Figure 6.5a) and 0.88 $\pm$ 0.09 (Figure 6.5b) respectively. Thus, the polymerization of ε-CL and $_L$-LA by **15** proceeded according to the overall kinetic law of the form represented in Equations 6.2 and 6.3 respectively.

$$-\frac{d[CL]}{dt} = k[CL][\mathbf{15}]^1 \qquad (6.2)$$

$$-\frac{d[L^{-LA}]}{dt} = k[L^{-LA}][\mathbf{15}]^{0.9} \qquad (6.3)$$

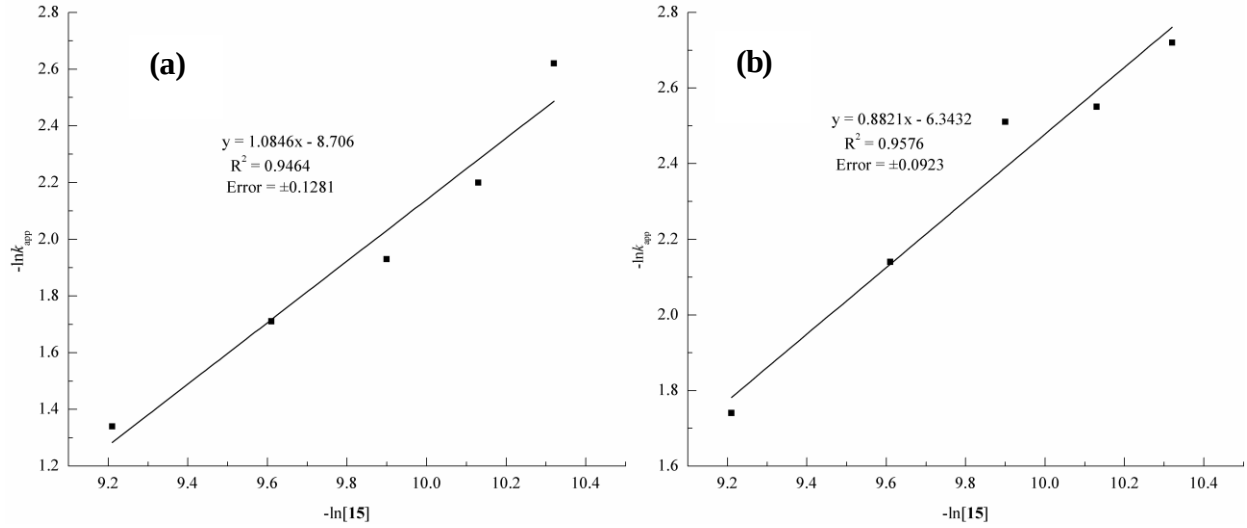

Figure 6.5: (a) Plot of $\ln k_{app}$ *vs.* ln[**15**] for the determination of order of reactions in the ROP of ε-CL and (b) for the determination of order of reactions in the ROP of $_L$-LA**.**

6.3.4 Assessment of the effect of alcohol initiators on the ROP kinetics of ε-CL

The ROP of ε-CL in the presence of BnOH and complex **15** was examined at different $[CL]_o$:$[I]_o$:$[BnOH]_o$ ratios(Table 6.3). The catalytic activity of **15** increased with increase in the concentration of BnOH. This probably resulted from the increase of catalytically initiating alkoxide sites in the system. For example, catalytic activities of Mg(II) alkoxide complexes reported by Kong and Zhong exhibited 83% conversion of 1000 equivalent of ε-CL in 80 min at 30 °C, whereas in $[Cat]_o/[CL]_o/[BnOH]_o$ ratio of 1:1000:10, 98% conversion of the monomer was obtained in 20 min.[25] The BnOH molecules added act as chain-transfer agents in the polymerization reaction, and the exchange between the growing alkoxide species and alcohol leads to chain transfer reaction, since the resulting benzyloxy-metal complex molecule is able to reinitiate the polymerization reactions.[26]

Table 6. 3: Studies for ROP of ε-CL in the presence of BnOH using complex **15**[a]

Entry	$[CL]_o:[I]_o:[BnOH]_o$	Time (h)	Conversion[b] (%)	k_{app} (h^{-1})	M_w (GPC)[c]	PDI[c]	IE[d]
1	200:1:5	22	95	0.1377 ±0.0073	1918	1.36	0.43
2	200:1:10	20	96	0.1588 ±0.0097	1506	1.33	0.66
3	200:1:20	18	96	0.1781 ±0.011	879	1.29	0.73
4	200:1:50	18	98	0.1998 ±0.0114	715	1.24	1.29

[a]Solvent: toluene, temperature, 110 °C. [b]Maximum conversion achieved [c]Molecular-weight average and PDI determined by GPC relative to polystyrene standard, values are the values obtained from GPC × correction factor of 0.56 for lactones.[18] [d]Initiator efficiency (IE) = M_{wexp}/M_{wcalc} where $M_{wcalc} = 114 \times ([CL]_o/([BnOH]_o) \times$ conv. (%) + 108.

6.3.5 Polymer molecular weight and molecular weight distributions

The polymers obtained from the ROP reactions were analyzed by GPC to determine the molecular weights and molecular weight distributions (Tables 6.1-6.3). The observed low weight average molecular weights (M_w) of the polymers obtained after corrections by a factor of 0.56 for PCL and 0.58 for PLAs[18], respectively, point to certain degree of intramolecular *trans*-esterification process (back-biting) during the polymerization reactions.[27] Increasing the concentration of benzyl alcohol initiator in the ROP reaction resulted in much more low molecular weight consistent with availability of many active initiating sites (Table 6.3).[25] Molecular weight distributions of between 1.42 to 1.58 were obtained and were relatively narrow

compared to previous reports using (benzomidazolylmethyl)amine Zn(II) and Cu(II) catalysts[17,28], where PDI values were as high as 3.97 for ROP reactions of ε-CL.

6.3.6 End-group analysis and ROP reaction mechanism

The kinetic data and the near integer order of ROP reactions obtained in the previous sections (**6.3.2.1** and **6.3.3**) pointed to a coordination-insertion pathway as the ROP mechanism. In order to gain more insight into the polymerization mechanism, end group analyses of polymers were performed using ^{1}H NMR spectroscopy Figures 6.6 and 6.7.

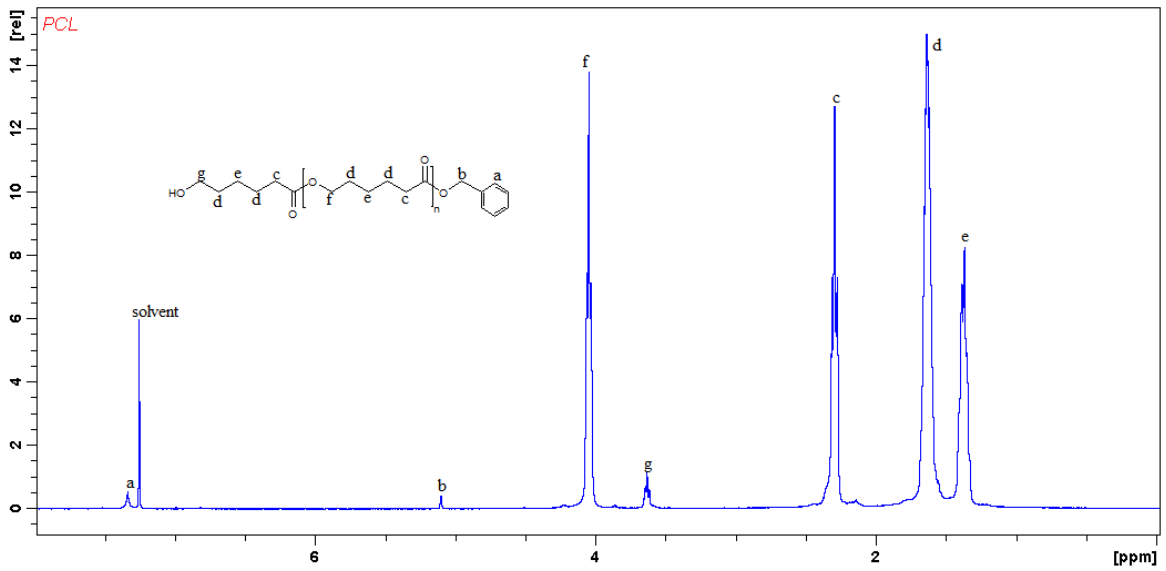

Figure 6. 6*:* ^{1}H NMR spectrum of PCL in $CDCl_3$ revealing the presence of phenyl ring protons (7.37 ppm) and CH_2 (5.12 ppm) signal of $–OCH_2C_6H_5$ group. Reaction condition:$[CL]_o$:$[I]_o$ = 200:1 in toluene at 110 °C, 12 h.

The presence of phenyl ring protons (7.37 ppm) and CH_2 (5.12 ppm) signal of :–$OCH_2C_6H_5$ group in the ^{1}H NMR spectra of PCL suggested that the polymer chain is capped with a benzyl ester group on one end and a hydroxyl group on the other end with the integration ratio of 3:1 (–$CH(CH_3)OH$:–$OCH_2C_6H_5$) (Figure 6.6). Also, the ^{1}H NMR spectrum of PLLA (Figure 6.7) indicated that the polymer chain was capped with one benzyl ester and one hydroxyl end in the ratio of 5:1. These results indicated that the ROP reactions occurred *via* coordination–insertion mechanism, proceeding through acyl-oxygen cleavage of the monomer.[29]

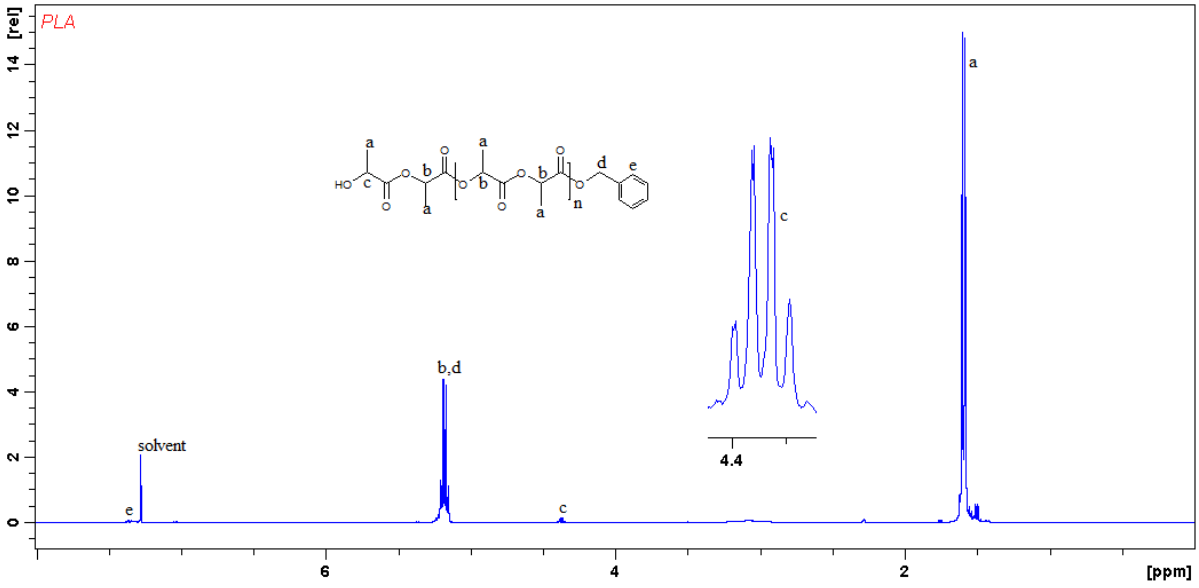

Figure 6. 7: ^{1}H NMR spectrum of PLA in $CDCl_3$ showing signals that the polymer chain is capped with one benzyl ester and one hydroxyl end. Reaction condition:$[CL]_o$:$[I]_o$ = 200:1 in toluene at 110 °C, 20 h.

However, analyses of the ESI-MS spectra showed Na^+–capped repeating units of the oligomers (Figure 6.8). The $–OCH_2C_6H_5$ and –OH groups observed in the ^1H NMR spectra of the polymers were also detected in the ESI-MS spectra, confirming coordination-insertion mechanism.[29,30,31]

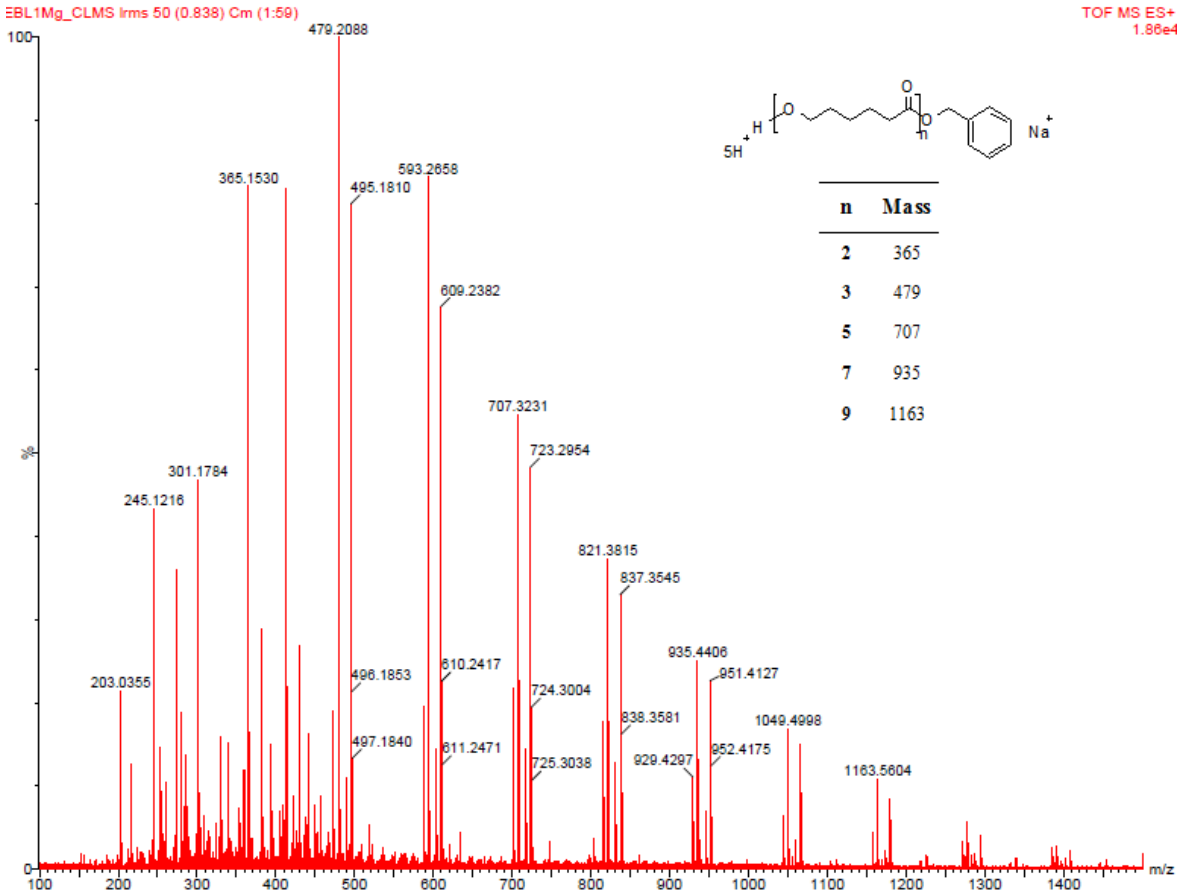

Figure 6. 8: ESI-MS spectrum of PCL obtained by using catalyst 15, Reaction condition:$[CL]_o$:$[I]_o$ = 200:1 in toluene at 110 °C, 12 h.

6.3.7 Microstructural analyses of the polymers

It is established that the physical, mechanical, and degradation properties of PLA are dependent on the stereochemistry of PLAs.[29,32,33] Determination of the stereochemical microstructures of

PLA was achieved through inspection of the methine region of homonuclear decoupled ^{1}H NMR, and ^{13}C NMR spectra of the polymers.[34,35] Microstructural analysis of homonuclear decoupled ^{1}H NMR, and ^{13}C NMR spectra of PLA formed from $_{L}$-LA polymerized by complex **15** revealed that the complex structures exerted a significant influence on the tacticity of the growing polymer chain producing a substantially isotactic PLA (Figures 6.9 and 6.10) without observable epimerization. This finding present an improvement in stereoselectivity compared to previous report in chapters **3** and **4**, when the occurrence of epimerization of $_{L}$-LA under our ROP reaction conditions produced moderate isotactic bias PLAs. Zn(II) carboxylate (benzimidazolylmethyl) complexes reported in literature[28] polymerized $_{L}$-LA to moderate isotactic PLA with observable epimerization.

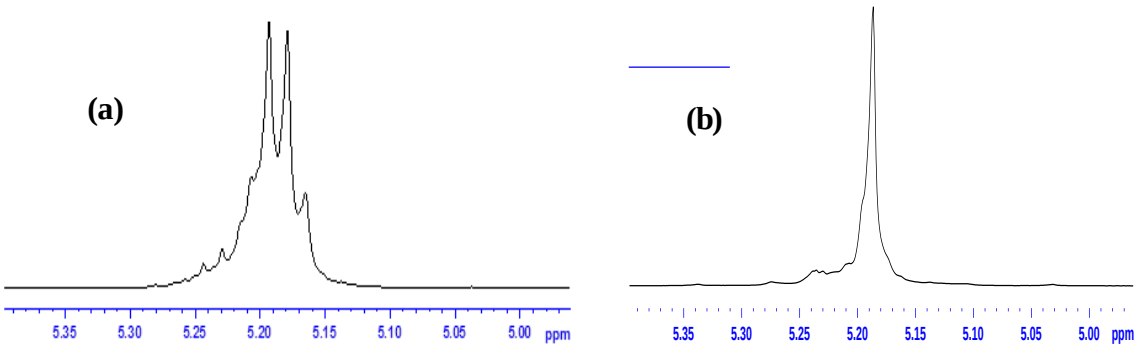

Figure 6. 9: (a) ^{1}H NMR (400 MHz, $CDCl_3$) spectra of the methine region of isotactic PLA prepared from $_{L}$-LA using catalyst **15** (b) Homonuclear decoupled ^{1}H NMR (400 MHz, $CDCl_3$) spectra of the methine region of isotactic PLA prepared from $_{L}$-LA using complex **15**

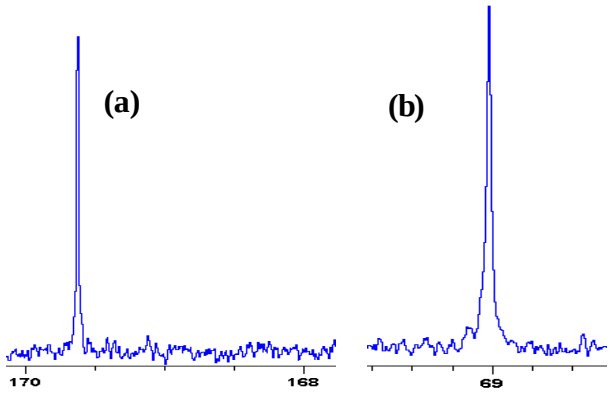

Figure 6. 10: (a) ^{13}C NMR spectra carbonyl region and (b) ^{13}C NMR methine region of poly($_{L}$-LA) supporting isotactic microstructure of PLA prepared from $_{L}$-LA using complex **15**. Reaction condition:$[CL]_o$:$[I]_o$ = 200:1 in toluene at 110 °C.

The stereochemistry of PLA obtained from the ROP of $_{D,L}$-LA was also investigated using homonuclear decoupled ^{1}H NMR spectrum of the methine region (Figure 6.11). The core tetrad stereosequences in poly($_{D,L}$-LA) are well resolved and peak assignments are consistent with literature [35-36] and production of atactic poly($_{D,L}$-LA) with *Pr* of 0.49.

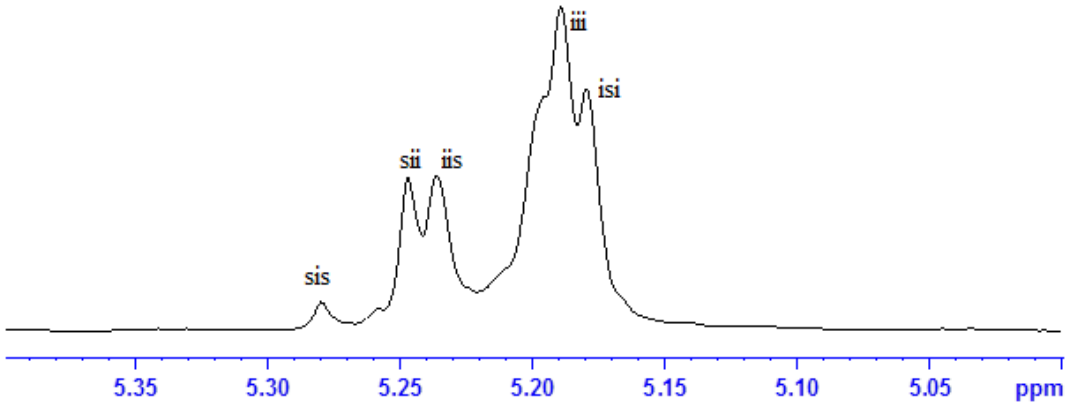

Figure 6. 11: ^{1}H homonuclear decoupled NMR of the methine region of poly($_{D,L}$-LA) obtained from complex **15** showing atactic microstructure.

6.3.8 TGA analysis of PLA

The melting points of polymers and the extents of crystallization depend on the composition of the isomers and sequences in the polymer.[37] The PLA obtained using complex **15** as catalyst was thermally analyzed by DSC-TGA and the results are presented in Figure 6.12. The initial decomposition temperature was around 256 °C. This can be attributed to the formation of a crystalline stereoblock PLAs.[38,39] Moreover, the temperature of complete decomposition was slightly higher than that reported in the literature. As illustrated in Figure 6.12, the DSC trace has a melting temperature (T_m) occurring at 183 °C which is similar to reports in literature.[38,40] The observed temperature at about 375 °C could not have been the glass transition temperature (T_g) because, only highly isotactic polymers have been reported to have very high glass transition temperature.[41]

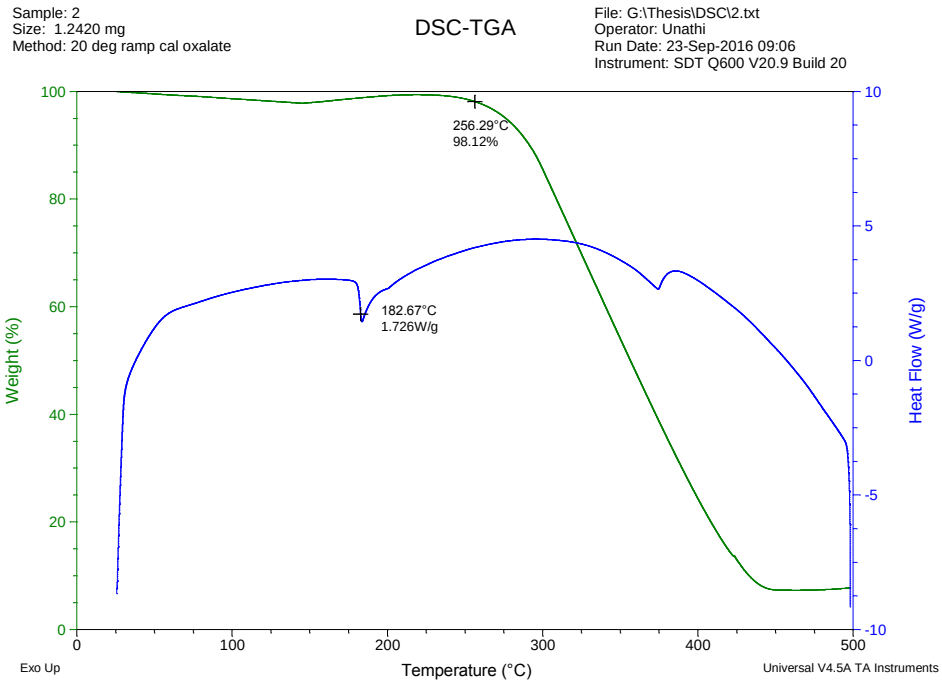

Figure 6. 12: DSC-TGA curves of PLA prepared from $_{D,L}$-LA at 110 °C, $[CL]_o/[I]$ = 200 using complex **15**.

6.4 Conclusion

Mg(II) alkoxides complexes bearing (benzimidazolylmethyl) amine ligands was synthesized and characterized. Each of complexes **14**–**17** catalyzed the ring opening polymerization of ε-caprolactone, $_{D,L}$-lactide and $_{L}$-lactide with the activity order of **15** > **14** > **16** >**17**. For the ring opening polymerization of ε-caprolactone, complex **15** showed the best control manifested by good molecular weight control and narrow molecular weight distributions. The resulted demonstrated an improvement ROP reactions by the alkoxide initiating group in comparison with the acetate and benzoate initiating groups resulted in controlled polymerization reactions demonstrated in relatively narrow molecular weight distributions and certain degree of streoregularity in the polylactides chains. The effect of employing alcohol as initiator in the polymerization process was also demonstrated as seen in the rate polymerization and the molecular weight of polymers obtained. The polymerization reactions proceeded *via* coordination-insertion mechanism to produce both atactic and isotactic polymers.

6.5 References

(1) Wood, R. J.; Suter, P. M.; Russell, R. M. *Am. J. Clin. Nutr.* **1995**, *62*, 493.

(2) Turnlund, J. R.; Betschart, A. A.; Liebman, M.; Kretsch, M. J.; Sauberlich, H. E. *Am. J. Clin. Nutr.* **1992**, *56*, 905.

(3) Darensbourg, D. J.; Karroonnirun, O. *Inorg. Chem.* **2010**, *49*, 2360.

(4) Labourdette, G.; Lee, D. J.; Patrick, B. O.; Ezhova, M. B.; Mehrkhodavandi, P. *Organometallics* **2009**, *28*, 1309.

(5) Chuang, H.-J.; Chen, H.-L.; Ye, J.-L.; Chen, Z.-Y.; Huang, P.-L.; Liao, T.-T.; Tsai, T.-E.; Lin, C.-C. *J. Polym. Sci. A: Polym. Chem.* **2013**, *51*, 696.

(6) Gao, Y.; Dai, Z.; Zhang, J.; Ma, X.; Tang, N.; Wu, J. *Inorg. Chem*. **2014**, *53*, 716.

(7) Wu, J.; Yu, T.-L.; Chen, C.-T.; Lin, C.-C. *Coord. Chem. Rev*. **2006**, *250*, 602.

(8) Ding, K.; Miranda, M. O.; Moscato-Goodpaster, B.; Ajellal, N.; Breyfogle, L. E.; Hermes, E. D.; Schaller, C. P.; Roe, S. E.; Cramer, C. J.; Hillmyer, M. A.; Tolman, W. B. *Macromolecules* **2012**, *45*, 5387.

(9) Miranda, M. O.; DePorre, Y.; Vazquez-Lima, H.; Johnson, M. A.; Marell, D. J.; Cramer, C. J.; Tolman, W. B. *Inorg. Chem*. **2013**, *52*, 13692.

(10) Attandoh, N. W.; Ojwach, S. O.; Munro, O. Q. *Eur. J. Inorg. Chem*. **2014**, 3053.

(11) Achar, K. C. S.; Hosamani, K. M.; Seetharamareddy, H. R. *Eur. J. Med. Chem*. **2010**, *45*, 2048.

(12) Campos-Vallette, M. M.; Figueroa, K. A.; Latorre, R.; Manriquez, V.; Diaz, G.; Costamagna, J.; Otero, M. *Vib. Spectrosc*. **1992**, *4*.

(13) O'Keefe, B. J.; Breyfogle, L. E.; Hillmyer, M. A.; Tolman, W. B. *J. Am. Chem. Soc*. **2002**, *124*, 4384.

(14) Hodgson, L. M.; Platel, R. H.; White, A. J. P.; Williams, C. K. *Macromolecules* **2008**, *41*, 8603.

(15) Gahleitner, M.; Severn, J. R. In *Tailor-Made Polymers Via Immobilization of Alpha-Olefin Polymerization Catalysts.*; Severn, J. R., Chadwick, J. C., Eds.; WILEY-VCH Verlag GmbH & Co. KGaA: Weinheim, 2008.

(16) Chang, M.-C.; Lu, W.-Y.; Chang, H.-Y.; Lai, Y.-C.; Chiang, M. Y.; Chen, H.-Y.; Chen, H.-Y. *Inorg. Chem*. **2015**, *54*, 11292.

(17) Attandoh, N. W.; Ojwach, S. O.; Munro, O. Q. *Eur. J. Inorg. Chem*. **2014**, 3053.

(18) Wu, J.-C.; Huang, B.-H.; Hsueh, M.-L.; Lai, S.-L.; Lin, C.-C. *Polymer* **2005**, *46*, 9784.

(19) Duda, A.; Kowalski, A. In *Handbook of Ring-Opening Polymerization*; Wiley-VCH Verlag GmbH & Co. KGaA, 2009.

(20) Liu, Y.-C.; Ko, B.-T.; Lin, C.-C. *Macromolecules* **2001**, *34*, 6196.

(21) Hancock, S.; Mahon, M.; Jones, M. *Chem. Centr. J.* **2013**, *7*, 135.

(22) Chamberlain, B. M.; Cheng, M.; Moore, D. R.; Ovitt, T. M.; Lobkovsky, E. B.; Coates, G. W. *J. Am. Chem. Soc.* **2001**, *123*, 3229.

(23) Rieth, L. R.; Moore, D. R.; Lobkovsky, E. B.; Coates, G. W. *J. Am. Chem. Soc.* **2002**, *124*, 15239.

(24) Appavoo, D.; Omondi, B.; Guzei, I. A.; van Wyk, J. L.; Zinyemba, O.; Darkwa, J. *Polyhedron* **2014**, *69*, 55.

(25) Kong, W.-L.; Wang, Z.-X. *Dalton Trans.* **2014**, *43*, 9126.

(26) Babu, H. V.; Muralidharan, K. *RSC Advances* **2014**, *4*, 6094.

(27) Stanford, M. J.; Dove, A. P. *Chem. Soc. Rev.* **2010**, *39*, 486.

(28) Attandoh, N. W.; Ojwach, S. O. *Polym. Korea* **2016**, *40*, 347.

(29) Dechy-Cabaret, O.; Martin-Vaca, B.; Bourissou, D. *Chem. Rev.* **2004**, *104*, 6147.

(30) Kamber, N. E.; Jeong, W.; Waymouth, R. M.; Pratt, R. C.; Lohmeijer, B. G. G.; Hedrick, J. L. *Chem. Rev.* **2007**, *107*, 5813.

(31) Platel, R. H.; Hodgson, L. M.; Williams, C. K. *Polym. Rev.* **2008**, *48*, 11.

(32) MacDonald, R. T.; McCarthy, S. P.; Gross, R. A. *Macromolecules* **1996**, *29*, 7356.

(33) Stevels, W. M.; Ankoné, M. J. K.; Dijkstra, P. J.; Feijen, J. *Macromolecules* **1996**, *29*, 6132.

(34) Thakur, K. A. M.; Kean, R. T.; Zell, M. T.; Padden, B. E.; Munson, E. J. *J. Chem. Commun.* **1998**, 1913.

(35) Thakur, K. A. M.; Kean, R. T.; Hall, E. S.; Kolstad, J. J.; Lindgren, T. A.; Doscotch, M. A.; Siepmann, J. I.; Munson, E. J. *Macromolecules* **1997**, *30*, 2422.

(36) Yang, Y.; Wang, H.; Ma, H. *Inorg. Chem*. **2015**, *54*, 5839.

(37) Drumright, R. E.; Gruber, P. R.; Henton, D. E. *Adv*. *Mater*. **2000**, *12*, 1841.

(38) He, Z.; Jiang, L.; Chuan, Y.; Li, H.; Yuan, M. *Molecules* **2013**, *18*, 12768.

(39) Chen, H.-Y.; Tang, H.-Y.; Lin, C.-C. *Macromolecules* **2006**, *39*, 3745.

(40) Petrus, R.; Sobota, P. *Organometallics* **2012**, *31*, 4755.

(41) Jamshidi, K.; Hyon, S.-H.; Ikada, Y. *Polymer* **1988**, *29*, 2229.

Chapter 7

Conclusions and future prospects

7.1 Research summary

In summary, this research project focused on the systematic investigations of Zn(II), Cu(II) and Mg(II) complexes of formamidine and benzimidazole derivatives ligands as catalysts in ring-opening polymerization of cyclic esters.

A series of formamidine (**L1**–**L3**) and benzimidazole derivatives (**L4**–**L6**) ligands were successfully synthesized in good yields. Ligands **L1**–**L3** coordinates to the metal centers through the imine nitrogen atom of the formamidine ligand in a monodentate fashion (Chapter **3**). Ligand **L1** form trinuclear Zn(II) complex with the three Zn(II) centers arranged in a linear fashion, and revealing two bridging modes of the acetate anions. Ligands **L2** and **L3** form dinuclear Zn(II) complexes with distorted trigonal bipyramidal and trigonal pyramidal geometries depending on the steric bulk of the ligand backbone and the flexibility of the bridging acetate anions. Ligand **L2** also exhibits a familiar dinuclear paddle wheel conformation in which the acetate anions bridges the Cu(II) centers in a bidentate mode. Introduction of benzoate ligand as an auxiliary ligand changes the coordination mode of **L1** around the Zn(II) center resulting in a dinuclear paddle wheel structure. Also, the ligand **L2** with auxiliary benzoate ligand in the other hand exhibit a distorted tetrahedral geometry around the Zn(II) atom possibly because of the steric contribution of the isopropyl and benzoate groups (Chapter **4**). The (benzimidazolylmethyl) amine ligands (**L4**–**L6**) were synthesized in good yields. The ligands were obtained by condensation reaction of 2-chloromethyl-1H-benzimidazole with appropriate

aromatic amines. Ligands **L4**–**L6** form dinuclear four-coordinate Zn(II) and Mg(II) complexes with the ligands binding in a bidentate fashion (Chapters **5** and **6**). The metal centers are bridged by BnO- or *t*-BuO- anions. All the compounds were comprehensively characterized using a range of analytical techniques which include ^{1}H and ^{13}C NMR spectrometry, FT-IR, mass spectrometry and elemental analysis. Single crystal x-ray diffraction was also employed in the characterization of complexes **1**, **2**, **3**, **4**, **5**, **6**, **7**, and **9**, respectively. The data acquired from all these techniques confirmed the nature of the ligands and metal complexes.

The activities of complexes **1**–**4** (Chapter **3)** as catalysts for the ROP reactions of ε-CL and $_{D,L}$-LA and $_{L}$-LA were evaluated. The reactions were performed in bulk and various reaction parameters including time, $[CL]_o/[Cat]$ ratio, temperature and solvent were investigated. Complexes **4**, **2**, **3**, and **1** showed moderate to high activity. However the low activity of **4** and **2** was attributed to the steric effected exerted by **L2**. The Zn(II) and Cu(II) complexes bearing *N*,*N'* diarylformamidines and benzoate ligands however, do form catalyst that catalyze ROP of cyclic esters producing moderate molecular weights polymers (Chapter **4**). The Zn(II) and Mg(II) alkoxide complexes (**10**–**17**) were active initiators for the ROP of ε-CL and $_{D,L}$-LA and $_{L}$-LA in toluene. All ROP reactions followed *pseudo*-first order kinetics with respect to the monomers. Best controlled ROP reactions with the alkoxide complexes **10**–**17** were manifested by good molecular weight control and narrow PDIs.

The benzoate initiating groups were inferior compared to the acetates, as depicted in lower reaction rates and poor stereoselectivity towards ROP of $_{D,L}$-LA. However, the alkoxides

initiating groups resulted in higher ROP reaction rates and improved polymer properties and stereoselectivity. Complexes with Zn(II) metal centers were better catalysts compared to complexes with Mg(II) and Cu(II) centers with activities in the following order; Zn>Mg>Cu. Bulky isopropyl substituents on the formamidine and benzimidazole derivatives ligands backbone hindered rapid coordination of the monomers to the metal centers, resulting in lower ROP reaction rates. Complexes of benzimidazole derivatives ligands compared with the formamidine complexes gave polymers with desirable properties such as narrow PDI and good stereoselectivity. The ring size and strain of the monomers played a role in the ring opening processes. Generally, higher polymer M_w were obtained with complexes with the acetates initiating groups, and from the experimental data obtained, the ROP reactions proceeded *via* coordination-insertion mechanism. The formamidines Zn(II) complexes displayed certain degree of control of polymer stereo-regularity producing predominantly heterotactic poly($_{D,L}$-LA) in the case of the acetate initiating groups, and atactic poly($_{D,L}$-LA) with the benzoates groups. Predominantly crystalline isotactic poly($_{L}$-LA) were obtained with the alkoxide complexes indicating stereoselectivity by the alkoxide initiating groups.

7.2 Conclusions

The findings in this research work are summarized as follows;

- ✓ The coordination chemistry and the effects of steric properties on the coordination behaviors of the ligands to the metal centers, and the applications of the complexes in the ROP of ε-CL and LAs have been demonstrated.
- ✓ The complexes formed active and stable catalysts in the ROP reactions of ε-CL and $_{D,L}$-LA and $_{L}$-LA

- ✓ The results demonstrated that the ROP reactions (mostly activities and M_w of polymers) depended largely on the steric properties of the ligands.
- ✓ The results showed that benzoate initiating groups are inferior in activity and polymer properties compared to the acetates and alkoxide groups with activities in the following sequence; alkoxide > acetates > benzoate.
- ✓ The kinetics of all the ROP reactions was *pseudo*-first order with respect to both ε-CL and LA monomers.
- ✓ Both the temperature, initiators (benzyl alcohol and methanol) and solvent (toluene) significantly influenced the ROP reactions.
- ✓ Based on the kinetic, Arrhenius and Eyring plots data, together with end group analyses using ^{1}H NMR and mass spectrometry, coordination-insertion mechanism as the predominant mechanism of the ROP reactions was confirmed.
- ✓ The catalysts display reasonable degree of control of polymer stereo-regularity.

In the area of ROP of cyclic esters, this work has significantly contributed to advances in the design and synthesis of catalysts/ initiators systems based on less toxic and cheap zinc, copper and magnesium metals, in the synthesis of biodegradable and biocompatible polymers from renewable bio-feedstock.

7.3 Future work

The findings reported in this study are significant contributions to the design and synthesis of active metal complexes as catalysts in ROP reactions. Further work towards finding more improved catalysts may be carried out as outline;

- Alkaline earth metals based catalysts have proven very attractive because of their good activity and low toxicity, and gives unique and controlled ROP reactions as demonstrated with the Mg(II) alkoxides systems reported in this studies. As such, synthesis of benzimidazole derivatives with calcium alkoxides, and their investigations as catalysts in ROP reactions would be useful.
- The benzimidazole derivatives ligands can be modified by introducing electron withdrawing groups to establish how that would compare to the complexes reported in these studies, and also how it would affect ROP processes and polymer properties. Also, varying R_1 with substituents as shown Figure 7.1 will result in a perfect bidentate ligand, and allow coordination to the metal center *via* the remaining secondary nitrogen atom and the lone pairs of the tertiary nitrogen atom. Depending on the R-groups, solubility of the resulting metal complexes could be enhanced thereby making it more suitable catalyst in ROP reactions.

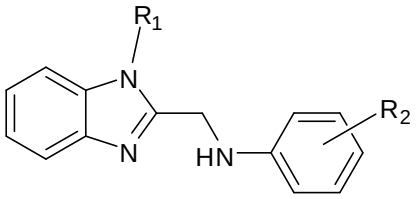

R_1 = CH_3, C_2H_5, benzyl, substituted phenyl
R_2 = OCH_3, Br, Cl, NO_2

Figure 7. 1: Possible modification of the benzimidazole derivatives ligands.

- Ligands precursors with chiral linkages (Scheme 7.1) with metal alkoxides may result in better stereoselectivity on the ROP of $_{D,L}$-LA, as such, this should be investigated.

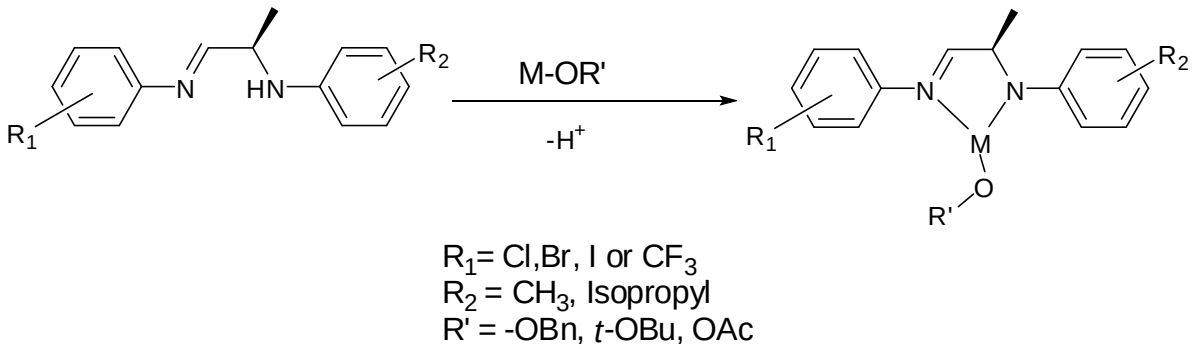

R_1= Cl,Br, I or CF_3
R_2 = CH_3, Isopropyl
R' = -OBn, *t*-OBu, OAc

Scheme 7. 1: Proposed simple ligand precursors with chiral backbone for the synthesis of stereoselective alkoxide complexes.

- ❖ DFT calculations to give more insight into the effect of steric and electronics on the coordination of monomers to the metal centers of catalysts to initiates ROP reactions should be given considerations.
- ❖ Crystal structure determination of metal alkoxides complexes in chapters **5** and **6** should be investigated.

APPENDIX A

Supporting information on single crystal XRD data (check cif) for reported complexes is provided as a PDF document on compact disc that accompanies this thesis.